Development and Characterisation of Skeletal Muscle Models for Secretome Investigation

Muna Nuh Ali

A thesis submitted in partial fulfilment of the requirements of

Sheffield Hallam University

for the degree of Doctor of Philosophy

December 2024

Candidate Declaration

I hereby declare that:

1. I have not been enrolled for another award of the University, or other academic or professional organisation, whilst undertaking my research degree.
2. None of the material contained in the thesis has been used in any other submission for an academic award.
3. I certify that this thesis is my own work. The use of all published or other sources of material consulted have been properly and fully acknowledged.
4. The work undertaken towards the thesis has been conducted in accordance with the SHU Principles of Integrity in Research and the SHU Research Ethics Policy, and ethics approval has been granted for all research studies in the thesis.

   The word count of the thesis is 53, 771.

Name	Muna Nuh Ali
Award	Doctor of Philosophy
Date of submission	11th December 2024
Research Institute	Industry and Innovation
Director of studies	Dr Daniel Kelly

Aqoon la'aan waa iftiin la'aan

To be without knowledge is to be without light

- Somali proverb

Acknowledgements

Alhamdulilah, to have reached this point.

To my hooyo and aabo, who sought, and continue to seek a better life for me and my siblings, mahadsaanid. In kasta oo aanad haysan shahaado aqooneed oo aad ku guulaysatay, haddana dadka ku yaqaana, ogow in aad leedahay aqoon aan la qiyaasi karin, oo dhaafsiisan waxa ay Jaamacaddu ku bari karto. Waan ogahay inay taasi run tahay sababtoo ah waxaad i siisay waxbarista noloshayda ugu muhiimsan. Hoyoo macaan, your humour and your warmth are always the first place I come to when I am unhappy or doubtful. I will forever be grateful for the nights you calmed me in your arms and helped me sleep. Aabaheey, to the most wonderfully kind and intelligent man I know. Your dependability has made me safe and reassured me when I have felt unsteady and anxious. Thank you.

To my womb-mates and walaalo: Fatemah, Mohamed, Hodan, Anisa, Abdulmalek, Abdisamad and Zakaria. I am so lucky to have 'whenever I need it' company, and unconditional love from you all. To my late brother Abdullah, you are always missed – I think you would have taken an interest in all the science-y things I had to say. I want to say a special thanks to my bestie, Hoon. How lucky am I that I get a best friend in you as well? Your scientific knowledge (as a design specialist) never fails to impress me. Thank you for showing me resilience and always cheering me on, no matter what you have going on. Finally, to the family I made along the way (Ibby, Abdek and Isdahil) and my OG sister in-law, Carin, thank you for your advice and kind words.

My forever girlies – Ameena, Henna, Manoshi and Taposhi. Thank you for your patience, for never making me explain myself and cheering me on what felt like a never-ending journey. Ameena, thank you for putting your hand up in school to volunteer to be my friend, and somehow communicating with me when I knew no English. Henna, the changes in your life have really put into perspective just how long this Ph.D. has taken. Thank you for your consistency and always being the glue to Pent. Manoshi and Taposhi – You are my favourite duo in the entire world. I laugh with you from the depths of my heart. Thank you for the most effortless and comforting sisterhood. Sharmila, thank you for planning and booking our amazing trips and always working around my schedule. Amani Handuleh, my Somali sis, I will never regret spending all my money on dinners and brunches with you and Taim. Our evening chai's is what I looked forward to most, after a long hard day.

Miss Kennedy, some of my best memories during my Ph.D. has been with you. Thank you for always giving me the perspective that I needed. Your Dicken's excerpts always

lifted my spirits when I was a wee down and your brilliant sense of humour always made me belly laugh. My Portuguese sister, Madalena. A wise man, dubbed ‘Italian ice-spice’ had once told us that soul mates can come in the form of friends – he was right. Thank you for the office dance parties, your hugs, coffee chats, your pick-me-up sticky notes, sushi dinners and in-depth analysis of the real housewives franchise. Filipe, my Virgo sis, your contagious energy and vibe was a bit of me from the start. You are amazing and I’ll never stop stanning! Laura, you started…and the rest was history. Thank you for your warmth and the endless fits of laughter. You are the plantain to my banana. Andrea, thank you for being such a great person, allowing me to share my concerns and anxiety. You have the biggest heart, and you will always have a friend in me. I promise to visit Switzerland someday, so you can teach me how to ski. To some of the amazing people who rode this journey with me; Sonia, Cris, Katie H, Alex Williamson, Chloe S and Lucy D - thanks for always being so kind and supportive.

I want to give a special thanks to my research team. Dr Daniel Kelly, my DoS, for giving me this opportunity. Our meetings were never dull, even when they lasted 3 to 4 hours (totally side-tracking). Your calm temperament always made things always feel lighter. Your compassionate words meant a lot and (almost) contended my imposter syndrome. Prof. David Smith, thank you for all the analytical support, humour and the PMA. I would like to give a special thanks to Prof. Christine Le Maitre, for encouraging my scientific creativity and helping me maintain my research spark. I hope you know that you have been an incredible mentor and support to me, who else would make their partner 3D print my little models for me on a Saturday night? Thank you to Dave Chorlton, who didn’t say no. Without you, the MTSIP would not exist! Finally, to the wonderful Orla Gallagher for all the support and access with imaging.

I would like to express a personal gratitude to all the staff and colleagues in the BMRC, however short our interaction was. I appreciate all the kind words from you all and wish you all the best in life.

Contents

Covid-19 impact statement

On 17th March 2020, the University announced a closure due to the COVID-19 pandemic, which restricted access to the BMRC laboratories and effectively halted all laboratory-based Ph.D. activities. Following government directives, a 'working from home' policy was implemented, severely impacting my ability to progress with my research. As my Ph.D. project is entirely laboratory-dependent, the six-month closure rendered it impossible to collect, analyse, or generate critical data essential for a viable thesis. Having only begun my Ph.D. four months prior to the closure, I had insufficient preliminary data to focus on during the remote working period. Instead, my time was largely occupied with literature reviews, attending webinars, instructor training, and an online conference. Data analysis was also constrained, as key softwares, including GraphPad Prism, ZEISS ZEN, Mass Lynx, and Progenesis, was inaccessible remotely. The BMRC laboratories reopened on 22nd September 2020 under stringent government restrictions. Laboratory access was limited to a three-day rota, with bench spaces, lab areas, and equipment requiring advance booking. Despite high demand, the restricted timetable and shorter working hours precluded the possibility of compensating for lost time. Progress was particularly impeded in cell culture work, which necessitated a minimum seven-day culture period; the rota rendered this unfeasible. Reliance on colleagues unfamiliar with the specific protocols led to frequent contamination, cell death, and loss of valuable resources. Additionally, prolonged shutdowns of critical instruments, such as mass spectrometers, caused startup delays, further hindering experimental workflows. Remote training for instrumentation via video conferencing further impacted effective learning and productivity. In summary, the prolonged lab closure and subsequent restrictions caused significant setbacks to the progress of my Ph.D. research.

Abstract

Exercise significantly reduces the risk of a spectrum of diseases and is increasingly prescribed as a therapeutic intervention, particularly for the management of chronic conditions including diabetes, cardiovascular diseases, musculoskeletal diseases, and neurological and psychiatric disorders. The skeletal muscle (SkM) secretome encompasses several hundred secreted proteins, forming a conceptual basis for understanding multi-organ crosstalk. During SkM contraction, myokines are secreted as proteins and proteoglycan peptides of approximately 5–35 kDa which mediate the protective and beneficial effects of exercise. Given the pivotal role of myokines, investigating their secretion patterns and responses to exercise-like stimuli is key to enhancing their therapeutic potential.

The complexity and redundancy of exercise as a biological stimulus, combined with the challenges of isolating specific myokine effects, necessitates *in vitro* models. Tissue-engineered SkM models were developed using a C2C12 murine myoblast cell line. From this, a foundational 2D SkM model and a novel tensile-strained 3D SkM construct was developed and characterised by structural and developmental myogenic markers. Histological and immunofluorescence analysis revealed aligned SkM fibres along a tension axis and deformation in the 3D construct. The application of electrical pulse stimulation (EPS) induced contraction and promoted myokine secretion. Nano-liquid chromatography mass spectrometry (nano-LCMS) facilitated the detection and profiling of the low-abundance myokines, validated through multiplex immunoassay (MIA). Untargeted data analysis revealed up to 1210 proteins from a single model. Secretome mining identified a putative novel myokine, serotransferrin (sTf), which contributes to the myokinome and demonstrates the effectiveness of the applied analytical and bioinformatics methodologies. Temporal myokine profiles, both transient and sustained, were observed in stimulated and unstimulated models, persisting up to 72 hours. Additionally, endogenous myokine secretion was observed in the *in vitro* models, which contributed to a baseline or spontaneous secretion profile.

The research presented in this thesis, developed a novel 3D muscle model where EPS stimulation effectively modulated myokine secretion, partially replicating the pleiotropic effects of exercise. Understanding how stimulation duration influences post-contraction myokine release offers valuable insights into the long-term effects of exercise on systemic health, including its role in chronic disease management, tissue regeneration, and sustained metabolic adaptations.

List of Figures

(p=0.0153), IL-15 +6 h (p=0.0211) and Irisin (p=0.0405) between 0 and 72 h; FSTL1 (p=0.0114) between 0 h and 48; and SPARC (p=0.0270) between 0 h and 24 h. Data was analysed by Kruskal-Wallis test, followed by Dunn's correction post-hoc test. ---210

List of Tables

List of abbreviations

ACTA1	Actin Alpha Cardiac Muscle 1
ACTN2	Alpha-Actinin-2
ALG	Alginate
AlgMA	Alginate Methacrylate
ALS	Amyotrophic Lateral Sclerosis
ATP	Adenosine Triphosphate
BAIBA	Beta-aminoisobutyric acid
BALB/3T3	BALB/c 3T3 (mouse fibroblast cell line)
BDNF	Brain-Derived Neurotrophic Factor
CAD	Computer-Aided Design
CCL2	C-C Motif Chemokine Ligand 2
CCL2/5/7/8	Chemokine Ligand 2/5/7/8
CCL5	C-C Motif Chemokine Ligand 5
CCL7	C-C Motif Chemokine Ligand 7
CCL8	C-C Motif Chemokine Ligand 8
cDMEM	Conditional Dulbecco's Modified Eagle's Medium
CM	Conditioned Media
CTRP15	C1q/TNF-related Protein 15/Erythroferrone
CTSB	Cathepsin B
CXCL1	C-X-C Motif Chemokine Ligand 1
CXCL1/5	C-X-C Motif Chemokine Ligand 1/5
DAPI	4',6-diamidino-2-phenylindole
DCD	Dermcidin
DCN	Decorin
DIA	Data-Independent Acquisition

DMD	Duchenne Muscular Dystrophy
DMSO	Dimethyl Sulfoxide
DPP4	Dipeptidyl Peptidase-4
DTT	DL-Dithiothreitol
ECM	Extracellular Matrix
ELISA	Enzyme-Linked Immunosorbent Assay
EPO	Erythropoietin
EPS	Electrical pulse stimulation
ERFE	Erythroferrone
ES	Electrical Stimulation
ESI	Electrospray Ionization
EV	Extracellular Vesicle
FA	Formic Acid
FASTA	FAST Alignment
FBS	Fetal Bovine Serum
FDR	False Discovery Rate
FFMT	Free Functional Muscle Transfer
FFPE	Formalin-Fixed Paraffin-Embedded
FGF15/19	Fibroblast Growth Factor 15/19
FGF15/21	Fibroblast Growth Factor 15/21
FGF2	Fibroblast Growth Factor 2
FGF21	Fibroblast Growth Factor 21
FNDC5	Fibronectin Type III Domain-Containing Protein 5
FSTL1	Follistatin-Like 1
GDF15	Growth Differentiation Factor 15
GDF15/8	Growth Differentiation Factor 15/8
GelMA	Gelatin Methacryloyl

hbFGF	Human Basic Fibroblast Growth Factor
hEGF	Human Epidermal Growth Factor
hESCs	Human Embryonic Stem Cells
hPSCs	Human Pluripotent Stem Cells
HSkMC	Human Skeletal Muscle Cells
IAA	Iodoacetamide
IGF-1	Insulin-like Growth Factor 1
IL-10	Interleukin 10
IL-15	Interleukin 15
IL-15/4/6/7	Interleukin 15/4/6/7
IL-1RA	Interleukin-1 Receptor Antagonist
IL-4	Interleukin 4
IL-6	Interleukin 6
IL-7	Interleukin 7
IL-8*	Interleukin 8
IMCT	Intramuscular Connective Tissue
INSL6	Insulin-like 6
iPSC	Induced Pluripotent Stem Cells
ITS-X	Insulin-Transferrin-Selenium-Ethanolamine
KLC	Kinesin Light Chain
LCMS	Liquid Chromatography-Mass Spectrometry
LIF	Leukaemia Inhibitory Factor
LN2	Liquid Nitrogen
MAGPIX	Magnetic Particle Imaging X-ray
Mag-TE	Magnetic Force-based Tissue Engineering
MALDI-QTOF	Matrix-Assisted Laser Desorption/Ionization Time of Flight
MAPK	Mitogen-Activated Protein Kinase

MCT6	MechanoCulture T6
MEF-2	Myocyte Enhancer Factor 2
Mefc2	Myocyte Enhancer Factor C2
MEMS	Microelectromechanical Systems
METRNL	Meteorin-like
MSCs	Mesenchymal Stem Cells
MFI	Mean Fluorescence Intensity
MIA	Multiplex Immunoassay
MLP	Muscle Lim Protein
MRF4	Myogenic Regulatory Factor 4
mTOR	Mechanistic Target of Rapamycin
MTSIP	Manual Tensile Strain-Inducible Platform
Myf-5	Myogenic Factor 5
MYHC	Myosin Heavy Chain
MyHC2	Myosin Heavy Chain 2
MyHC-E	Myosin Heavy Chain-E
MyHC-F	Myosin Heavy Chain-F
MyHC-IIa	Myosin Heavy Chain IIa
MyHC-IIb	Myosin Heavy Chain IIb
MyHC-IId/x	Myosin Heavy Chain IId/x
MyHC-pn	Myosin Heavy Chain-Pn
MyHC-S	Myosin Heavy Chain-S
MYOD	Myogenic Differentiation 1
Myog	Myogenin
NGF	Nerve Growth Factor
NMJ	Neuromuscular Junction
OGN	Osteoglycin

OSM	Oncostatin M
OSTN	Osteocrin
PAX7	Paired Box 7
PBS	Phosphate Buffered Saline
PBST	Phosphate Buffered Saline with Tween
PCM-1	Pericentriolar Material 1
PDGF	Platelet-Derived Growth Factor
PDMS	Polydimethylsiloxane
PEDF	Pigment Epithelium-Derived Factor
PEEK	Polyether Ether Ketone
PI3K	Phosphoinositide 3-Kinase
PLGA	Poly(lactic-co-glycolic acid)
PLLA	Poly-L-lactic acid
PMTs	Post-Translational Modifications
PPI	Protein-Protein Interactions
QTof	Quadrupole Time-of-Flight
rhFGF	Recombinant Human Fibroblast Growth Factor
RT	Room Temperature
SDS-PAGE	Sodium Dodecyl Sulphate Polyacrylamide Gel Electrophoresis
SFM	Serum-Free Medium
SILAC	Stable Isotope Labelling with Amino Acids in Cell Culture
SkM	Skeletal Muscle
SPARC	Secreted Protein, Acidic and Rich in Cysteine
STRING	Search Tool for the Retrieval of Interacting Genes/Proteins
TBS	Tris-Buffered Saline
TGF	Transforming Growth Factor
TGF-β	Transforming Growth Factor Beta

TMSB4X	Thymosin Beta-4
TNF	Tumour Necrosis Factor

1 General Introduction

1.1 Skeletal muscle structure and function

Skeletal muscle (SkM) accounts for around 40% of the total body mass in the human adult (Deshmukh *et al*., 2015a; Schnyder and Handschin, 2015; Olfert *et al*., 2016; Etienne *et al*., 2020) and primarily serves a mechanical function, generating force for movement and maintains posture. SkM roles include metabolism (Hingst *et al*., 2018; Huh, 2018), mass regulation (Lee and Jun, 2019) and thermoregulation (Rowland, Bal and Periasamy, 2015). SkM tissue has a hierarchical arrangement (**Figure 1.1**). It is primarily composed of fascicles (bundles) aligned under the epimysium, which ensheaths the entire organ. A perimysium surrounds the fascicles containing organised subsets of muscle fibres known as myofibers. The myofibers are long multinucleated muscle cells that align unidirectionally and are activated by motor neurons during contraction. A layer of connective tissue endomysium surrounds single myofibers and encapsulates a scaffolding basal lamina within the myofiber and contains satellite cells, the muscle specific progenitor cells, and differentiating myoblasts (Purslow, 2020). Myofibers are further made up of myofibrils containing the cytoskeletal thin actin and thick myosin myofilaments arranged to form sarcomeric functional units. A myofibril is made up of repeating portions of sarcomeres which form boundaries at Z-discs (Washio *et al.*, 2019). Most skeletal muscles are attached to bones via tendons, which function as flexible anchor points. Tendons are essential for conserving tissue structure and transmit the force generated by muscle contraction (Lovering *et al.*, 2011).

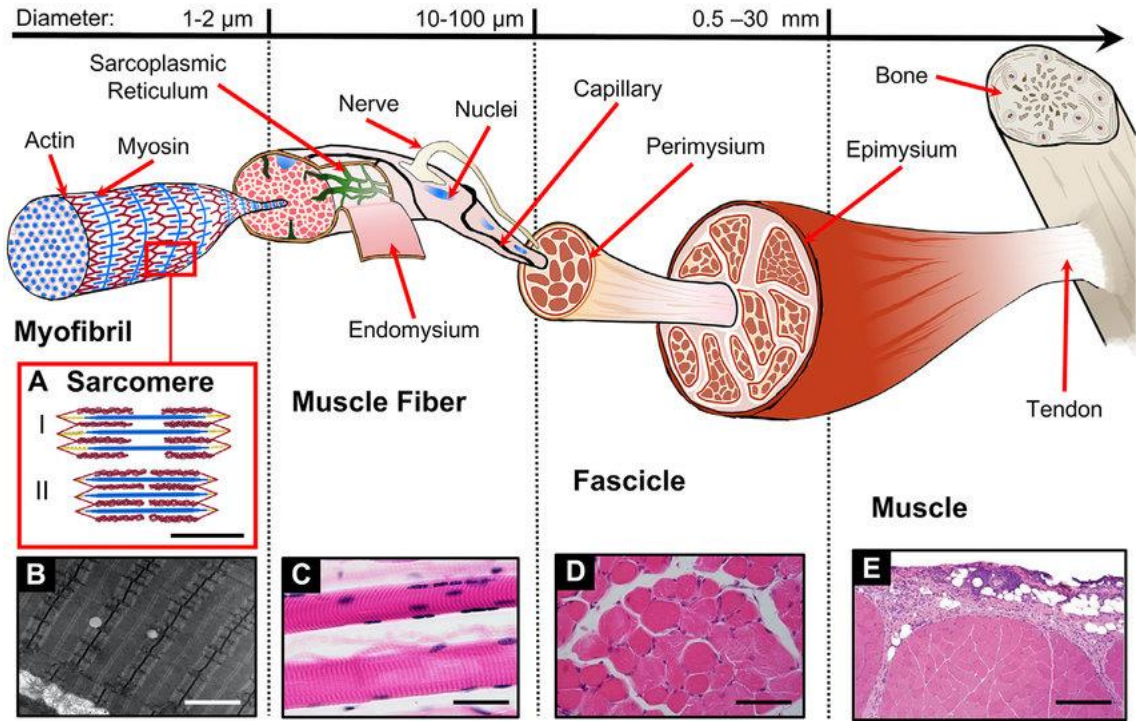

Figure 1.1 Structural hierarchy of SkM. (A) *Sarcomere structure, showing actin (red), myosin (blue), and titin (yellow) filaments in relaxed (I) and contracted (II) positions (scale bar: 0.5 nm).* ***(B)*** *Myofibrils imaged via TEM highlights the myofibril structure (scale bar: 1 nm).* ***(C)*** *Muscle fibres (pink) and nuclei (dark purple, scale bar: 50 µm).* ***(D)*** *Histological image of fascicle cross-section reveals perimysium membranes of muscle fibres, and nuclei (scale bar: 100 µm).* ***(E)*** *Histology cross section showing the epimysium membrane (scale bar: 0.5 mm). Image adapted from Gotti et al. (2020).*

1.2 SkM myogenesis

To form the highly ordered structure of skeletal muscle, a specific process of tissue development and maturation takes place. In embryonic development, myoblasts derived from pluripotent stem cells proliferate within the developing muscle tissue and align along the extracellular matrix. Myoblasts then fuse in two stages, first to each other, then to already multinucleated myotubes. It has been reviewed that mechanisms of fusion involve two proteins: Myomaker and Myomerger with roles in fusion competence and fusogenicity, respectively (Sampath, Sampath and Millay, 2018). While early myofibers are smaller, less nucleated and possess less contractile force generating capabilities, they exist as initial architectural patterning for future muscle cells to be built upon (Murphy *et al*., 2011). Subsequent rounds of myoblast differentiation and fusion enables larger secondary myofibers to be formed following the same pattern as preceding structures continuing until mature adult-like myofibers develop. Much like during development, in muscle growth and repair satellite cell-derived myoblasts differentiate and fuse with existing secondary fibres to expand or maintain the mature muscle tissue. It is these fundamental developmental processes that researchers aim to achieve when

generating *in vitro* models. Therefore, when evaluating developmental SkM models, it is important to consider indicators of functionally mature tissue.

1.3 SkM disease

Myopathies can be characterised as acquired (drug-induced or inflammatory/immune-related) or hereditary (such as Muscular dystrophies) and vary in prognosis. These disorders share common symptoms such as atrophy, hypertrophy, exercise intolerance and weakness (Barohn, Dimachkie and Jackson, 2014). Muscle atrophy is also a symptom of many neuromuscular disorders such as amyotrophic lateral sclerosis (ALS) and even cancer (Powers *et al.*, 2016). The effects of atrophy include decreased immunity, wound healing and increased risk of infection and muscle weakness, and in the worst case, death (Argilés *et al*., 2016a). This highlights the importance of maintaining SkM mass. Physical therapy for most myopathy patients has benefits beyond strength (King and Kissel, 2013) and rehabilitation has been shown to improve muscle repair and recovery following injury or disease (Liu *et al*., 2018) and also contributes to supporting whole-body homeostasis. Although SkM has the ability to regenerate after injury (Yoshimoto *et al*., 2020), there are some constraints such as volumetric muscle loss, which limits the muscle's full regenerative capacity (del Carmen Ortuño-Costela *et al*., 2019; Gholobova *et al*., 2020; Khodabukus *et al*., 2018; Piersma *et al*., 2013; Sicari *et al*., 2015; Wang *et al*., 2019). Treatments seldom restores full function. Furthermore, there has not been much success with free functional muscle transfer (FFMT) and other muscle flap procedures (Mertens *et al*., 2014). Therefore, there is a need for *in vitro* models to replace lost or damaged tissue.

1.4 Towards 3D *in vitro* models

The use of human subjects and tissues have ethical implications and greatly depend on availability. SkM tissue samples are obtained from invasive biopsies, and the cells extracted have limited expansion potential and differentiation ability, which is key for development of physiologically relevant functional myotubes *in vitro*. *In vitro* models limits the use of animal models, particularly with induced pluripotent stem cells (iPSc) (Maffioletti *et al*., 2018). Therefore, *in vitro* biocompatible tissue engineered biomimetic models are needed for the purposes of studying SkM health and disease. Indeed, 3D SkM modelling has significantly advanced since the initial development using avian myotubes embedded in a type collagen I gel (Vandenburgh, Karlisch and Farr, 1988). Despite these advances, ongoing challenges remain due to the diversity of the *in vivo* microenvironment, the plasticity of SkM tissue and specifically the complex tissue structure. Consequently, there is a lack of standardised protocols or guidance for the fabrication and characterisation of mature and physiologically relevant SkM models as

laboratories strive to design and develop models tailored to their specific research objectives.

1.5 Indicators of SkM Maturity

1.5.1 Structural maturity features

1.5.1.1 Myotube structure

When characterising myotubes within SkM models, conventional morphological features including length, width, diameter, total number of cells, number of nuclei per myotube, fusion index scores and number of myotube branches are often used to assess development and progression to maturity (Jones *et al.*, 2018). Measuring width and diameter of myotubes provides information about the growth and hypertrophy of muscle fibres, and higher number of nuclei per myotube indicates successful fusion of myoblasts into multinucleated myotubes, a critical step in muscle maturation. Fusion index is calculated as the ratio of nuclei within myotubes to the total number of nuclei in a given field of view as a measure of the efficiency of myoblast fusion into myotubes and better myogenic differentiation and maturation. The presence and complexity of branching patterns can provide insights into the structural organisation and regenerative capacity of the muscle tissue. These parameters are typically quantified using microscopy and image analysis software following H&E and immunofluorescent images. Therefore, researchers look for signs of well-formed, elongated, and thick myotubes with multiple nuclei, which indicate successful differentiation and maturation (Jiao *et al.*, 2018). High fusion index scores and appropriate branching patterns further confirm that the myotubes are mimicking the native muscle tissue structure and function.

However, mimicking native SkM dimensions is highly dependent on the muscle region. Although native SkM cells are considered 'large' cells in humans, they can still range from 20 µm to 100 µm in diameter with length cans reaching 12 cm (Feher, 2012). Fibre length is further complicated by other differences including gender of muscle origin (Kawakami *et al.*, 2006). In *in vitro* myooids, myotube diameter can range from <10 µm (Huang *et al*., 2005; Khodabukus *et al*., 2019) to 450 µm (Yamasaki *et al*., 2009). Comparatively, 2D model myotubes have presented diameters up to 25 µm (Bakooshli *et al*., 2019) and when measuring whole myooids, these can reach up to 3mm (Chen *et al*., 2019). This suggests that 3D microenvironments promote comparatively increased myotube size in culture.

Other structural features include striations of myotubes visualised by sarcomeric actin, myosin and α-actinin proteins via immunofluorescence. Striations are indicative of the highly ordered arrangement of myofibrils and the alignment of actin and myosin filaments

within the sarcomeres which are necessary for muscle contraction and overall functionality. Immature muscle cells, or myoblasts, lack this organised structure and detectable striations. *In vitro* models present these key sarcomeric proteins (**Table 1.1**). The presence of both the endosarcomeric and exosarcomeric cytoskeleton in *in vitro* models best represents native muscle and light and electron and microscopy images reveal distinct isotropic (light) and anisotropic (dark) bands (Rall, 2018), which give myofibrils their characteristic striations. A schematic representation of sarcomeres and intrinsic bands are seen in **Figure 1.1**. Anisotropy is a notable feature that is important for mimicking native SkM architecture. Indicated by alignment of fibres, it reflects directional dependence of structural and functional properties in SkM that necessitates force transmission and contraction (Jana, Levengood and Zhang, 2016). Details of tissue-engineered approaches to promote alignment is discussed hereafter. Furthermore, some labs adopt other assesment methods in SkM models, such as a 'slack test' (Krieger *et al.*, 2018) to indirectly measure and compare tissue integrity, ECM maturity, and muscle fibre development between engineered samples by assessing their shortening after being released from tension. Two variations are employed: the whole tissue slack test, which measured the shortening of tissue rings after removal from agarose posts, and the cleaved tissue slack test, which evaluated the internal tension in the tissue by measuring changes in length after the tissue was cut and placed in culture media.

Table 1.1 Relevant EPS stimulated 3D SkM models with key characteristics of maturity. *Active models refer to models that demonstrate contractility (spontaneous or induced) and passive models are inactive or non-contractile. MyHC- F, -S, -E; Myosin Heavy Chain -Fast, -Slow, -Embryonic; MyHC-MF20; Myosin Heavy Chain-MF20; (Human) epidermal growth factor, hEGF, EGF; (human) basic fibro-blast growth factor; hbFGF, FGF; (recombinant human) fibro-blast growth factor, rhFGF; Vascular Endothelial Growth Factor, VEGF; NR, Not reported.*

Model construct	Cell type	Substrate	Growth factor	Structural and Developmental markers	Reference
ACTIVE MODELS					
Bioprinted four-layer dumbbell-shaped micro tissue models printed on agarose substrates	Primary human muscle precursor cells	Matrigel, agarose substrates	NR	MyHC α-actinin F-actin Myf5 MyoD Myog Actn2 MyHC1, 2,3, 7&8	(Alave Reyes-Furrer *et al.*, 2021)
Hydrogels formed within dumbbell-shaped channel moulds in 12 well-plates from PDMS and anchored by nylon hooks at each end.	Co culture: Primary human myoblasts, primary human muscle fibroblast-like cells	Fibrin/Geltrex hydrogel (3D), Geltrex (2D) or a fibrinogen/Geltrex mix	bFGF	α -actinin β -tubulin MyHC MyHC, MF20	(Bakooshli *et al.*, 2019)
Bio- well-insert moulds with fixed twin posts	C2C12 myoblasts and Human Derived	Collagen/Matrigel hydrogel	NR	F-actin MyHC Desmin	(Capel *et al.*, 2019)

Model construct	Cell type	Substrate	Growth factor	Structural and Developmental markers	Reference
	Muscle Cells				
Bio-hydrogels and bulk-hydrogel constructs.	Co-culture: C2C12 myoblasts and fibroblasts (BALB/3T3)	ALG blended with semi-synthetic biopolymer	NR	MyHC-MF20 Actin -ACTA1 MYOD1 MYH2 Myog	(Costantini, Testa, Mozetic, *et al*., 2017)
µ-molded gelatin hydrogels: patterned and unpatterned (as per Bettadapur *et al*. (2016) protocol below).	C2C12 myoblasts and primary myoblasts	Gelatin hydrogels	bFGF	α-actinin-2 - ACTN2 Actin MyHC	(Denes *et al*., 2019)
Cells embedded into bio-printed ring-shaped models	Co-culture: C2C12 and Human SkM myoblasts	GelMA-AlgMA-Fibrin bioink	NR	MyHC (MF20) α-actinin (ACTN2) F-actin Myf5, Myod1, Myog, Actn2, Tnnc2, Myh4 and Myh7	(García-Lizarribar *et al.*, 2023)
Human bio-artificial muscle (BAM) made using silicone rubber moulds with end	C2C12 or human myoblasts	Fibrin gel	hEGF (HM and MM)	Desmin MyHC-MF20 Tropomyosin MYH1 MYH8	(Gholobova *et al*., 2018)

Model construct	Cell type	Substrate	Growth factor	Structural and Developmental markers	Reference
attachment sites in 6-well plate.				MYH3 Myog	
Magnetic force-based tissue engineering (Mag-TE)	C2C12/FST myotubes	Collagen solution, Matrigel	NR	α -actinin	(Ikeda *et al.*, 2017a)
Myobundles formed within PDMS moulds containing two semi-cylindrical wells with PDMS posts.	Primary human myoblasts	Matrigel, fibrinogen	hEGF	α-actinin Dystrophin MyHC α-tubulin F-actin	(Khodabukus *et al.*, 2019)
Human myogenic precursors cast within fibrin/Matrigel matrix in PDMS moulds to achieve myobundles.	Primary human myoblast	Matrigel and fibrinogen	EGF, bFGF	F-actin MyHC α-actinin Myog	(Madden *et al.*, 2015)
Spun nanofibers embedded in hydrogels.	C2C12	Gelatin and alginate hydrogel	NR	MyHC F-actin MyoD Myog	(Mao *et al.*, 2019)
Cell-culture inserts fabricated using standard photolithography and PDMS moulding.	Primary human myoblasts	Matrigel	NR	Titin Desmin MyHC 1 MyHC 2 MyHC 3	(Mills *et al.*, 2019)

Model construct	Cell type	Substrate	Growth factor	Structural and Developmental markers	Reference
				MyHC 7 MyHC 8	
Biohybrid robot with flexible substrate and embedded gold electrodes, operated in open air	Single-cell myoblast suspension (hind limbs of 1–2 days old Wistar neonatal rats)	Collagen (Cellmatrix), sacrificial alginate gel	NR	a-actinin	(Morimoto, Onoe and Takeuchi, 2020)
Elastase-treated porcine aorta as artificial tendons fixed on silicone sheet by stainless-steel pins.	C2C12	Collagen type I (Cellmatrix)	NR	MyoD MRF4 Myog	(Nakamura *et al.*, 2017)
Cells encapsulated in micromoulded GelMA hydrogels.	Co-culture: C2C12 and PC12	Micropatterned methacrylated gelatin, GelMA hydrogels	NR	Actin α-actinin - ACTA1 MyHC-IId/x MyHC-IIa MyHC-IIb MyHC-pn MyHC-F/-MY32 Myog Mefc2	(Ostrovidov *et al.*, 2017)

Model construct	Cell type	Substrate	Growth factor	Structural and Developmental markers	Reference
				Myf-5 MLP	
Three-dimensional engineered muscle tissues (iSkM bundles) formed within polydimethylsiloxane (PDMS) moulds containing two semi-cylindrical, cast from 3D-machined Teflon masters.	Human pluripotent stem cells	Fibrin based hydrogel	bFGF	F-actin – phalloidin α-actinin Myf5 MyHC-MF20 Dystrophin MyoD Myog	(Rao *et al.*, 2018)
3D free-standing muscle tissue made using culture stage and stamp.	Human myocyte cell line	Collagen (Cellmatrix) and Matrigel	IGF-1	α-actinin Myosin Myog	(Shima *et al.*, 2018)
Chamber slide with three rectangles of polyethylene meshwork bars as flotation bars, fixed at two ends	Primary rat muscle derived cells	Collagen I	NR	Desmin	(Smith *et al.*, 2012)
Aligned myoblast transfer from micropatterned UpCell®	Tri-culture: Human myoblasts and	Fibrin gel and Matrigel	NR	α-actinin F-actin – phalloidin	(Takahashi, Shimizu and Okano, 2018)

Model construct	Cell type	Substrate	Growth factor	Structural and Developmental markers	Reference
dish to fibrin-based gel containing silicone ring.	human dermal fibroblast			MyHC Myog	
Polyacrylamide-based hydrogel with microchannels made from a PDMS mould on a petri dish.	C2C12, human primary myoblasts, hESCs myoblasts	Matrigel	EGF, bFGF	α-actinin Desmin Dystrophin Vinculin MyHC Myog MyHC3 MyHC2	(Urciuolo *et al.*, 2020)
Cells embedded in collagen scaffold held with two stainless steel pins on polycarbonate plate.	C2C12 myoblasts	Collagen type I (Cellmatrix)	NR	None studied	(Yamasaki *et al.*, 2009)
PASSIVE MODELS					
Cell-laden core-shell hydrogel microfiber (formed by a double co-axial laminar flow)	C2C12 myoblasts	Collagen gel in the core region of alginate fibres	NA	Actin	(Bansai *et al.*, 2019)
Micro-printed and isotropic substrate	C2C12 myoblasts	Fibronectin solution, gelatin	NR	α -actinin MyHC	(Bettadapur *et al.*, 2016)

Model construct	Cell type	Substrate	Growth factor	Structural and Developmental markers	Reference
constructs (micro-moulded gelatin hydrogels, isotropic gelatin hydrogel, fibronectin coated on PDMS and soft PDMS)				Actin-phalloidin	
Scaffold/dual-scaled cell culture system using electro- spinning and PEG hydrogel micropatterning	C2C12 myoblasts	Electrospun nanofiber and PEG hydrogel	NR	MyHC	(Cha, Lee and Koh, 2017)
Multiple cell culture platforms: 3D printed scaffolds, 2D PLGA films, PLGA-based 3D scaffolds, 3D spheroid	C2C12 myoblasts	Stimulated by E-jet 3D printer	NR	MyHC F-Actin-phalloidin Vinculin Myog	(Chen *et al.*, 2019a)
Agarose casting mould made using Teflon spacer in 24-well plates, supported by two silicone posts.	Primary cells	Fibrin gel	rhFGF	α -actinin MyHC α-tubulin α5 integrin Vinculin Actin MYH3	(Chiron *et al.*, 2012)

Model construct	Cell type	Substrate	Growth factor	Structural and Developmental markers	Reference
				ACTN2 Myog	
Myoblasts encapsulated in GelMA hydrogels	C2C12	Gelatin	NR	MyHC-MF2	(Costantini, Testa, Fornetti, *et al.*, 2017)
Cross-linked protein films and collagen and gel scaffolds	Fibroblast: HT1080, Myoblast: C2C12, C2C12-α2+ (L3 cells) and Rugli (rat glioma)	Collagen, gelatin	NR	None studied	(Davidenko *et al.*, 2016)
PLLA nanofibrous scaffold and micropatterned PDMS polymers.	C2C12 myoblasts	Gelatin or fibronectin	NR	F-actin – phalloidin MyHC-F MyoD	(Huang *et al.*, 2006)
Stacked multilayer cell sheet on thermoresponsive nanofabricated substratum	C2C12	Gelatin	NR	F-actin	(Jiao *et al.*, 2018)

Model construct	Cell type	Substrate	Growth factor	Structural and Developmental markers	Reference
TE SkM constructs fabricated in a precision manufactured and commercially available polyether ether ketone (PEEK): TE culture chambers	C2C12	Type I collagen	NR	F-actin-phalloidin Myog	(Jones *et al.*, 2018)
3D printed construct: a sacrificing acellular gelatin hydrogel bioink, and a supporting poly(ε-caprolactone) (PCL) pillar	Human muscle progenitor cell (biopsies of human gracilis muscles)	Collagenase type I	hEGF, hbFGF, dexamethasone	MyHC	(Kim *et al.*, 2018)
Myogenic cells in polymerized fibrin hydrogels between silicone posts	hESCs and hiPSCs (hPSCs)	Fibrin hydrogels	VEGF, bFGF	Desmin MyHC MyoD Actin	(Maffioletti *et al.*, 2018)
3D printed muscle-tendon unit with a thermoplastic polyurethane and poly(epsilon-	C2C12 myoblasts and NIH/3T3 fibroblasts	Hydrogel-based bioink of hyaluronic acid, gelatin, and fibrinogen	NR	MyHC Desmin Vinculin	(Merceron *et al.*, 2015)

Model construct	Cell type	Substrate	Growth factor	Structural and Developmental markers	Reference
caprolactone) on either two different sides					
Sculpting PDMS chamber with surface functionalised anchorage nodes	Mouse embryonic fibroblasts, normal human lung fibroblasts, human MSCs and human skeletal myoblasts	Collagen I, Matrigel	NR	Myogenin MyHC	(Mondrinos *et al.*, 2021)
3D printed gelatin methacryloyl (GelMA)-alginate	C2C12	Gelatin, alginate	NR	Desmin F-actin	(Seyedmahmoud *et al.*, 2019)
Silicone tube secured in 4 or 24 well plate with sylgard to form a chamber.	C2C12/Primary human myoblasts	Collagen I/Matrigel hydrogel	FGF	Actin - Phalloidin Desmin	(Snyman *et al.*, 2013)
Scaffold-free cell sheets via thermoresponsive poly(N-isopropylacrylamide)	Human SkM myoblasts	Gelatin gel	NR	MyHC Actin	(Takahashi *et al.*, 2013)

Model construct	Cell type	Substrate	Growth factor	Structural and Developmental markers	Reference
grafted on a cell culture substrate					
Microporous cryogel scaffolds with incorporated carbon nanotubes	C2C12	Gelatin, carboxymethyl cellulose	NR	MyHC F-actin	(Velasco-Mallorquí *et al.*, 2020)

1.5.1.2 Sarcomeric proteins

The sarcomere is the most basic functional and structural unit of SkM. The presence of a mature contractile apparatus can be considered a basic requirement for the development of valid *in vitro* models and most studies characterise myosin, actin and α-actinin as the fundamental sarcomeric proteins in muscle models (**Table 1.1**). Although there is a correlation between increased sarcomere formation and increased contractile activity present in both 2D and 3D constructs (Ikeda *et al*., 2017b), sarcomeres are also characterised in passive models (**Table 1.1**) which demonstrates they are not always consistent with functional maturity. Thus, sarcomeres are better depicted as a structural feature of maturity that should be combined with other parameters to assess functionality. Sarcomeres are altered during contraction; change in sarcomere length and rate of change from myofibers to myofibrils can be a measured using light microscopy (Moo and Herzog, 2018).

1.5.1.2.1 Actin and Actinin

Actin is a widely characterised sarcomeric protein. There are two types of cellular actin: F-actin, which is the linear polymeric microfilament form and G-actin, the free monomeric globular form which F-actin is formed from via ATP regulated polymerisation (Oosterheert *et al.*, 2022). F-actin forms the thin filaments of the sarcomeres, interacting with myosin filaments to produce muscle contraction through the sliding filament mechanism. Most SkM models characterise F-actin, visualised by conjugated phalloidin antibody, as an indicator of a structurally well-developed model with functional capabilities (**Table 1.1**).

Actinins are also sarcomeric markers of SkM structure. Broadly, α-actinins play a crucial role within cells by cross-linking actin filaments, a process that contributes significantly to the structural integrity and function of the cytoskeleton. Beyond their structural role, α-actinins are integral to the formation and maintenance of focal adhesions with the extracellular matrix transmitting mechanical signals bidirectionally (Seto *et al.*, 2011). Moreover, through their interactions with actin filaments, α-actinins exert control over intracellular tension, influencing the mechanical properties and stability of the cell as well as facilitating the dynamic rearrangement of the cytoskeleton necessary for the regulation of cell migration during development, wound healing, and other physiological processes. Although there are four α-actinin isomers, α-actinin-2 and α-actinin-3 are mainly expressed in muscle cells (Shao *et al*., 2010). The isomers are functionally different in relation to their roles in F-actin crosslinking, protein interactions and subsequent contractile function (Hsu *et al*., 2018). Although less abundant in SkM, actinin-1 is involved in general cytoskeletal organisation also cross-linking actin filaments

in the Z-discs at the boundaries of each sarcomere and anchors them stabilising the sarcomeric structure and ensuring efficient force transmission during muscle contraction (Hamill *et al.*, 2015). Actinin-2 is the main actin cross-linker in the sarcomere of muscle tissue. Actinin-3 plays a specific and essential role in fast glycolytic muscle fibres, which rely on glycogen-fuelled anaerobic metabolism to rapidly produce energy (Murphy and Young, 2015). Therefore, classification of alpha-actinin type can better characterise the type of tissue model developed *in vitro*.

Other sarcomere structures such as titin, nebulin, troponin and tropomyosin can further characterise the extent of functional machinery present in SkM models. Titin, the largest known SkM protein, spans half of the sarcomere and contributes to its elasticity and stability playing a crucial role in muscle contraction by connecting the Z-disc to the M-line and providing a scaffold within the tissue (Trinick and Tskhovrebova, 2010). Nebulin regulates the length of actin filaments within the sarcomere, which is essential for maintaining uniform sarcomere structure and function (Mijailovich *et al.*, 2019). Troponin and tropomyosin regulate actin and myosin interactions during muscle contraction (Lehman *et al.*, 2009). Troponin is a complex of three subunits (troponin C, troponin I, and troponin T) that bind to calcium ions and initiate conformational changes in tropomyosin to induce a conformational change that exposes myosin-binding sites on actin filaments, allowing cross-bridge cycling and muscle contraction.

1.5.1.2.2 Myosin Heavy Chain (MyHC)

Myosin is one of the key proteins in determining the structural and functional phenotype of myofibers. It is composed of two globular head units and tails that intertwine to form an α-helical structure. The combination of a single head unit and its corresponding tail is known as a myosin heavy chain (MyHC). Different isoforms or versions of MyHC correspond to distinct myofibril phenotypes, which emerge at various stages of muscle growth and development (Schiaffino *et al.*, 2015). MyHC-perinatal (MyHC-pn), is typically expressed at the end of gestation, during the first weeks of life, and in regenerating muscles. It plays a crucial role in the initial stages of muscle development, helping to establish the initial functional properties of muscle fibres in newborns. Embryonic MyHCs are critical for myoblast differentiation and regulation of other MyHCs (Sharma *et al.*, 2018) and although they have been identified in adult human muscle (Schiaffino *et al.*, 2015), they are expressed before adult fast myosin (MyHC-IId/x, MyHC-IIa, MyHC-IIb) in mammals (Ostrovidov *et al.*, 2017). Skeletal muscles exhibit different MyHC isoforms that define their characteristics. Slow twitch/type I fibres are made of MyHC-I and the fast twitch/type II fibres contain type II MyHC sub types, namely MyHC-IIa or MyHC-IId (Neunhäuserer *et al.*, 2011).The fast or slow fibre type correlates to a high or low actin-dependent ATPase. The fast or slow fibre type in muscle correlates with high or low actin-

dependent ATPase activity, respectively (Lee *et al*., 2019). Oxidative fibres express MyHC I and are associated with endurance and a slower, more sustained contraction. Glycolytic fibres, which come in two types – medium speed (MyHC IIx) fibres that provide intermediate contraction speed for moderate-intensity activities, and fast speed (MyHC IIb) fibres that enable rapid contractions for high-intensity, short-duration activities (Lee *et al*., 2019). The expression patterns of these MyHC isoforms can determine the functional properties and maturity stages in muscle models, providing critical insights into muscle development and regeneration (Ostrovidov *et al*., 2017). Therefore, characterisation of MyHCs can inform the developmental stage of myoids and may be useful in determining model maturity *in vitro*.

Indeed, human SkM cells used in models have been shown to express genes including MYH7 (Abdelmoez *et al.*, 2020) which code for MyHC-beta (β) that is associated with mature type I (slow twitch) muscle fibre. Some models show a transformation from immature to mature MyHC forms by demonstrating upregulated expression of the fast and slow adult MyHC isoforms and downregulation of embryonic MyHC expression (Bakooshli *et al*., 2019), demonstrating expression of these structural proteins is indeed a dynamic process. Thus, identifying and confirming MyHC class switching from embryonic to neonatal forms within a model could be a valuable tool for determining muscle type and developmental stage of maturation. Complicating this, hybrid fibres (I/IIa, IIa/IIx, IIx/IIb) in SkM also exist in transitional phases in response to mechanical or electrical stimulation and the transition of fibre types being expressed typically moves from type I to IIa to IId to IIb (Medler, 2019). Following endurance exercise, fibre type switches and transitions have been observed with increased protein expression of MYH7B, a slow-twitch myosin, and decreased expression of MYH2, a fast-twitch myosin (Mills *et al*., 2019). Additionally, cell type (discussed later) can influence MyHC content as expression in humans compared to mice can differ; for example, MyHC-IIx encoded by MYH1 is expressed in late human foetal muscle or early postnatal mouse muscle but also in adult muscle (Schiaffino *et al.*, 2015). This complexity and dynamic nature of MyHC within SkM may explain why most reported models lack specification of MyHC type(s) favouring a pan marker, such as MF20 antibody which recognises all MyHCs isoforms, and regarding MyHC as a general late-stage structural marker in myogenesis (Cha *et al*., 2017).

1.5.1.2.3 Intermediate filaments

Intermediate protein filaments in muscle are characterised due to their diameter of approximately ten nanometres which is intermediate between smaller microfilaments (about 7 nm) and larger microtubules (about 25 nm) (Costa *et al.*, 2004). Desmin is the largest intermediate filament in SkM providing structural integrity and alignment of

myofibrils and is often identified in models as a characteristic marker of development of these contractile units (**Table 1.1**). It is considered one of the first appearing structural muscle-specific protein in development, essential for mechanotransduction, stability and organisation of the cytoskeleton. Due to these structural roles, desmin positive models have been reported in contractile and non-contractile models (**Table 1.1**). Earlier research suggested desmin cross-striations are associated with high maturity (van der Ven *et al.*, 1992), however it is now considered that desmin exists in both early and late stages of differentiation in both active (Gholobova *et al.*, 2018; Urciuolo *et al.*, 2020) and in passive models (Snyman *et al.*, 2013; Maffioletti *et al.*, 2018). Higher expression levels of desmin can be observed later in differentiation, compared to intermediate filament proteins, like vimentin, which are present earlier in the process of myogenesis. This distinction therefore indicates that while desmin alone cannot determine terminal maturation, it has useful application in the confirmation of the stage of cellular differentiation. Loss of desmin causes a disruption of muscle fibre organisation and decreases force-generating ability highlighting a role in SkM function (Lovering *et al.*, 2011). The dystrophin-glycoprotein complex and the vinculin-talin-integrin system have structural and signalling roles to support the interaction of muscle fibres to the ECM. However, these are not typically characterised in SkM models (Khodabukus *et al.*, 2019).

1.5.1.3 Myotube orientation

Myotube orientation is essential to generate a mature and functional model as it correlates with contractility as unidirectional fibre orientation leads to physiological contractile forces (Bian *et al.*, 2012; Okano and Matsuda, 1997). Most 3D models reported in **Table 1.1** have produced longitudinal myotubes aligned in parallel and, more specifically where cells are in hydrogels, along a force/tension axis. This orientation supports the force that is created by actin–myosin cross bridges that are transmitted longitudinally along the myotube axis and then laterally within the fibre (as reviewed by Frontera & Ochala, 2015). Most 3D SkM models give rise to uniform myotubes with polar alignment (**Table 1.1**). However, there are some exceptions with some multidirectional myotubes (Mills *et al.*, 2019) or with diffuse sarcomeric α-actinin (Bettadapur *et al.*, 2016). Tissue-engineered models have shown that when myotubes are organised to resemble native tissues with primarily unidirectional orientation, contraction has always resulted (**Table 1.1**). Studies from **Table 1.1** have shown that random myotube orientation following differentiation, resulted in fewer or no myogenic regulatory factor (MRF) expression or proteins such as MyHC (Yamasaki *et al.*, 2009).

1.5.2 Developmental maturity features

1.5.2.1 Myogenic regulatory factors (MRFs)

Myogenic development is controlled by extrinsic and intrinsic regulatory mechanisms whereby SkM cell differentiation and development is coordinated by the expression of MRFs or myogenic factors (Myf) (Hernández-Hernández *et al.*, 2017). SkM can be characterised according to a hierarchy of these transcription factors with expression profiles differing throughout the coordinated process of myogenesis from activation of precursor cells to development of mature myofibers (Bakooshli *et al.*, 2019). Therefore, establishing expression of early and later differentiation stage MRFs can be used as indicators of SkM developmental maturity. The key MRFs are Myf5, myoblast determination protein 1 (MyoD or Myf3), Myogenin (Myog), and MRF4 (also known as Myf6/herculin) and can be utilised as important indicators of myotube maturity and functionality as they are present sequentially at different stages of myogenesis (Braun and Gautel, 2011) (**Figure 1.2**). MyoD and Myf5 appear in the early stages of myogenesis in undifferentiated myoblasts but are not expressed in later stages as they are known to regulate the cell cycle which is absent in mature adult myofibers incapable of undergoing mitosis (Mueller *et al.*, 2021). Both Myf5 and MyoD act genetically upstream of MRF4 and Myog to increase their expression (**Figure 1.2**) (Bentzinger, Wang and Rudnicki, 2012). Myog and MRF4, are exhibited in late myogenic differentiation and are required for the fusion of myoblasts and the formation of myotubes, respectfully (Nakamura *et al.*, 2017). Expression levels of MRF4 are significantly elevated in adult mature muscle and are considered to reflect high muscle fibre maturity (Yoshimoto *et al.*, 2020). MRF4 additionally has an inhibitory effect on early-stage MRFs and commits the cells to terminal differentiation (Asfour, Allouh and Said, 2018). Despite this unique pattern of expression through muscle development, there is evidence of regulatory factor interchangeability where each MRF can convert many types of non-myogenic cells into myogenic cells *in vitro* (Wang and Jaenisch, 1997). Indeed, functional redundancy of MRFs is an important evolutionary advantage of SkM, enabling compensation between factors under certain conditions and ensures that muscle development can proceed even if one pathway is disrupted, safeguarding essential biological processes against genetic mutations or environmental challenges. An example of this is the ability of Myog to substitute for Myf5 *in vivo* as these factors have overlapping molecular pathways and target genes (Zammit, 2017). Similarly, MRF4 can functionally replace myogenin in early myogenesis to activate myogenin expression profiles (Zhu and Miller, 1997). While this interchangeability ensures that essential myogenic signals are maintained even in the absence of one factor, it highlights the complexity of the natural regulatory pathways. Furthermore, the wide range of

environmental cues that up-regulate or down-regulate specific genes within the dynamic SkM tissue further complicates the characterisation of robust MRF markers of maturity. This could account for the lack of MRF characterisation as a high order maturity factor in SkM tissue constructs. One study demonstrated the maximal expression of myogenic genes – MyoD, myogenin, MRF4 at 2 weeks of culture with significant decrease a week after (Nakamura *et al*., 2017). This suggests that culture period is reflective of myogenic development and appropriate culture times can therefore assist in yielding mature tissue. Myog presents one of the most reported MRFs (**Table 1.1**), suggesting most models in the field are composed of differentiating or differentiated myotubes. In summary, detection of MRFs via gene expression, immunofluorescence or western blots may be useful in the determination the developmental staging of a model but must be interpreted.

1.5.2.2 Nuclear localisation

Nuclear localisation and morphology are important for the formation of fully functioning healthy tissues. Mispositioning or abnormalities in the morphology of the nuclei may contribute to, or is a consequence of, muscle dysfunction and disease (Cadot *et al*., 2015; Roman and Gomes, 2018). Significantly elongated nuclei have been reported in laminopathic muscle constructs which have been recapitulated in cell culture, to model disease (Maffioletti *et al.*, 2018). In healthy tissues, the position of nuclei within cell fibres can be indicative of cell maturity. The nucleus migrates during myogenesis and reaches a specific peripheral location in mature fibres. Accordingly, myofibers isolated from mature human muscle strips exhibit peripheral nuclei located near the sarcolemma (Gholobova *et al*., 2018). Nuclear migration during myogenesis occurs in stages (**Figure 1.2**). In fusing myoblasts, the nucleus rapidly moves towards the myotube centre down microtubule networks via dynein motor proteins. Concurrently, previously centred nuclei help pull microtubules attached to the nuclei of newly fusing myoblasts towards the centre of myofibers. This cooperative movement ensures a uniform distribution of nuclei within the myotube. As myofibers mature, the uniformly distributed nuclei then migrate from the centre to the myotube periphery as the final location (Cadot *et al*., 2015; Roman and Gomes, 2018). The function of the characteristic peripheral nuclei localised below the sarcolemma remains largely unknown, however positioning may be linked to acetylcholine receptor clustering in innervated muscle fibres, close to the motor end plates and receptor binding site. While there is clearly a predominance for peripherally located nuclei, a smaller proportion of myotubes may additionally be present displaying central nuclei before they migrate during cell fusion and localised maturation as they develop in muscle growth or repair. Collectively this suggests that nuclear location and morphology form important aspects of muscle development that can be used as indicators of tissue maturity whereby models exhibiting nuclei at the centre are

considered less mature or at a transitioning phase of myogenic development (Cadot *et al*., 2015; Roman and Gomes, 2018).

A significant factor that drives movement of the nuclei to the periphery is contraction (Roman and Gomes, 2018), and with the centrally located nuclei of non-contractile models (**Table 1.1**), highlights the importance of functionality and contractility in both the assessment and development of mature SkM models. As most *in vivo* muscle receives some degree of contraction stimulation, even during development, it may be necessary to apply low level stimulus during model construction to achieve more physiological nuclear localisation indicative of muscle maturity. In this way, tissue engineered constructs still have a way to go in recapitulation nuclei positioning *in vivo*.

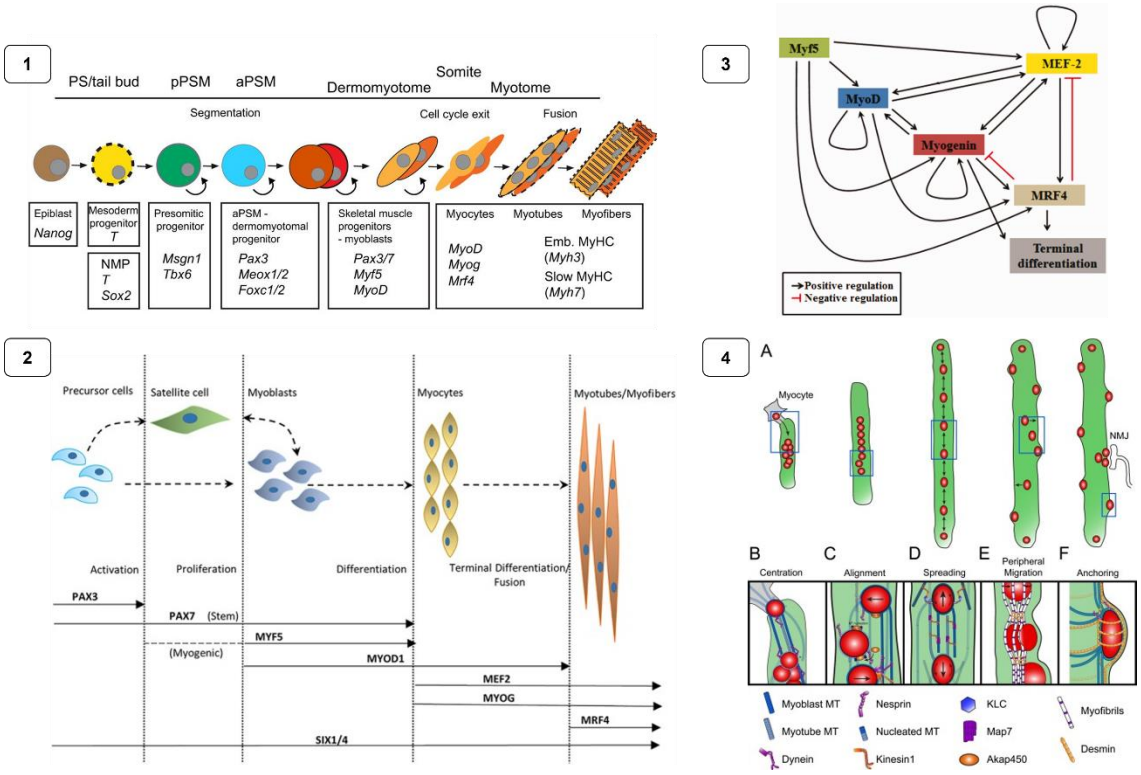

Figure 1.2 Schematic representation of the crucial events during myogenesis, which determine myotube morphology and nuclear localisation within myotubes.

1. ***The development and differentiation of muscle paraxial progenitors to myofibers and the corresponding transcription factors involved at each stage.*** *In in vitro muscle models, cells reported are at the myotome stage, however where fused fibres express MYHC and mature MRFs including MRF4* (Chal and Pourquié, 2017).
2. ***Transcription factors regulation of the myogenic lineage.*** *These MRFs determine myogenic development. PAX3/7 progenitors initiate temporal sequence of activation during myogenesis. Satellite cells express PAX7 whereas the myogenic satellite cells additionally present MYF5 activation. Myoblasts then express MYF5 and MYOD1. Activation of MYOG and MEF2C, coupled with the downregulation of MYF5 and subsequently MYOD1, observes the start of terminal differentiation. MRF4 is activated a few days post differentiation induction, after decreased MYOG expression* (Mukund and Subramaniam, 2020).
3. ***Crosstalk of MRFs and their signalling mechanisms.*** *Myf5 activates all other MRFs (MyoD, Myogenin and MRF4) and MEF-2 proteins. MyoD has an auto-regulatory mechanism and cross-activation mechanism with Myogenin. Myogenin has an auto-regulatory mechanism and can induce terminal differentiation directly or/and indirectly via activation of MRF4. MRF4 directly induces terminal differentiation and can be activated by all other MRFs and MEF-2. MRF4 can inhibit both Myogenin and MEF-2 expressions. MEF-2 has an autoregulatory mechanism and can reciprocally activate both MyoD and Myogenin (Asfour, Allouh and Said, 2018).*
4. ***Migration of the cellular nuclei during myogenesis****. A is an overview of nuclei migration within the myocyte. B-F are zoomed in pictures regions of A which depict the migration stages. Various microtubular proteins, signalling proteins and linkers are involved in the process as illustrated in the above key. (B) Centration: The nuclei first toward the centre of the myotube by dynein and microtubules. (C) Alignment. Centrosomal and motor proteins are recruited to the nuclear envelope via Nesprin-1 and PCM-1. (D) Spreading: Kinesin-1 and Map7 bound to microtubules cause the spread of nuclei along the myotube length. Nuclear rotation is induced by kinesin-1 and kinesin light chain (KLC) at the nuclear envelop by their movement towards the positive end of the microtubules. (E) Peripheral migration: Myofibrils crosslink, regulated by desmin and nuclear movement to the periphery are promoted by contraction and nuclear stiffness. (F) Anchoring. Finally, nesprin arranges microtubular network which allows nuclei to anchor (again, directed by desmin) just below the plasma membrane* (Roman and Gomes, 2018).

1.6 Functional maturity features

1.6.1 Contractility

The primary function of SkM is contraction, consequently the goal of all engineered SkM models is the generation of a contractile force-generating fibres or tissue-mimetics. The degree of functional capability is intrinsically linked to the maturity of muscle models and contractile capability of myotubes can be a promising indicator for physiological relevance of a model as it requires high myotube differentiation, presence of appropriate ECM properties and mature sarcomere formation. It could therefore be argued that contractile force is the ultimate assessment of a muscle model's maturity and functionality. Muscle contraction is also necessary for the proper formation and development of Z-discs in muscle fibres, *in vivo* (Geach, Hirst and Zimmerman, 2015).

Contractility can be measured via changes in sarcomere length, formations of actin and myosin cross-bridges and the subsequent concentric (active shortening) and eccentric (active lengthening) velocities as they contribute to force generation (Franchi *et al*., 2017). Calcium transient amplitude can alter contraction kinetics and therefore serve as a measure of contraction too (Khodabukus *et al*., 2019). Displacement (Shima *et al*., 2018) or deformation of entire models as a result of contraction can also be considered as a measure, while changes in morphology to produce a ‘bowing effect’ also provides evidence of contraction (Smith *et al*., 2012), this is characteristic of chamber type models with anchors at each end (Okano and Matsuda, 1997; Chiron *et al*., 2012; Jones *et al*., 2018) and unique biohybrid robots (Morimoto, Onoe and Takeuchi, 2020), using collagen substrates. As SkM cells contract, they pull on the collagen fibres in the matrix causing the collagen matrix to shrink or deform and change its surface area. This phenomenon can therefore be measured via the change in substrate surface area during culture (Shima *et al*., 2018). Direct measurement of contraction itself, involving the immediate biochemical and biophysical events within the muscle fibres as they contract, is technically more challenging and often not feasible with current *in vitro* techniques.

1.6.2 Force production

Force production following contraction is an additional measure of SkM functional maturity (Capel *et al.*, 2019). The ability of muscle tissues to generate force is usually assessed through physiological measures like peak twitch force (Pt) and excitability (Ito *et al.*, 2014). Forces generated in the muscle fibres are transmitted from the contractile sarcomere to the ECM by integrins and dystrophin-glycoprotein complex (Gumerson and Michele, 2011; Peter *et al*., 2011). Force production of muscle fibres depends on several factors including arrangement of fibres, their length, activation, contraction velocity and the muscles contraction history (Tomalka *et al.*, 2017). There are many factors that

influence the maximal force and force output of muscle including fibre type and the force-velocity relationship of the contractions (Alcazar *et al.*, 2019). MyHC I fibres are found predominantly in muscles related to postural and endurance whereas MyHC IIA and IIX fibres are related to muscles responsible for rapid, high-power, shorter bouts of movements. Fibre maturity, and the presence of MyHC, particularly types IIA and IIA/X give rise to greater forces and isometric forces compared to MyHC I types (Miller, Bedrin, Ades, Palmer, & Toth, 2015). Therefore, presence of type II fibres in *in vitro* models can determine greater capability of physiological force production. Yet the force-velocity relationship that exists in muscle fibres dictates that the slower the muscle shortens, the superior its force generation is during contraction (and vice versa) (Alcazar *et al.*, 2019). Typically, contractile force in 2D and 3D models are measured via cantilever deflection, post deflection and force transducers (Vesga-Castro *et al.*, 2022). Furthermore, microelectromechanical systems (MEMS), have been used in a variety of ways to interact with SkM models, but more so for dynamic mechanical analysis (Fujita *et al.*, 2011; Shimizu *et al.*, 2013, 2010). Electrical stimulation has also successfully increased specific forces of a human myobundles model and has resulted in production of the highest specific force described for human engineered muscle (19.3 mN/mm^2) (Khodabukus *et al.*, 2019). Though, this was still significantly lower than that of native human SkM (ranging 150 – 250mN/mm^2). Reproducing native adult function requires specific forces above 200 mN/mm^2 and myofiber diameters of 50–100 μm (Khodabukus *et al.*, 2018). Contractile force of myobundles can be measured by dividing force contraction with cross-sectional areas (typically at the centre of the bundle), which equates to a contractile force measure of a muscle bundle (Sebille *et al.*, 2017). Force is influenced by many factors such as cell density because increased cell density increases the chance of packed and aligned syncytia which creates unified movement of fibre sheets with greater force. Most studies in **Table 1.1** which report high cell density correspondingly show increased force generation (Ikeda *et al.*, 2017b; Mills *et al.*, 2019). These methods capture the contractile properties of muscle constructs, providing critical data on their functional maturity. Hereafter, we examine how current SkM models achieve maturity through some of these aforementioned structural, developmental and functional features of maturity (**Figure 1.3**).

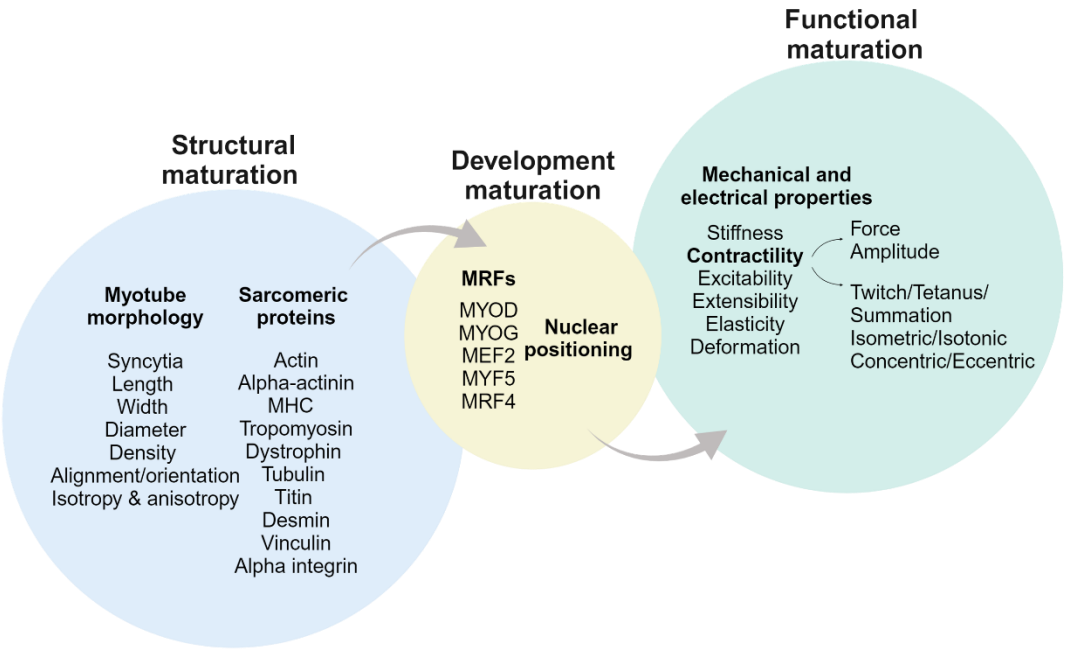

Figure 1.3 Characterisation of in vitro SkM models. *Models should be assessed for key structural, developmental, and functional maturity features to meet physiological relevance and establish a mature model.*

1.7 3D Engineered SkM Models

An array of more complex, 3D SkM models are now reported in the literature which serve various research purposes, including study of contractile dynamics, drug testing, drug disposition and toxicity, neuromuscular junction physiology, cell binding and surface chemistry, injury, disease and myogenesis (**Table 1.1**). In addition to the diverse study aims and research laboratories across the globe, there is a lack of standardised protocols to guide the fabrication and characterisation of mature and physiologically relevant SkM models. This is further complicated by short culture times and custom tissue-engineered approaches *in vitro*. In SkM tissue engineering, key modifiable components include cells, biomaterials and stimulation which provide biochemical and biophysical stimuli for SkM tissue development, growth, and maturity. The challenge in standardising these models arises from the variability and customisation inherent in each of these components. Different cell types or sources can lead to variations in tissue properties and behaviour, the choice of biomaterials affects the structural and mechanical environment of the developing tissue, and the methods of stimulation can significantly influence muscle contraction, alignment, and maturation. Therefore, reproducibility between laboratories, development of standardised protocols and validating new models is challenging with this high degree of customization and variability.

1.7.1 Cellular composition

Cells are a distinguishable feature of SkM models and selecting an appropriate cell type is critical for the specific aims of a study. This necessity arises partly due to species-specific differences in mRNA composition among cells, with genes being differentially expressed and enhanced in various states across different cell types. For instance, rat myotubes (L6) have been shown to exhibit the lowest expression of genes related to function and contraction compared to C2C12 and human SkM cells, rendering them unsuitable for generating functional SkM (Sato *et al*., 2019). Furthermore, cell density significantly impacts functional maturity, as higher cell density promotes the formation of densely packed and aligned syncytia, resulting in coordinated fibre sheet movements with substantial force. Consistently, studies have reported that increased cell density correlates with enhanced force generation (Ikeda *et al*., 2017b; Mills *et al*., 2019). Increased cell density can also lead to nutrient and oxygen deprivation, waste accumulation, and physical interference between cells. Additionally, excessive density may disrupt the balance between cell proliferation and differentiation, and introduce mechanical stress, all of which can negatively impact muscle development. This can differ between cell types and therefore, optimising cell density specific to the selected cells is crucial to achieving functional SkM constructs. Comparison of advantages and disadvantages of different cell strains for use in SkM models have been previously discussed.

1.7.1.1 C2C12

Murine C2C12 cells are immortalised myoblast cell line established from adult mouse satellite cells by (Yaffe, 1968). They are commercially available and display rapid proliferation, large expansion capabilities in culture and have inexpensive differentiation conditions making them a widely used cell choice in 3D SkM models (**Table 1.1**). Compared to primary cell cultures, cell lines provide more consistent and standardised preparations, making them invaluable tools for drug screening and toxicological studies. C2C12s are capable of cell fusion, with nuclei aggregation in the centre resulting in the formation of immature myotubes and even myofibers. While the frequency of use of C2C12 cells in SkM constructs encourages replicative and cohesive model development across different labs, C2C12s have some limitations. Deep muscle proteomic and bioinformatic investigation has shown that C2C12 myotubes do not have many of the specialised *in vivo* muscle characteristics (Deshmukh *et al*., 2015b). As a result, C2C12 cells show less maturation compared to primary muscle progenitor cells, indicating potential limitations in achieving full functional maturity and complexity in SkM tissue engineering (Langelaan *et al.*, 2011). Additionally, the C2C12 cell line has a limited lifespan and can only be passaged 10–50 times before senescence, with differentiation

requiring earlier passages (Adams, 2018). Finally, species difference preside in translation whereby C2C12 cell models may not fully recapitulate human SkM physiology.

1.7.1.2 L6

The L6 cell line, originating from rat SkM myoblasts was first isolated by Yaffe (Yaffe, 1968) abundantly expresses acetylcholine receptors and contains numerous contractile units that can organise into myofibrils, facilitating their differentiation into contracting myotubes. As with C2C12s, they are a well-established cell line that are easy to handle, relatively inexpensive and proliferate well in culture to facilitate large-scale experiments (Li *et al*., 2023). They also exhibit genetic stability over extended passages, providing consistent experimental outcomes. L6 cells have been shown to demonstrate a force-Ca^{2+} concentration curve that closely mimics that observed *in vivo* SkM making them a valuable tool for studying muscle physiology and cellular responses to various stimuli (Ojuka *et al*., 2003; Balu *et al*., 2016). Resultingly, L6 cells are widely used in muscle research. Conversely, it has been shown that the myotubes that L6 cells form do not contain alpha-actin and myosin I and have lower expression levels of nicotinic acetylcholine receptors (Niu *et al.*, 2010). In fact, L6 have been demonstrated lower expression levels of several genes associated with muscle function and contraction compared to C2C12 and human SkM cells and have previously been considered inadequate for producing functional SkM (Sato *et al*., 2019). Furthermore, lower myofibrillar protein synthesis rates are seen in L6 cells compared to other cell lines, indicating potential differences in metabolic function and anabolic signalling that might not be representative of physiological SkM tissue (Uranga *et al., 2022*).

1.7.1.3 Myok9

Due to dogs being more like humans at the pathophysiological and immunological level than rodents, a canine muscle cell line, Myok9, has been recently developed from primary myoblasts isolated from healthy tissue and immortalised via SV40 viral transfection, enabling continuous proliferation (López *et al.*, 2020). Characterisation indicated stability and the muscle-specific nature of Myok9 cells at different growth stages and during differentiation, along with the presence of muscle-related genes, including dystrophin, MRF4, myogenin, MyoD, desmin and PAX7 suggesting a comprehensive expression of key proteins associated with muscle biology and function in the Myok9 cells. Relatively few studies have used Myok9 cells in SkM model development and accordingly further investigations are needed to fully understand cell behaviour, functionality, and response to various stimuli or treatments. Similarly to L6 cells, research indicates that Myok9 myotubes exhibit lower myofibrillar protein synthesis rates compared to other SkM cells, lower still than L6 myotubes, suggesting lower overall

protein synthesis rates (Uranga *et al.,* 2022), with the use of all animal cells in research, translation to humans may also be limited.

1.7.1.4 Primary SkM Cells

Primary human cells offer significant advantages over murine C2C12 and L6 cells in tissue engineering of SkM models due to their physiological relevance and ability to closely mimic the biological and functional properties of human skeletal muscle. These cells maintain authentic gene expression profiles, facilitating the study of human-specific muscle functions and disease mechanisms. Additionally, they have a higher potential to achieve full functional maturity, closely replicating *in vivo* conditions. Myocytes of human primary cells have displayed greater maturation and spontaneous contraction compared to C2C12 cells, demonstrating functionality without stimulation (Urciuolo *et al*., 2020). Human muscle cells are considered optimal cells for secretome study due to similarities to native muscle secretome (Hartwig *et al*., 2014). Primary cell models have been used to create myobundles with hallmarks of disease such as Pompe disease (Wang *et al*., 2021). The use of primary human cells also enables the creation of personalised models for studying specific muscle diseases and testing therapeutic interventions, as they can be derived from patients. However, there are several challenges associated with their use. Obtaining primary human cells can be difficult due to limited tissue availability and ethical considerations of the invasive biopsies needed to collect them. Donor variability can also lead to inconsistencies, affecting reproducibility and experimental results. Therefore, most primary cell SkM models use isolated mouse cells (**Table 1.1**). Additionally, myotubes have been successfully generated from non-human primate myogenic progenitor cells under appropriate *in vitro* differentiation conditions (Baik *et al.*, 2023). Primary cells often require more stringent and complex culture conditions to maintain viability and promote differentiation, and culturing and maintaining them can be more expensive compared to immortalised cell lines. Additionally, inducing primary myoblast differentiation into myotubes can be time-consuming, taking approximately 8–10 days (Vaughan and Lamia, 2020). Moreover, cell yield may vary during the culture process, and as time progresses, cells may become senescent, thus limiting the passage capacity and *ex vivo* cell expansion potential, which can constrain long-term experiments and large-scale studies.

1.7.1.5 iPSCs

iPSCs created by artificially inducing specific genes in non-pluripotent cells, exhibit many of the same characteristics as native pluripotent stem cells, including the ability to differentiate into various cell types. Therefore, iPSCs offer significant advantages for the development of SkM models as they can proliferate indefinitely, providing a limitless source of material for research, and can differentiate into SkM cells allowing for the

generation of muscle tissue from a single cell source. iPSCs have shown a notable advantage in their speed of differentiation into myotubes, achieving this in roughly half the time required by C2C12, L6, and primary myoblasts, forming myotubes in just three days (Uchimura *et al*., 2017; Sasaki-Honda *et al*., 2018; Kokubu *et al*., 2019; Honda *et al*., 2022). However, only a few human pluripotent stem cells (hiPSCs) mimetics exist (Maffioletti *et al.*, 2018), with fully functional 3D SkM tissue (myobundles) produced from human pluripotent stem cells being functionally immature (Rao *et al*., 2018).

iPSCs can be derived from individual patients, facilitating the creation of personalized models that reflect patient-specific genetic and phenotypic characteristics. This is particularly valuable for studying disease mechanisms and testing tailored therapies. Indeed, iPSc can be differentiated towards specific fibre types that are selectively affected by diseases such as Duchenne muscular dystrophy (Webster *et al.*, 1988) or to investigate human fibre involvement in pompe disease (van den Berg *et al.*, 2011). Additionally, iPSCs can be genetically manipulated, to enhance the study of gene function in muscle development and disease. In a recent 2023 study, researchers used a newly generated blood cell-derived iPSC line, ORIONi003-A, to model Duchenne muscular dystrophy *in vitro* (Hajduchova *et al.*, 2023). This cell line was created by reprogramming peripheral blood mononuclear cells from a paediatric patient using the Sendai virus encoding Yamanaka factors. The use of iPSCs also reduces variability in experiments, as they can be cultured under defined conditions, and circumvents ethical concerns associated with embryonic stem cells. These advantages make iPSCs a powerful tool for advancing our understanding of SkM biology and developing new therapeutic approaches.

1.7.1.6 Co-Cultures

The native SkM tissue microenvironment consists of multiple cell types that additionally interact with myocytes to facilitate differentiation, maturation, structural organisation, and functionality. Heterocellular models aim to mimic this environment and the direct and indirect crosstalk between native muscle which include not only myocytes but also endothelial, connective tissue and nerve cells.

While co-culture enhance SkM cells, fibroblasts specifically promote myoblast differentiation and maturation through ECM components and growth factor secretion (Cooper *et al.*, 2004). Fibroblasts also support vascular lumen formation, making them a practical cell choice for engineering vascularised SkM models (Khodabukus *et al.*, 2018). Also, C2C12 cells on a feeder layer of fibroblast have generated mature fibres with peripheral nuclei (Cooper *et al.*, 2004). Incorporation of other cell types creates a multi-cell model with motor neurons and vascular cells which support native physiology. Furthermore, co-cultures also increase cell size and myotube area coverage compared

to monocultures (Ostrovidov *et al*., 2017). There is difficulty in mimicking the muscle vasculature due to heterogeneity of fibres (Olfert *et al*., 2016). However, to date, studies consistently integrate endothelial cells (EC) with myoblasts to represent *in vivo* tissue and most of the studies incorporating vascularisation into *in vitro* muscle constructs are passive models (Perry, Flugelman and Levenberg, 2017; Bersini *et al*., 2018; Maffioletti *et al*., 2018; Osaki, Sivathanu and Kamm, 2018).

Models can achieve a further level of complexity with neuromuscular junction (NMJ) formation. The NMJ is a specialised synapse (neuronal junction) between the terminal end of a motor neuron and a muscle fibre that allows the transmission of electric impulses from an innervating motor neuron to an innervated muscle fibre. This is important because it drives SkM contraction (Mukund and Subramaniam, 2020). Native SkM tissue encompasses capillaries and are innervated by motor neurons. In this way, they stimulate fibres to contract (Maleiner *et al*., 2018).

As SkM matures and differentiates in 3D, there are increased acetylcholine receptor (AChR) clustering as a NMJ feature. *In vitro* models, aim to recapitulate this process of electrical stimulation via co-culture of SkM cells with neuronal cells. Models have incorporated motor neuron clusters into cell suspensions and mixtures (Bakooshli *et al.*, 2019). Three dimensional models that incorporate neuronal cells, which result in the presence of neuromuscular junction markers are scarce (Ostrovidov *et al*., 2017; Bakooshli *et al*., 2019). These types of co-culture have increased differentiation and induction of NMJ formation survival (Kim *et al*., 2020). Further evidence of NMJ formation with the addition of neuronal cells in models have shown improved myotube morphology, increased striations, contractility and contractile force (Martin *et al*., 2015). However, these few studies do demonstrate contractility, showing promising functionality. To visualise AChRs, cells can be stained with α-bungarotoxin which allows them to quantify AChR clusters (Madden *et al*., 2015; Bakooshli *et al*., 2019).

1.7.2 Growth Factors and Supplements

The unique physiological and chemical environment of muscle tissue orchestrates the myogenesis and functionality within *in vivo* SkM. While many of the chemical pathways that promote muscle development, maturity and regeneration have been studied, the complex mechanisms and interactions of these factors at different stages of development are not fully understood. Despite this, exploiting chemical stimuli to enhance *in vitro* SkM development is advantageous for successful functional model generation. SkM model development can, therefore, be augmented and/or functionalised by the addition of bioactive molecules such as growth factors and supplements which are aimed at

promoting myoblast proliferation or differentiation as well as inducing myotube hypertrophy and production of important SkM ECM components.

1.7.2.1 Insulin-like growth factor (IGFs)

IGF-1/Akt/mammalian target of rapamycin (mTOR) pathway (IGF-1/Akt/mTOR) has been known to be the most important pathway to muscle protein synthesis (Zhang, Chen and Fan, 2007). IGF-1 is a commonly used growth factor and has a role throughout myogenesis promoting mature myotube formation and functional muscle tissue development (Shima *et al*., 2018). Through activation of p38 mitogen-activated protein kinase (MAPK) and phosphotidylinositol 3-kinase (PI3K) signalling pathways, IGF-1 promotes myoblast differentiation and the hypertrophy of differentiated myotubes during later stages of embryogenesis, where larger more functional secondary myofibers are formed (Syverud, VanDusen and Larkin, 2016). Mesenchymal stem cells (MSCs) are multipotent stromal cells capable of differentiating into various lineages, including myogenic cells, and the transition from myoblasts to myocytes is driven by key regulators such as MyoD, myogenin, and external cues like growth factors and extracellular matrix interactions. Indeed, IGFs have been shown to upregulate the expression of MRFs, MyHC, MyoD, myogenin, and tropomyosin associated with mature muscle in mesenchymal stem cells (Aboalola and Han, 2017; Husmann *et al*., 1996; Mueller *et al*., 2021). Through the same p38 MAPK and Phosphoinositide 3-kinases (PI3K) signalling pathways, IGF-1 influences SkM regeneration following damage of muscle fibres by promoting satellite cell and satellite cell-derived myoblast proliferation and differentiation as well as increasing satellite cell proliferation and force production in atrophied gastrocnemius muscles of aged rats (Chakravarthy *et al*., 2000). IGF-2 is known to have similar effects by promoting satellite and myoblast cell proliferation and differentiation (Husmann *et al*., 1996). Insulin-like growth factor-1 isoforms, particularly IGF-1Ea, promote myogenic differentiation, hypertrophy, and muscle fibre growth *in vitro* and *in vivo*, enhancing muscle strength and regeneration processes (Ascenzi *et al*., 2019; Yoshida and Delafontaine, 2020).

1.7.2.2 Transforming growth factor (TGF)

TGF-β plays a key role in reorganizing the basement membrane and extracellular matrix during regeneration by promoting the production and deposition of extracellular matrix components, inhibiting proteases that degrade the matrix, and stimulating the activity of protease inhibitors (Husmann *et al*., 1996). Collagen production by muscle cells has been induced by TGF-β (Csapo, Gumpenberger and Wessner, 2020). Furthermore, when TGF-β1 is added to the cell culture medium of scaffold-less engineered 3D SkM tissue, an increase in construct contractility demonstrated via EPS (Weist *et al*., 2013). This was accompanied by denser regions of better organized myofibers indicated by

sarcomeric myosin heavy chain and collagen type I staining (Weist *et al.*, 2013). TGF-β has been shown to inhibit satellite cell differentiation *in vitro*, potentially as a mechanism to hold the cells in a proliferative state which may be important for muscle regeneration (Husmann *et al.*, 1996). Furthermore, TGF-β treatment can lead to muscle fibre atrophy without the need for physical injury. It also diminishes the force-producing ability of untreated, intact muscle (Mendias *et al.*, 2012).

1.7.2.3 Fibroblast growth factor (FGF)

FGFs are the most used growth factors in tissue engineering of SkM, having beneficial effects on proliferation of myocytes and the delaying of terminal differentiation of myofibers (Syverud, VanDusen and Larkin, 2016). Specifically, FGF-19 has been demonstrated to increase extra-cellular-signal-regulated protein kinase 1/2 (ERK 1/2) phosphorylation involved in satellite cell proliferation and differentiation into myotubes (Marshall, 1995) as well as inducing muscle hypertrophy and enhanced functionality in adult murine muscle (Kim, Kim and Asada, 2019). FGF-21, however, was shown to have no effect on SkM cell proliferation or differentiation indicating the unique impact of growth factor isoform on muscle development (Kim *et al*., 2019). FGF-1 and FGF-2 have been shown to stimulate myoblast proliferation yet repress differentiation to myotubes in mouse SkM cell lines to provide enough muscle precursor cells to allow muscle regeneration to occur (Yu *et al*., 2004). Normally, FGF-2 promotes angiogenesis (Jia *et al.*, 2021) and therefore may be a growth factor of choice in representing vascularised models (Carnes and Pins, 2020).

1.7.2.4 Other growth factors

Platelet-derived growth factor (PDGF) and Hepatocyte growth factor (HGF) promote proliferation of myocytes where HGF and FGF delay terminal differentiation of myofibers (Syverud, VanDusen and Larkin, 2016). Furthermore, EGF on myobundles produced better contractile function compared to cells cultured in FGF (Madden *et al*., 2015). As the process of muscle regeneration has many similarities to muscle development and growth factors are indicated in both regenerative and developmental processes, the inclusion of specific growth factor stimulation in engineered tissue model generation is recommended. Several commercially available matrices, including Matrigel® and PuraMatrix® (Corning), incorporate growth factors including IGF-1, TGF-b, EGF, PDGF, bFGF, NGF and VEGF to promote tissue maturation. Matrigel incorporating myooids therefore have multifunctional advantages. A benefit of fibrin as another matrix is that it interacts well with integrins and has specific binding to growth factors (Chiron *et al*., 2012).

1.7.2.5 Ascorbic Acid

Vitamin C or L-ascorbic acid is an essential co-factor for collagen synthesis (Pinnell, 1985). Furthermore, as an antioxidant that reduces inflammation and promotes pro-inflammatory markers (Fischer *et al.*, 2004; Işin *et al.*, 2023). It restores muscle atrophy and physical inability in mice which lack vitamin c synthesis (Takisawa *et al.*, 2022). Several studies have reported the addition of ascorbic acid to their SkM models, more commonly in differentiation media (Asano *et al*., 2015; Ikeda *et al*., 2017b; Merceron *et al*., 2015; Rao *et al*., 2018; Shima *et al*., 2018; Weist *et al*., 2013) and rarely used in growth media (Hurd *et al.*, 2015).

1.7.2.6 Insulin

Additionally, insulin acutely influences the expression of genes involved in muscle differentiation and growth, promoting myogenic growth factors while reducing muscle hypertrophy suppressors, ultimately stimulating muscle development and maturity. Insulin acutely upregulates myogenic growth factors like MyoD and myogenin, supporting muscle differentiation and growth, while suppressing MRF4, indicating a role in modulating anabolic actions in SkM (Dhindsa *et al.*, 2019). Insulin supports SkM growth by activating the PI3K-mTOR pathway, enhancing protein synthesis, and influencing myoblast activity, crucial for muscle hypertrophy and development *in vitro* and *in vivo* (Sylow *et al.*, 2021).

1.7.2.7 Glucose

Glucose supplementation is crucial for promoting SkM recovery and replenishing glycogen stores following exercise (Sonou *et al.*, 2007). Research has shown that glucose, especially when combined with protein, significantly boosts glycogen levels in rats (Morifuji *et al.*, 2010) and impacts muscle cell differentiation (Su *et al.*, 2021). In tissue-engineered human SkM myobundles, insulin significantly enhances glucose uptake, with a 50% increase in 2-deoxyglucose uptake observed (Kondash *et al.*, 2020).

1.7.2.8 AICAR

SkM cells can also be treated with the AMP kinase (AMPK) agonist 5-aminoimidazole-4-carboxamide-1-β-D-ribofuranoside (AICAR) (Moon *et al*., 2019, 2016; Wang *et al*., 2022), which affects SkM muscle contraction and metabolism via AMPK activation (Bergeron *et al*., 1999; Smith *et al*., 2005; Wang *et al*., 2022) and mTOR signalling (Thomson, Fick and Gordon, 2008). AICAR act as an exercise mimetic (Guerrieri, Moon and van Praag, 2017) and often AICAR treatment is established alongside insulin in *in vitro* models (Deng *et al*., 2015; Gonzalez-Franquesa *et al*., 2021a). Thus, AICAR is crucial to developing SkM models that are capable of secreting exercise induced myokines.

1.7.3 Biomaterials

1.7.3.1 Scaffolds

3D models have been developed that can be scaffold dependant or scaffold-free and provide the surface that the cells are seeded on. The former consists of integrating myoblasts into a 3D matrix which supports a mechanical environment. The tissues then form into myotubes and myobundles. **Table 1.1** lists models which are constructed with and without scaffolds.

Examples of scaffold material include polystyrene (plastic cell culture plates), Polydimethylsiloxane (PDMS) which boasts a high transparency, biocompatibility and gas permeability; however, it can absorb hydrophobic materials, thus potentially having an effect on the cellular interaction (Reid *et al*., 2020). Interestingly, cells seeded on a scaffold may not entirely produce a 3D model structure, as cells can be seeded on 2D surfaces within 3D scaffolds. Therefore, it is important to establish a true 3D environment that allows for cells to self-organise into 3D structures as *in vivo*. Advancement in tissue engineering has produced moulds and channels (as scaffolds) to allow cells and matrices to assume 3D structures (Takahashi *et al*., 2013; Jensen *et al*., 2020).

Cell morphology including cell orientation and alignment and contractile function are all affected by a model' architecture and dimension. Furthermore, biological activity such as a cell adhesion is also affected by model dimension (Davidenko *et al*., 2016). Therefore, choosing the appropriate scaffold is crucial in SkM tissue-engineering.

Both synthetic and biological scaffolds have been produced to create myooids. Synthetic scaffolds are made from PDMS, a popular silicon-based organic polymer biomaterial bio-printed or electrospun to create nanofibers to produce parallel aligned fibres or a meshwork (Cha *et al*., 2017; H. Chen *et al*., 2019b; Mao *et al*., 2019). PDMS can be used to create open and enclosed moulds that form channels (Bakooshli *et al*., 2019; Madden *et al*., 2015; Mills *et al*., 2019; Urciuolo *et al*., 2020; Wang *et al*., 2019). The moulds can be stamped or micropatterned to create a surface topography (Bettadapur *et al*., 2016; Ngan F Huang *et al*., 2006; Shima *et al*., 2018). Biological scaffolds can be made from ECM components including collagen as a biopolymer scaffold (Yamasaki *et al*., 2009; Davidenko *et al*., 2016; Nakamura *et al*., 2017). Scaffolds and hydrogels in 3D construct also support culture time (Bettadapur *et al*., 2016; Denes *et al*., 2019) and to our knowledge, the longest myogenic culture time is reported in a 3D bio-printed fibrous hydrogel structure, lasting up to 21 days(Costantini *et al*., 2017). The surfaces of PDMS stamps can also be treated with 2-methacryloyloxyethyl phosphorylcholine, to prevent cell adhesion and enable easy detachment of hydrogel sheets from the PDSM stamp (Morimoto, Onoe and Takeuchi, 2020).

Comparative assessment of muscle models reveals thick elongated ellipsoid nuclei of both myoblasts and myocytes positioned along a longitudinal axis of a 3D fibrin gel, in contrast to the round myoblast with flat disc-like nuclei and multiple cell orientations in 2D (Chiron *et al.*, 2012). The elongated nuclei observed in 3D were considered reminiscent of physiologically observed in native SkM tissue (Aminoff, 2005). In contractile tissue engineered constructs, the nuclei can be at the centre of the cells, suggestive of an early-stage model with developing myotubes (Gholobova *et al*., 2018). Passive models also present the same centronucleated fibres (Davidenko *et al*., 2016; Maffioletti *et al*., 2018) and to date, there is a lack of contractile models which report peripherally nucleated fibres.

1.7.3.2 Hydrogels

Gelatin hydrogels have been found to be closer to that of muscle tissue compared to plastics and other substrates like PDMS (Bettadapur *et al*., 2016). Mechanical tests can characterise gels according to their compressive stiffness (Costantini *et al*., 2017). To mimic native muscle, substrate stiffness of engineered constructs such as hydrogels (made from gelatin, collagen and/or fibrin (as seen in **Table 1.1**) need to achieve young's modulus of about 12-18 kPa, to mimic resting human SkM (Yin, Price and Rudnicki, 2013; Khodabukus *et al*., 2018). The constructs listed in **Table 1.1** demonstrate a range between ~12 kPa to 15 kPa during differentiation, within physiological range. Myotubes cultured on micropatterned surfaces like soft gels < 5 kPa and stiff gels > 15 kPa, have demonstrated diffuse actin and MyHC staining unlike human muscle. Substrate stiffness therefore influences functional sarcomeric components. In support of this, stiffness of 8–11 kPa has been shown to produce distinct striations, representing sarcomeres in myotubes (Engler *et al.*, 2004). However, outside this physiological range, soft hydrogel models with ≤ 6kPa stiffness demonstrate self-organised, highly aligned, and contractile myotubes (Jensen *et al.*, 2020). This reinforces SkM constructs are highly multifactorial. Fibrin aggregation in SkM ring models have increased the stiffness and the compressive modulus of the hydrogels (with 0.02 % Lithium phenyl-2,4,6-trimethyl-benzoyl phosphinate) increased to 11.4 kPa, close to the SkM tissue stiffness range (García-Lizarribar *et al*., 2023).

Proliferating myoblasts at high density are usually seeded on these micro-platforms described, typically in a hydrogel suspension (Ostrovidov *et al*., 2017; Shima *et al*., 2018). A well-known hydrogel used in SkM tissue engineering is GelMA (Gelatin Methacryloyl) (Nichol *et al.*, 2010). Cells that are commonly encapsulated hydrogels have previously been used as a bioink for 3D printed models (Seyedmahmoud *et al.*, 2019). Hydrogels can polymerise in moulds to form scaffolds have been widely adopted in muscle constructs including the gelatin hydrogels which support structural maturation

and increase sarcomeres and contractile proteins such as MyHC (Denes *et al*., 2019). Collagen-encapsulating models can also be used to maintain humidity of constructs operated outside of typical incubation conditions (Morimoto, Onoe and Takeuchi, 2020).

1.7.3.3 Substrates

Substrates are amenable to surface treatments (i.e., laminin, fibronectin coating) depending on the desired cell fate. Nonetheless, the ideal substrate will permit cell mechanosensing upon cell binding, to activate and cluster integrins for focal adhesion formation, subsequent recruitment of cytoskeletal and signalling proteins to determine cell fate including proliferation, differentiation, and maturation. The ECM is complex and can be defined as both a substrate (in direct contact with the cells) and as a scaffold (which maintains tissue structure). The ECM has further physical roles; it creates a boundary between other tissues, provides mechanical signal transduction, regulates the activity of soluble factors and a role in signal transduction via interaction with integrins (Hoshiba and Yamaoka, 2019).

Scaffolds and matrices all demonstrate a stiffness, measured by Young's elastic modulus, (*E*). A tissue's elastic modulus is defined as the resistance offered by tissues to deformation effects i.e. the tissue stiffness (Engler *et al.*, 2004). Substrate stiffness close to the human muscle physiology of 12-18 kPa aids maturation (Engler *et al.*, 2004) and myoblasts depend on substrate stiffness to spread, elongate, and align, as exhibited in native muscle. Myotubes differentiate optimally on substrates with tissue-like stiffness (Hong *et al.*, 2019). Stiff substrates can affect SkM maturity by decreasing muscle specific genes (Khodabukus *et al.*, 2018). However, human myoblasts cultured on stiff substrates have been shown to enhance contractility and proliferation compared to those on softer substrates, with fibronectin promoting stronger stiffness-dependent responses of myoblasts (Nguyen *et al.*, 2024). Dependently, myoblast adhesion to compliant substrates is arguably the most important step in achieving myoblasts that attach and spread in a controlled manner and fuse into myotubes using microenvironmental cues. This in turn, leads to formation of structurally mature multinucleated fibres, able to contract. Substrate stiffness can influence spontaneous self-organisation of cells and alignment during fusion (Jensen *et al.*, 2020). Furthermore, substrate stiffness can affect myogenesis – as matrix stiffness increases, myogenesis decreases (Costantini *et al*., 2017). Substate stiffness may also influence functionality as sarcomerogenesis (the formation and serial deposition of new sarcomeres) is favoured between ~10 and 14 kPa (Engler *et al.*, 2004). Furthermore, stiff substrates can cause detachment of myotubes (Khodabukus *et al.*, 2018), which has been linked to synthetic substrates that are matrix coated (Bettadapur *et al*., 2016). This presents a major issue in model development as it limits culture time. Substrate stiffness is achieved via appropriate matrix choice and

increased with greater myoblasts density and differentiation (Chiron *et al.*, 2012). Stiffness is also highly dependent on the ECM (Krieger *et al.*, 2018). In the first instance, native ECM mimicry has not necessarily produced the best *in vitro* tissues. For example, fibrin is considered the 'gold standard' in SkM tissue engineering due to stiffness corresponding to human physiology of 12-18 kPa (Engler *et al.*, 2006). However, it is not the major component in native ECM, collagen is. Type I collagen specifically, supports migration and differentiation of C2C12 myoblasts (Liu *et al*., 2020). The most used matrix is Matrigel®, which can be complemented with collagen or fibrin as a hydrogel mix, as seen in **Table 1.1**. It contains abundant laminin and collagen IV like native muscle basal lamina matrix. Human myotubes cultured on laminin have shown to be more than 3 times longer than those on collagen I, IV and fibronectin, demonstrating that myotube size is greatly influenced by ECM components (Duffy, Sun and Feinberg, 2016). Matrix porosity is an important consideration as myoblast division and fusion are affected by matrix porosity (García-Lizarribar *et al.*, 2023).

1.7.3.4 3D printing and micropatterning

Moulds and channels like those described earlier can be used to align myoblasts, guiding their orientation during differentiation. In this way, the ultrastructure and organisation of SkM can be controlled. Random myotube orientation is also present on unpatterned surfaces Huang *et al*., 2006; Ostrovidov *et al*., 2017), confirming that topographical substrates encourage true myotube alignment. To quantify myotube orientation on micropatterned surfaces, 'global myotube alignment' can measured since sarcomeres show definite structure along their longer axes (Bettadapur *et al*., 2016). Another method could be the degree of alignment, in relation to the (angle) deviation from a printed pattern direction. Micropatterning can control tissue orientation (Takahashi *et al.*, 2013) and has been shown to improve muscle's developmental maturity via the increase in expression of genes that encode sarcomeric proteins and contractile protein content is increased in micropatterned hydrogels (Denes *et al*., 2019). Myotube size can be controlled and guided by geometric cues. Scaffolds that are micropatterned to improve myotube dimensions and increase myotube length. A 40% increase in length due to micropatterning surfaces compared to non-patterned surfaces has been shown (Huang *et al*., 2006). Increased striations (repeating bands of actin and myosin filaments) on micropatterns along the myofibril length, has inferred increased myofiber length (Huang *et al*., 2006). Therefore, it is possible to manipulate myotubes into increase their size using bio-printed scaffolds. Myotube lengths to be extend up to 346 µm (Costantini *et al*., 2017) or beyond. Extraordinarily, 1.5 mm length were reported for myotubes on µ-moulded gelatin hydrogels, which extended beyond the field of view during imaging (Bettadapur *et al*., 2016). Furthermore, myotubes grown on micropatterned gelatin

hydrogels have demonstrated to be more physiological with lengths, compared that of *in vivo* plateau phase of length-tension relationship (Denes *et al*., 2019). Patterned substrates further positively influence the structural maturation of *in vitro* muscle and can form wider myotubes, particularly in myotubes were significantly wider on μ-moulded gelatin hydrogels (Bettadapur *et al*., 2016). Therefore, micropatterning develops superior myotubes compared to those cultured on non-patterned surfaces, with increased cell maturation (Young *et al.*, 2018). Anisotropic scaffolds have been fabricated that guide cell behaviour and produce unidirectional cells. ECM components can be used in models to promote anisotropy when compared to random orientation of fibres seen without an anisotropic ECM component e.g. laminin (Takahashi, Shimizu and Okano, 2018). 3D printed ring models of up to 4.5 mm diameter and 1 mm height, anchored around (5 × 1 mm) silicon pillars, promoted the concentric alignment of the myotubes, and myoblasts which were immobilised around the pillar-like structures (García-Lizarribar *et al.*, 2023).

1.7.4 Exogenous stimuli

1.7.4.1 Anchorage

3D muscle can recapitulate tendons by creating two adhesion points which anchor tissue constructs in cell culture dishes. An *in vitro* tissue model can be pinned at either ends of a culture vessel. In this way, mechanical tension is created which promotes uniaxial myotube orientation during early differentiation (Nakamura *et al*., 2017), alignment in the direction of the anchor points (Gholobova *et al*., 2018) or force axis (Maffioletti *et al.*, 2018) and longitudinal arrangement (Lee *et al.*, 2018). Tensile force created by anchor points causes reorientation and supports reorganisation of disorganised fibres, allowing them to become parallel, under contraction (Huang *et al*., 2005). Anchoring a myooid offers further advantages including protection of myotubes from detachment (Osaki, Sivathanu and Kamm, 1980) and elimination of shrinkage (Costantini *et al*., 2017). Long term EPS and/or culture can lead to detachment, due to sarcomerogenesis (Yamasaki *et al*., 2009; Duffy, Sun and Feinberg, 2016), which can lead to cell death and limit a model's lifespan. Therefore, anchorage is important to maintain tissue integrity. A method of anchoring cells without the use of physical fixtures is also possible. For example, myocytes have been anchored to a fibrin ECM and shown to spread and form actin stress fibres (Chiron *et al.*, 2012). A 3D sculpted model anchored anisotropic boundary constrains as anchor points which caused anisotropic deformation. As such, this model showed increased density of type III collagen, which also transitioned from a granular morphology to aligned ECM fibres (Mondrinos *et al.*, 2021).

Native SkM tissues present spatial and directional anisotropy (Chanda and Callaway, 2018). Both muscle cells, and the surrounding ECM contribute to anisotropy. Anchorage to mimic native myotendinous junctions of a tissue construct have been shown to

enhance polarisation and therefore increase tissue tension and anisotropy (Mondrinos *et al.*, 2021). Previously, it was discussed that achieving the anisotropy of SkM is a prerequisite to functional maturity (force transmission and contraction) through alignment and orientation. Furthermore, models which are functionally mature or contractile, tend to be anchored (**Table 1.1**). Therefore, anchorage influences maturation by promoting alignment and organisation of fibres which creates functional maturity.

There are several materials used to fabricate adhesions which exhibit variability. 3D models commonly use stainless steel pins as anchor points (Yamasaki *et al.*, 2009; Snyman *et al.*, 2013; Nakamura *et al.*, 2017; Gholobova *et al.*, 2018). These anchor points are fabricated using silicone, PDMS, stainless steel and nylon as artificial tendons (Bakooshli *et al.*, 2019). Other anchor materials used in myooid engineering include polyethylene mesh (Mudera *et al.*, 2010) and glass (Okano and Matsuda, 1997). Stainless-steel pins can also be used and can be attached to electric motors such as a stepper motor to stimulate the muscle model (through direct contact) or a sensor such a force transducer (Powell *et al.*, 2002). Other materials used in the fabrication of anchors include Sylgard, which is a silicone-based encapsulant and is typically used as a base or coating for anchors in cell culture dishes (Gholobova *et al.*, 2018; Snyman *et al.*, 2013). Muscle-tendon myooids can of course be bio-printed too, to form innovative structures that combine synthetic biomaterials and numerous cell types (Merceron *et al.*, 2015). Specific anchor shapes can also be useful in controlling the deformability of substrates (Morimoto, Onoe and Takeuchi, 2020). Furthermore, anchors can also be coated with ECM proteins such as fibronectin, to support cell adhesion (Morimoto, Onoe and Takeuchi, 2020).

1.7.4.2 Mechanical loading

Depending on the type of exercise model desired, mechanical loading is important in controlling concentric or eccentric contractions. The type of load the muscle experiences also determines the force-velocity it experiences (Alcazar *et al.*, 2019). . Under compression, the anisotropic response of tissues can be tested, and it has been proven that human SkM does indeed demonstrate anisotropy (Talbot, Mavez and Maves, 2016). Stress loading has been found to achieve the high organisation and density of myotubes required for maturation within cell models (Okano and Matsuda, 1997). However, under tension, the fibre direction is mainly transversely isotropic (Böl *et al.*, 2014). Examination of limb and facial morphogenesis in zebrafish and mouse has also shown cartilage generates tension at muscle attachment points. Thus, mechanical forces guide the orientation and stretching of myocytes (Sunadome *et al.*, 2023).

1.7.4.3 Chemical and Optical

Several methods have been employed in SkM models to induce contraction. Chemical stimulation has been achieved using caffeine and acetylcholine (Madden *et al*., 2015). Other stimulation methods, such as optical stimulation enables contraction by light-induced membrane depolarization (Asano *et al*., 2015; Bakooshli *et al*., 2019; Mills *et al*., 2019). However, the most common method by far in the use of stimulating *in vitro* SkM models is via ES or EPS, which remains the focus in this body of work.

1.7.4.4 Electrical

For optimal contractile functionality of a model, and therefore maturity, a threshold for maximal electrical stimulation duration, frequency and voltage needs to be established as specific parameters for each model in line with the objectives of the investigation. Achieving muscle contraction is a key functional indicator of maturity. While spontaneous contraction is achievable in some muscle models (Bakooshli *et al*., 2019; Denes *et al*., 2019; Shima *et al*., 2018; Urciuolo *et al*., 2020; Yamasaki *et al*., 2009), the majority utilise an applied electrical or chemical stimulus to mimic this primary functionality.

Studies successfully achieve isometric twitch contractility (Nakamura *et al*., 2017; Takagi, Nakamura and Fujisato, 2018). However, this does not necessarily mimic native muscle where large proportions of muscle activity happen during eccentric contractions. Therefore, it is important to consider producing models with matched active lengthening or isometric shortening to resemble the contractile physiology of the muscle or exercise relevant to the investigation. Additionally, the eccentric muscle force *in vivo* is generally lower than that seen *in vitro*, yet still higher than forces produced by isometric or concentric contractions generation (Franchi, Reeves and Narici, 2017).

Many studies utilise sensitive optical force transducers and computer-controlled linear actuators, where tissues are placed under electrical stimulation as previously described and isometric (active, constant length) twitch and tetanic contractions are recorded in muscle bundles and a contractile force measure of a muscle bundle is measured (Sebille *et al.*, 2017). Furthermore, fibre alignment and geometrics strongly influences contractile function (Bian *et al.*, 2012). EPS has been shown to enhance myogenic maturation (Velasco-Mallorquí *et al.*, 2020).

EPS of muscle cells is an *in vitro* method to achieve contractility and produce an exercise model that mimics adaptation in native SkM (Tarum *et al*., 2017). Commonly, measurable stimulation parameters include pulse or voltage output, frequency, and pulse duration (**Table 1.2**). These can be refined to induce contraction of different models and produce different exercise protocols. Models are subjected to electrical stimulation ranging from 0.3 V – 50 V, 0.5 Hz to 50 Hz and 1 ms – 200 ms. According to the studies reported, the

average stimulation programmes applied to mouse (C2C12) cells is 17.8 V and 3.7 Hz. For human SkM cells, 13.1 V is the average voltage applied with a similar frequency of 3.8 Hz (**Table 1.2**).

The frequency of stimulation dictates contractile patterns (Takahashi, Shimizu and Okano, 2018) and the active state of SkM tissue is dependent on the EPS frequency (Yamasaki *et al*., 2009). Muscle contractions are characterised as twitch, tetanus, or summation. Following stimulation due to a single action potential the moment of contraction and relaxation is known as twitch. Repeated twitch contractions, where the previous twitch has not relaxed completely are called a summation. If the frequency of these contractions increases to the point where maximum tension is generated and no relaxation is observed, then the contraction is termed a tetanus (Smith *et al*., 2020).The fast-twitch and slow-twitch fibres can be further explained by the kinetics of cross-bridge cycling (Feher, 2012). Altering the frequency of EPS over time has significant effects on metabolic activity. Application of low, frequency EPS (such as 2 ms, with 30 V and 1 Hz for last 24 h or 48 h of differentiation) has been shown to increase glucose uptake and oxidation and fatty acid oxidation (as seen in exercised *in vivo* fibres (Nikolić *et al*., 2012). By altering the frequency as described, we can better simulate *in vivo* metabolism. Additionally, EPS of C2C12 cells for 2hrs at low frequency (40 V, 10 ms and 1 Hz) and stimulates calcium signalling, and decreases sodium and potassium content, respectively which regulate SkM contraction (Sidorenko *et al*., 2018).

Myotube size can be further increased by electrical stimulation (Mills *et al*., 2019; Ostrovidov *et al*., 2017; Takahashi *et al*., 2018). Furthermore, alignment is supported by excitation as myotubes appear to exhibit anisotropy in their response to stimulation. Electrical stimulation enhanced actomyosin rearrangement into sarcomeres and increased the width of fibres (García-Lizarribar *et al*., 2023).

Contractile patterns seen *in vitro* are largely twitch contractions at low frequency or sustained unfused tetanus contractions, determined by EPS (Bakooshli *et al*., 2019; Huang *et al*., 2005; Khodabukus *et al*., 2019; Mills *et al*., 2019; Nakamura *et al*., 2017; Yamasaki *et al*., 2009).

Table 1.2 Electrical pacing parameters to induce active SkM cells in 3D models. *The systems listed in the table include a commercially available Ion Optix system (Ion Optix Corp., Milton, MA, USA) and unconventional systems which include customised stimulators and actuators. The C-Dish™ by Ion Optix features carbon electrode elements that are placed into wells and are compatible with many other systems. As described in the table, the different ES can apply the same conditions to cells, therefore stimulation comparisons can be made. ES, electrical stimulator; human SkM, HSkM; NR, not reported.*

Culture dish	Electrical generator	Cells	Pulse output (V)	Frequency (Hz)	Pulse duration (ms)	Stimulation duration	Reference
CONVENTIONAL ION OPTIX ES							
6-well/C-Dish	C-Pace EP	C2C12 & SOL8	14	50	1	90 min, 24 h	(Burch *et al.*, 2010)
8-well or Cell-Disk LF/C-Dish	C-Pace 100	C2C12 &HSkMC	20	1	4	16 h	(Chen *et al.*, 2019c)
6 well/ C-Dish	C-Pace EP	C2C12	40	1	10	4 h	(Danilov *et al.*, 2017)
6-well/C-Dish	C-Pace 100	C2C12	11.5	1	2	24 h	(Evers-Van Gogh *et al.*, 2015)
4-well/ C-Dish	C-Pace 100	C2C12	40	1	24	1,2, 6 h	(Fujita, Nedachi and Kanzaki, 2007)
6 well plate/ /C-Dish	C-Pace 100	HSkM	11.5	1	2	2, 8, 12 and 24 h	(Lambernd *et al.*, 2012a)
6-well/ C-Pace 100	C-Pace EP	C2C12	0.3	1	4	4 days	(Lee *et al.*, 2018)
4 or 8-well/C-Dish	C-Pace 100	C2C12	40	1	2	24 hrs	(Nedachi *et al.*, 2008)

Culture dish	Electrical generator	Cells	Pulse output (V)	Frequency (Hz)	Pulse duration (ms)	Stimulation duration	Reference
6-well.C-Dish	C-Pace 100	HSkM	11.5	1	2	4-24 h	(Raschke *et al.*, 2013)
6-well/C-Dish	C-Pace EM	C2C12 & C2 myoblasts	10 - 12	0.5	4	16 - 24 h	(Reimann *et al.*, 2017)
6-well/C-Dish	C-Pace EP	HSkM	14	5	4	24 h	(Scheler *et al.*, 2015)
6-well/C-Dish	C-Pace EP	HSkM	14	5	2	2, 4, 8, and 24 h	(Scheler *et al.*, 2013)
6-well/C-Dish	C-Pace EP	C2C12	20	30	2	5 s	(Shimizu *et al.*, 2017)
6-well	C-Pace EP	C2C12	40	1	10	2 h	(Sidorenko *et al.*, 2018)
6-well/C-Dish	C-Pace	HSkM	10	1, 2 or 15	10	5 s, 1 h for 3 days or 2 weeks	(Takahashi, Shimizu and Okano, 2018)
6-well	C-Pace EP	HSkM	12	1	2	8 h	(Tarum *et al.*, 2017)
MatTek dishes	C-Pace	C2C12	20	0.5	12	2 h	(White *et al.*, 2014)
6-well/C-Dish	C-Pace EP	C2C12	20	1	24	12 h	(Zhao *et al.*, 2018)
CUSTOMISED ES							

Culture dish	Electrical generator	Cells	Pulse output (V)	Frequency (Hz)	Pulse duration (ms)	Stimulation duration	Reference
35 mm petri-dish	Function generator (Rigol DG1022U).	HSkM	5	1,20	-	-	(Bakooshli *et al.*, 2019)
4 well C-Dish	Uchida-denshi, (Hachioji, Japan)	C2C12	0.03	1	50	1 h	(Furuichi *et al.*, 2018)
2 semi-cylindrical wells	D330 Multistim system (Digimeter Limited)	HSkMC	0.07	1	2	1 h	(Khodabukus *et al.*, 2019)
-	Force transducer &controlled motorized linear actuator (Thor Labs, Newton, NJ)	HSkM	40	1, 5, 10, and 20 Hz were	10	1 sec	(Madden *et al.*, 2015)
4 or 8-well/C-Dish	Uchida-denshi, (Hachioji, Japan)	C2C12	50	1	3	1, 2, or 3 h	(Manabe *et al.*, 2012b)

Culture dish	Electrical generator	Cells	Pulse output (V)	Frequency (Hz)	Pulse duration (ms)	Stimulation duration	Reference
8-well/C-Dish	Uchida-denshi, (Hachioji, Japan)	C2C12 & primary mouse cells	0.005, 0.010, 0.015	1	-	3 h	(Manabe *et al.*, 2016)
4-well/C-Dish	Uchida-denshi, (Hachioji, Japan)	C2C12	50, 30, 12, 10	1	3	1, 3, 6 and 24 h	(Manabe *et al.*, 2014)
-	EP generator	C2C12	5	1	1	-	(Mao *et al.*, 2019)
6 or 24-well plate	Grass S-48 stimulator (Grass Instruments, Quincy, MA, USA)	C2C12	50	3	30	90 mins	(Marotta, Bragós and Gómez-Foix, 2004)
Matrigel coated wells	Panlab/Harvard Apparatus Digital Stimulator	HSkMC	0.02	1, 2, 5 and 20	5	4 days	(Mills *et al.*, 2019)
Biohybrid robot operate din open air	Electrode tip on both side of two anchors	Rat myoblasts	3V/mm	1 and 50	2	-	(Morimoto, Onoe and Takeuchi, 2020)
Polycarbonate plate	WF1974 generator,bipolar amplifier	C2C12	1	0.5	2	-	(Nakamura *et al.*, 2017)

Culture dish	Electrical generator	Cells	Pulse output (V)	Frequency (Hz)	Pulse duration (ms)	Stimulation duration	Reference
	(HSA4101, NF Corporation)						
12-well plates	Grass S88 Dual Output Square Pulse Stimulator (Warwick, RI).	C2C12	1.5	1	6	-	(Nieuwoudt *et al.*, 2017)
6-well plates	Muscle stimulator built at the Electronics Lab, Institute of Chemistry, University of Oslo.	HSkMC	30	1	2 or 200	5 - 60mins	(Nikolić *et al.*, 2012)
60mm petri dishes	ES (Nihon Koden, SEN-8203, Japan) coupled with an isolator unit (Nihon Koden, SS-104 J, Japan)	C2C12	6	1	1	2 days	(Ostrovidov, *et al.*, 2017)
10cm dish	Force transducer	Induced myogenic	40	1, 10, 20 and 40	10	15 days	(Rao *et al.*, 2018)

Culture dish	Electrical generator	Cells	Pulse output (V)	Frequency (Hz)	Pulse duration (ms)	Stimulation duration	Reference
	&controlled motorized linear actuator (Thor Labs, Newton, NJ)	progenitor hPSCs					
6-well plate	AFG1000 Series Arbitrary/Function Generator	C2C12	2.2 - 2.5	1	4	24 h	(Seyedmahmoud *et al.*, 2019)
4-well/C-Dish	SEN-3401	L6.C11	50	100	NA	0.5, 1,3, 5 h	(Sato *et al.*, 2019)
-	Function generator (Agilent Technologies) & power amplifier (Mess-Tek, Japan)	HSkMC	1	1	2	-	(Shima *et al.*, 2018)
100-mm collagen-coated dish	WF1974 generator	C2C12	20	0.5 – 10Hz	10	-	(Yamasaki *et al.*, 2009)

1.7.5 Force output

iPSC myobundles can produce 1.5 ± 0.1 mN twitch and 2.7 ± 0.2 mN tetanus forces which are lower than primary human myobundles, human adult muscle and even native foetal muscle (Rao *et al*., 2018). By comparison, the first engineered functional 3D myobundles that were made from primary human myoblasts (Madden *et al*., 2015), demonstrated 2.1 ± 0.9 mN twitch and much greater tetanus force of 7.0 ± 2.2 mN, and an average tetanus- to-twitch ratio of 3.5 ± 0.8 – within a normal adult range. Other human primary human models have shown similar contractile features (2.0 ± 0.7 mN twitch and 4.9 ± 0.8 tetanus), however more reflective of foetal human muscle and lower than those for adult human muscle forces (Mills *et al*., 2019). In a C2C12 3D model, similar twitch contractile forces to the stem cell and human model of 2 mN was achieved (Nakamura *et al*., 2017). This suggests that in response to electrical stimulation, higher forces are present in primary cells compared to pluripotent stem cells.

1.8 SkM secretomics and myokines

1.8.1 Exercise and its therapeutic application

Exercise involving contractile SkM cells offers significant health benefits (Nishii *et al*., 2023). Part of this is due to muscle secreted factors termed ‘myokines’ (Pedersen *et al*., 2003) which are known to have roles in metabolic homeostasis (Lee and Jun, 2019), muscle atrophy (Piccirillo, 2019) and angiogenesis and immunoregulation (Nielsen and Pedersen, 2008). With the added knowledge that regular physical activity can reduce the risk of development of cardiometabolic diseases (Lacombe *et al*., 2019; Pinckard *et al*., 2019), it becomes significant to understand the underlying mechanisms of exercise and the wider communication network between organs, tissue and SkM (Delezie and Handschin, 2018; Gamas *et al*., 2015; Hamrick, 2012; Pedersen, 2019a). There is great potential to upregulate myokines for positive metabolic effects, for instance, to increase glucose sensitivity through EPS (Nikolić *et al*., 2017). Therefore, development of physiologically relevant *in vitro* models is a key first step towards targeting myokines for therapeutics.

1.8.2 IL-6: the prototype myokine

The mechanism by which factors produced by SkM during physical activity influence other tissues, thereby promoting the overall health benefits of exercise, was previously referred to as the 'exercise factor' or 'work stimulus' (Pedersen *et al*., 2003; Pedersen, 2010). The humoral factors described are a diverse group of SkM-secreted proteins, peptides, and metabolites, which exert autocrine, paracrine, or endocrine effects, thereby

regulating various physiological processes. IL-6 is a prototypical myokine, playing a central role in early research and discovery within this field and remaining the most extensively studied myokine. Elevated IL-6 levels in the circulation were initially observed following marathon running and was originally attributed to immune cell activity during exercise (Ostrowski *et al.*, 1998). Circulating IL-6 levels were found to increase up to 100-fold compared to resting levels after a single intense bout of exercise, highlighting the significant response of IL-6 to physical exertion (Ostrowski *et al.*, 1998). Since then, several studies identified SkM as the source of IL-6 secretion (Steensberg *et al*., 2000; Starkie *et al*., 2001; Febbraio *et al*., 2003; Hiscock *et al*., 2004). The term 'myokine' was then coined by Bente Pedersen and colleagues while considering IL-6 as a SkM secreted exercise factor (Pedersen *et al*., 2003). More recently, the term 'exerkines' has been used to describe exercise secreted factors, although this does not specifically ascertain the tissue origin of the exercise factor (Brooks *et al*., 2023; Gonzalez-Franquesa *et al*., 2021b; Magliulo *et al*., 2021). Pedersen has since built on the myokine concept, with a focus on exercise as prescription to treat treatment of chronic disease (Pedersen, 2019b; Pedersen and Saltin, 2015).

Since their initial identification in 2003, over 650 myokines are currently recognised and with growing interest and research activity surrounding myokines, this list is continuously expanding (Lee and Jun, 2019). Despite this progress, challenges remain in the discovery and therapeutic application of myokines, including the need for advanced techniques to identify and analyse their functions.

1.8.3 SkM secretomics

Myokines can be detected following secretome analysis, of the metabolites and proteins released from SkM, usually following exercise of muscle contraction. In the analysis of the secretome, it is important for myokines to be validated by multiple methods. This is because of 654 SkM secretome proteins reviewed by Florin *et al*. (2020) and only 30 were differentially regulated by exercise. The remaining proteins were regulated during myogenesis (130), by dystrophin deficiency (114), muscle atrophy (26), insulin stimulation (27) and secreted by insulin-resistant muscle cells (176) (Florin *et al*., 2020).

Bioinformatic filters are typically applied to the secretome data, to concur myokines discovery, through signal peptide prediction (SignalP, SecretomeP) and network analysis (STRING, Cytoscape, Ingenuity Pathway Analysis (IPA)). The second method consists of the targeted identification of myokines, which may be prompted by comparative evidence of similar proteins that are identified as myokines, that have been previously documented in the literature. Bioinformatics tools can be incorporated into analytical workflows to identify cell secreted proteins. For instance, the Lysate and Secretome

Peptide Feature Plotter (LSPFP) can be employed to detect and visualise proteolytic protein processing events that might occur during secretion. This method enables the validation of proposed signal peptide cleavage as well as detects unknown proteolytic processing events (Grube *et al.*, 2018). Alternatively, by blocking of classical secretory processes, using Brefeldin A, altered sensitivity to classically secreted proteins can be identified (Grube *et al.*, 2018). One of the major challenges in secretome studies is to distinguish cell-derived proteins from residual serum proteins. Applying the SILAC approach offers an advantage compared with other labelling strategies because metabolic labelling of cells facilitates the discrimination between secreted proteins *versus* contaminating serum proteins due to the incorporation of the isotope-labelled amino acids into the proteins during their synthesis inside the cell (Henningsen *et al.*, 2010).

The secretome or CM of exercised SkM models can be used to investigate the endocrine effects of SkM. The entire secretome or CM can be applied to other cells to elicit effects in other cells/tissues/organs. The secretome or CM of rat L6 SkM cells (treated with AICAR) influences the brain through enhancement of neural differentiation (Moon *et al.*, 2019). Further studies show that CM from EPS-induced C2C12 myotubes establish a crosstalk between SkM and pancreatic β-cells whereby acute insulin release from normal cultured β-cells, nondiabetic islets and Type-2 diabetic islets was potentiated and associated with enhanced mitochondrial substrate oxidation (Barlow and Solomon, 2019). In a separate study, a connection between SkM and β-cells, modulated by the insulin-resistant state of the muscle was revealed following incubation of rat primary β-cells with TNF-treated CM media from muscle cells (Bouzakri *et al.*, 2011).

A curated list of key secretome studies which identify >10,000 proteins in the secretome of SkM cells (from a single study) are listed in **Table 1.3**, discriminating rodent and human derived sources.

Table 1.3 Characteristics of key studies investigating the SkM secretome. *5-aminoimidazole-4-carboxamide-1-β-D-ribofuranoside, AICAR; Matrix-Assisted Laser Desorption/Ionization Quadrupole Time-of-Flight, MALDI-QTOF; Multiplex immunoassay, MIA; Enzyme-linked immunosorbent assay, ELISA; Conditioned media, CM; SkM, Skeletal muscle; Lysate and Secretome Peptide Feature Plotter, LSPFP; Stable isotope labelling by amino acids in cell culture, SILAC; Pigment epithelium derived factor, PEDF; Dipeptidyl peptidase 4, DPP4.*

Study	Key Insights	Exogenous stimuli	SkM source	Sample	Techniques	No. protein IDs
(Deshmukh *et al.*, 2015b)	SkM secretome altered by lipid-induced insulin-resistance model	None	Mouse C2C12 cells	CM	Mass spectrometry	1073
(Catoire *et al.*, 2014)	CX3CL1 and CCL2 as novel exercise-induced myokines in humans, showing increased expression at both mRNA and plasma levels following acute endurance exercise	Acute and endurance exercise	Human participants	Plasma	MIA Elisa	86 (acute) and 69 (endurance)
(Chan, McDermott and Siu, 2007)	Identification of secreted proteins during SkM development	None	Mouse C2C12 cells	CM	1D-SDS-PAGE, Mass spectrometry (MALDI-QTOF)	80 total, 27 secretory proteins
(Gonzalez-Franquesa *et al.*, 2021a)	Insulin and AICAR differently influence the SkM secretome. Insulin boosts mitochondrial respiratory capacity in myotubes, highlighting distinct metabolic roles	Insulin and AICAR	Mouse C2C12 cells	CM	Mass spectrometry	858 total, 377 Insulin - and 118 AICAR-altered proteins.
(Grube *et al.*, 2018)	A two-step secretomics approach combining LC−MS/MS, LSPFP	None	Mouse C2C12 cells	CM	Mass spectrometry	672
(Gueugneau *et al.*, 2018)	Increased Serpina3n release into circulation during	None	Mouse C2C12 cells	CM	Immunoblot, Mass spectrometry	739 total, 26 differentially secreted between control

	glucocorticoid-mediated muscle atrophy					and glucocorticoid-treated groups
(Hartwig *et al.*, 2014)	Extensive secretome profiling to identify novel myokines	None	Human primary cells	CM	Mass spectrometry, Antibody-based	548 total, 305 secretory, 12 novel myokines
(Henningsen *et al.*, 2010)	Secretome comparison at three different time points of muscle differentiation	None	Mouse C2C12 cells	CM	SILAC, Mass spectrometry	635
(Le Bihan *et al.*, 2012)	Identified three major independent secretory pathways in myoblasts	None	Satellite cells from human primary cell culture	CM	MIA 2D gel electrophoresis Mass spectrometry	954
(Raschke *et al.*, 2013)	Validated the regulation and release of two selected myokines, PEDF DPP4	EPS	Human primary cells	CM	ELISA Cytokine antibody arrays	52 novel myokines from human SkM cells, 48 contraction-regulated
(Mengeste *et al.*, 2022)	Enhanced oxidative metabolism in EPS-exposed myotubes observed	EPS	Human primary cells	CM	Mass spectrometry, MIA, ELISA	1,215 total, 81 (differentially regulated proteins)
(Moon *et al.*, 2019)	CM from AICAR-treated SkM cells Increase neuronal differentiation of adult neural progenitor cells	AICAR	L6 (rat)	CM	Western blot, Mass spectrometry	74 total, 38 differentially secreted proteins by AICAR
(Norheim *et al.*, 2011)	Identification of proteins secreted by SkM cells *in vitro* facilitated the	None	Human primary cells	CM	SDS-PAGE,	236

	discovery of novel responses in skeletal muscles of strength-training individuals				Mass spectrometry	
(Ojima *et al.*, 2014)	Proteomic analysis of secreted proteins from skeletal muscle cells during differentiation	None	Mouse muscles biopsies	CM	Mass spectrometry	437 proteins, 8% as myokines
(Roca-Rivada *et al.*, 2012)	The secretome characterisation and the comparative 2-DE secretome analysis among fast-glycolytic (gastrocnemius) and slow-oxidative (soleus) rat muscle explants and its variation after exercise intervention	1 week of endurance exercise training	Sprague–Dawley rats explants	CM	2-DE immunoblotting Western blot Mass spectrometry	19 (soleus vs. gastrocnemius) 10 (gastrocnemius) 17 (soleus)
(Yoon *et al.*, 2015)	Identification of skeletal muscle-derived proteins whose secretion is modulated by palmitate-induced insulin resistance.	None	L6 (rat), myoblast cells	CM	Mass spectrometry	36 secretory proteins modulated by palmitate-induced insulin resistance
(Yoon *et al.*, 2011)	Comparative analysis of TNF-induced insulin resistant vs. wild type SkM cells	None	L6 (rat) myoblast cells	CM	Mass spectrometry	28 TNF-modulated secretory proteins

1.8.4 Characterisation of myokines

Following their identification, myokine characterisation has revealed a broad spectrum of functions, highlighting their role in maintaining systemic homeostasis and their potential therapeutic relevance in metabolic and inflammatory diseases (**Table 1.4**). Myokines are implicated in the metabolic and physiologic responses to exercise in various organs, including the SkM itself, however only a few myokines have been linked to specific biological functions. The roles of myokines have expanded since earlier reports (Manabe *et al*., 2012a) and their roles have been more recently reviewed, specifically in the prevention and treatment of metabolic conditions such as type 2 diabetes (Carson, 2017), muscle wasting (Belizário *et al*., 2016; Piccirillo, 2019), in regulating muscle mass (Lee and Jun, 2019) and bone-crosstalk (Hamrick, 2012; Gomarasca, Banfi and Lombardi, 2020). Indeed, several key myokines, such as irisin and IL-6, have been well-characterised, however, the vast majority remain poorly understood. Characterising myokines is essential for understanding their role in muscle-to-organ crosstalk and their impact on systemic health. This knowledge is crucial for identifying new therapeutic targets for metabolic disorders, such as diabetes and obesity, and for addressing age-related conditions like sarcopenia and chronic inflammation

The pleiotropic nature of myokines, which makes their characterisation inherently challenging, has been emphasised in various studies (Boesten *et al*., 2005; Li *et al*., 2020; Lin *et al*., 2015; Little *et al*., 2018) and reviews (Belizário *et al*., 2016; Gonzalez and Trigatti, 2017; Gonzalez-Gil and Elizondo-Montemayor, 2020; Jin *et al*., 2016; Leal *et al*., 2018; Muñoz-Cánoves *et al*., 2013; Pal *et al*., 2014). Myokines are involved in a wide range of biological processes, including metabolic regulation, immune modulation, and tissue repair (**Table 1.4**), making it challenging to define their specific physiological roles and classify them within a standardised system. In the context of exercise, the secretion of myokines is influenced by variables including the modality, intensity, and duration of exercise (Egan and Zierath, 2013). Physiological differences such as age and gender further influence myokine response (Lundsgaard and Kiens, 2014; Ruan *et al*., 2019). Furthermore, myokines operate within complex signalling networks, making it difficult to pinpoint their precise mechanisms of action. Furthermore, the classification of myokines can overlap with other definitions when they are secreted by non-SkM tissue, such as adipokines (Raschke and Eckel, 2013). Indeed, exercise produces integrative, systemic effects, which involve hepatokines, osteokines, and adipokines (Gonzalez-Gil and Elizondo-Montemayor, 2020), whereby known myokines such as FGF-21 and FSTL1 are identified as hepatokines too, due to being released from the liver during or immediately after an exercise bout (Weigert, Hoene and Plomgaard, 2019). This reinforces the cross-functional roles of non-myocyte derived ‘exerkines’ in vivo (Magliulo

et al., 2021), such as thymosin β4 (TMSB4X), which has a role in osteoblast proliferation and neurite outgrowth (Gonzalez-Franquesa, *et al*., 2021).

The absence of a comprehensive database for myokine discovery underscores the need for ongoing literature reviews to identify newly reported myokines. Rigorous validation of their presence in secretomics studies is imperative, followed by the application of post-experimental bioinformatic approaches, to elucidate their underlying pathways and functional associations. Furthermore, SkM cells can secrete different types of myokines at different developmental stages (Ojima *et al.*, 2014). In the literature, three key factors are typically considered when characterising myokines, which are: reliable detection, demonstrated metabolic effects, and their response to exercise (i.e. changes in levels following exercise or contraction). Below is a list of myokines reported to date, including evidence for SkM-organ crosstalk and thus, establishing the endocrine effects of these myokines (**Table 1.4**).

Table 1.4 Purported endocrine effects of commonly reported myokines. *Detail of established myokine roles are described. Information is obtained from reviews* (Legård and Pedersen, 2019; Severinsen and Pedersen, 2020) *or individual references that are detailed within the table. *Mice lack the IL-8 gene.*

Common names	Abbreviation	Endocrine target

Angiopoietin-like protein 4	ANGPTL4	• Adipose tissue –
		  • Increase lipolysis
		  • Endothelium – decrease LPL activity
		• Pancreas – α cells – hyperplasia

β-aminoisobutyric acid	BAIBA	• Adipose tissue – browning, increase thermogenesis
Brain-Derived Neurotrophic Factor	BDNF	• Brain – neurogenesis, synaptic plasticity • Fat oxidation (Matthews *et al.*, 2009)
Cathepsin B	CTSB	• Brain – Hippocampal neurogenesis via BDNF • increased cognitive function
C-C Motif Chemokine Ligand 2/MCP-1	CCL2	• Immune cells – monocyte – increase ell attraction
C-C Motif Chemokine Ligand 5/ Rantes	CCL5	• Adipocytes – promote the migration of subcutaneous adipocytes to SkM and induce the intramuscular fat content (Yu *et al*., 2024)
C-C Motif Chemokine Ligand 7	CCL7	• Cardiovascular disease, diabetes mellitus, and kidney disease – inflammation progression (Chang, Chen and Chen, 2022)
C-C Motif Chemokine Ligand 8	CCL8	• SkM – initiation of myogenic differentiation during injury-induced muscle regeneration (Boss-Kennedy *et al.*, 2024)
C-X-C motif chemokine ligand 1	CXCL1	• SkM – promotes myogenesis from satellite cells (Masuda *et al.*, 2018)
Decorin	DCN	• Bone – promote formation
Dermcidin	DCD	• Heart – modulates cardiomyocyte survival (Esposito *et al.*, 2015)
Erythropoietin	EPO	• Adipose tissue – browning (W. Yin *et al*., 2024)
Fibroblast Growth Factor 15/19	FGF15/19	• SkM - regulates SkM mass through enlargement of muscle fibre size and protects muscle from atrophy (Benoit *et al.*, 2017)
Fibroblast Growth Factor 2	FGF2	• Bone – promote formation

Fibroblast Growth Factor 21	FGF21	• SkM – promotion of muscle atrophy (Oost *et al.*, 2019) • Bone – reduced mineral density (Staiger *et al.*, 2017) • Stress-induced myokine, released during starvation, ER stress, and mitochondrial dysfunction (Tezze, Romanello and Sandri, 2019) • WAT – Energy metabolism, thermogenesis (Kim *et al.*, 2013) (Keipert *et al.*, 2014) • SkM – insulin resistance (Lindegaard *et al.*, 2013) • Heart – Cardiac protection (Planavila *et al.*, 2013)

Follistatin-related protein 1	FSTL1	• Heart –
		  • positively regulate myocardial substrate metabolism
		  • promotes endothelial cell function

Growth Differentiation Factor 8/Myostatin	GDF8	• SkM - inhibits hypertrophy • Bone – negative regulation of formation
Growth Differentiation Factor 15	GDF15	• Adipose tissue - increased lipolysis (Laurens *et al.*, (Broo
Insulin Like 6	INSL6	• SkM – Myogenic regenerative factor
Insulin-like Growth Factor 1	IGF-1	• Bone – positive regulation of formation, increased mineralisation and formation
Interleukin-1 receptor antagonist	IL-1RA	• Immune cells – IL1α/β – reduce inflammation
Interleukin-4	IL-4	• SkM - promotes hypertrophy

Interleukin-6	IL-6	• SkM - promotes hypertrophy (cell proliferation)
		• Brain - appetite suppressant
		• Adipose tissue - stimulates lipolysis to decrease visceral fat mass, browning
		• Bone – promote formation
		• Liver – glucose production
		• Pancreas –
		  • positive regulation of insulin secretion
		  • stimulates GLP-1 secretion, positive regulation of β-cell mass (by stimulating

		• β-cell proliferation and preventing apoptosis induced by metabolic stress) • α cells – hyperplasia • Intestine – stimulates GLP-1 secretion from L-cells • Vasculature – anti-inflammatory (by inhibition of TNF production and stimulation of IL-1ra and IL-10 production) • Immune cells – macrophages – increase activation • Adrenal gland - stimulates cortisol production and induces neutrocytosis and lymphopenia
Interleukin-7	IL-7	• SkM - promotes hypertrophy
Interleukin-8*	IL-8*	• Vasculature – Increase in angiogenesis (prevention of arteriosclerosis) (Nishii *et al.*, 2023)
Interleukin-10	IL-10	• Liver – Immune cells – decrease inflammation • Immune cells – T cells – reduces inflammation
Interleukin-15	IL-15	• SkM – promotes hypertrophy • Bone – positive regulation • Skin – retards skin aging • Vasculature – endothelium – decrease LPL activity • Bone – positive regulation of formation • Increased mineralisation and formation
Irisin	FNDC5	• Adipose tissue – browning, increase thermogenesis • Brain – Hippocampal neurogenesis (via BDNF)
Leukaemia inhibitory factor	LIF	• SkM – promotes hypertrophy (satellite cell proliferation) (Broholm *et al.*, 2011; Broholm and Pedersen, 2010)
Meteorin Like	METRNL	• Adipose tissue – • Browning

		• Macrophages – increase thermogenesis, reduces myostatin, decrease fat mass
Myonectin/erythroferrone	CTRP15/ERFE	• Adipose tissue – promotes fatty acid uptake (Seldin *et al.*, 2012) • Liver – lipid homeostasis (Seldin *et al.*, 2012)
Oncostatin M	OSM	• Breast tissue – decrease breast cancer cell proliferation (Negrini *et al.*, 2024) • Immune cells – increase macrophage and neutrophil expression (Komori and Morikawa, 2022)
Osteocrin/musclin	OSTN	• SkM – promotes hypertrophy (mitochondrial biogenesis)
Osteoglycin	OGN	• SkM – inhibit myoblast migration during myogenesis
Secreted protein acidic and rich in cysteine/ Osteonectin	SPARC	• Bone – positive regulation of formation • Increased mineralisation and formation
Tumour Necrosis Factor	TNF	• Pancreas – inhibit β-cell function
Transforming Growth Factor-beta	TGF-β	• Bone – negative regulation

1.8.5 Myokines and EVs

Extracellular vesicles (EVs) released during physical activity may facilitate intercellular communication, supporting tissue and organ signalling during exercise-induced adaptations (Romancino *et al*., 2013; Aswad *et al*., 2014; Frühbeis *et al*., 2015). Myokines can therefore be secreted both via the classical secretory pathway and by EVs. Quantitative proteomic analysis of EV fractions has revealed a net flux of over 600 proteins, with 35 proteins showing significant release rates during exercise or recovery (Whitham *et al*., 2018). Additionally, a correlation between circulating microRNAs and the myokine response after strenuous exercise suggests that EVs are involved in this response (Faraldi *et al.*, 2022). Evidence for myokine release via EVs is further supported by the detection of endogenous IL-6 in vesicle-like structures within resting muscle fibres, with muscle contraction reducing these IL-6-containing vesicles (Lauritzen *et al.*, 2013). However, findings on EV quantity during exercise are inconsistent. For instance, EV protein yield has been shown to increase after acute exercise in sedentary youth with obesity (Pierdoná *et al.*, 2022), while a similar study in adults with obesity found a decrease in EV concentration immediately after exercise and at 3 h and 24 h post-exercise (Rigamonti *et al.*, 2020). A reduction in EV protein content 4 hours post-exercise has also been reported, suggesting partial clearance through tissue absorption (Trovato *et al*., 2019). Therefore, EV characterisation in the context of SkM myotube formation and acute contractile activity is important (Bydak *et al.*, 2022).

1.9 Summary

Initiation of *in vitro* model development should involve selection of species-specific cell selection, to best mimic the organism and disease pathology of investigation. Central to obtaining structurally mature 3D models thereafter is due to cell alignment. It is the prerequisite for development of contractile tissue and facilitates adequate force transmission. Advanced 3D models provide mechanical tension to produce highly myogenic, aligned, and contractile myofibers. Furthermore, the SkM secretome could be viable indicator of SkM contraction. The literature reviewed in this chapter offers a characterisation guide for *in vitro* model development which can be useful in the development of physiological models, particularly concerning EPS-induced models. Building on the development of SkM models, an exploration of contraction-inducible factors, particularly myokines, reveals their critical role in mediating the systemic benefits of exercise and their potential therapeutic applications. Myokines may explain the beneficial effects of exercise and therefore, can be targeted for potential therapeutic intervention. Myokine characterisation, however, remains challenging due to limitations in detection methods. This is further complicated by the multiplicity of many myokines originating from alternate tissues with duality of function, their pleiotropic effects and role

in inter-organ communication. Further consideration of myokine transport mechanisms, biological roles, population samples, exercise and exercise-like factors such as mode, frequency, intensity, duration, should all be considered when characterising both existing and novel myokines.

1.10 Project overview

The development of a functionally contractile SkM model is essential for advancing the study of myokine research. In this thesis, *in vitro* models were developed, informed by the myogenic maturation features ascertained from the literature. Although *in vivo* research established decades ago, that muscle contractions drive IL-6 secretion (Ostrowski *et al.*, 1998), the first definitive *in vitro* evidence of contraction-induced myokine release from cultured C2C12 SkM was only recently reported (Furuichi *et al*., 2018). This emphasised the need for further development of *in vitro* models. Unlike *in vivo* systems, *in vitro* models provide a controlled environment where variables can be precisely manipulated, eliminating the confounding effects of exercise. In this way, researchers are able to isolate the specific mechanisms driving myokine secretion without the complexity of whole-organism interactions. This thesis utilised EPS to regulate myokine secretion through intensity, pulse duration and frequency. The first study to show EPS-evoked muscle contractile stimulation increased irisin from a 3D engineered model was only recent (Sugimoto *et al.*, 2022). This underscored the importance of investigating and validating myokine profiles and their secretion dynamics using *in vitro* models. Thereby, the central hypothesis of this thesis postulates that myokine secretion can be altered through EPS induction and secretions are sustained following the induction period. To address the main hypothesis, the aims of this thesis were as follows:

- Explore tissue engineering strategies to develop 2D and 3D SkM models, characterised by myogenic features of maturation.
- Investigate the effect of EPS induction and duration on myokine profiles of 2D and 3D SkM models.
- Determine the temporal dynamics of myokines post ± EPS.

2 Methods

2.1 Cell Culture

2.1.1 C2C12 cell line maintenance

C2C12 (CRL-1772™, ATCC) cells were used as one of the most popular mouse immortalised myogenic cell lines, established by Yaffe (1968). The spindle-shaped cells with a single nucleus rapidly proliferate and readily differentiate to produce elongated, and multinucleated contractile myotubes to provide a dynamic platform for studying SkM myogenesis, function and disease. The C2C12 cells were cultured in complete Dulbecco's Modified Eagle Medium (cDMEM; Gibco, cat. no. 10569010) containing high glucose, GlutaMAX and pyruvate, 10 %(v/v) foetal bovine serum (FBS; Gibco, cat. no. 10082-147), 1 % (v/v) L-glutamine (Gibco, cat. no. 25030-081) and 1 % (v/v) Penicillin/streptomycin (P/S; Gibco, cat. no. 15140-122). Cells were either sub-cultured in T75 flasks or seeded in Nunc™ Treated Multidishes (Thermo Scientific, cat.no. 140675) for differentiation when they reached approximately 70-80 % confluency. Cells were maintained at 37°C and 5 % CO_2 and routinely tested for infections including mycoplasma using the MycoAlert™ Mycoplasma Detection Kit (Lonza, cat. no. LT07-318).

During cell passage, the culture medium was removed, and cells were rinsed twice with Phosphate-buffered saline (PBS; Gibco, cat. no. 14190-094). Afterwards, cells were incubated with 3 mL (T75) or 6 mL (T175) of trypsin-EDTA (Gibco, cat. no. 25300-062) at 37ºC for approximately 3-5 minutes (min). To neutralize trypsin-EDTA, cells were resuspended in 7 mL (T75) or 24 mL (T175) of complete DMEM and transferred to falcon tubes for centrifugation at 1000 *x g* for 5 min. Subsequently, the supernatant was discarded, and the pelleted cells were re-suspended in 1 mL of fresh DMEM. Cellular viability and concentration was determined by mixing 1:1 ratio of cell suspension and Trypan Blue (Gibco, cat. no. 15250-061) and loading 10 µL of this final suspension into a Countess™ Cell Counting Chamber Slides (Invitrogen, cat. no. C10228). Percentage viability (live/dead) of cells and concentration (1×10^4–1×10^7 cells/mL) were measured using the Countess™ II Automated Cell Counter (Thermo Scientific). The C2C12 cell suspension was aliquoted into T75 or T175 flasks containing fresh cDMEM, based on the intended split ratio (i.e. 1:5). Cells were used between 1 and 10 passages for experiments. Cells were cryopreserved in 1 mL of 90:10 FBS/DMSO (ATCC, CRL-1772™) (DMSO; Bio-Techne, cat.no. 3176) suspension in Nunc™ Biobanking and Cell Culture Cryogenic Tubes (Thermo Scientific, cat. no. 377267) and stored at -80ºC short-term (in Nalgene® Mr. Frosty, Thermo Scientific, cat. no. 5100-0001) or transferred to liquid nitrogen (LN_2) for long-term storage.

2.1.2 Optimisation of a two-dimensional model

2.1.2.1 Proliferation and differentiation

A 2D model was initially developed, based on established C2C12 culture protocols, which produced district myocyte fibres (Jang *et al*., 2022). Cells of 70-80 % confluency were seeded at a density at $5x10^5$ cells/mL in 6-well plates. After 24 hours, fully confluent cells were switched from growth medium to differentiation medium containing DMEM (high glucose, GlutaMAX and pyruvate), supplemented with 1% (v/v) Horse Serum (HS, Sigma-Aldrich, cat. no. H1138), 1 % (v/v) L-glutamine and 1% (v/v) P/S (defined media 1). The cells were differentiated for 7 days at 37°C and 5 % CO_2. Differentiation media was changed every 48 hours and cells were checked for infection as previously stated. To enhance myoblast differentiation, the aforementioned differentiation conditions were supplemented with 50 ug/mL L-Ascorbic acid-2-phosphate (AA2P; Sigma-Aldrich, cat. no. A8960) and 50 ng/mL Insulin-like growth factor 1 (IGF-I/IGF-1; Bio-Techne, cat. no. 791-MG) (defined media 2), prepared fresh upon media change, following concentration optimisation.

2.1.3 Optimisation of a three-dimensional model

2.1.3.1 Overview of model development

The 3D hydrogels were cultured for up to 21 days (D21) under 3D differentiation conditions consisting of further supplementation of defined media 2 (Section 2.1.2.1) with 1.25 mg/mL AlbuMAX (Gibco, cat. no. 11020021), 40 µg/mL L-Proline (Sigma-Aldrich, cat. no. P5607) and 0.1 % (v/v) ITS-X (Insulin-Transferrin-Selenium-Ethanolamine; ITS-X; Gibco, cat. no. 10524233) (defined media 3). 3D model development considered cell density, matrix composition, model morphology and tethering, as key factors influencing cellular alignment, differentiation, response to tensile loading, contractility, and secretory function.

2.1.3.2 Hydrogel spheroid: Col-Tgel

Collagen transglutaminase (Col-T; 101 Bio, cat. no. P720M) was used to produce hydrogel spheroids. The Col-T gel provided a medium stiffness of 14-20 kPa for muscle cells, correlating human SkM physiology of 12-18 kPa (Engler *et al*., 2006; Khodabukus *et al*., 2018; H. Yin *et al*., 2013). Furthermore, sarcomerogenesis is critical to muscle function (Zöllner *et al.*, 2012) and is favoured between 10 and 14 kPa (Engler *et al.*, 2004). Col-T was therefore used as the first 3D culture matrix attempted. The following cell densities: $2.5x10^6$, $5x10^6$ and $1x10^7$ cells in Col-Tgel at a 1:20 ratio of A to B Col-Tgel components were prepared. Gell-cell suspensions were pipetted into 48-well plates (200 µL) and left to set for 1 hour to allow gelling at 37°C and 5 % CO_2. The gels were topped with growth media for 24 hours, then switched to differentiation media.

2.1.3.3 Hydrogel spheroids: Collagen-Geltrex

Native SkM ECM comprises a basal lamina and intramuscular connective tissue (IMCT). Myofibers are surrounded by a basal lamina which is made up of non-fibrillar collagen IV, laminin, heparin sulphate proteoglycans, and glycoproteins (Csapo *et al*., 2020; Gillies & Lieber, 2011; Khodabukus *et al*., 2018; H. Yin *et al*., 2013). To mimic this, Geltrex™ (Gibco, cat. no. A1413202) was used. The basement membrane extract similarly contains laminin, collagen IV, entactin, and heparin sulphate proteoglycans. Collagen-geltrex hydrogel spheroids were cultured as the second 3D model, at a higher density of $1x10^7$ cells/mL . The cell-hydrogel suspension was prepared on ice by resuspending a pellet of $1x10^7$ cells in 100 µL growth media with the following order of hydrogel components: 525 µL Type I collagen (Collagen type 1; Rat Tail, Corning, cat. no. 354236) in 0.02 N acetic acid (concentration range 3-4mg/mL), 175 µL Geltrex™ 200 µL growth media and 18 µL Sodium hydroxide (NaOH pellets, Thermo Scientific, cat. no. 15433117). The cell-laden gel mixture (2.5 mL) was pipetted into a 96-well plate (125 µL). The gels set after 1 hour at 37°C and 5 % CO_2 and subsequently removed from the wells and placed in 6-well plates with 2 mL of growth media. 24 hours later, the media was switched to differentiation media (D0).

2.1.3.4 Hydrogel rods: Collagen-Geltrex

Smaller rods (rod v1) moulds were prepared from plastic tubes (BD Microlance™ syringe cap), cut to approximately 25.0 mm (length) and 5.0 mm (diameter). Subsequently, larger rods (rod v2) were prepared from pasteur pipettes as moulds, with approximately 57.0 mm (length) and 15.8 mm (diameter). The moulds were sterilised with 70 % IMS and rinsed with PBS. Sterile BD Microlance™ Stainless Steel Needles (Fisher Scientific, Gauge 30G, 0.3 x 13 mm length) were used to puncture holes into the tubes to allow efficient transfer of nutrients and oxygen to the hydrogel. For rod v1, $1x10^7$ cells per 1018 uL gel were prepared and $2x10^7$ per 1018 uL gel for rod v2. For the preparation of two 'large' hydrogels (rod v2), 5x the hydrogel components and cells in Section 2.1.3.3 was used, consisting of 2625 µL Col type I, 1000 µL growth media, the dropwise addition of 90 µL of 1M NaOH, 875 µL Geltrex™ and finally $5x10^7$ cells previously resuspended in 500 µL growth media. A total 2,500 µL of the cell-laden gel mixture was pipetted into two tube moulds and the ends were sealed with sterilised parafilm. The cell-gel suspension was incubated for 1-2 hours to allow gelling at 37°C and 5 % CO_2. Following gelation, hydrogels were removed from their moulds and placed in growth media in Nunc™ Cell Culture/Petri Dishes (Thermo Scientific, cat. no. 150318). Due to the size of the cell-hydrogel model and to avoid fungal infections, 1 % (v/v) Amphotericin B (AmB; Gibco, cat. no. 15290026) was added to the cell culture (**Figure 2.1**).

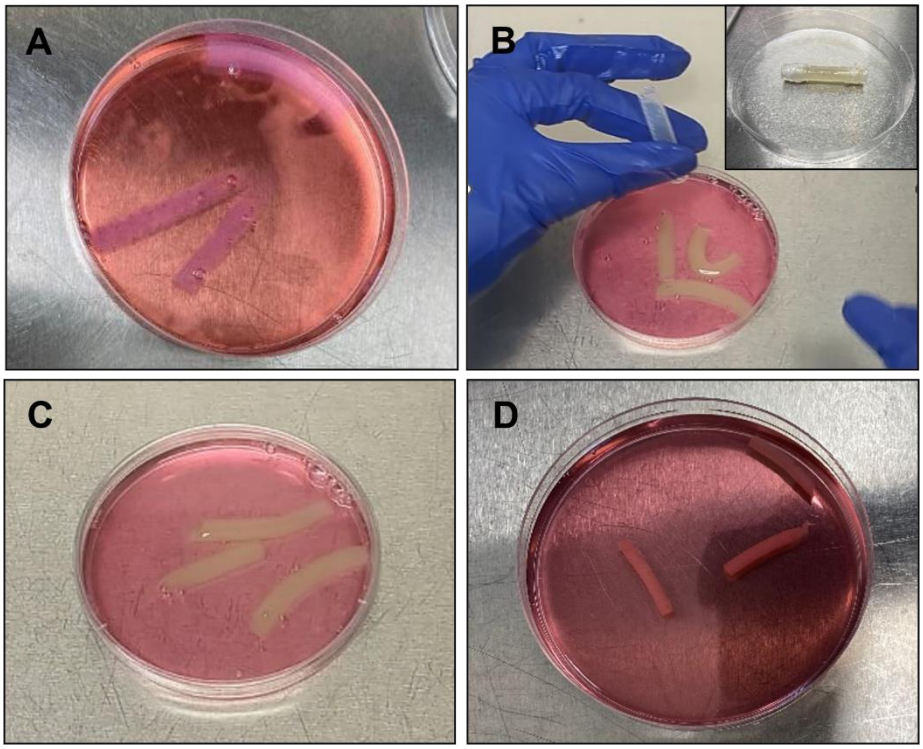

Figure 2.1 Preparation of 'large' cell-hydrogel rods (v2). (A) *Acellular hydrogels.* ***(B)*** *Casting and removal of hydrogel rods, following thermal gelling.* ***(C)*** *Hydrogel rods in growth media before 48 h incubation (D-2).* ***(D)*** *Hydrogel rods after 48 h incubation (D0).At this stage, the cell-hydrogels decreased in size and were subjected to differentiation and tensile strain.*

The hydrogels were then stretched using the MechanoCulture T6 (MCT6), following 2-day incubation under proliferation conditions at D0. The key target features of the final hydrogel rod model were: (1) an elongated fibrillar shape, reminiscent native fibrillar myofibers and myofibrils, (2) anchorage and tethering as with bone and tendon interaction *in vivo* and (3) an optimal size for tethering and post formalin-fixed and paraffin-embedded (FFPE) processing.

2.1.3.4.1 Metabolic activity

Alamar blue assay was performed to determine the metabolic activity of the cells within their matrix. This was assessed in the rod models only, up to 24 h post casting of hydrogels, before differentiation. Acellular hydrogel (negative) controls were used, to determine background fluorescence. The cell-hydrogels were also normalised to the negative controls. Resazurin sodium salt (Sigma-Aldrich, cat. no. R7017) was resuspended in the media of cell models, including an acellular well at a concentration of 3 mg/mL . The cells were incubated at 37°C and 5 % CO_2 for up to 24 h. The resazurin was reduced to resorufin and subsequently, the media was removed and the resorufin was quantified by measurement of the relative fluorescence units (RFU, Ex=530 nm, Em=590 nm) using a Clariostar microplate reader (BMG Labtech, UK).

2.1.3.5 Anchorage and loading using the MechanoCulture T6 (MCT6)

The initial rod model (v1) was anchored and stretched to recapitulate the properties of strain-dependent skeletal muscle. The primary goal of incorporating anchorage and stretching of the model, was to support the orientation and maturation of myotubes within the hydrogel. Hydrogels with a cell density of $1x10^7$ were cultured for 7 days (D7) then the differentiated cell-hydrogel was stretched for further 7 days via the MCT6, (D7MCT6-7) (**Figure 2.2**). The models were therefore cultured for a total of 14 days in defined media 2. The hydrogels were stretched by ~ 100 % (i.e. twice its original length).

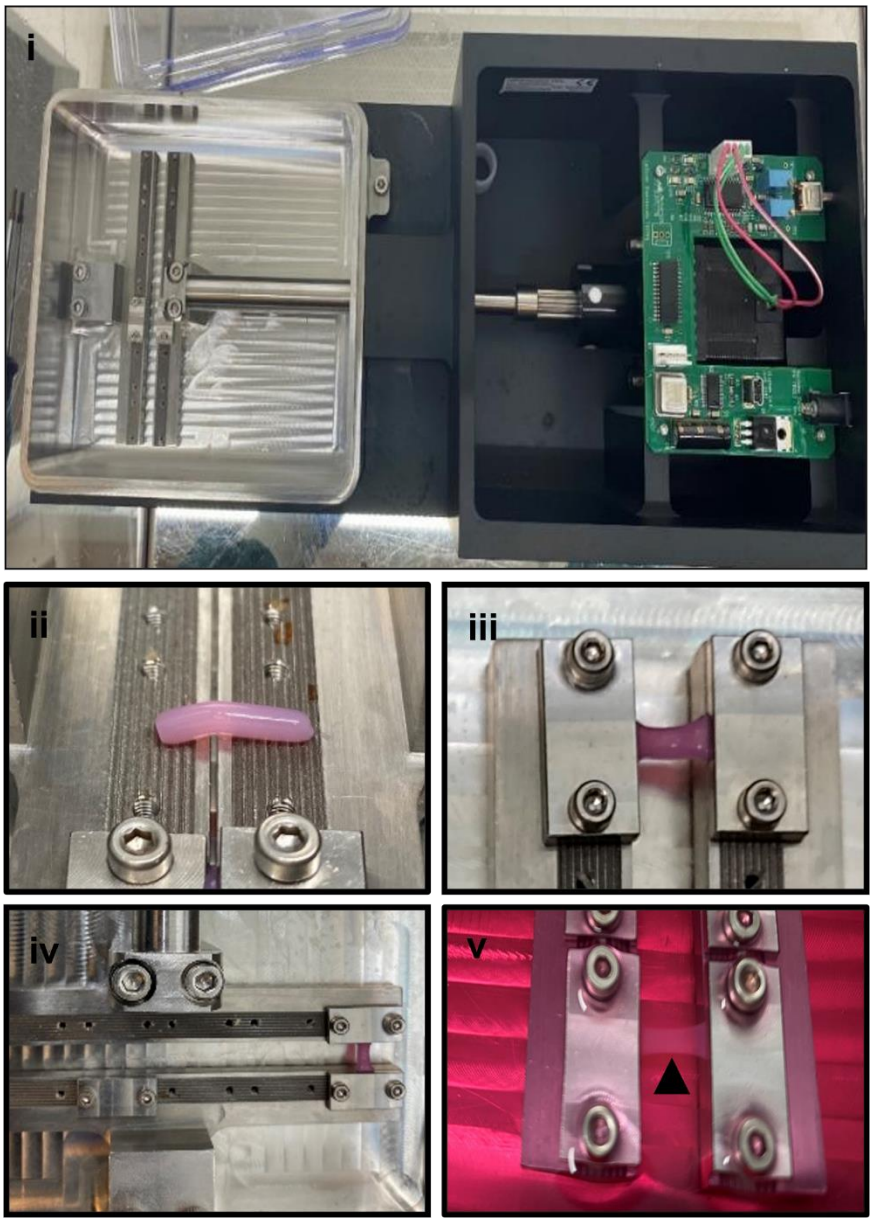

Figure 2.2 ***Tethering and stretching of hydrogels using the MCT6 platform****. **(i)** The MCT6 system consists of an actuator and screw-driven clamps. **(ii)** The cell-hydrogel rod (v1) placed on sterile grip bars. **(iii, iv)** The anchored hydrogel between two clamps being uniaxially stretched hydrogel. **(v)** 30 mm stretched hydrogel in differentiation conditions, black arrow shows point of tension in the centre of the gel).*

2.1.3.6 A manual tensile strain-inducible platform (MTSIP)

The concept of anchorage and strain was carried forward to develop a custom system that was designed and 3D printed together with Mr David Chorlton, University of Manchester. The aim was to generate a system to facilitate simultaneous tensile strain and electrical stimulation of cell-hydrogels (**Figure 2.3**). The final 3D CAD design is included in the Appendix (**Figure A1**). The first step of the design process consisted of the development and 3D-printed stage with fixed arced ends, with pin-like structures. Rod v1 (Section 2.1.3.4) was placed between the arced points, to support the pinning of the tubular-shaped hydrogel ends. This system produced poor grip and tension which resulted in a slack centre region of the cell-hydrogel. Furthermore, the ends cell-hydrogels were not secured and therefore, detached in culture later, particularly following 48 h, as they reduced in size due to contraction. After several design iterations, a 3D printed strain-inducible system was developed. The system consisted of a sliding unit (**Figure 2.3, Ai,** slider), which enabled the cell-hydrogel to be stretched first, by sliding across a stage (**Figure 2.3, Ai,** stage). Anchored clips (**Figure 2.3, Ai,** clip) with multiple projections, provided a strong grip (**Figure 2.3, Ai,** grip region) and ensured fixed tethering. The slider, clip, and grip regions all formed components of the hydrogel anchor arrangement (**Figure 2.3, Ai,** anchor). To compensate for shrinkage and ease of tethering the model, a larger (v2) rod was developed. Lastly, the tensile strain was controlled via a 'spacer' (**Figure 2.3, Ai**, spacer) with a viewing window to observe potential contractions in the stretched region of the cell-hydrogel. The spacer was placed in the central region of the cell-hydrogel after sliding and anchoring. A MTSIP was developed (**Figure 2.3, Aii, B**) which fit into a single well of a 6-well plate (**Figure 2.3, D**). The cell-hydrogel models, stretched via MTSIP were cultured in 5 mL of defined media 3, up to D21.

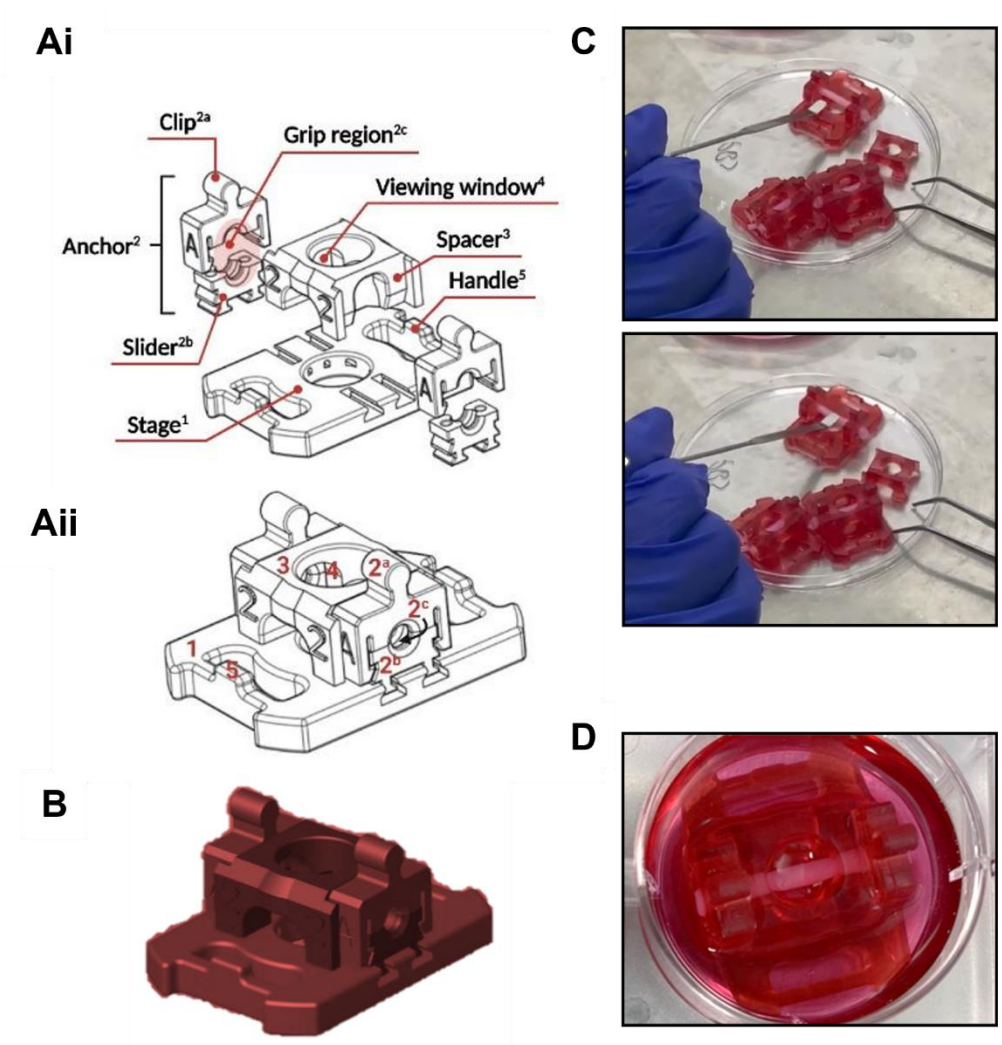

Figure 2.3 Presentation of the custom 3D manual tensile strain-inducible system (MTSIP). (Ai) *Drawing of the annotated disassembled MTSIP components. Aii) Drawing of the annotated assembled system components. The anchor components consist of a top feature that clips over a bottom sliding element for stretching of anchored hydrogels. The anchor components assemble to grip the ends of a hydrogel rod, supported by ridged surfaces in the grip region.* ***(B)*** *A 3D image of the assembled MTSIP.* ***(C)*** *Demonstrating the deformation of a 30 mm stretched, and anchored cell-hydrogel with excess gel at the ends.* ***(D)*** *The complete MTSIP-cell-hydrogel system with finished ends, in a standard Nunc™ 6-well dish with 5 mL of media.*

2.1.3.7 EPS

Cells were seeded in 6-well culture dishes with integrated electrodes (**Figure 2.4**). These dishes supported the IonOptix the stimulation system. Models were electrically pulse stimulated using the C-Pace EP Stimulator (IonOptix) (**Figure 2.4**). The strength of stimulation, the rate at which the electrical pulses were delivered, and the length of each EPS pulse was modulated by the stimulator. The C-dish and C-Pace EP were connected via a ribbon cable that provided access to the field stimulating electrodes in the dish. Carbon electrodes on the C-Dish™ (BD Falcon, IonOptix , cat. no. 353846) were placed into compatible 6-well culture dishes with cells in media. Bipolar pulses delivered 20 V, 1 Hz and 10 ms to cells via media contact. The C-dish was sterilised with 70 % IMS (Fisher Scientific, cat. no. M/4470/17), followed by UV sterilisation for 15 minutes before use. After several uses, the electrodes were gently brushed, and the C-dish was placed in distilled water overnight. An Olympus CK40 microscope (Evident Corporation, Tokyo, Japan) and Moticam 1080 camera (Motic, Hong Kong) captured ~20-second recordings of contractions, with the 2D and 3D models, connected to the C-Pace EP and C-dish and stimulated (+ EPS) or unstimulated (- EPS).

A single EPS protocol was selected based on previous literature (Nikolić *et al.*, 2017), following optimisation of voltage and frequency, to achieve contractile fibres visualised by microscopy as twitching myotubes. Final bipolar pulses delivered of 20 V, 1 Hz and 10 ms via media contact to cells (+ EPS). Time-matched unstimulated control cells (- EPS) were kept in the incubator in serum free media (SFM). The *in vitro* 'exercise' regime selected was determined by the type of physiological mimicry desired and was characterised as acute and chronic exercise. For 2D models, acute exercise consisted of a single bout of stimulation of 1 h or 3 h, while continuous stimulation of 6 h or 24 h, mimicked chronic exercise. The cell-hydrogel samples were Formalin Fixed and Paraffin embedded (FFPE) and subsequently sectioned for analysis. 3D models underwent the same EPS protocols as in 2D except cell-hydrogels remained under tensile strain via the MTSIP for 21 days. The 3D model was subjected to 1 h of EPS on D21 as the acute stimuli and subsequent daily 1 h EPS from D16 to D21 as the chronic stimuli.

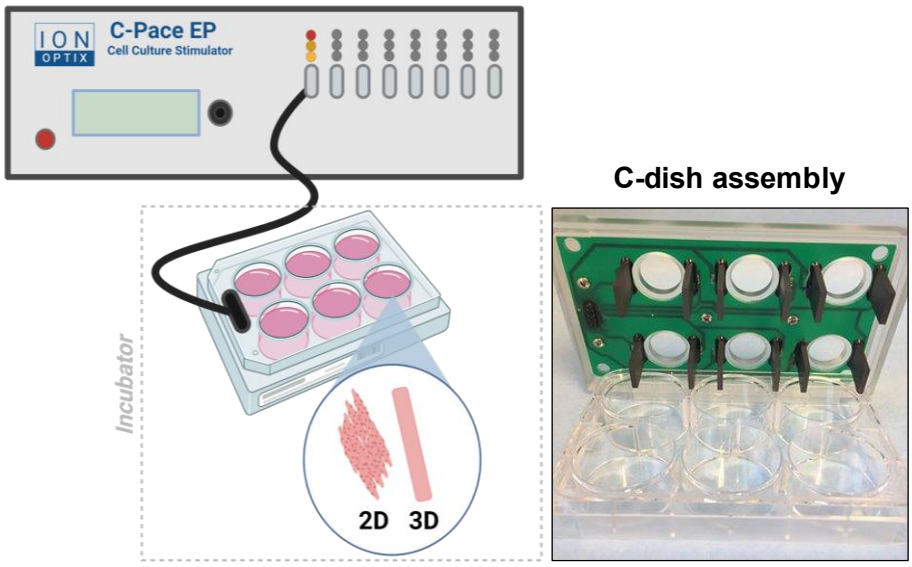

Figure 2.4 Culture pacing system and assembly for stimulation experiments. *The C-dish is a two-part assembly consisting of a standard 6-well plate and a plate lid with carbon electrodes attached. The C-Pace EP connects to the C-dish via a ribbon cable that provides access to the field stimulating electrodes inserted in the culture well with media. The C-dish with C2C12 models of SkM are placed inside an incubator at 37°C and 5 % CO_2. Cartoon created in Biorender.com.*

2.2 Histological and Immunofluorescence staining

2.2.1 Sample preparation

Cell-hydrogel samples underwent FFPE, according to standard Leica histological protocols. Briefly, samples were fixed for 24 hours in 10% neutral buffered formalin (Merck). Then, on an automatic benchtop tissue processor (Leica TP1020), samples were dehydrated in IMS, cleared in Xylene substitute (Sub-X; Leica microsystems) and embedded in melted paraffin wax (Leica microsystem). Tissue sections of 4-6 µm were mounted onto X-tra™ adhesive glass slides and dried at 37°C. The sections were stored at RT until analysis. In preparation for staining, slides with sections were deparaffinised in Sub-X (3x5 min). Prior to staining, sections were rehydrated in graded IMS (100 % x 2 min, 90 % x 2 min, 70 % x 2 min) and rinsed in water. For batch processing and longer-term storage, fixed hydrogels were kept in 30 %distilled H_20, 70 %IMS.

To elucidate the morphology, organisation, and spatial distribution of cells within 3D structures, a cell-hydrogel was sectioned serially. Regional sections were selected to represent the 3D model. Reliable comparison of hydrogel models required comparison of sections from similar regions. Therefore, upper (U), central (C) and lower (L) longitudinal central sections were obtained from experimental models (**Figure 2.5**).

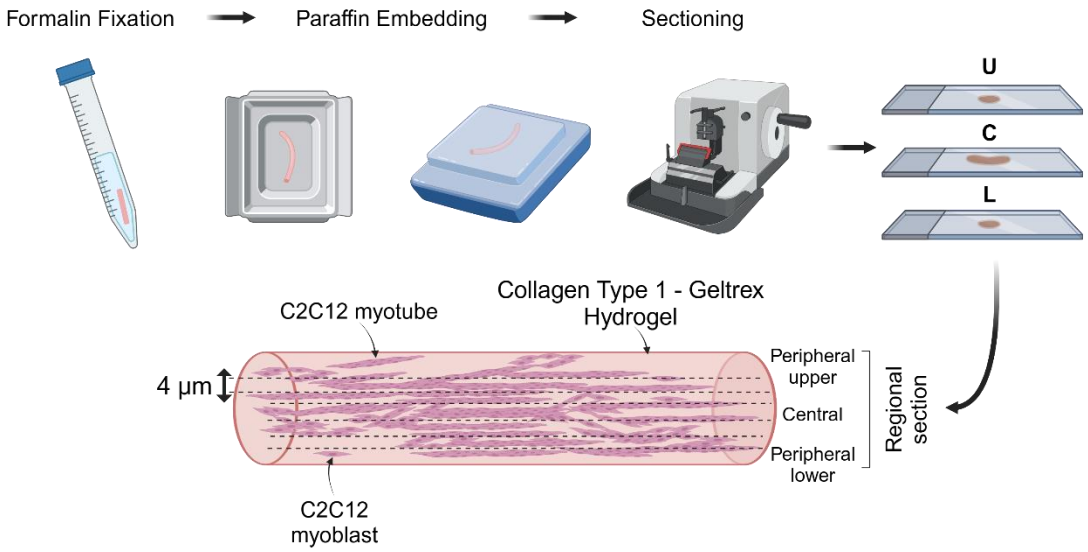

***Figure 2.5 Schematic of direction of embedding and sectioning of cell-hydrogel rods**. Cell-hydrogels are into 4 µm longitudinal sections before staining for analysis. Upper and lower peripheral sections are essentially obtained from peripheral regions of the hydrogel. Sections are U , Upper; C, Central; and lower, L sections.*

2.2.2 H&E and Masson's Trichrome

H&E (Mayer's Haematoxylin, Merck) staining was completed to assess the cellular morphology within the 3D models. Mayer's Hematoxylin was applied to 4 µm sections for approximately 3 min to stain the nuclei (dark purple). Sections were then blued in running tap water for 6 minutes before being subjected to a 1 % aqueous Eosin Y solution (Leica biosystems) for 4 min to stain cytoplasmic regions (pink/red). Subsequently, the sections underwent dehydration in IMS for 5 minutes, repeated thrice, and the IMS was clarified using Sub-X for 5 minutes, repeated thrice. Finally, the sections were mounted with 1-2 drops of Pertex (Leica biosystems) per slide, and 22 x 50 mm Academy glass coverslips (Smith Scientific, cat. no. NPS13/2250) were affixed. Masson Trichrome (Methyl Blue) Stain Kit (Atom Scientific, cat. no. RRSK20) was utilised to differentiate the myofibers from the collagenous matrix in the hydrogel. The steps were followed as per the manufacturers protocol, but briefly 4 µm sections underwent staining with Weigert's Iron hematoxylin for 20 min, followed by rinsing in a 1 % acid alcohol solution and blueing in tap water. Ponceau fuchsin was applied for 5 min, and differentiation occurred in phosphotungstic acid for 15 minutes. Subsequently, samples were directly transferred, without rinsing, into a methyl blue solution for 5 min. Sections were then rinsed with water, dehydrated in IMS, and cleared via Sub-X. Finally, sections were mounted and fixed as described above. All H&E and MT images were taken on a Leica DMRM microscope and viewed on Wacom Cintiq 27Q creative pen display.

2.2.3 Immunofluorescence

2.2.3.1 2D C2C12 cells

Cells were seeded on 22 x 22 mm Academy squared glass coverslips (Smith Scientific, cat. no. NPS13/2222) that were previously sterilised and washed with 70 % IMS and PBS, at a cell density of $5x10^5$ cells/mL in 6-well plates. Cells were switched to differentiation media (day 0, D0) and fixed with ice-cold methanol (Fisher Scientific, cat. no. M/3950/17) for 15 minutes at -20°C on day 1 (D1), day 3 (D3), day 5 (D5) and day 7 (D7) of differentiation. Thereafter, cells were washed with 0.5 % (v/v) Tween-20 (Sigma-Aldrich, cat. no. P1379) in PBS (PBST) 3 times for 4 minutes each, and subsequently blocked with 1 % (w/v) Bovine serum albumin (BSA; Sigma-Aldrich, cat. no. A7906), 75 % (v/v) tris-buffered saline (TBS; 20 mM Tris (hydroxymethyl methylamine, Fisher Chemical, cat. no. T/3710/60), 150 mM Sodium chloride (NaCl, Fisher Chemical cat.no. S/3160/60), pH 7.5 and 25 % (v/v) goat serum (Merck, cat. no. G9023) for 2 hours at room temperature (RT). Cells were then probed with primary antibodies diluted in blocking solution and incubated overnight at 4°C, in a humidified environment with gentle agitation. Successively, cells were washed with PBST three times, for 4 min each and subsequently probed with fluorophore-conjugated secondary antibodies diluted in

blocking buffer for 30 min at RT. The antibodies used, and their corresponding dilutions are listed in **Table 2.1**. Cells were finally washed with PBST as before and coverslips were mounted using VECTASHIELD® HardSet™ Antifade Mounting Medium with 4′,6-diamidino-2-phenylindole (DAPI) (Vector Laboratories, cat. no. H-1500). In the instance where primary antibodies conjugated to fluorophores were used, no secondary antibody was applied afterwards. Application of ActinRed™ 555 ReadyProbes™ was performed following fixation and washing of cells. Two drops of F-actin probe per 1 mL of PBST was added to each well, containing cell-adhered coverslips. After 30 minutes, the cells were washed in PBST and mounted as mentioned earlier.

2.2.3.2 Cell-hydrogel sections

To characterise the structural and developmental features of the cell-hydrogel model, IF was performed for the primary antibodies followed by secondary antibodies (enlisted in **Table 2.1**) to visualise the staining. After deparaffinisation and rehydration, enzymatic antigen retrieval was performed by placing sections of the cell-hydrogel in 100 µg/mL of α-chymotrypsin A (Sigma-Aldrich, cat. no. C4879) from bovine pancreas in 0.1 % (w/v) Calcium Chloride dihydrate (Merck, cat. no. 10035-04-8) in TBS, warmed to 37°C. Sections were then permeabilised in in 0.05 % (v/v) Tween-20/TBS for 15 min was then blocked in 1 % (w/v) BSA in 75 % (v/v) TBS and 25 % goat serum (Sigma-Aldrich, cat. no. G9023) for 2 h at RT. After the blocking step, sections were incubated with primary antibodies in 1 % BSA/TBS overnight, at 4°C in a humidified environment. The following day, 3 washes in 0.05 % (v/v) Tween-20/TBS was performed followed by the incubation with secondary antibodies in 1 %BSA/TBS for 1 hr at RT. Three more washes were performed and then VECTASHIELD® HardSet™ Antifade Mounting Medium was used to mount the coverslips. F actin was applied as above.

Table 2.1 List of antibodies for IF staining. *Published species reactivity is as per the manufacturer.*

Antibodies	Supplier	Catalog No.	Final concentration
Rabbit anti-Sarcomeric α-actinin	Abcam	ab137346	10 µg/mL
Mouse anti-Myogenin (F5D)	Abcam	ab1835	5ug/mL
Mouse anti-Myosin 4/MF20 eFluor™ 660	Thermo Fisher Scientific	50-6503-82	10 µg/mL
Rabbit anti-Dystrophin	Abcam	ab15277	10ug/mL
Rabbit anti-MYF6	Thermo Fisher Scientific	PA5-97990	10 µg/mL
ActinRed™ 555 ReadyProbes™ (Rhodamine phalloidin)	Invitrogen™	R37112	~5.2 U/mL
Goat anti-Rabbit, AlexaFluor 488	Abcam	ab150077	2µg/mL

Goat anti-Mouse, AlexaFluor 488	Abcam	ab150113	2µg/mL
Goat anti-Rabbit, Cyanine5	Thermo Fisher Scientific	A10523	4µg/mL
Rabbit IgG, Isotype Control	Abcam	ab37415	10 µg/mL
Mouse IgG1, kappa (15-6E10A7), Isotype Control	Abcam	ab170190	5ug/mL
Mouse IgG2b kappa Isotype Control (eBMG2b), eFluor™ 660	Thermo Fisher Scientific	50-4732-82	10 µg/mL

2.3 Imaging

2.3.1 Confocal Zeiss LSM 800

Images were acquired using a Zeiss LSM 800 confocal microscope (Germany) For 2D analyses, three random regions per slide were imaged on D1, D3, D5, and D7 to assess four protein markers: myogenin, F-actin, α-actinin, and MyHC. Myotube differentiation in 2D was assessed through immunofluorescence (IF) imaging and quantified as the fusion index, calculated as the percentage of nuclei within myotubes containing two or more nuclei relative to the total nuclei per field of view. The number of myotubes per field of view for each experimental condition also indicated the morphological differentiation potential.

For 3D hydrogel analysis, orthogonal projection of a Z-stack, of automatically calculated increments, produced a 3D projection. The Zeiss ZEN 2.3 (blue edition) software was used to delineate the areas of protein expression, then automatically calculated their *mean area of fluorescence* and *mean fluorescence intensity (MFI)* (**Figure 2.6**). Any aggregated cells located outside or at the edge of the tissue were excluded from the analysis to focus on cell processes within the hydrogel (**Figure 2.6, Aiii**). Three to six regions were obtained for four protein markers including myogenin, F-actin, α-actinin, MyHC and dystrophin and MRF4 for sections of each experimental condition (**Table 2.2**).

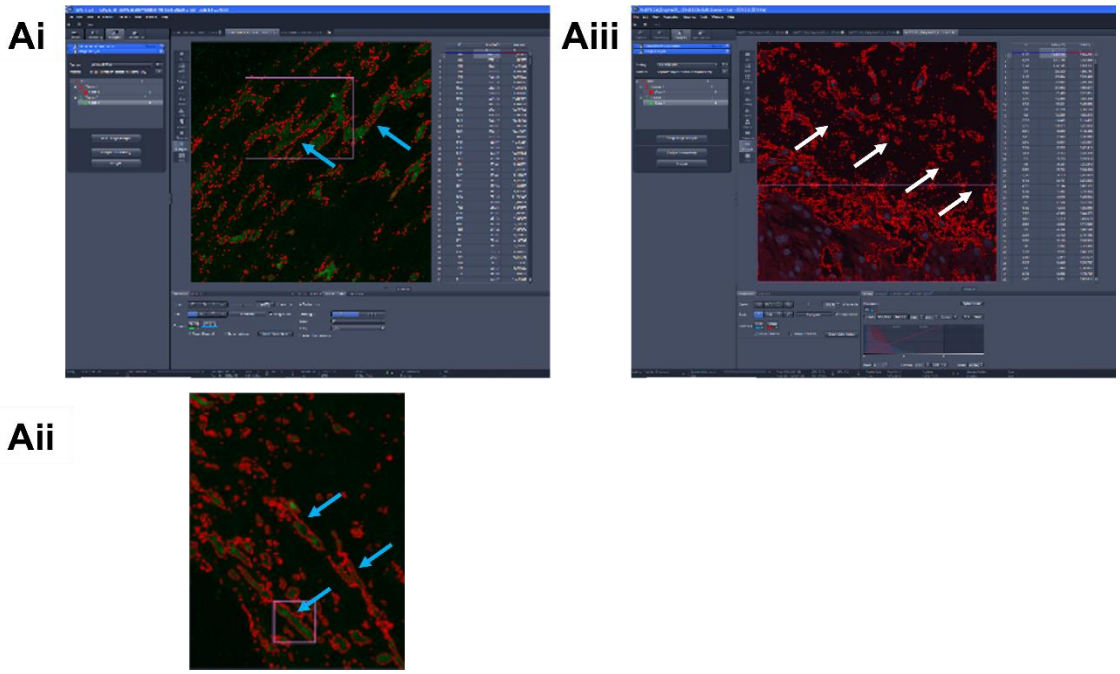

Figure 2.6 Screen capture of representative image analysis using the Zeiss Zen 2.3. (Ai-ii) *Detection of α-actinin staining (green) showing areas of fibre regions within the hydrogel (Blue arrows).* ***(Aiii)*** *Detection of MyHC staining (red) showing areas of cell aggregates and cells outside the tissue section (white arrows). The MFI and the mean area of fluorescence was calculated automatically. Cellular regions (myotube fibres) are outlined in red.*

Table 2.2 Outline of proteins analysed from experimental conditions per 3D cell-hydrogel section, from upper (U), central (C), and lower (L) sections of hydrogel. *Ctrl, control.*

Model		Characterisation marker	Replicate (*n*)	Section region
Acute	**+ EPS & strain**	α-actinin	3	6
		MyHC	2	6
		MRF4	3	6
		Dystrophin	3	6
	- EPS & strain Ctrl	α-actinin	3	6
		MyHC	2	6
		MRF4	3	6
		Dystrophin	3	6
Chronic	**+ EPS & strain**	α-actinin	1	3
		MyHC	2	3
		MRF4	2	6
		Dystrophin	2	6
	- EPS & strain Ctrl	α-actinin	1	3
		MyHC	1	3
		MRF4	2	6
		Dystrophin	3	6

IF images of 3D sections were also observed via an Olympus BX60 microscope and images captured by a digital camera Olympus XC30 and Olympus CellSens software (Media Cybernetics, Buckinghamshire, UK). These images provided analysis for the effect of α-actinin on cellular strain via MCT6.

2.3.2 Scanning electron microscopy (SEM)

3D spheroids only were removed from culture and flash frozen with liquid N_2 and stored at - 80°C. The sample was freeze dried overnight under vacuum at -50°C (Labconco, cat. no. 7752060, S/N 140795377). Before imaging, the samples were attached onto an aluminium stub, coated with carbon (20mA sputter current for 120 s) and images were captured on a Quanta 650 SEM scanning electron microscope (SEM) with a with tungsten electron gun.

2.4 Secretome analysis

The C2C12 models were prepared for EPS by washing and incubating in SFM, to prevent contamination of non-specific proteins. The EPS apparatus and protocol used are detailed in the in Section 2.1.3.7, but principally, 20 V, 1 Hz and 10 ms was applied to for 1 h EPS as the acute protocol and a sustained period of 6 h EPS (2D) or repeated bouts of 1 h EPS over 6 days (3D) as the chronic protocol. Prior to detection of myokines, post-translational modifications were considered for mass spectrometry detection. Post-translational glycosylation can reduce proteomic coverage due to the additional and variable mass of glycans (DeRosa *et al.*, 2022). Thus, its removal reveals the base peptide of interest. The proteins and peptides were then detected via multiplex

immunoassay (MIA) and Liquid Chromatography with Mass Spectrometry with Elevated Energy (LCMS^{E}) (**Figure 2.7**

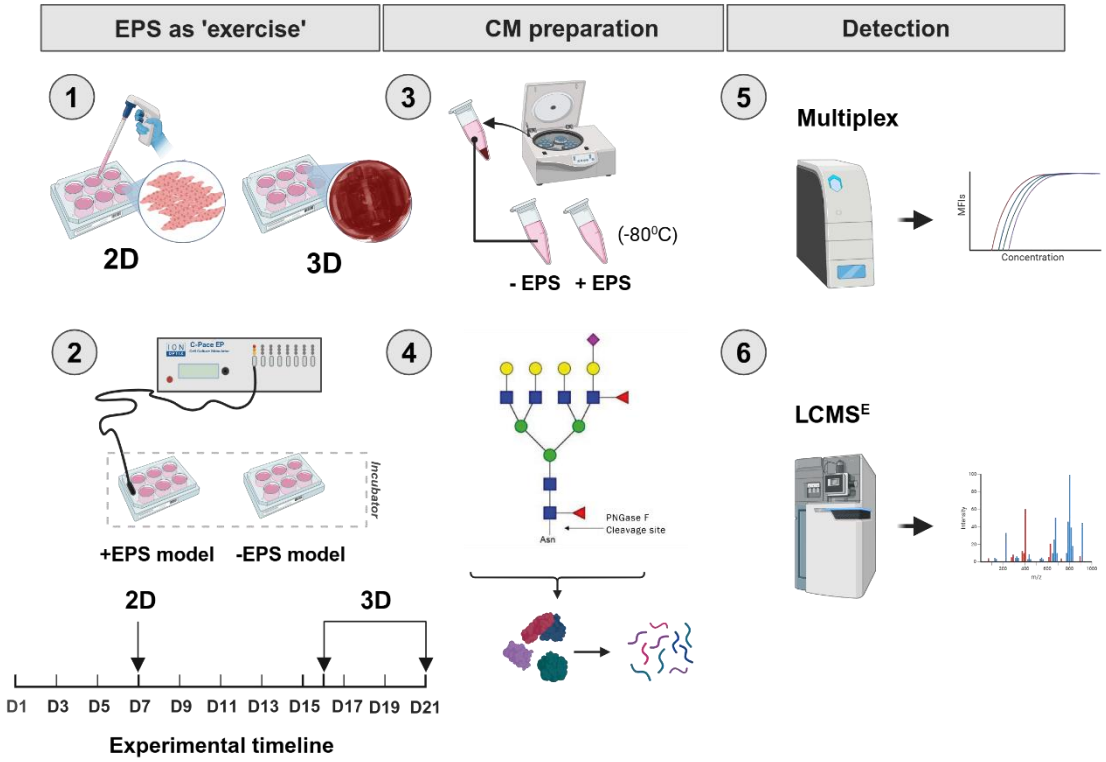

Figure 2.7 An overview of the methodologies employed for detecting myokines in the CM of 2D and 3D C2C12 cultures. ***(1)*** *Differentiated C2C12 cells as 2D monolayers or laden in a collagen-geltrex hydrogel were washed in SFM twice then incubated in SFM for 1h, EPS.* ***(2)*** *2D cells were subjected to a single bout of 1 h or 6 h EPS on D7. The 3D cell-hydrogel was subjected to 1h EPS on day D21 and 1h EPS from day 16 (D16) until D21.* ***(3)*** *CM was collected immediately after EPS and centrifuged twice at 4^{0}C at 1000rpm, to remove dead cells and debris. The samples were stored in LoBind® eppendorf tubes at -80°C until further analysis.* ***(4)*** *Following protein quantitation, samples were prepared for mass spectrometry analysis by deglycosylation and protein digestion.* ***(5)*** *Myokines within CM samples were detected via Multiplex immunoassay (Luminex) or* ***(6)*** *LCMS^{E}. Illustration was created in Biorender.com.*

2.4.1 Protein Quantitation

Prior to secretome analysis, the concentration of CM samples was analysed using the Qubit™ Protein Assay Kit (Invitrogen, cat. no. Q33212), with a range of 12.5µg to 5mg/mL. Unknown samples and known standards were diluted in Qubit™ tubes (Invitrogen, cat. no. Q32856): 2µL CM samples were diluted in 1998µL of Qubit™ buffer and 10µL of assay standards (1-3) were diluted in 190µL of Qubit™ buffer. Samples and standards were incubated for 15 minutes at RT in the dark. The known standard concentrations were used to generate a calibration curve of relative fluorescence units (RFUs) using the Qubit™ fluorometer (via selection of fluorometer mode, protein assay, reagent calculator). Unknown CM concentrations were determined by comparison to the standard RFUs. If the concentration was greater/less than a desired sample concentration of 1mg/mL, the sample was diluted with SFM or lyophilised, accordingly. All samples were transferred to Eppendorf Protein LoBind® tubes (Scientific Laboratory Supplies, cat. no. 0030108094) and undergo preparation for LCMS^E analysis, namely deglycosylation, reduction, alkylation, and digestion steps were performed (**Figure 2.8**).

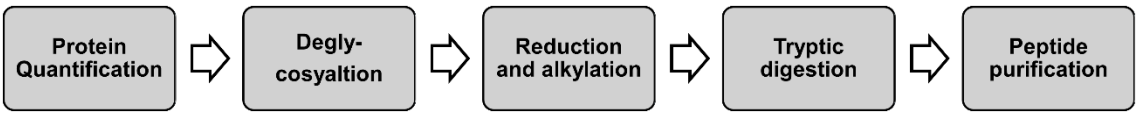

Figure 2.8 Summary of key stages of CM sample preparation for nano-LCMS^E analysis

2.4.2 Liquid Chromatography-Mass Spectrometry with Elevated Energy LCMS^E analysis

2.4.2.1 Deglycosylation of proteins

Proteins were deglycosylated under non-denaturing conditions prior to tryptic digestion. Two microliters of Peptide-N-Glycosidase F (PNGase F; Promega, cat. no. V4831) was added to 15µL (15 µg) of protein mixture (CM) from 1mg/mL CM stock. Following gentle mixing, samples were incubated overnight for approximately 16 h to 18h (overnight) at 37 °C, with constant shaking at 500rpm.

2.4.2.2 Reduction and alkylation of proteins

Fifteen microlitres (15 µg) of deglycosylated CM sample was reduced with 2µL of 85mM DL-Dithiothreitol (DTT; Sigma-Aldrich, cat. no. D0632) in 50mM (v/v) Ammonium bicarbonate (ABC; Fisher Scientific, 10207183) for 40min at 56°C. Subsequently, 7µL of 55mM Iodoacetamide (IAA; Sigma-Aldrich, I6125) in 50mM (v/v) ABC was added to a reduced sample and incubated for 30 min in the dark at RT. The samples were reduced again, to remove excess IAA via addition of 3µL of 85mM DTT in 50mM (v/v) ABC. This final incubation was for 10min in the dark at RT. Samples were then dried using an Eppendorf™ Vacufuge™ Concentrator and the mixed peptide sample was resolubilised in 27µL of 50mM (v/v) ABC, ready for tryptic digestion.

2.4.2.3 Tryptic digestion of proteins

Sequence grade trypsin (Promega, cat. no. V5111), 20µg/mL of (in 50mM v/v ABC) was added to the CM sample at 1:20 (w/w) and incubated overnight at 37 °C, with constant shaking at 500rpm. The following day, the tryptic reaction was stopped by the addition of 0.1 % (v/v) Formic acid in Ultrapure H_20 (FA; HiPerSolv CHOMANORM®, VWR International, cat. no. 84865.180). Sample acidification was checked using pH test strips. Acidified samples were dried again using an Eppendorf™ Vacufuge™ Concentrator. Dried sample peptides were resolubilised with 10µL of 0.1 % (v/v) FA in µL in ultrapure H_20.

2.4.2.4 Peptide purification

Tryptic digests (peptides) were concentrated and purified for sensitivity analysis using C18 ZipTips (Millipore®, Sigma-Aldrich, cat. no. Z720070-96EA): (1) First, the tips were equilibrated by aspiration of 10µl Buffer B (80 % and 20 % (v/v) H_20 and 0.1 % (v/v) FA and disposed into waste, twice ; (2) Aspiration of 10µl of Buffer A (98 %µL in ultrapure H_20 and 2 % ACN and 0.1 % (v/v) FA and disposal to waste, twice; (3) Binding and washing of peptides by aspirating and dispensing (x10 cycles) into sample; (4) Aspiration of 10 µl Buffer A and dispensed to waste (x4) and (5) Eluting with Buffer B in a new

LoBind tube. Samples were dried in an Eppendorf™ Vacufuge™ Concentrator then resuspended in Buffer A (50µL). Samples were transferred to total recovery vials for nanoLC-MS^E. The pH of samples were checked using a Universal pH Indicator Paper (Fisher scientific, cat. no. 12345378).

2.4.2.5 Data-Independent nano LC-MS^E acquisition

Data-independent acquisition via LC-MS^E allowed for parallel multiplex fragmentation (all peptide precursors are fragmented) throughout the separation process regardless of intensity (Silva *et al.*, 2006). The process enabled identification of low abundance peptides and gives a wide proteome coverage and large dynamic range of protein identification. Therefore, this unbiased and continuous untargeted approach is ideal for detection of myokines in secretome. LC-MS^E was performed on an Synapt XS® (Waters Corp, Manchester, UK) – a hybrid, quadrupole, orthogonal acceleration-time-of-flight (QTof) mass spectrometer, coupled with a nano-HPLC for nanoflow chromatography and Zspray^{TM} NanoLockSpray (Waters cat. no. 289004103, S/N 1071014) as the exact mass ionization source.

The tryptic digest (10 µL) was loaded into a nanoEase M/Z Symmetry C18 Trap Column (Waters, cat. no. 186008815, 100A, 5 µm, 180 µm x 20mm). Reverse-phase-trapping was achieved by injecting 97 % of Buffer A, Water with 0.1 % FA (Optima™, Fisher Scientific cat. no. 10229884) at 3µL/min for 3 min. The loading flow rate was 400 nL/min and peptides were separated using a C18 nano-LC resolving column at a flow rate of 0.3 µL/min across a 60 min linear gradient of Buffer B, Acetonitrile with 0.1 % FA (Optima™, Fisher Scientific cat. no. 10678935) from 3 % to 40 %. Buffer B was increased to 60 % within 20 min, then to 95 % and maintained for 7 min to rinse the stationary phase. The column was then equilibrated with 97 % Buffer A for 10 min. Both trapping and resolving columns were maintained at a constant temperature of 40°C to ensure consistent chromatography. The Synapt Q-Tof was operated in LCMS^E positive Electrospray Ionisation (ESI) resolution mode. Samples were analysed for 83 min, over a *m/z* range of 50 to 1500 with a scan time of 0.5 seconds. The capillary, sample cone, and collision energy were 3 kV, 40 V, and 4.0 V respectively. During elevated energy scan, the collision energy was ramped from 14 V to 40 V. [Glu1]-fibrinopeptide (Glu-Fib; Waters, cat. no. 700004729B) standard was used as the lock mass for mass correction (m/z 785.84).

Trypsin Digested Methylated BSA Standard (Agilent Technologies, cat. no. G1990-85001) was used as a reference sample. At least 3 biological replicates were analysed per condition. The analytes were analysed via a data-independent acquisition (DIA) method, whereby molecular structure determination in which all ions within a selected *m/z* range were fragmented and analysed in a second stage of tandem mass spectrometry. Data was collected using MassLynx™ v4.2.

2.4.2.6 Progenesis QIP analysis

The RAW files (Waters) were analysed using the Progenesis QI for proteomics software v28 (QI-P; Nonlinear Dynamics, Newcastle, UK). A Label-free analysis workflow was performed for myokine peptide identification. Raw, profile (continuum) MS^E data files were imported into the software and a quality check of ion intensity maps and alignment variation between runs was assessed. A representative, single run was automatically selected as an alignment reference to align the retention times of all other sample runs. The following automatic peak-picking steps were applied to all runs: a signal-to-noise of 3 times the baseline, no minimum chromatographic peak width specification (to include all ions eluted over the entire run time) and a maximum ion charge of 20+ was applied for detection. This allowed for correction of potential drift in retention time. Following review of proteins, experimental runs were sorted into two groups. Firstly, to analyse a broad range of EPS timepoints in order to confirm the acute and chronic timepoints chosen in MIA analysis. A subsequent review of peak picking and peptide statistics was performed. Peptide IDs were made using the ion accounting workflow as the peptide identification method. Peptide identifications with a mass error tolerance ≤ ±10 ppm were removed from the data set. Further search tolerance parameters applied for protein identification are listed in **Table 2.3**. Protein identifications were made by peptide matches to previously identified myokines and against the mouse proteome.

Table 2.3 Search tolerance parameters and ion matching requirements applied for protein-level identifications. *FDR, false discovery rate; ppm, parts per million.*

Parameter	Result
Digestion enzyme	Trypsin
Missed cleavages	2
Post-translational modifications (PMTs)	Carbamidomethyl C (fixed) Methionine oxidation (variable)
Peptide tolerance	10ppm
Fragment tolerance	Auto
FDR	4 %
Fragments/peptide	1
Fragments/protein	3
Peptide/proteins	1

2.4.2.6.1 Relative quantification

The relative quantitation of protein abundance in each condition was confirmed by peptide discrimination i.e. non-conflicting peptides that were present in more than one protein were excluded. The relative mean abundance of a protein was calculated as the sum of its ion abundances. Thus, the sum of normalised unique (non-conflicting) peptide ion abundances determined the normalised abundance of a corresponding protein from

a condition. Repeated measures ANOVA was automatically performed on Progenesis QIP for proteomics to determine individual differences between conditions. Analysed data was plotted as normalised mean abundance for each myokine (n=3), in GraphPad™ Prism® software (version 10.1.0). Threshold for significances were *p > 0.05, **$p \leq 0.01$, *** p >0.001 and **** $p = \leq 0.0001$.

2.4.2.7 Functional analysis: Gene ontology

Gene Ontology (GO) and statistical overrepresentation analysis were performed on proteins detected from the conditioned media of 2D and 3D ± EPS conditions via LCMS^E. GO terms related to muscle functions were identified to characterise known myokines and pinpoint potential myokines based on functional classifications. Protein accession numbers (UniProtKB) were entered into the PANTHER Classification System's gene list analysis tool. A statistical overrepresentation test compared specific GO terms in the dataset against the mouse genome background. Proteins were categorised into biological process, molecular function, and cellular component domains. Fisher's Exact Test, with a significance threshold of 0.05, was used alongside FDR correction to adjust for multiple testing. The analysis included the number of genes per GO term, fold enrichment, and FDR-adjusted p values. Only parent genes were reported in the results, to control the level of granularity related to gene hierarchy.

2.4.3 Identification of novel myokine candidates

2.4.3.1 Secretome pathway analysis

The secretory pathways of the top 10 proteins with the highest confidence score from the CM of all conditions (2D and 3D ± EPS CM) was analysed to identify potential novel myokines. Confidence scores were determined using 14 software-based criteria. To confirm myokine secretory function and exclude passive release into SFM, FASTA sequences of candidate proteins were obtained from UniProtKB and analysed using SignalP v6.0 to predict canonical secretion via signal peptides (SP). For proteins with SP, cleavage sites and probabilities were reported, with the highest probability SP annotated. Proteins without signal peptide predictions were further analysed using SecretomeP v2.0 to predict non-classical secretion pathways (**Figure 2.9**).

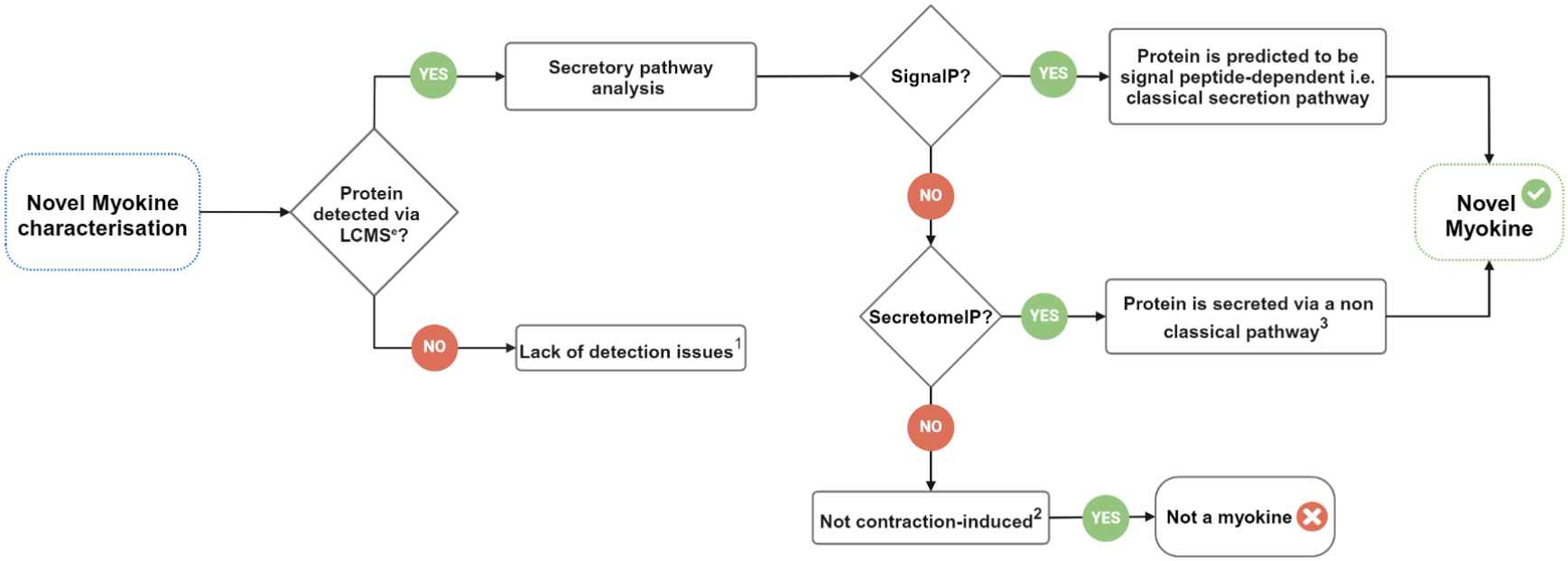

Figure 2.9 A flowchart illustrating the steps towards novel myokine characterisation using proteomic and bioinformatic analysis. *Proteins were identified via global mass spectrometry analysis from secretome of ± EPS conditions. Lack of protein identifications could have been due to low abundance, sample complexity, poor ionisation efficiency and protease resistance (1). Following secretome pathway analysis, if a protein was not characterised via its secretory pathway, it was not contraction-induced and instead could be a serum component, intracellular protein (i.e. released via cell lysis), contaminant (such as BSA, keratin, trypsin) or an extracellular vesicle (2). Proteins secreted via non-canonical pathway and identified via SecretomeP included those with a NN/SecP score exceeding 0.6 and lacking a signal peptide. Validation of novel myokine identification would confirm its presence. Further gene expression analysis would verify muscle-specific expression of the gene encoding protein and downstream functional assays would determine its biological activity. Illustration was created in Biorender.com.*

2.4.3.2 Protein network analysis

To further characterise novel proteins in the context of existing biological systems, protein network analysis was performed using the STRING database (v12.0) as a systemic perspective for understanding the broader biological significance of potential novel myokines, which can be challenging to deduce through direct analysis alone. This approach allows researchers to identify potential interactions and functional associations of a novel protein with other well-characterised proteins. Analysis of networks can infer the potential roles of proteins in cellular processes, predict specific pathway involvement and identify potential targets for further experimental validation. The full string network, including direct physical and indirect functional protein associations was selected. A medium confidence score of 0.4 was chosen as a moderate threshold for including broader range of potential interactions, capturing both well-established and less obvious connections. Kmeans clustering was applied with a minimum of 3 clusters to ensure that the protein network is sufficiently subdivided to capture distinct functional modules or interaction patterns.

2.4.4 Validation of myokine detection via MIA

MIA was performed using a the MILLIPLEX® Mouse myokine magnetic bead assay kit (Merck Millipore, cat. no. MMYOMAG-74K) employing Luminex® xMAP® bead-based technology. The assay kit was utilised, covering 12 well-studied analytes (BDNF, EPO, IL-6, IL-15, FGF21, FSTL1, Myostatin, Irisin, LIF, OSM, OSTN and SPARC) according to their dynamic range, to measure the concentrations of myokines from CM. The experiments were undertaken according to the manufacturer's protocol, using a handheld magnetic 96-well separator (Invitrogen, cat. no. A14179). In brief, standards were provided for each mouse myokine, from which standard curves were generated. CM samples were assayed neat, in duplicate. CM samples (n=3), standards and controls and were analysed using a Luminex MAGPIX® xMAP® instrument (Luminex, Austin, TX) and XPonent 4.2 Software. Concentrations were determined for the aforementioned myokines, relative to an appropriate five parameter logistic (5PL) regression standard curve, in which the mean fluorescence for each myokine standard was transformed into known concentrations (pg/mL). Due to manufacturing issues Osteocrin (OSTN)/ Musclin was only included in a single assay – the 2D acute detection panel. The multiplex analysis was performed for CM from 4 conditions: 2D and 3D acute (1 h) ± EPS, and chronic (6 h) ± EPS. Daily and weekly maintenance of the MAGPIX® was applied using calibration (Merck Millipore, cat. no. MXP-CAL-K25, Lot no. B93651) and verification (Merck Millipore, cat. no. MXP-PVER-K25, Lot no. B92571) kits. The MAGPIX® was maintained via routine software-controlled cleaning protocols using 10-20 % (v/v)

household bleach, 70 % (v/v) ethanol (Fisher Chemical, cat. no. 10048291) and 0.1N NaOH (w/v) (Sigma-Aldrich, S5881) diluted in distilled water. Myokines were detected in xMAP® sheath fluid (Merck Millipore, cat. no. 40-50021).

2.5 Statistical analysis

Data was subjected to Shapiro-Wilk normality test. If parametric, data was analysed by one-way ANOVA test (for comparison of three of more groups), followed by Tukey's correction post-hoc test. Parametric data was presented as mean ± s.d. If non-parametric, data was analysed either by the Mann-Whitney test with Holm-Šídák's post hoc procedure for comparison of two time-matched groups (i.e. - EPS 1 h vs + EPS 1 h , EPS 6 h vs + EPS 6 h) or via Kruskal-Wallis test, followed by Dunn's correction post-hoc test for comparison of more than two groups. Non-parametric data was presented as median with range to provide a more accurate measure of central tendency for non-normally distributed data, with the range presenting the variability within the data. All analysis was performed using GraphPad (v.10.1). Significance threshold was $p \leq 0.05$. Asterisks indicated respective statistical significance as *$p > 0.05$, **$p \leq 0.01$, *** $p > 0.001$ and **** $p = \leq 0.0001$.

3 Development of *In vitro* Skeletal Muscle Models

3.1 Introduction

Review of tissue-engineered constructs in Chapter 1, highlighted the need for further *in vitro* model development. Currently, diverse *in vitro* SkM models exist for drug testing applications (Alave Reyes-Furrer *et al*., 2021; Gholobova *et al*., 2018; Ikeda *et al*., 2017b) and for accurately modelling severe genetic muscle diseases such as Duchenne muscular dystrophy (DMD) (Maffioletti *et al*., 2018) and Pompe disease (J. Wang *et al*., 2021). 3D SkM models have even seen the development of 3D human primary muscle progenitor cells (hMPCs)-derived construct with the capability to restore defects (Kim *et al*., 2018) as well as implantable systems for mice that have generate organised artificial muscle tissue *in vivo* (Costantini *et al*., 2017). Furthermore, size variability and mechanistic approach of models leads to discrepancies in experimental outcomes. Bio-robotic 'ExoMuscle' has been developed to mimic the behaviour of pectoralis major (Xie *et al*., 2023). On the other size spectrum, miniaturized 96-well micro-muscle platforms have been, better for high-throughput study for human SkM (Mills *et al*., 2019). Technological advancements have further complicated *in vitro* SkM model reproduction, increasingly incorporating bioprinting technologies (Costantini, Testa, Mozetic, *et al*., 2017; García-Lizarribar *et al*., 2023; Merceron *et al*., 2015), adding to biomaterial complexity. Nevertheless, even sophisticated systems, such as electrospun nanofibrils in nanohybrid hydrogels (Mao *et al*., 2019), often rely on C2C12 cells, as with the models developed in this study.

Most models have the common goal of producing 3D models aiming to engineer microphysiological, aligned myofibers as functionally organised tissue mimetics (Bettadapur *et al*., 2016; Costantini, Testa, Mozetic, *et al*., 2017; Jiao *et al*., 2018; Maffioletti *et al*., 2018; Mondrinos *et al*., 2021; Shimoyama *et al*., 2010; A. S. T. Smith *et al*., 2012; Velasco-Mallorquí *et al*., 2020). Multidimensional scaffolds with micropatterns to promote cell alignment and elongation of fibres have also been studied (Cha *et al*., 2017). Such models are not easily scalable or replicable in standard laboratory settings, especially for short-term downstream analyses. Existing *in vitro* 3D SkM models (as outlined in **Table 1.1**), fail to replicate the full complexity of native tissue, particularly the tissue maturity observed *in vivo*. Furthermore, many models lack higher order MRFs, such as MRF4. Thus, there remains a need for facile, physiologically mature SkM models.

Mechanical loading as an external stimulus continues to feature in advanced SkM models (Franchi, Reeves and Narici, 2017). Early models have showed that cyclic stretching produced oriented SkM myofibers (Okano and Matsuda, 1997; Shimoyama *et*

al., 2010). More recently, loading has controlled of the orientation of myoblast-like cells to reconstruct them into maturated muscle tissues (Bansai *et al.*, 2019). Further benefits of SkM stretching includes hypertrophy (Aguilar-Agon *et al.*, 2019) and activation and proliferation of satellite cells, which are important to recapitulating models of repair and growth (Passey *et al.*, 2011). Stretching protocols can be produced to mechanically exercise the SkM models, in order to study adaptive responses. The purpose of developing *in vitro* exercise models, also known as 'exercise in a dish', include exploration of the cellular impacts of exercise physiology such as SkM contraction or the activation of exercise-responsive signalling pathways. Additionally, such models facilitate the examination of exercise-induced communication between various cell types, such as secreted factors including myokines. The development of EPS to induce contraction has enabled some protocol comparison between laboratories (Nikolić and Aas, 2019). This study uncovers the systematic development and characterisation of a 3D model, guided by and maturity features outlined in Chapter 1, to determine its physiological relevance and application for secretome study. Several methods exist to stimulate SkM contraction – via optogenetic (Asano *et al.*, 2015; Sebille *et al.*, 2017), mechanical induction (Aguilar-Agon *et al*., 2019; G. Huang *et al*., 2020; Powell *et al*., 2002; Riehl *et al*., 2012) or combinations of external stimuli (Kim, Kim and Asada, 2019), which can all influence the development, differentiation, and function of SkM models. EPS is a widely applied stimuli (Vepkhvadze, Vorotnikov and Popov, 2021) and the most commonly used commercial EPS system is the Ion Optix C-Pace coupled with a C-Dish culture plate.

Within the last 3 decades, tissue-engineered, 3D SkM models have advanced significantly, carefully considering cells, biomaterials and growth factors (**Figure 3.1**), to better replicate the native muscle microenvironment for improved functionality and extended culture durations. However, the complex and dynamic nature of SkM has challenged these advances and researcher-specific criterion for model development has resulted in many different context-dependent models within the research field.

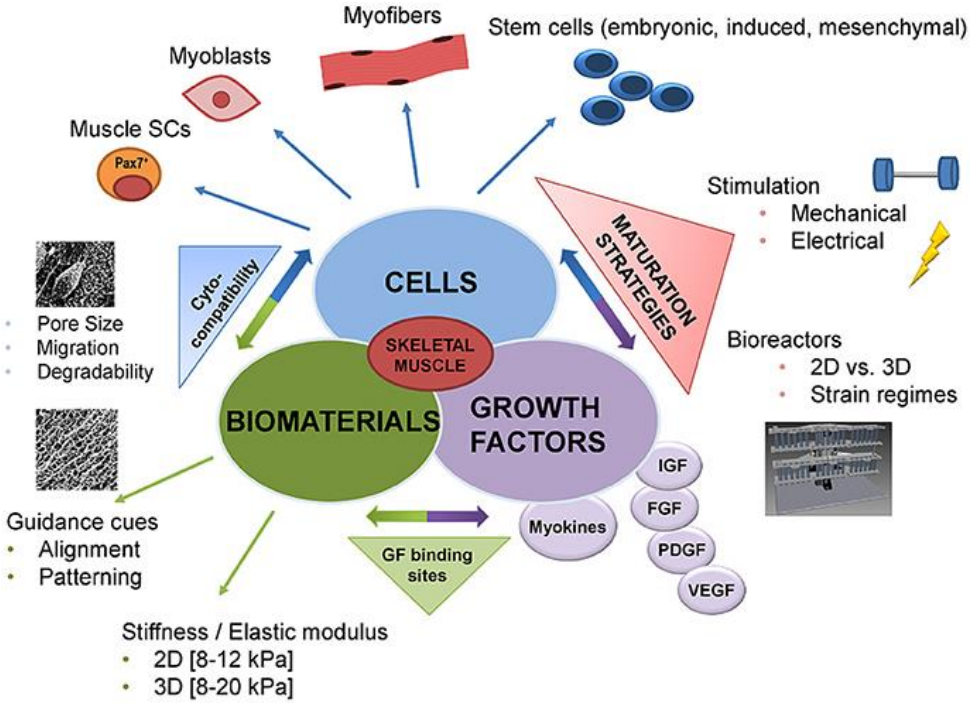

Figure 3.1 Progress in skeletal muscle tissue engineering – from traditional to functional methods. *Historically, tissue engineering has combined biomaterials, cells, and growth factors. Recently, this approach has been refined with new methodologies, enhancing biomimetic strategies. These advancements include cross-linking growth factors to biomaterials, patterning to encourage cellular alignment, multicellular systems, application of external stimuli and dynamic cell culture systems. Together, these approaches were considered in this Chapter to support the development of mature of SkM models. Figure was reproduced from Maleiner et al., (2018).*

3.2 Aims and Objectives

Previously, this thesis reviewed tissue-engineered strategies of *in vitro* models to incite maturity characterisation and presented indicators of functionally mature SkM models (Chapter 1). The aim of the current chapter was to apply that knowledge to develop an *in vitro* SkM models, which could be used to investigate the contraction-induced secretome analysis. Initial work aimed to develop a 2D myotube model, which was characterised utilising SkM maturation phenotypic markers and acted as a basis for the comparative characterisation of a novel 3D model. To develop a 3D model of SkM; substrate composition, model architecture, cell density, differentiation conditions, anchorage and tethering, and EPS conditions were optimised to support SkM phenotype and function. The final 3D model was developed which was electrically pulse stimulated while under strain via a manual tensile strain-inducible platform (MTSIP). SkM models were analysed to investigate their structural, developmental and functional maturity to assess model mimicry and physiological relevance.

3.3 Experimental overview of SkM models

Phenotypic SkM markers were optimised to assess the developmental and structural maturity of a prototypic 2D SkM model, to confirm optimal myotube differentiation and evaluate structural and developmental maturity features. First, a 2D model was established under low serum conditions (Section 2.1.2.1), then supplemented with Insulin-like growth factor 1 (IGF-1, 50 ng/mL) and L-ascorbic acid 2-phosphate (AA2P, 50 µg/mL) to enhance myoblast differentiation and contraction. Following this, a series of 3D models were tested (Sections 2.1.3.1 to 2.1.3.4), considering factors such as morphology, cell density, substrate composition, differentiation conditions, anchorage, tensile strain and EPS. A final 3D model consisted of a Collagen type I and Geltrex hydrogel rod, encapsulating C2C12 cells (Section 2.1.3.4). The model was anchored and tethered using a manual tensile stain-inducible platform (MTSIP) (Section 2.1.3.6) and exposed to EPS protocols (Section 2.1.3.7). Immunofluorescence and histology (H&E and Masson's Trichrome staining) were used to visualise model features (Section 2.2).

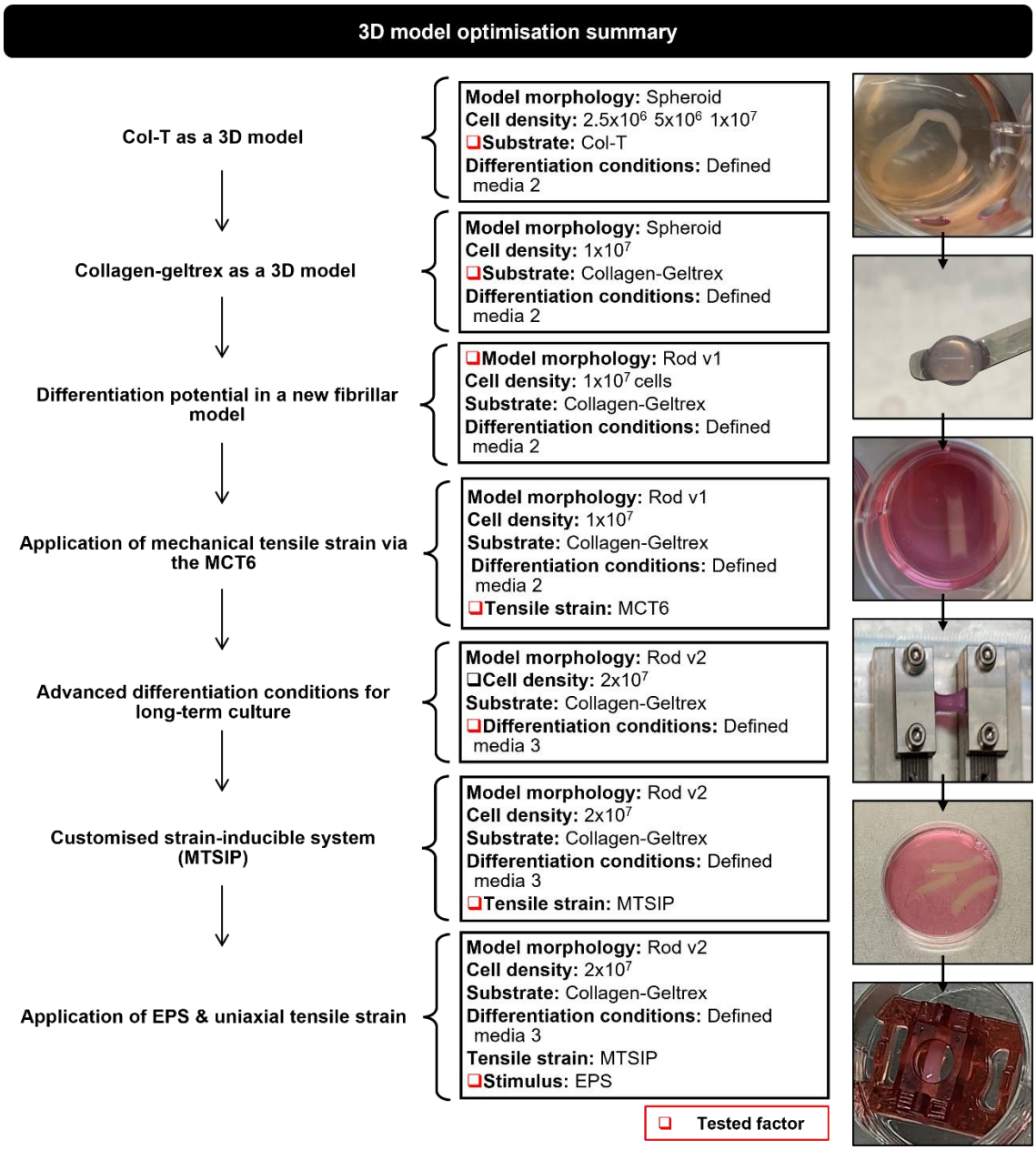

Figure 3.2 3D model development: progression towards a final anchored and stretched SkM model. *Tissue engineering aspects were tested. Two size variations of hydrogel rod models were developed as version (v1) and version 2 (v2) as outlined in chapter 2, section 2.1.3.3. The cell density is per 1018 µL of hydrogel constitution. Media compositions are outlined in sections 2.1.2.1 and 2.1.3.1.*

3.4 Results

3.4.1 Optimisation of a 2D SkM model

A 2D model was developed in standard low sera conditions to promote differentiation. A brightfield time-lapse video of C2C12 differentiation, showing round, single nuclei myoblasts fusing to form elongated, multinucleated myotubes in low-sera conditions (section 2.1.2.1) is included in the appendix (**Appendix data, Table A1, video 1**). The 2D model, under basic differentiation conditions produced distinct myotube fibres by day 7 (D7)*.* This 2D model was characterised by the presence of developmental (myogenin) and structural sarcomeric markers (F-Actin, α-Actinin and MyHC II) (**Figure 3.3 A**). Myogenin was present throughout differentiation (**Figure 3.3 A,** myogenin). The mean fluorescent areas of the remaining markers were quantified. F-Actin area remained persistent day 1 to day 7 (D1-D7) and staining revealed disorganised cells at D1 (24322.5 μm^2) to aligned fibres by D7 (24169.4 μm^2) (**Figure 3.3 Bi,** F-Actin). The mean area of sarcomeric proteins; α-Actinin increased throughout differentiation up to D5 (14297.0 μm^2) and remained consistent up to D7 (14380.6 μm^2). MyHC II was also greatest by D7 (16056.6 μm^2, **Figure 3.3 Bii, Biii,** α-Actinin and MyHC II). Furthermore, the percentage fusion index used to quantify the number of nuclei inside MyHC-positive myotubes as a percentage of the total number of nuclei present, also increased up to D7. D1 vs. D3, D1 vs. D5, D1 vs. D7 (p<0.0001), D3 vs. D5 (ns), D3 vs. D7 (p=0.0011) and D5 vs. D7 (p=0.0162) (**Figure 3.3 Biv)**.This confirmed the differentiation potential of myotubes by D7, indicating it as the appropriate time for EPS application.

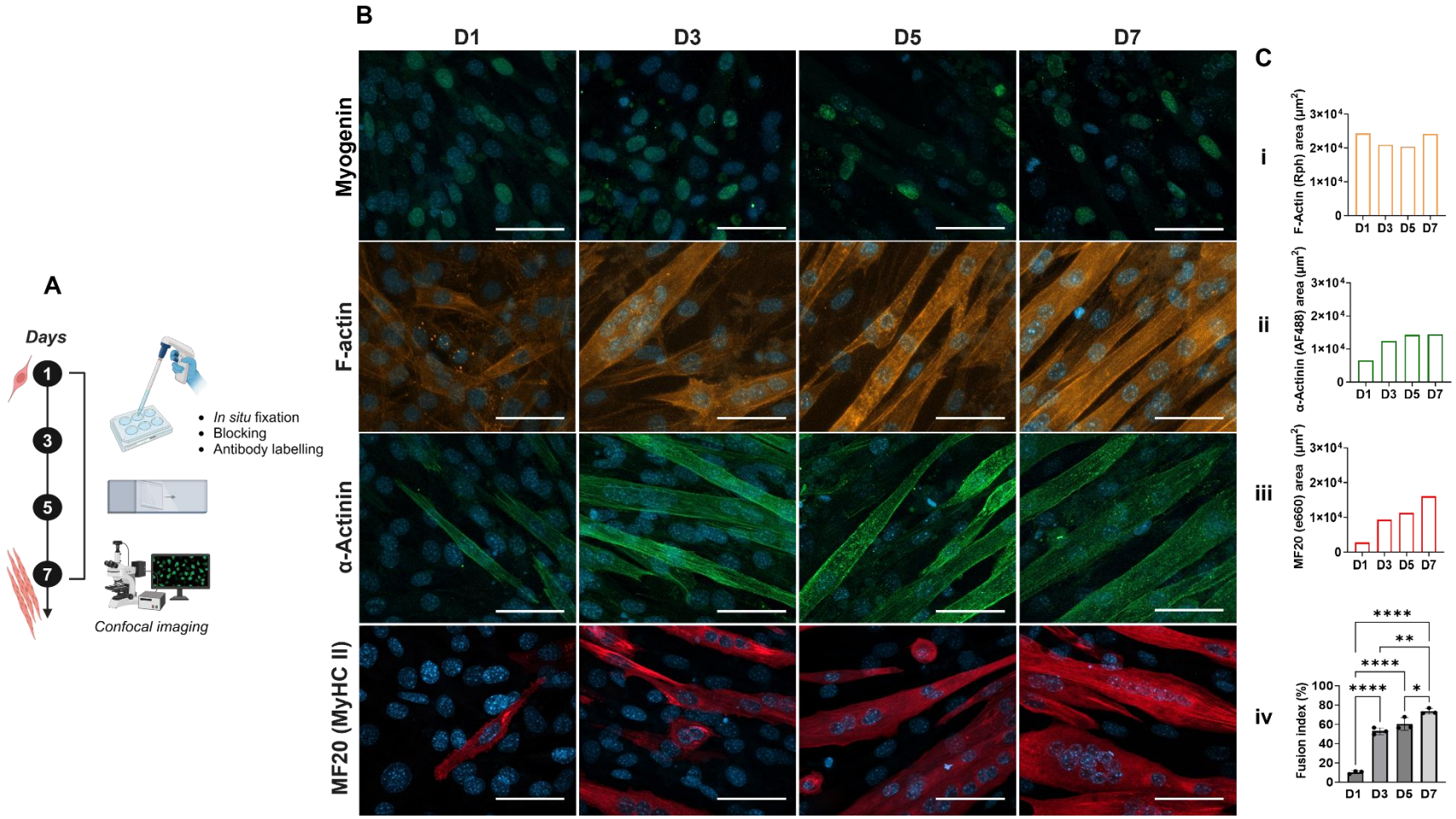

Figure 3.3 Determination of myogenic potential in 2D C2C12 cells. (A) *Schematic of steps for immunofluorescence staining of SkM cells.* ***(B)*** *Merged confocal images of C2C12 myotubes, differentiated for 7 days (from D1 to D7). Cells were stained for myogenin (green) as a developmental marker of maturity, F-Actin (amber), α-Actinin (green) and MF20 (Myosin II heavy chain marker, red) as structural markers of maturity. Cell nuclei were counterstained with DAPI (blue). Scalebar: 50 µm.* ***(Ci-iii)*** *Area of IF staining during differentiation of markers, data is mean (ROI=5, n=1). Rph, Rhodamine phalloidin.* ***(Biv)*** *The percentage fusion index, calculated as the number of nuclei incorporated into MyHC II-positive myotubes as a proportion of the total number of nuclei present, data is mean ± s.d, analysed via One-Way ANOVA followed by Tukey's range test (ROI=5, n=3). Schematic was created in Biorender.*

The 2D model was then adapted as outlined in the Methods (Section 2.1.2.1, to enhance differentiation using IGF-1 and AA2P included in the media. Optimisation demonstrated that a combination of 50 ng/mL IGF-1 and 50 µg/mL AA2P, induced significantly more myotubes (*p=0.0293*) (**figure 3.4, Ai**). The addition of the supplements also altered the fibre morphology during contractions – the mouse C1C12 cells contracted mostly as distinct single myotubes (morphology 1) in defined media 1 (section 2.1.2.1) (**Appendix data, table A1, video 2**), however in defined media 2 (section 2.1.2.1), the 2D model developed three further morphologies. Myotubes contracted as cross-linked fibres (morphology 2) and as merged supercontractions with poor distinction of individual fibres, described as 'sheets-like' contraction (morphology 3) (**Appendix data, table A1, videos 3, 4 and 5**). Furthermore, myotubes exhibited spontaneous contractions, in the absence of external stimuli (EPS), however no deviation in morphology (from morphology 1) was observed (**Appendix data, table A1, video 6**).

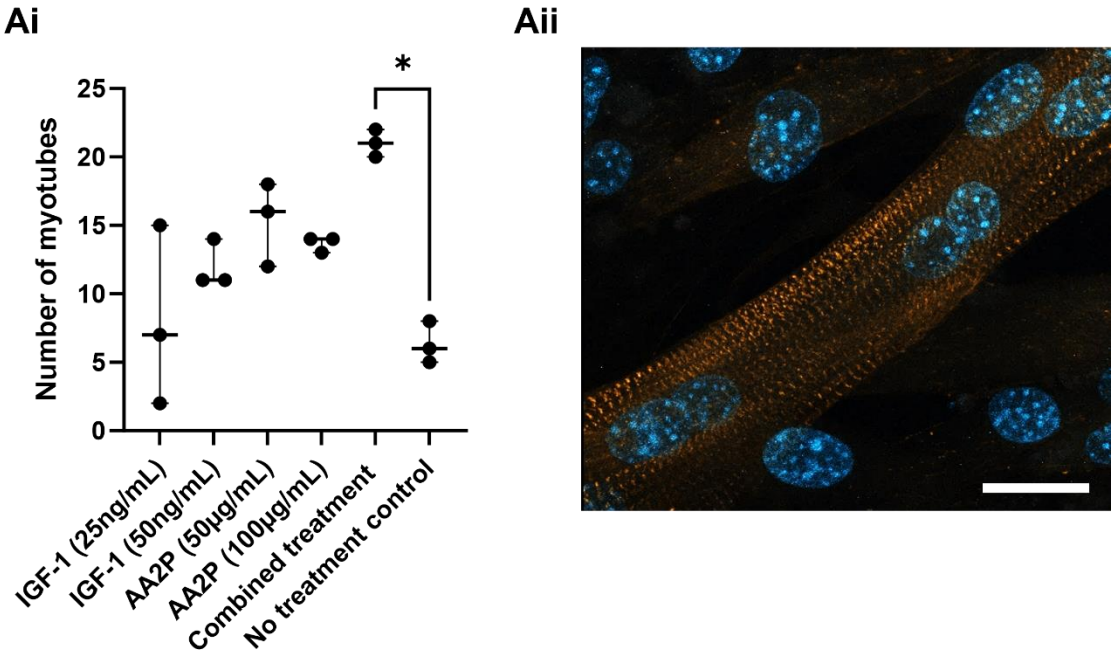

Figure 3.4 The effect of IGF-1 and AA2P on myotube formation. (Ai) *Differences between treatments at two concentrations were compared to a no treatment control on D7 cells and analysed via the Kruskal-Wallis test with Dunn's post-hoc correction, *p=0.0293 (5 ROI, n=3 hydrogels).* ***(Aii)*** *Representative IF confocal micrograph of stained myoblasts at D7 with combined treatment. F-Actin (amber) staining shows characteristic Z-discs marking the presence of sarcomeres. Cell nuclei were counterstained with DAPI (blue); scalebar: 20 µm.*

3.4.2 Optimisation of a 3D model

Two separate 3D cell culture models were developed, consisting of hydrogel-based spheroids and rods. Two substrates were also tested consisting of a Col-Tgel and a Collagen type 1 and Geltrex (Collagen-Geltrex) combination, primarily to optimise myogenic differentiation potential. The influence the physical structure and arrangement of polymer of the substrates on C2C12 myogenesis analysed via histology, SEM and IF imaging.

3.4.2.1 Cell-laden Col-Tgel spheroid

The first 3D model developed was a collagen spheroid model, using Col-Tgel (Sections 2.1.3.1 – 2.1.3.2). A range of cell densities of $2.5x10^6$, $5x10^6$, and $1x10^7$ cell/mL were applied (**Figure 3.5, Bi, ii, iii**) and the models revealed migration of the cells from the gels to the media and wells, even at high cell density (**Figure 3.5, Bi, ii,** black arrows). Histological analysis confirmed poor retention of cells within the gel by D21 in defined media 2 conditions (section 2.1.2.1) **(Figure 3.5, B)**. Furthermore, the model did not retain its shape, became involuted at the circumference and produced a disc-like morphology from D7 in culture (**Figure 3.5 B, Ci**). Therefore, Col-Tgel was considered an unsuitable matrix for the proliferation and subsequent differentiation of C2C12 cells. The model was omitted from further investigation.

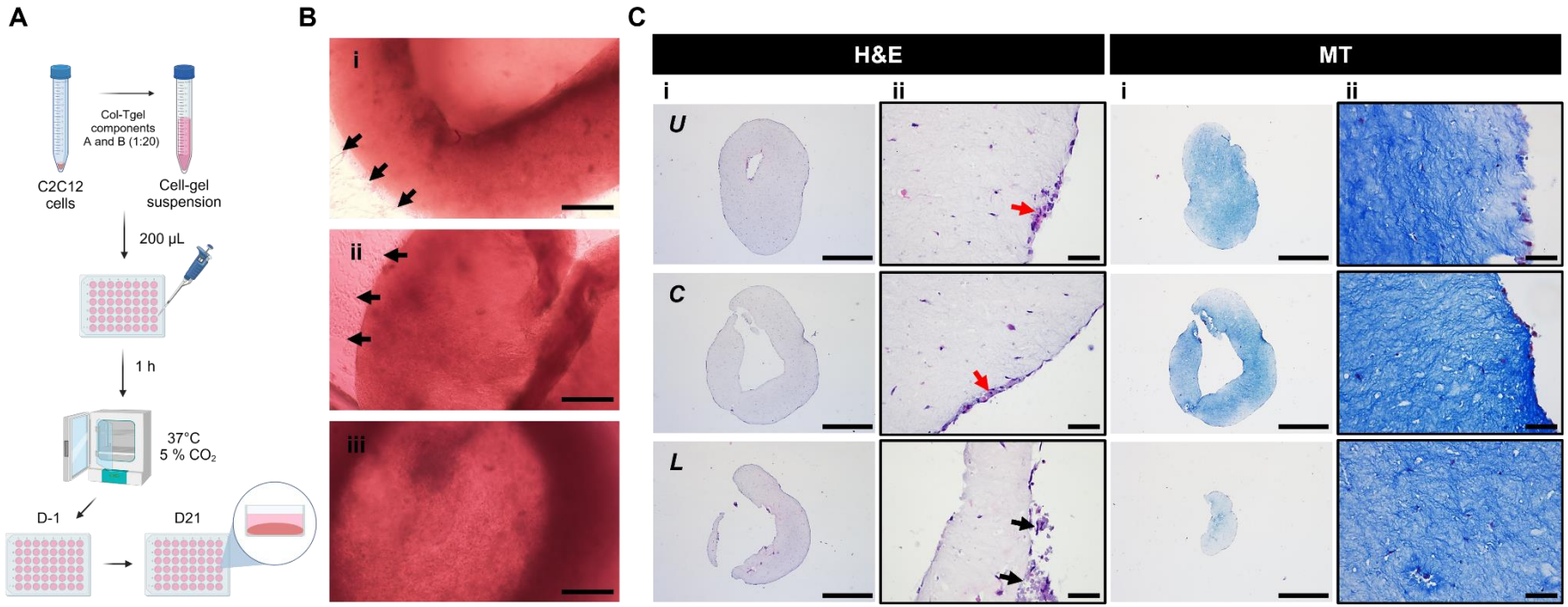

Figure 3.5 Proliferation and differentiation of cells within Col-Tgel spheroid models. ***(A)*** *Schematic of development and culture of Col-Tgel model.* ***(B)*** *Live images of 3 hydrogel spheroids in culture, with the following cell densities (i) 2.5x10^6 cells/mL (ii) 5x10^6 cells/mL and (iii) 1x10^7 cells/mL in 48-well plates in 200 µL of defined media 2 for 21 days. Scale bar: 500µm.* ***(C)*** *H&E and MT of 5x10^6 cells/mL seeded in a hydrogel spheroid. Images represent* ***(Ci)*** *whole gel sections and (****Cii****) higher magnified ROIs (n=1). Regional sections of the cell-hydrogel model are represented as (top-bottom) upper (U), central (C), and lower (L) longitudinal sections. Black arrows show the migration of the cells from the hydrogels to into the surrounding media and well. Red arrows show the alignment of cells at the tissue edge. Scale bar: whole gel sections* ***(i)****, 1mm; higher magnified ROIs* ***(ii)****, 50µm. Schematic was created in Biorender.*

3.4.2.2 Cell-laden Collagen-Geltrex spheroids

Following testing of the Col-Tgel matrix, the substrate of the spheroid model was altered to a Collagen-Geltrex matrix (prepared as described in Sections 2.1.3.1 and 2.1.3.3, **Figure 3.6, A**). This model resembled both oblate and prolate structures (**Figure 3.6**). There was improved cell retention within the gel, with no cell outgrowth (**Figure 3.6, Ci, ii**) compared to that of the cells in the Col-Tgel (**Figure 3.5**). Furthermore, the C2C12 cells demonstrated differentiation potential, observed by the presence of extended fibres, however, they assumed multiple cellular orientations within the spheroid model (**Figure 3.6, Di, ii**). H&E images further revealed dense cytoplasmic regions at the gel periphery (**Figure 3.6, Ei, ii**). In an attempt to align disoriented fibres within the matrix, freely suspended hydrogel spheroids in media were briefly stimulated with 20 V, 1 Hz, and 10 ms pulses for 1 h on D21. While individual myotube fibres were visible, their contractions were not observed. Instead, the entire spheroid responded to EPS, particularly contracting at the periphery (**Appendix data, table A1, video 7**).

SEM imaging (**Figure 3.7**) revealed the surface structure and composition of the model was dense and amorphous (**Figure 3.7 Bi**). However, the interior appeared porous with small dendritic-like projections (**Figure 3.7, Bii**). Evidence of myoblast fusion (**Figure 3.7, Biii**) and myocyte adhesion to the matrix was present by D7 (**Figure 3.7, Biv**). Fibre-like projections protruding from inside the cell-hydrogel model was observed by D21 (**Figure 3.7, Bv**).

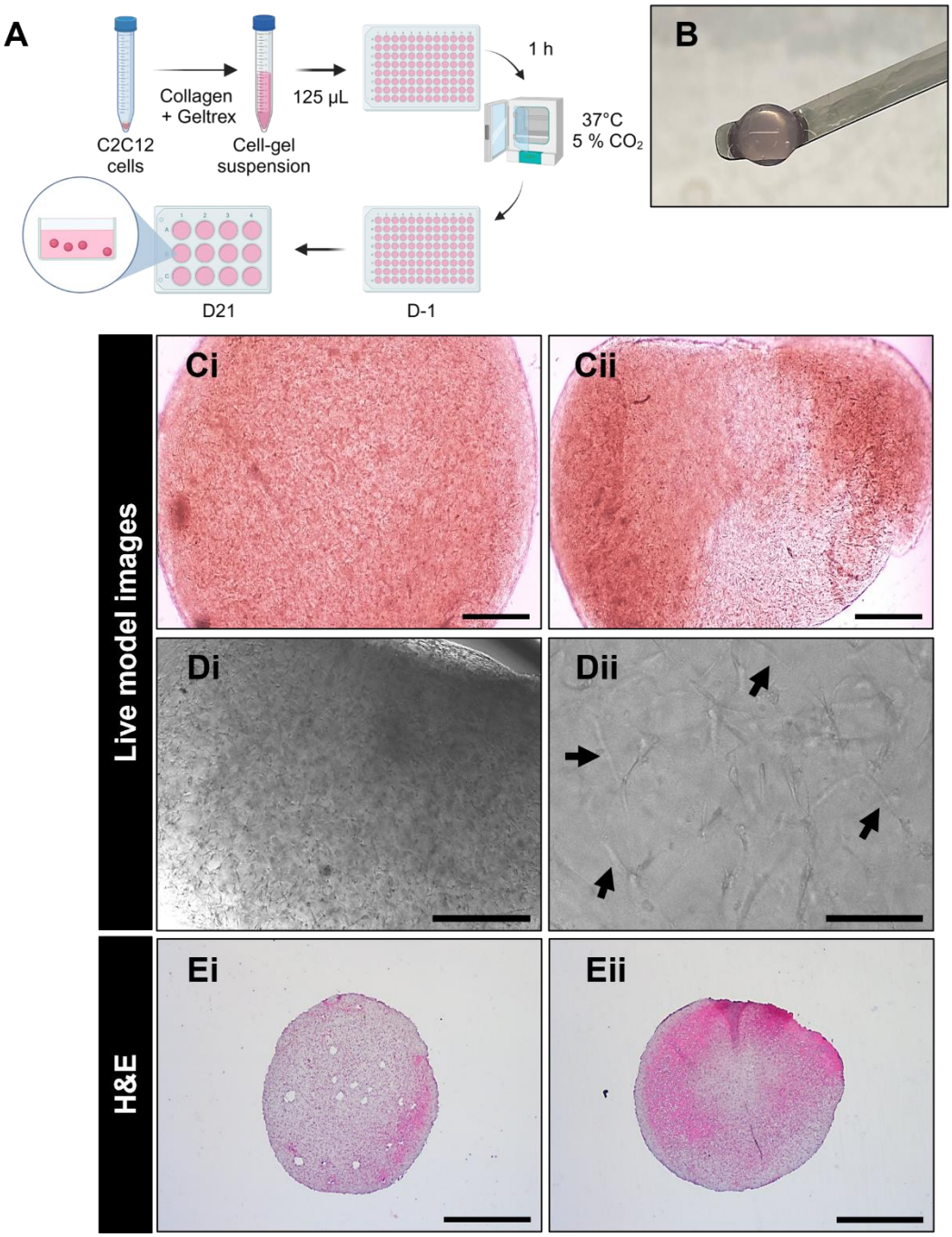

Figure 3.6 C2C12 Collagen-Geltrex spheroid. ***(A)*** *Schematic of development and culture of Collagen-Geltrex spheroid model.* ***(B)*** *Cell-hydrogel spheroid after 1 hour casting, balanced on a spatula.* ***(Ci-ii)*** *Live images of whole cell-laden gels at D7, scalebar: 500 µm.* ***(Di-ii)*** *Differentiation and multidirectional orientation of myotubes within the matrix by D7 (black arrows), scalebar: 1000 µm, 100 µm.* ***(Ei-ii)*** *H&E sections (6 µm) of cell-hydrogel spheroids at D21 under defined media 2 differentiation conditions, scalebar: 1mm. Schematic was created in Biorender.*

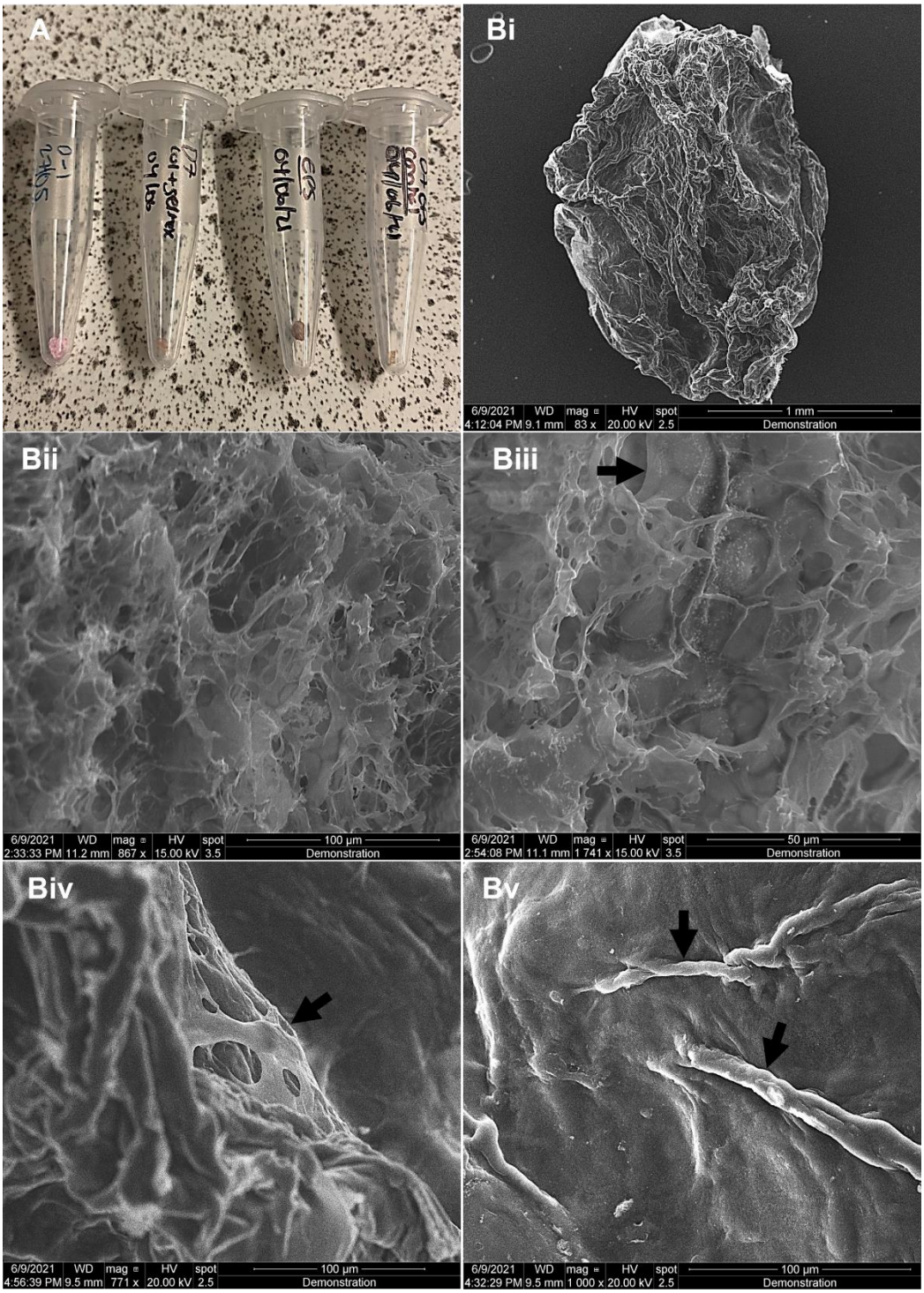

Figure 3.7 Early representative SEM analysis of C2C12 proliferation and differentiation within Collagen-Geltrex spheroids. ***(A)*** *Freeze-dried cell-hydrogel spheroids after culture in defined media 2.* ***(Bi)*** *Spheroid overview, scalebar: 1mm.* ***(Bii)*** *Internal matrix without cells, scalebar: 100µm.* ***(Biii)*** *Cell-laden spheroid at 1x10^{7} cells/mL, black arrow shows potential early myoblast fusion at D7, scalebar: 50 µm.* ***(Biv)*** *D7 hydrogels showing likely cell adhesion to the porous collagen matrix (black arrow).* ***(Bv)*** *Potential myotube fibre protrusions at D21 after 1 h EPS (black arrow), scalebar: 100µm.*

3.4.2.3 Collagen-Geltrex hydrogel rods

Promotion of cellular maturation was achieved by optimisation of cell density, substrate composition, model architecture, differentiation condition, anchorage and tethering, and EPS.

The first hydrogel rod model was produced as described previously (Section 2.1.3.4) (**Figure 3.8, A**). During culture, the hydrogel rods decreased in size at several stages – following casting then again after 2-day culture in proliferation media (data not shown). The models underwent further shrinkage during FFPE processing (data not shown). Hematoxylin and Eosin stain (H&E) and Masson's trichrome (MT) staining of the cell-hydrogel rod (v1) highlighted regions that were stained dark pink via H&E and red via MT and revealed that myotubes were arranged at the cell periphery by D21 (**Figure 3.8, B,** red arrows), mainly in the upper (U) and central (C) longitudinal sections. By D21 there was decreased cell density which could be attributed to the lack of nutrient delivery deeper into the gel that is necessary for the development and maintenance of mature SkM tissue. There was minimal evidence of myoblasts fusion to form myotubes (**Figure 3.8 B,** back arrows) and elongated syncytium across the tissue section was also limited. At this stage, the conditions of this fibrillar model did not produce optimal myocyte fusion and myotube formation.

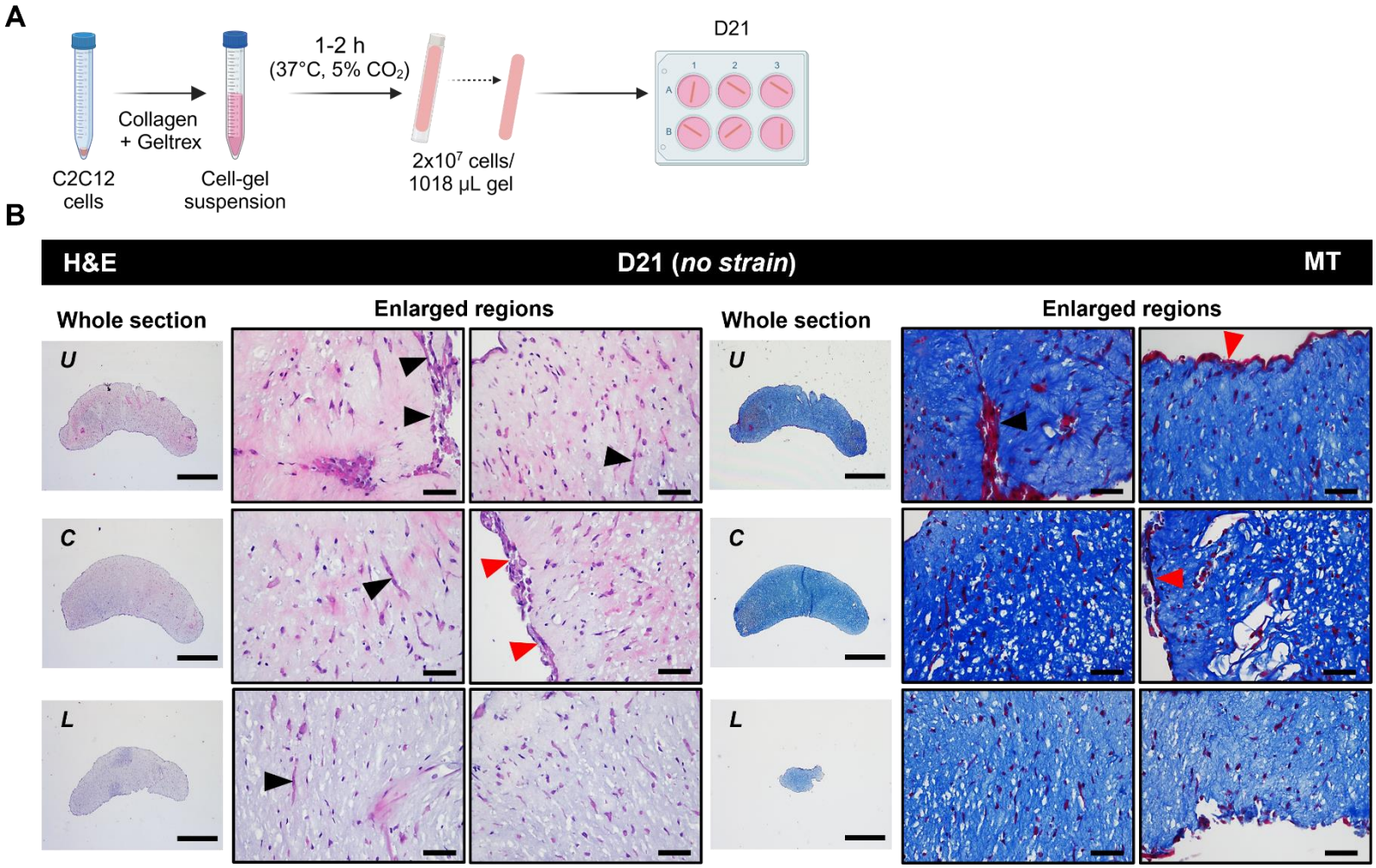

Figure 3.8 Assessement of differentiation in Collagen-Geltrex hydrogel rods. *(A) Schematic of development and culture of Collagen-Geltrex model. Cells were seeded at 1x107 cells/hydrogel and cultured in defined media 2. (B) H&E and MT staining of regional sections of the cell-hydrogel model are represented as (top-bottom) upper (U), central (C), and lower (L) longitudinal sections. Black arrows show prominent myotubes at the periphery. Red arrows show preferential peripheral alignment of myocytes at the tissue edge. Scalebar: whole section, 1mm; enlarged regions, 50 µm. Schematic was created in Biorender.*

3.4.2.4 Application of static tensile strain to influence cellular maturation via the MechanoCulture (MCT6).

Native SkM tissues are attached to bone via tendons and are therefore under constant tensile strain (Lieber and Ward, 2011). Furthermore, recapitulating the tension and anchorage of skeletal muscle has been shown to increase structural and developmental maturation of fibres (Powell *et al.*, 2002), as evidenced in tissue-engineered models described in Chapter 1. Consequently, the next optimisation step involved using the MCT6 system (Section 2.1.3.5) to apply anchorage and tensile strain, to promote myotube formation. Hydrogels were differentiated for 7 days followed by ~ 100% uniaxial strain for 7 days using the MCT6 (D14-MCT6). Therefore, models stretched via MTC6 experienced 14 days in differentiation media (**Figure 3.9, A**). Representative sections from Collagen-Geltrex hydrogels were stained with H&E and α-Actinin to assess the structural integrity of cells and differentiation under tension. By D14, hydrogels showed some indication of directional alignment under tension, as suggested by α-Actinin staining in cells loosely aligned with the direction of strain and anchorage (**Figure 3.9, B, C**, arrows). However, no significant differences were found in α-Actinin MFI between unstrained (D7, D14) and strained (D14-MCT6) conditions (**Figure 3.9, D**). While the mean α-Actinin MFI was highest in the D14-MCT6 group (3.24 a.u.) compared to D7 (1.32 a.u.) and D14 (2.63 a.u.), these values should be interpreted with caution due to the lack of statistical significance. Nuclear counts were slightly higher at D7 (286.3) and showed a modest decrease by D14 (168.3) and D14-MCT6 (149), though overall trends were not pronounced. EPS was introduced following the 7-day MCT-6 strain period, during which the models remained in suspension in differentiation media.

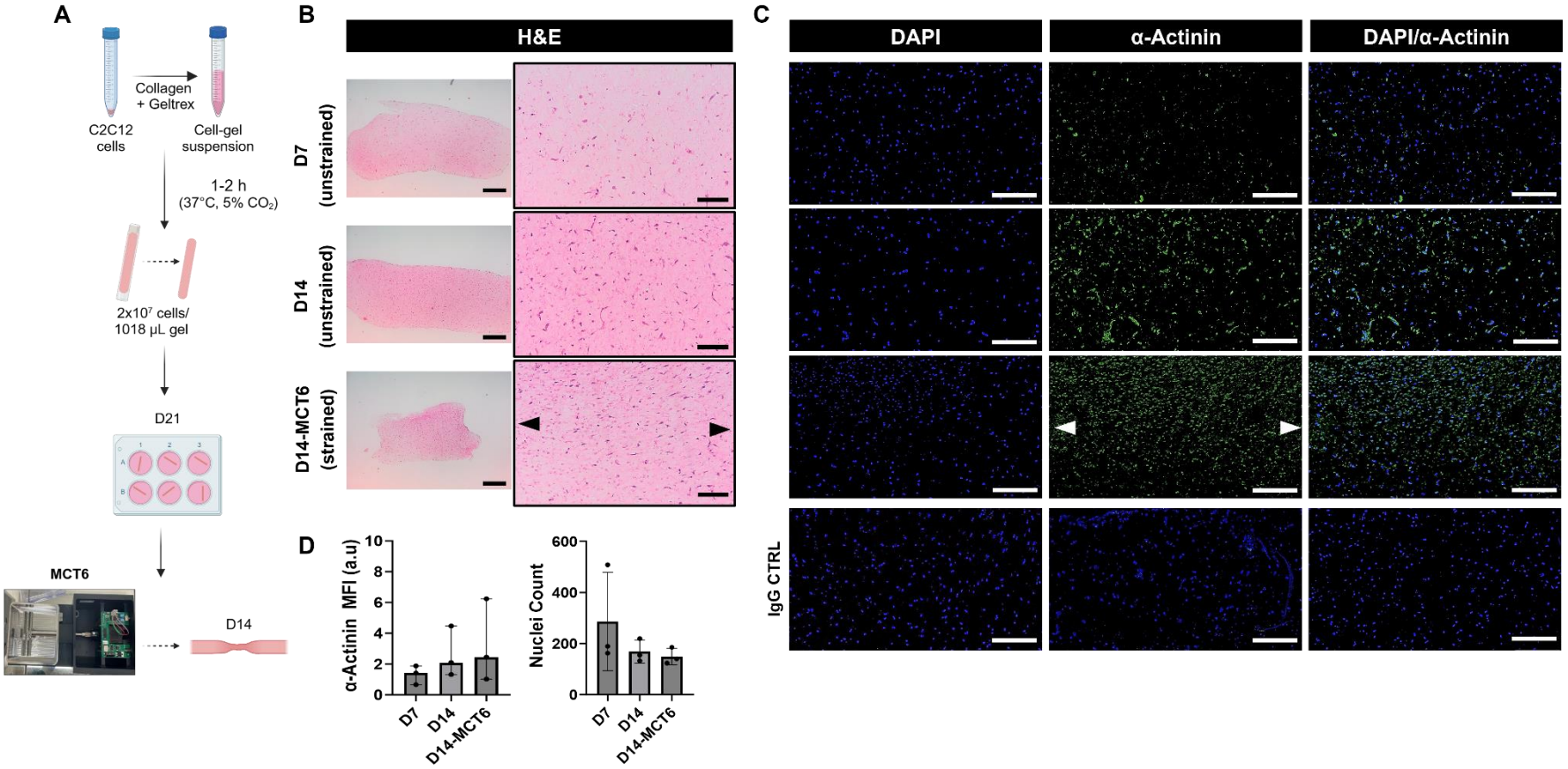

Figure 3.9 The effect of anchorage and strain via MTC6 on the structural maturity of hydrogel rod models. ***(A)*** *Schematic of development and culture of Collagen-Geltrex rod v1 under MCT6 strain. D7 and D14 unstretched models were compared to D7 stretched models that were stretched while differentiating for a further 7 days via the MCT6 (D14MCT6). The arrows represent the direction of tension in a stretched hydrogel. (B) H&E staining of cell-hydrogel sections. Scalebar: whole gel sections, 500 µm; high magnification area, 100 µm.* ***(C)*** *α-Actinin-stained C2C12 cells. IF – 200 µm. Images represent central longitudinal sections of the cell-hydrogels.* ***(D)*** *Graphs show differences between D7, D14 and D14MCT6 models. α-Actinin MFI shows median and range, analysed via Kruskal-Wallis test with Dunn's post-hoc correction; nuclei count shows mean with ± s.d, analysed via One-Way ANOVA followed by Tukey's rage test. Sections were analysed via Image J (n=3). Schematic was created in Biorender.*

The stretching of hydrogel rods (v1) via the MCT6 was challenging, particularly due to the inconsistency between the size of the hydrogel and the anchored area. A tensile strain of ~ 100% was applied for 7 days and the effects of this included tearing and detachment during culture (**Figure 3.10, A,** black arrow) while other hydrogels withstood strain. However, H&E staining exposed the loss of mass and nuclei in the anchored regions of the hydrogel (**Figure 3.10, B, '1**') while the stretched region (**Figure 3.10, B, '2**') had retained cells. The MCT6 functioned to promote the structural maturity of hydrogels, however the large surface area of the screw-driven clamps for anchorage created loss of the tissue-like structure (**Figure 3.10**). Furthermore, the MCT6 was incompatible with the simultaneous application of EPS. Further optimisation involved the development of larger hydrogels rod (v2) for long-term culture. A refined strain-inducible system with improved anchors to better retain cell density and cell-hydrogel mass was

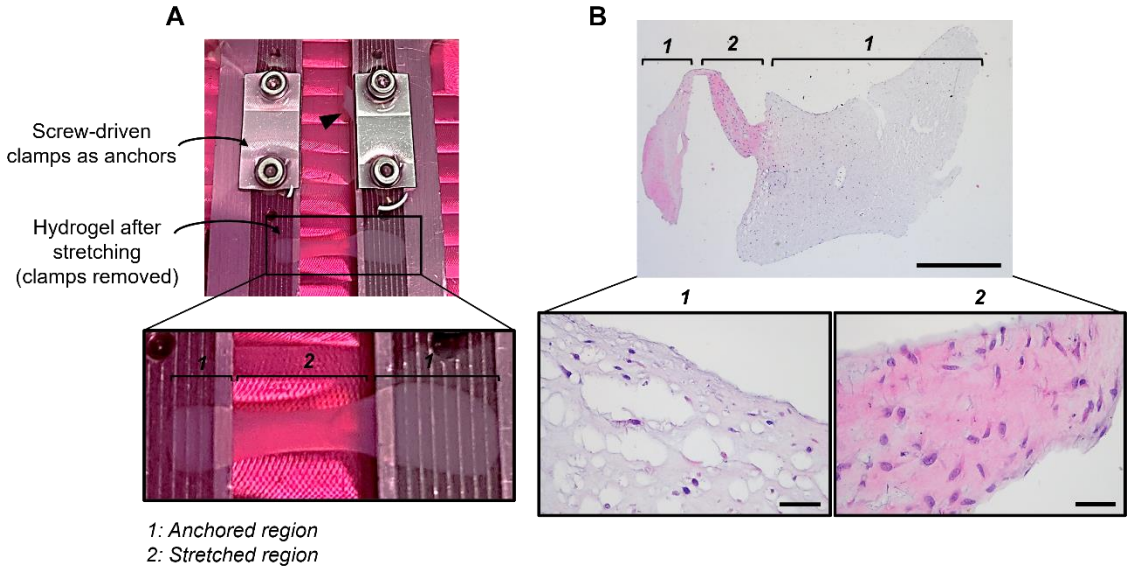

Figure 3.10 Incompatibility of the MCT6 with the cell-hydrogel rod model (v1). (A) *Hydrogel ends were compressed by the clamps, leaving the strained regions intact.* ***(B)*** *Histology showed significant shrinkage of strained regions post-FFPE, compared to anchored areas, with the strained regions exhibiting higher cell density and increased nuclei. Scalebar: H&E: whole gel sections, 1mm; higher magnified ROIs, 50 µm.*

3.4.2.5 Promoting cellular differentiation

A larger hydrogel rod was produced (Section 2.1.3.4) to facilitate better anchorage and strain application (**Figure 3.11, A**). Increased cell density was also incorporated, which theoretically necessitated enhanced nutrient support to ensure sufficient diffusion and availability of essential factors for effective differentiation and myotube fibre formation (**Figure 3.11, A**).

The relative metabolic activity of the high cell density hydrogels (3.5 x 10^7 cells/mL) was measured up to 24 h during differentiation (**Figure 3.11, B**). The metabolic activity of SkM cells were initially increased within the first few hours of culture (1-4 h), however, decreased minimally at 24 h ($p > 0.05$), which could indicate the shift from proliferation to differentiation, where cells may reduce their metabolic rate as they mature. Alternatively, it could reflect nutrient depletion, accumulation of metabolic waste or changes in cellular stress, all of which could have affected metabolic function. To promote differentiation, cell-hydrogels were cultured under defined differentiation conditions (Section 2.1.2.1), from D0 (**Figure 3.11, Ci**) to D21 (**Figure 3.11, Cii**). Cells were enriched in the central regions of the hydrogel compared to the lower regions at both D0 and D21 (**Figure 3.11, Ci, Cii**). Furthermore, myocytes did not produce elongated myotubes by D21 (**Figure 3.11, Cii**). Therefore, the models were supplemented with AlbuMAX, L-Proline and ITS-X (defined media 3, section 2.1.3.1, **Figure 3.11, Ci**) to support long-term differentiation. There was marked improvement by way of homogenous regions of cell density throughout the gels, including the central and lower regions, indicated by the red MT staining (**Figure 3.11, Ciii**). There were also dense collagen regions throughout the hydrogels. Interestingly, extended fibres were present at the periphery of constructs both in central and lower regions of the gel, towards the surrounding nutrient-rich media (**Figure 3.11, Ciii,** white arrows).

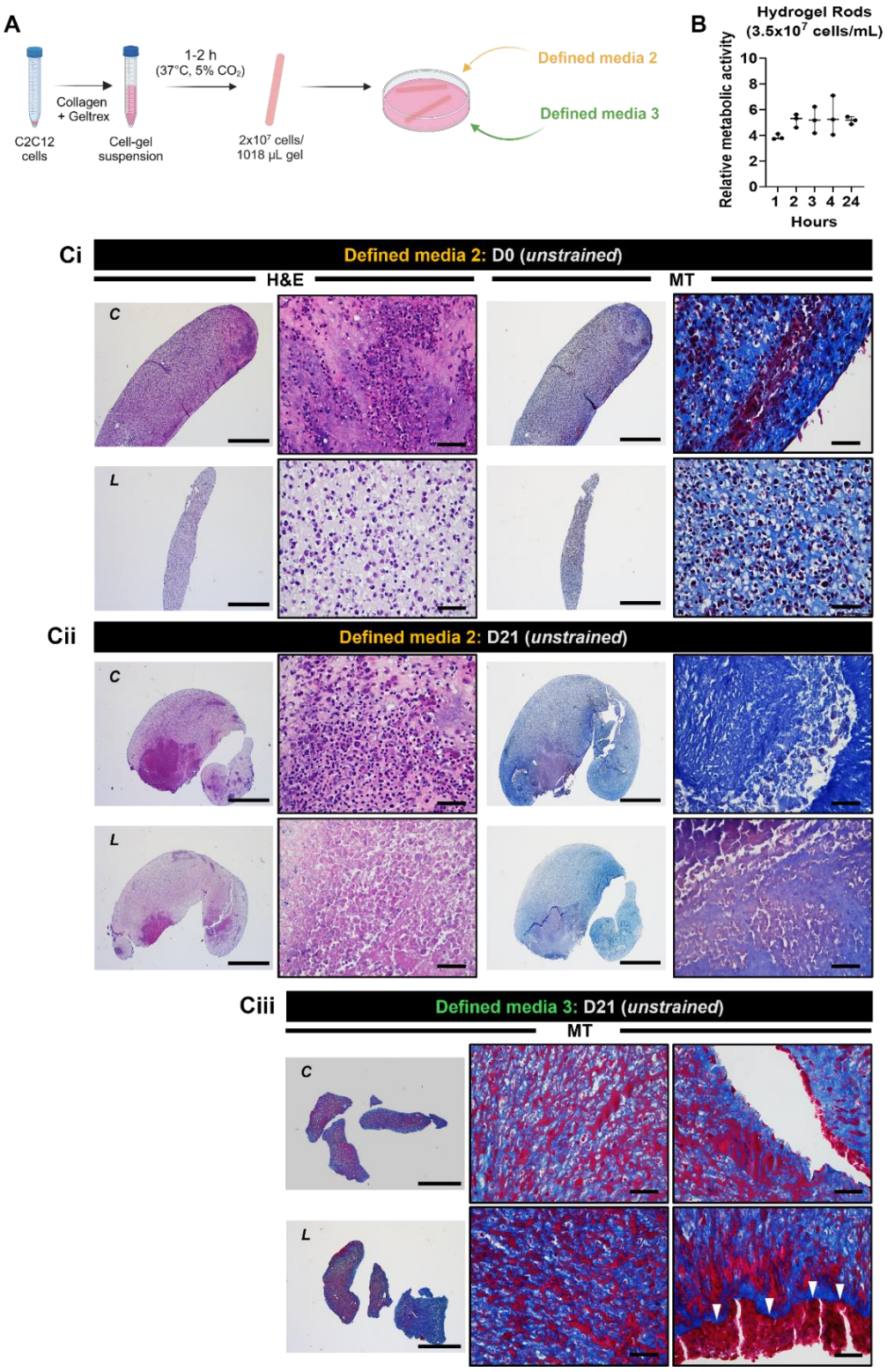

Figure 3.11 Optimisation of culture conditions for Collagen-Geltrex rod models. (A) *Schematic of two differentiation conditions for culture of 'large' (v2) hydrogel rods.* ***(B)*** *The metabolic activity of high cell density hydrogels in defined media 2 were measured via Alamar blue assay, up to 24 h. Data shows median and range, analysed via the Kruskal-Wallis test with Dunn's post-hoc correction, p>0.05 (n=3).* ***(Ci)*** *H&E and MT staining of 2x10^7 cells/hydrogel at D0.* ***(Cii)*** *H&E and MT staining of cells ay D21 in defined media 2.* ***(Ciii)*** *MT staining of cells enriched in defined media 3 by D21. White arrows show areas of cell migration towards the periphery. Sections represent central (C) and lower (L) longitudinal regions of the cell-hydrogels. Scalebar: whole gel sections, 1mm; higher magnified ROIs, section, 50 µm. Schematic was created in Biorender.*

3.4.2.6 Application of static tensile strain to influence cellular maturation via the MTSIP.

A novel manual tensile strain-inducible platform (MTSIP) was developed, which permitted simultaneous strain of hydrogel rods (v2) inside 6-well plates with C-Dish application and EPS via the C-Pace EP. The MTSIP also mitigated the challenges associated with MCT6 anchorage. Details of the MTSIP development are outlined in Section 2.1.3.6.

An ~ 60% strain was applied to the cell-hydrogel rod (v2) models via the MSTIP in defined media 3 (**Figure 3.12, A**). This altered the collagen-cell distribution of the models by D21 (**Figure 3.12, B**) compared to the D21 unstrained hydrogels in defined media 3, reported previously (**Figure 3.11, Ciii**). Collagenous areas (stained blue) were interspersed throughout the hydrogels after MTSIP application and did not dominate the SkM network (**Figure 3.12, B**) unlike the unstrained model shown above (**Figure 3.11, Ciii)**. The MTSIP model created a homogeneous fibre network and cells migrated from the tissue edge to reveal a collagenous (blue) border (**Figure 3.12, B**). This suggests maturation of muscle fibres and a remodelling response to static strain. By comparison, the cells (red) of the unstrained models migrated towards the periphery (**Figure 3.11, Ciii**). Indeed, the MTSIP-strained models produced distinct, longitudinal SkM fibres which were accentuated along, the longitudinal tension axis (**Figure 3.12,** black bidirectional arrows). Thinner regions of the cell-hydrogel revealed the high strain areas (**Figure 12,** single black arrows). Overall, the D21 strained models had greater cell prominence (**Figure 3.12, B**) compared to unstrained D21 models (**Figure 3.11, Ciii)**, which suggests that tensile strain enhanced differentiation and structural maturation. Thus, strain via MTSIP can sufficiently produce SkM fibres.

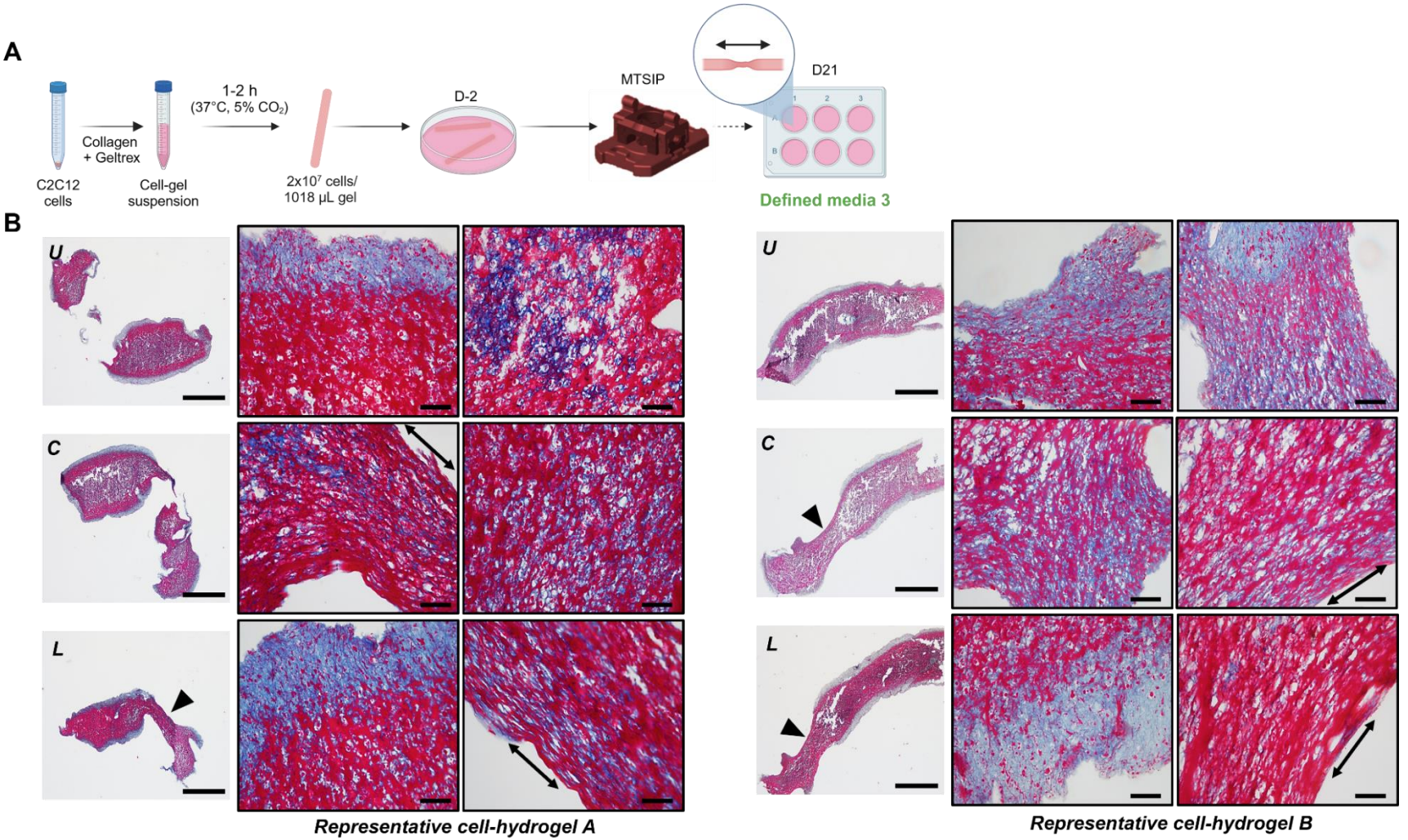

Figure 3.12 The effect of tensile strain via the MTSIP on the maturation of SkM hydrogel rods. (A) *Schematic of tensile strain application via MTSIP to C2C12 Collagen-Geltrex rod v2. A 60 % strain was applied to the hydrogels, as they were cultured under defined media 3 differentiation conditions.* ***(B)*** *Two representative hydrogels (A and B) show the following MT-stained sections: upper (U), central (C) and lower (L). MT staining differentiates collagenous (blue) and SkM (red) regions. Single black arrows show high tension regions in the whole gel sections, while bidirectional black arrows show the alignment of the SkM fibres along the longitudinal tension axis. Scalebar: whole gel sections, 1mm; two higher magnified ROIs, 50 µm.*

3.4.2.7 The effect of EPS on SkM maturation

EPS was next applied to the cell-hydrogel rod models (v2), while stretched by the MTSIP (**Figures 3.13, 3.14, A**). To test whether EPS affected the maturation of the cells within the 3D model, the median area and MFI of α-Actinin, MyHC II, MRF4 and Dystrophin was analysed per hydrogel region. The effect of EPS was assessed by analysis of the fold change (FC) difference of corresponding sections from unstimulated (- EPS) and stimulated (+ EPS) cell-hydrogel sections. This was completed for both acute (**Figure 3.13**) and chronic (**Figure 3.14**) EPS conditions. To review the effect of EPS on entire cell-hydrogels were analysed as the pooled medians by condition and sample size (**Figure 3.14**).

Visualisation of α-Actinin, MyHC II, MRF4, reveal aligned multinucleated fibres along the longitudinal tension axis (**Figure 3.13, B**). Conditions of - EPS to + EPS sections following acute EPS revealed no remarkable fold-change for α-Actinin, MyHC II and Dystrophin. However, there was a 2.04-fold increase in MRF4 area from the upper - EPS section to the upper + EPS section (**Figure 3.13, B, C**). Apart from MRF4, no differences were observed in marker area or MFI between corresponding sections with or without EPS (**Figure 3.13, B C**). Similarly in the chronic condition (**Figure 3.14, B, C**), There was no observed difference in marker area between related sections with or without 6 h of EPS. However, following 6 h + EPS, the MFI of α-Actinin and MyHC II increased by 2.28-fold and 5.71-fold, respectively (lower peripheral sections, **Figure 3.14, B, C**). No differences in MFI were observed for the remaining markers between the corresponding sections with or without EPS. (**Figure 3.14, B, C**).

Analysis of pooled maker area of all sections (whole gel analysis, **Figure 3.15**) revealed a 3.52-fold increase in MyHC II from acute - EPS to + EPS and a 2.03-fold increase in MyHC II in chronic - EPS to + EPS (**Figure 3.15, C**). Pooled maker MFI of all sections showed a 3.52-fold increase in MyHC II only from acute - EPS to + EPS, and a 2.03-fold increase, again in MyHC II, from chronic - EPS to + EPS (**Figure 3.15, C**).

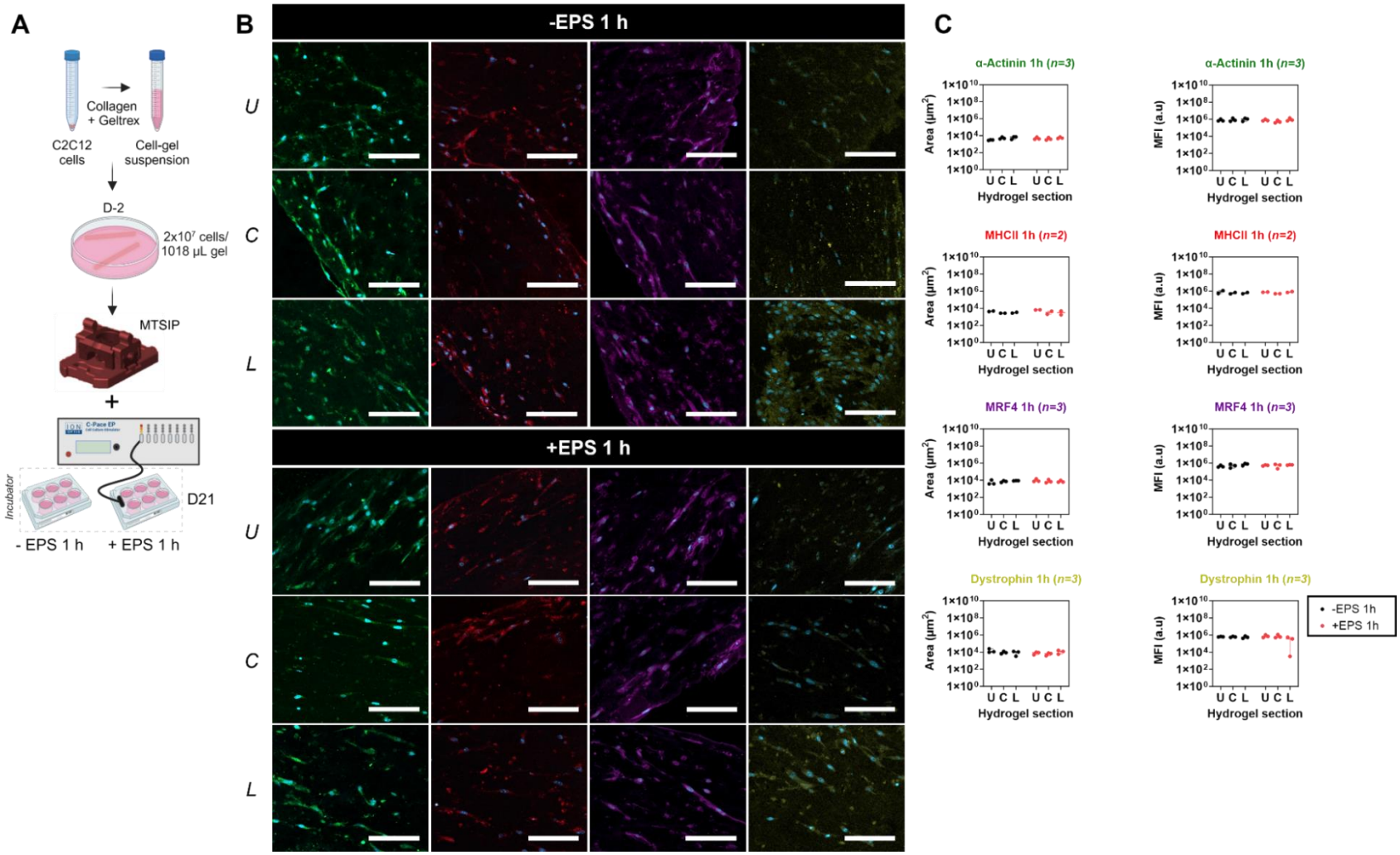

Figure 3.13 The application of MTSIP ± EPS 1 h of 3D hydrogels. ***(A)*** *Schematic of MTSIP and ± EPS stimuli to C2C12 Collagen-Geltrex rods (v2).* ***(B)*** *Merged IF confocal images displaying maturity markers: α-Actinin (green), MyHC II (red), MRF4 (magenta), and Dystrophin (yellow). Cell nuclei were counterstained with DAPI (blue).* ***(C)*** *Quantified mean fluorescence area and MFI of regional sections (U, C, L) for ± EPS conditions. The Mann-Whitney test with Holm-Šídák's post hoc procedure revealed no significant differences ($p > 0.05$) between sections. Data shown as log_{10} median and range (n=1–3).*

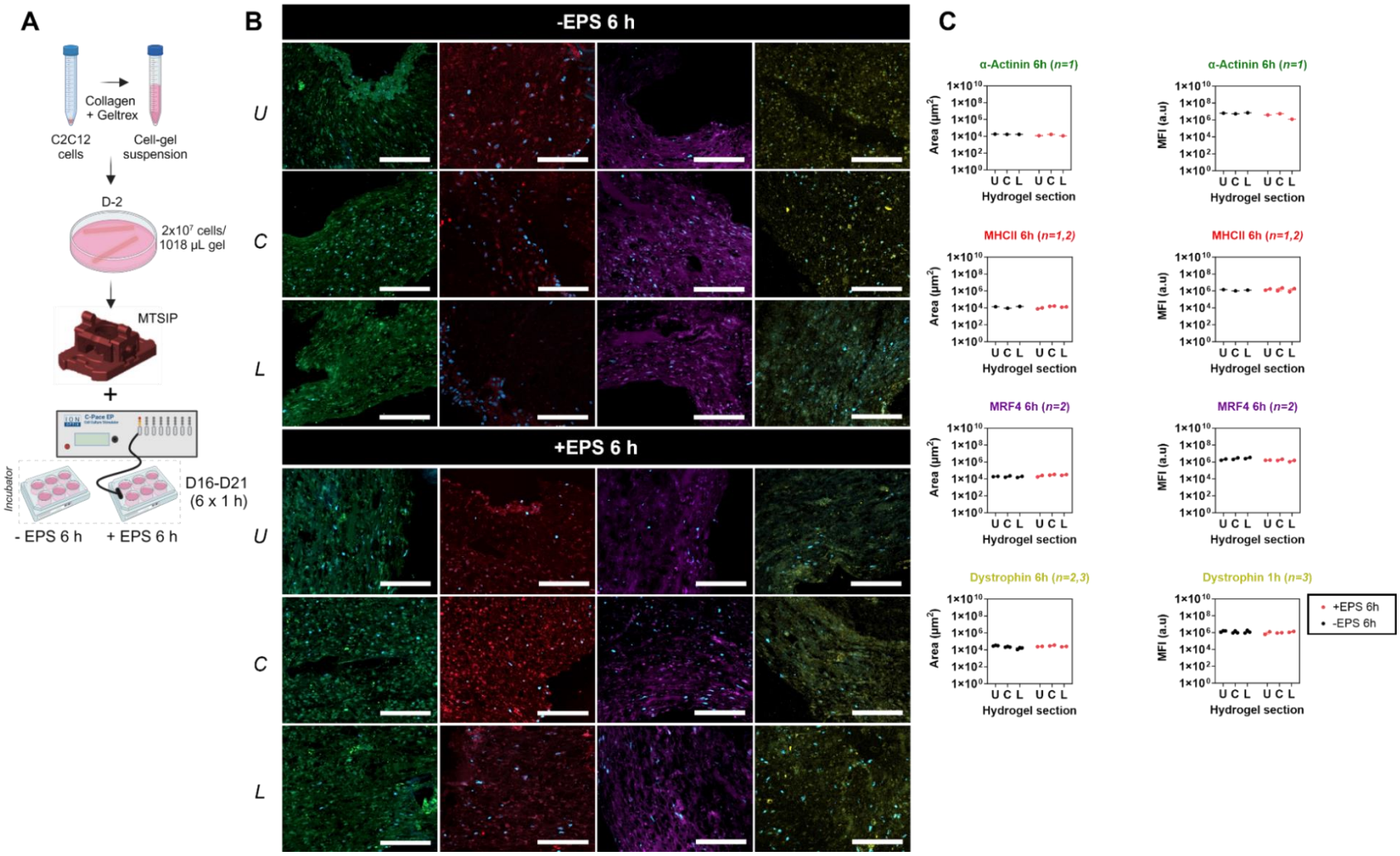

Figure 3.14 The application of MTSIP ± EPS 6 h of 3D hydrogels. ***(A)*** *Schematic of MTSIP and ± EPS stimuli to C2C12 Collagen-Geltrex rods (v2).* ***(B)*** *Merged IF confocal images display maturity markers: α-Actinin (green), MyHC II (red), MRF4 (magenta), and Dystrophin (yellow). Cell nuclei were counterstained with DAPI (blue).* ***(C)*** *Quantified mean fluorescence area and MFI of regional sections (U, C, L) for ± EPS conditions. The Mann-Whitney test with Holm-Šídák's post hoc procedure revealed no significant differences ($p > 0.05$) between sections. Data shown as log_{10} median and range (n=1–3).*

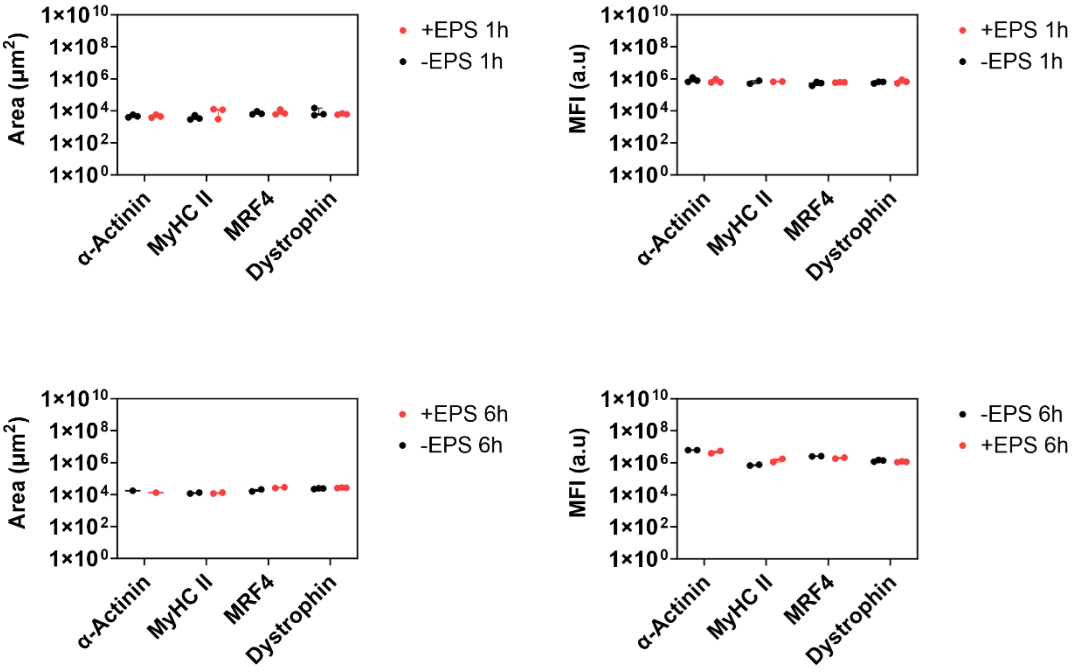

Figure 3.15 Analysis of ± EPS 1 h and 6 h of whole gels. *Scatter graphs shows pooled means by condition & sample size for the mean fluorescence area and MFI of α-Actinin, MyHC II, MRF4, and Dystrophin. Differences between - EPS and + EPS was analysed via Mann-Whitney test with Holm-Šídák's post hoc procedure revealed no significant differences ($p > 0.05$) between - EPS and + EPS sections for all markers. Data shown as log_{10} median and range (n =1–3).*

3.4.2.8 Histological assessment of EPS

Histological analysis of chronic ± EPS (6 h) on MTSIP stretched models was completed to further assess the effects of chronic EPS. MT staining of + EPS 6 h hydrogels revealed dense and with closely packed fibres in the matrix (**Figure 3.16,** representative cell-hydrogel A) as well as a likely porous tissue structure (**Figure 3.16,** representative cell-hydrogel B, black arrows). MT staining show cells (red) were maintained in the centre of the hydrogel and formed a distinct cell-free collagenous border (**Figure 3.16**), as seen previously (**Figure 3.12**). With + EPS 6 h, the cell-hydrogels appeared to withstand the tension as the models lack the narrow, high tension observed previously (**Figure 3.12**).

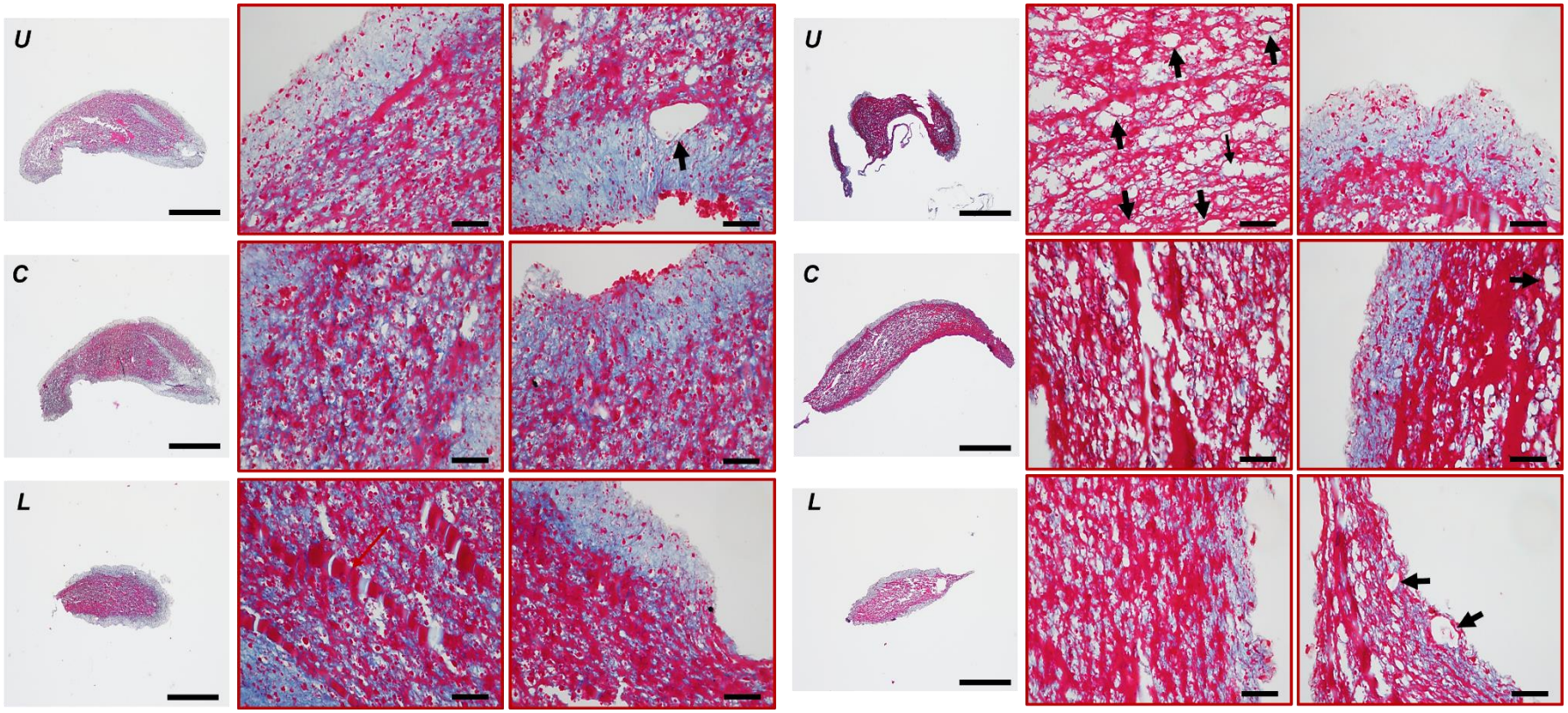

Figure 3.16 Histological assessment of the effect of chronic EPS on cell-hydrogel models under stretch. *A 60% strain was applied to the hydrogels as they were cultured under defined media 3 for 21 days. At D EPS was applied. Three representative hydrogels (A, B and C) show upper (U), central (C) and lower (L) longitudinal MT-stained sections. Staining differentiates blue (collagenous), and red (SkM) regions of the model Black arrows highlight tissue-like sections pores. Scalebar: whole gel sections, 1mm; two higher magnified ROIs, 50 µm.*

3.5 Discussion

This chapter contributed to the development of a scalable and controllable SkM model for secretome analysis. This study successfully developed and characterised a novel 3D SkM model, derived from a foundational 2D model. The final 3D model was optimised through a systematic development process, incorporating key factors such as substrate composition, architecture, cell density, growth factors, supplements, anchorage, tethering, and the application of EPS. Iterative modifications culminated in a hydrogel-based fibrillar (rod-shaped) construct, generated using a mould-based scaffold. The 3D model's innovation lies in its integration of concurrent tensile strain and EPS, facilitated by the Ion Optix C-Pace EP system. Furthermore, it's scalability and feasibility makes it an ideal model for high throughput studies, particularly for the investigation of secretomics.

3.5.1 Enhanced differentiation conditions produced variable morphologies in 2D

Differentiation of 2D myotubes under low-sera conditions was optimal by D7, based on imaging analysis revealing elongated syncytium and mature contractile proteins- and developmental MRFs (i.e. MyHC II, MRF). The substitution of FBS with HS is common practice for differentiating C2C12 myotubes (Asano *et al*., 2015; Denes *et al*., 2019; Nieuwoudt *et al*., 2017) and optimal results were observed between D5 and D7 in 2D. Aligned, parallel fibres are essential for force generation and transmission (Jana, Levengood and Zhang, 2016). To enhance differentiation and subsequent contractility in 2D, IGF-1 and AA2P was applied. IGF-1 plays a pivotal role in myogenesis (Ahmad *et al.*, 2020)**,** promoting mature myotube formation and functional development by stimulating myoblast proliferation and differentiation, enhancing protein synthesis, and inhibiting atrophy-associated pathways (Shima *et al*., 2018). The additional supplements including IGF-1 may have contributed to contraction alone as a primary human model was shown to contract following stimulation with 100 ng/ mL of IGF1, developing differentiation and myotube phenotype (Dreher *et al.*, 2024). AA2P is a stable derivative of L-ascorbic acid, has been shown to promote myotube formation (Ikeda *et al.*, 2017a) and is critical for collagen synthesis (Takisawa *et al.*, 2022), a major component of the ECM. Moreover, a well-structured ECM provides mechanical support and signalling cues necessary for myoblast alignment and fusion into parallel myotubes. Thereby, facilitating collagen production, AA2P improves ECM structural integrity, creating an environment conducive to myotube formation. Increased contractility requires enhanced nutrient and energy availability to support the metabolically active tissues during muscle contractions. When supplemented with IGF-1 and AA2P, the 2D SkM model exhibited spontaneous contractions and produced diverse phenotypes, including sheet-like structures, cross-

linked fibres, in addition to distinct myotubes. Sheet-like structures have been uniquely developed as SkM models before (Bian *et al*., 2012; Takahashi *et al*., 2013; Nakamura *et al*., 2017; Jiao *et al*., 2018; Takahashi, Shimizu and Okano, 2018). In fact, one of the earliest 3D models was a cell 'sheet' phenotype (Vandenburgh, Karlisch and Farr, 1988). However, without appropriate quantification of contractility, the functional efficacy of the cellular model phenotype in the model could not be determined. However, F-Actin staining revealed enhanced sarcomere localisation in the myotubes. Lastly, the effect of altered morphology on the contractility of the fibres need further investigation.

3.5.2 Refining matrix composition, morphology and SkM architecture in 3D

The initial 3D model developed using Col-Tgel demonstrated poor cell retention and significant migration of cells into the surrounding media, resulting in limited cell proliferation and differentiation. Substrate stiffness, a critical factor in cellular behaviour, may have influenced the cells' ability to proliferate and differentiate (Nguyen *et al.*, 2024). C2C12 cells exhibit a passive Young's modulus~12 kPa (Pang *et al.*, 2023), alike physiological SkM stiffness (12–18 kPa) and they differentiate on tissue-like stiffness (Engler *et al.*, 2004). Thus, the lack of proliferation, differentiation, and retention is more likely attributed to matrix rigidity than to intrinsic cellular properties.

Although the Col-Tgel matrix is reported by the manufacturer to have a stiffness of 14 ~ 20 kPa, within the physiological SkM range, substrate stiffness plays a pivotal role in myoblast behaviour. Myoblasts require substrates with appropriate stiffness to spread, elongate, and align, mimicking native muscle tissue (Engler *et al.*, 2004; Gilbert *et al.*, 2010). Previous studies investigating Col-Tgel stiffness found that medium-stiffness matrices produced dot-like actin-microfilaments and filopodia, while softer matrices supported mesh-like or extended actin filaments, facilitating myoblast-like cell differentiation (Tan *et al.*, 2015). Skeletal muscle stiffness is primarily determined by ECM composition, particularly fibrillar collagen, which significantly influences matrix rigidity(Meyer and Lieber, 2011), notably fibrillar collagen, which affects stiffness (Trensz *et al.*, 2015). The limited proliferation and differentiation observed in the Col-Tgel model necessitated the transition to a Collagen-Geltrex ECM, leading to the development of the next-generation model.

Collagen is commonly incorporated into 3D SkM models (**Table 1.1**), and its peptides have also been found to promote myoblast differentiation and myotube hypertrophy *in vitro* by activating the mTOR signalling pathway in mouse skeletal muscle cells (Kitakaze *et al.*, 2016). Pertinent to the downstream analysis of contraction induced secretomics, Collagen type 1 is found to promote C2C12 cell migration and myogenic differentiation

by inducing IL-6 release through activation of the FAK/NF-κB p65 signalling pathway (X. Liu *et al*., 2020). With the Collagen-Geltrex model, there was evidence of myoblast fusion into myocytes, but these assumed multiple orientations in the spheroids. Using SEM analysis, distinction of myotube fibres from the collagen fibres was not conclusive without further analysis such as Energy-Dispersive X-ray Spectroscopy (EDX) SEM or discriminative histological analysis such as MT staining. Subsequent contraction in the Collagen-Geltrex model was minimal. Similarly, models which lacked alignment have reported fewer or no MRF expression (**Table 1.1**) or contractile proteins such as MyHC (Yamasaki *et al*., 2009).

Spheroid models pose challenges in physical tethering and sectioning, particularly for generating longitudinal arrangements needed to confirm myotube formation. To support fibre alignment, the model required fibrillar structure, reflecting inherent fibrillar SkM, from sarcomeric myofilaments to fascicles arranged laterally (Rall, 2018b). Fascicle arrangements vary, including fusiform, parallel, convergent, and pennate structures (Xie *et al.*, 2023). While circular tissue models, such as the orbicularis oculi (a sphincter-like muscle), are arranged concentrically around the eyelids, their fibres remain longitudinally aligned, despite circular morphology (Sekulic-Jablanovic *et al.*, 2016). Model morphology was critically evaluated, as architectural variations influence the tension generated between muscle tendons (Böl *et al.*, 2014; Washio *et al.*, 2019).

3.5.3 2D and 3D *in vitro* models

The 2D model developed long, elongated syncytia with aligned fibres, sarcomeric protein expression, and an increased fusion index by D7. In contrast, the primary 3D hydrogel rod model exhibited minimal fibre fusion in the same media by D21. This likely stemmed from the 3D model relying solely on IGF-1 and AA2P without additional growth factors or optimised culture conditions necessary to mimic the complexity of *in vivo* environments (Urzì *et al.*, 2023). In 3D systems, cells are encapsulated in a matrix that partially replicates the extracellular environment and depends on external cues such as growth factors to drive differentiation. Incorporating AlbuMAX, L-Proline, and ITS-X enhanced model development, producing a SkM tissue analogue with distinct fibres within a collagenous matrix.

The 3D hydrogel rod model in defined media generated SkM regions, indicated by MT staining and peripheral extensions. AlbuMAX, a lipid-rich BSA supplement, supported myoblast proliferation and fusion into multinucleated myotubes by enhancing membrane stability and protein synthesis. L-Proline promotes collagen synthesis, which is essential for ECM integrity and myotube formation. Insulin aids cell survival, transferrin provides iron, and selenium acts as an antioxidant, optimising conditions for myoblast proliferation

and myotube differentiation in both 2D and 3D cultures. These factors facilitate muscle fibre development by supporting growth, fusion, and alignment, while culture conditions ensure long-term survival and proper function. The high cell density in the 3D model, maintained for 21 days, requires sufficient nutrient supply to support muscle fibre maturation and contraction, which is important for muscle development (Bakooshli *et al*., 2019). This may also be linked to the ability of developing models of high maturity, which can contract without external stimuli (reviewed hereafter).

The 2D model revealed centrally aligned nuclei. The 3D rod models showed myotube alignment and peripheral clustering, with and without defined media 3. Similar to mature human muscle fibres, peripheral nuclei in myofibers (Brunetti *et al*., 2021; Gholobova *et al*., 2018) reflect *in vivo* nucleus movement (Roman and Gomes, 2018). Indeed, nuclei are positioned at the fibre periphery, adjacent to the myofibrils and sarcolemma, near the T-tubules (Rossi *et al.*, 2022). Nuclear positioning as part of model development and functional implications in 3D models are discussed in Chapter 1.

3.5.4 Tensile strain increased structural maturity in 3D

SkM maturation was further promoted via application of strain, which has been shown to influence cell orientation, proliferation and differentiation, promoting maturation (G. Huang *et al*., 2020; Riehl *et al*., 2012). Several studies have indicated an increased myotube diameter and area (Powell *et al.*, 2002) and alignment (Heher *et al.*, 2015) under strain. Enhanced maturation was achieved in the current study by placement of the cell seeded collagen-hydrogel between two fixed points, which led to the generation of isometric strain in the construct as the cells pulled against these stationary posts. A strain of ~60%, which is considered high (Y. Li *et al*., 2016), was applied. Cell-mediated tension provided a mechanical stimulus that promoted the organisation and alignment of the seeded cells along the principal strain produced by the MCT6. The tensile strain produced aligned and elongated SkM fibres, stained distinctly MT. Early models have demonstrated that repetitive cyclic stretching increases SkM elasticity, two- to three-fold compared to static controls (Powell *et al.*, 2002). In a more recent model, applying cyclic strength as mechanical stimulation produced oriented and mature myotubes (Bansai *et al.*, 2019). By comparison, the tension applied in this study was static and the C2C12 cells responded by an increase in sarcomeric protein. The mean MFI of α-Actinin increased from D7 to D14, therefore 7 day differentiated hydrogel rods combined with 7-day MCT6 strain was adopted, which produced the greatest expression of α-Actinin. The increase in the expression of sarcomeric proteins, may be evidence for sarcomerogenesis, which is not only considered the gold standard marker of advanced myotube maturation but is considered to be essential for contractile function (Costantini, Testa, Mozetic, *et al*., 2017). Furthermore, SkM responds to passive overstrain through

sarcomerogenesis, in response to chronic longitudinal muscle growth (Zöllner *et al.*, 2012), presumably to maintain optimal sarcomere length. The increase in α-Actinin demonstrated the structural integrity SkM adaptation to greater functional demands.

Tension was associated with a modest reduction in nuclei count alongside higher α-Actinin levels, suggesting a possible inverse relationship. Nuclei count decreased under static conditions from D7 to D14 and was lowest under strain. This study's findings of increased α-Actinin and decreased cell nuclei during MTC6 strain align with previous research, which demonstrated a reduction in satellite cell population in response to chronic strain, without impeding serial sarcomere addition. This response also maintained both fibre cross-sectional area and ECM structure in a transgenic Pax7-DTA mouse model (Kinney *et al.*, 2017). If nuclei are lost at a slower rate than α-Actinin, the remaining nuclei would be linked to higher α-Actinin levels (relative amount of α-Actinin per nucleus), potentially explaining the observed increase in α-Actinin despite the decrease in nuclei. However, α-Actinin changes were evaluated only after the 1-week strain, limiting the ability to assess the long-term relationship between α-Actinin and nuclei under strain. Furthermore, the 'myonuclear domain' theory is relevant here, as it suggests that muscle fibre growth, including lengthening, may be constrained when the upper threshold of each domain within the syncytium is exceeded (Conceição *et al.*, 2018; Snijders *et al.*, 2021). Reduction in nuclei under strain may also suggest evidence of atrophy and myonuclei loss via apoptosis (Gundersen and Bruusgaard, 2008), suggesting an alternative, negative effect of strain on the 3D SkM models. Furthermore, it is indeed challenging to differentiate between true myonuclei and neighbouring mononuclear cells (Schwartz, 2019).

3.5.5 MTSIP-models altered the SkM architecture and is sufficient for SkM maturation

The differences between the unstrained and strained models underscored the importance of tensile strain. Stretched models, despite undefined orientation, exhibited alignment, showcasing anisotropy. The unstimulated models under tensile strain showed evidence of collagen-cell remodelling, anisotropic tissue formation, and uniform SkM coverage across stained sections.

The mechanical constraints, such as the anchor points, ultimately dictated the direction in which strain was applied, directing contractile forces to shape the tissue and influence its microarchitecture. A 3D sculpted model anchored anisotropic boundary constrains as anchor points which cased anisotropic deformation. As such, this model showed increased density of type III collagen, which also transitioned from a granular morphology to an aligned ECM fibres (Mondrinos *et al.*, 2021). Similarly, the 3D model in this work

exhibited high points of tension with anchorage and strain; there was deformation in the stretched (high tension) regions of the model, which at times tore at this point. Thereby, the entire tissue-mimetic resembled a 'bundle' alike previous studies of 3D SkM models (Shimoyama *et al*., 2010; Kim *et al*., 2018, 2020; Osaki, Sivathanu and Kamm, 2018; Rao *et al*., 2018; Mills *et al*., 2019).

In a similar way, models strained via the MTSIP experienced deformation which altered its shape. This 'bowing effect' is commonly observed in anchored models, particularly chamber-like models (Chiron *et al*., 2012; Jones *et al*., 2018; Okano & Matsuda, 1997). Similar models produce the same dumbbell morphology as a result of constraints (Alave Reyes-Furrer *et al*., 2021; Bakooshli *et al*., 2019). Tissue under tension alone has some cells protruding outside the sections and collagen distributed within the tissue. The opposite is for EPS tissue under tension, whereby the cells remain within the tissue and diffuse collagen, around the periphery too.

It is commonly theorised that collagen fibres dynamically increase alignment in response to muscle strain, and this change in alignment is related to passive muscle stiffness. Using dynamic imaging of collagen in skeletal muscle we demonstrate that as skeletal muscle is stretched, collagen fibres re-orient themselves along the axis of strain and increase their alignment. The degree of alignment and the increase in alignment are each weakly related to passive muscle stiffness in a DMD mouse models (Wohlgemuth *et al.*, 2024). The density of the collagenous tissue regions appeared altered in our final 3D rod model. Collagen remodelling has been reported *in vivo* as collagen peptide supplementation has promoted architectural remodelling, specifically improving the angle of fibre pennation in healthy males during resistance training, also increasing both whole quadriceps and total muscle volume (Balshaw *et al.*, 2023).

Unstimulated C2C12 models stretched via the MTSIP expressed the same maturity markers, including MRF4, as the stimulated models, with intact myotubes confirmed by histology. This suggests that strain alone may be sufficient to promote maturity. A study supports this, showing that mechanical stimulation alone aligned fibres more effectively than EPS, though less so than co-stimulation, which enhanced contractile force (Kim, Kim and Asada, 2019).

3.5.6 Effect of EPS on SkM models under tensile strain

EPS is bifunctional as it can be used as part of model development to promote skeletal muscle maturation and as an exercise model. Both are invariably linked as skeletal muscle contraction is characterised as a functional maturity feature. EPS was used to establish acute (1h) and chronic (6h) *in vitro* 'exercise' to the final MTSIP model. Histological and IF analysis in 3D, revealed the presence of structural sarcomeric

markers including α-Actinin, MyHC II, Dystrophin; and developmental MRF4. In native muscle, MRF4 is significantly elevated in mature adult muscle, indicating advanced fibre maturity (Yoshimoto *et al.*, 2020). It also inhibits early-stage MRFs, driving cells toward terminal differentiation (Asfour, Allouh and Said, 2018), contributing to a mature muscle model. Distribution of the markers was assessed throughout the cell-hydrogel models and the effect of maturity (via markers) ± EPS. Uniform sectioning of hydrogels revealed structural consistency between upper and lower slices, but initially hypothesised differences in cell density, nutrient availability, and oxygen levels would arise due to environmental factors during culture.

3.5.7 Contraction induction vs. spontaneous contraction

The key benefits of EPS induction is that the desired type of EPS response could be controlled, by voltage and duration and frequency. Furthermore, the type of EPS response can be modelled such as eccentric contraction could be modelled by combining EPS on elastic substrates with strain (Orfanos *et al.*, 2016). Myotube size can be increased by EPS (Ostrovidov *et al*., 2017; Takahashi, Shimizu and Okano, 2018; Mills *et al*., 2019) to improve structural maturity. Increasing the frequency of contractions has been shown to increase myotube length reaching up to 577 μm (Khodabukus *et al*., 2019). Similarly, following EPS, constructs produce larger fibre diameters, up to 450 μm (Yamasaki *et al*., 2009).

A SkM model, capable of spontaneous and EPS-controlled contraction, has been considered a highly mature and functional model (Guo *et al.*, 2014). In some models, spontaneous contraction is defined by specific developmental stages, such as by day 11, myofiber-like structures, striated MyHC patterns, and peripheral nuclei are observed (Mondrinos *et al.*, 2021). In this study, only the 2D model exhibited spontaneous contractions under defined media 2 differentiation conditions. However, without real-time analysis of 2D and 3D models in culture, visualisation of sporadic spontaneous contractions linked to a single model or event cannot be determined. Besides, models without external stimulation such as EPS can still be functionally bioactive and secrete proteins (revealed in subsequent chapters).

Chronic EPS may have produced a porous model, with MT images revealing mesh-like morphology and pockets in the cell-tissue network, particularly in comparison to the non-EPS model presented earlier. The ECM can also produce porous networks that could be cell-derived and formed with the elongated and aligned architecture observed within muscle samples (Hurd *et al.*, 2015). Porosity has also been favoured as a feature to 3D models (Davidenko *et al*., 2016). The potential of pores in the tissue structure as a result of the histological preprocessing steps including FFPE or sectioning cannot be ignored.

Analysis of maturity was assessed via area and MFI of in α-Actinin, MCHII, and dystrophin as structural markers, essential for contraction. Both sectional and entire gels were analysed (as the average of all the sections within it) revealed no statistical difference between – EPS and + EPS models. It can be argued that the 3D model produced homogenous myofiber throughout the gel, with the upper and lower sections being analogous. Furthermore, this also provided further evidence of static strain, without EPS as sufficient for development of a mature SkM model.

3.5.8 Study limitations

Although C2C12 are commonly applied unicellular models, they do not fully replicate the complexity of native SkM tissue. In fact, C2C12 cell cultures do not contain satellite cells equivalent to adult mouse skeletal muscle tissues (Snijders *et al.*, 2021), or possess many of the specialised features of skeletal muscle *in vivo* (Deshmukh *et al*., 2015a).

Contraction in the final MTSIP-strained hydrogels were not observed; thus, their contractile ability remains undetermined. Moreover, the hydrogel models were indeed stimulated in SFM, for the purpose of secretome analysis. Metabolic analysis of C2C12 myoblasts and myotubes in different SFM (B27 and AIM-V) has been investigated and showed varying metabolic profiles compared to conventional serum-supplemented culture (Jang *et al*., 2022). Furthermore, histological analysis of + EPS 1 h was not documented, however a non-EPS histological control model was not used, albeit supplemented. Therefore, this study was largely dependent on IF analysis. Additionally, commercial platforms like C-Dish™ often overlook the efficacy and electric field distribution of EPS models (Nagamine *et al.*, 2018), leaving their impact on SkM structural integrity undetermined. Conventional metrics, such as fibre length, width, orientation, and diameter, should have also been considered to better understand the effect of the variables investigated on the structural maturity of the final model (Moo and Herzog, 2018). Measurement of sarcomere lengths would provide better insights into sarcomere formation and consolidate the sarcomerogenesis premise of muscle lengthening under tensile strain.

3.6 Conclusion

This work successfully developed 2D and 3D models, characterised by key structural, and developmental features. Alongside this, a novel strain inducible platform was developed which promoted direction-dependent properties in C2C12-laden hydrogels. The lack of significant differences between hydrogel region, with and without stimulation, suggested a homogeneous model was produced. Contraction was not quantified in this study, and the similarity in maturity characterisation between the stimulated and unstimulated models prompted further investigation into secretomic characterisation,

with the secretion of myokines serving as evidence of the model's contractile functionality. Finally, the analysis of both acute and chronic effects of ± EPS on the developed models was explored in the subsequent chapter.

4 Proteomic Analysis of the Skeletal Muscle Secretome

4.1 Introduction

The effects of physical activity are long-lasting, contributing to improved health outcomes and reduced mortality (Lacombe *et al*., 2019). Exercise is increasingly being reviewed as a medicine (Pedersen, 2019b), with evidence for prescribing exercise as therapy for 26 diseases (Luan *et al*., 2019; Pedersen & Saltin, 2015) and even as therapy for cancer, cachexia (Hesketh, 2024) and cardiovascular disease (Ahmadi *et al*., 2023; Gronek *et al*., 2020). Myokines as exercise factors, following contraction, play crucial roles in intercellular communication, particularly in the regulation of metabolic processes (Argilés *et al*., 2016b; Eckel, 2019) . Thus, it is important to establish which myokines are released following SkM contraction, prior to investigation of systemic effects. The exploration of myokine adaptations to various exercise protocols, has provided insights into how different types of physical activity mimetics can differentially modulate myokine secretion (Nikolić *et al*., 2017). In human studies, different training modes (aerobic and resistance) altered the expression of several myokines including IL-15, SPARC, OSM and Decorin, and their effects were observed immediately following 1 h exercise in healthy adults (Bettariga *et al*., 2024). Furthermore, plasma concentrations of FGF21, IL-6, IL-8, IL-15, and IL-18 have also been found to be regulated by acute exercise (Garneau *et al*., 2020).

Myokines as contraction-induced proteins can help validate the functional properties of tissue-engineered SkM models. Many recent bioengineered *in vitro* SkM models that apply external stimuli for contraction, fail to report secretome factors (Bakooshli *et al*., 2019; Capel *et al*., 2019; Costantini, Testa, Mozetic, *et al*., 2017; Denes *et al*., 2019; Gholobova *et al*., 2018; Khodabukus *et al*., 2019; Madden *et al*., 2015; Mao *et al*., 2019; Morimoto *et al*., 2020; Nakamura *et al*., 2017; Ostrovidov *et al*., 2017; Rao *et al*., 2018; Shima *et al*., 2018; Urciuolo *et al*., 2020; Yamasaki *et al*., 2009). However, some models that induce contraction do report single secreted factors such as TNFα soluble receptor I (García-Lizarribar *et al*., 2023) and IL-6 (Alave Reyes-Furrer *et al*., 2021; Bakooshli *et al*., 2019; Denes *et al*., 2019; Khodabukus *et al*., 2019; Takahashi *et al*., 2018). Meanwhile, other studies report differentially expressed proteins such as follistatin but are not defined as myokines (Mills *et al*., 2019; Ikeda *et al*., 2017b).

Exercise-induced myokine secretion can vary depending on the intensity, duration, and type of exercise performed. EPS can mimic muscle contraction patterns observed during different types of physical activity and is a valuable model for studying myokine release *in vitro* (Nikolić & Aas, 2019; Valero-Breton *et al*., 2020). Application of EPS has allowed researchers to delineate the specific myokines involved in various physiological processes, including glucose metabolism, fat oxidation and inflammation (Brandt *et al*., 2015).

In order to characterise myokines from skeletal muscle, robust detection is required. Over 3000 myokines have been identified to date (Piccirillo, 2019) but most remain uncharacterised, specifically in their alterations to exercise. Mass spectrometry-based methods have contributed to secretome-wide analysis and identification of thousands of proteins in the conditioned media (CM) of C2C12 cells (Deshmukh *et al*., 2015a; Grube *et al*., 2018), primary human SkM cells (Hartwig *et al*., 2014) and human myoblasts (Le Bihan *et al*., 2012). Furthermore, for the identification of myokines, liquid chromatography mass spectrometry (LC-MS) is considered a gold-standard detection method (Albrecht, *et al*., 2020) and it is a particularly valuable technology for the identification of novel myokines due to high sensitivity and dynamic range offered (Esposito *et al*., 2015; Gonzalez-Franquesa *et al*., 2021; Ishiuchi, Sato, Komatsu, *et al*., 2018; Mittenbühler *et al*., 2023; Piccirillo, 2019; Yoon *et al*., 2011).

The detection and quantification of myokines, however, presents significant challenges, mainly due to their low abundance in biological fluids (Sarihan *et al*., 2023; Tu *et al*., 2010) and the complexity of the muscle secretome (Florin *et al*., 2020). Beyond mass spectrometry techniques, several alternative methods have been employed to successfully detect myokines including Enzyme-Linked Immunosorbent Assay (ELISA), Multiplex Immunoassay (MIA), Western blotting (WB) and Polymerase chain reaction (PCR). ELISA's reliance on antibody specificity can limit its ability to detect all isoforms or post-translational modifications of a given myokine (Le Goff *et al*., 2021). This approach is also biased and targeted and thus cannot detect potentially novel myokine proteins. Comparatively, MS allows for the identification and quantification of a broad range of myokines simultaneously. However, while relative quantification is possible, this does not provide absolute quantitative information as with ELISA, which can only be achieved through the use of a targeted MS approach using labelled standards. As a result, this can lead to discrepancies when comparing to other methods. MS is highly sensitive, detecting low abundance myokines in complex biological samples, but it can be challenging and prone to errors including inefficient protein extraction, digestion or protein loss during sample clean-up, all of which can potentially lead to underrepresentation of myokines. Furthermore, the stepwise methodology can be time-consuming and requires validation of the secreted factors. MIA enables the simultaneous detection of multiple myokines in a single sample, offering a modest profile of myokine secretion. However, cross-reactivity can arise and the approach is targeted and limits novel myokine discovery. WB is often used to validate findings from ELISA or MS; however, it is semi-quantitative when compared to other methods. Finally, PCR, used to quantify the mRNA levels of various myokines like IL-15 and FNDC5 in muscle tissues, can show how exercise can regulate their expression (Huh *et al*., 2018), however, mRNA levels do not necessarily translate to changes at protein level. These discrepancies

underscore the importance of cross-validating findings using multiple methods to ensure the accuracy and reliability of myokine quantification. These challenges also highlight the need for ongoing methodological advancements to improve the detection sensitivity and specificity for myokine targets.

4.2 Aims and objectives

The aim of this chapter was to detect and quantify putative myokines in the secretome of stimulated and unstimulated 2D and 3D SkM models developed in chapter 2. We hypothesised that myokines are secreted directly after contraction and that the secretion is altered by the duration of stimulation i.e. acute and chronic duration. To test this, the following experimental objectives were employed:

- Establish acute and chronic *in vitro* exercise-mimicking timepoints.
- Analyse changes in myokine abundance between acute and chronic conditions, via Liquid Chromatography with Mass Spectrometry with Elevated Energy ($LCMS^E$).
- Validate the presence of $LCMS^E$-detected myokines in conditioned media (CM) samples and quantify changes in concentration between acute and chronic ± EPS conditions, via multiplex immunoassay (MIA).
- Verify detected myokines through comprehensive, global profiling and reveal novel candidate myokines.

4.3 Experimental design

This chapter examined myokine secretion following contraction of 2D and 3D C2C12 SkM models. To establish the ideal time course for acute and chronic exercise-mimicked durations, broader timepoints (1 h, 3 h, 6 h, and 24 h) were analysed via $LCMS^E$ in the 2D C2C12 model first (not shown in the schematic, **Figure 4.1**). Following data collection, 1 h and 6 h timepoints were then confirmed for acute and chronic exercise mimicry. Two detection methods were employed. The primary approach utilised $LCMS^E$ to detect peptides, while MIA analysis was employed to quantify myokines using a commercially available panel of target proteins. $LCMS^E$ enabled both selective and global analysis; in selective analysis, known myokines were matched to peptide sequences within the secretome. Identified myokines were then assigned GO terms, facilitating their categorisation by biological processes, molecular functions, cellular components, and the identification of potential biological pathways. Novel candidate myokines were identified by virtue of their secretion from C2C12 cells via canonical (SignalP) or non-canonical (SecretomeP) pathways. Potential novel myokines were functionally characterised and network analysis was performed (via String DB) to predict interactions

between candidate myokines and other proteins and infer potential roles in muscle communication (**Figure 4.1**).

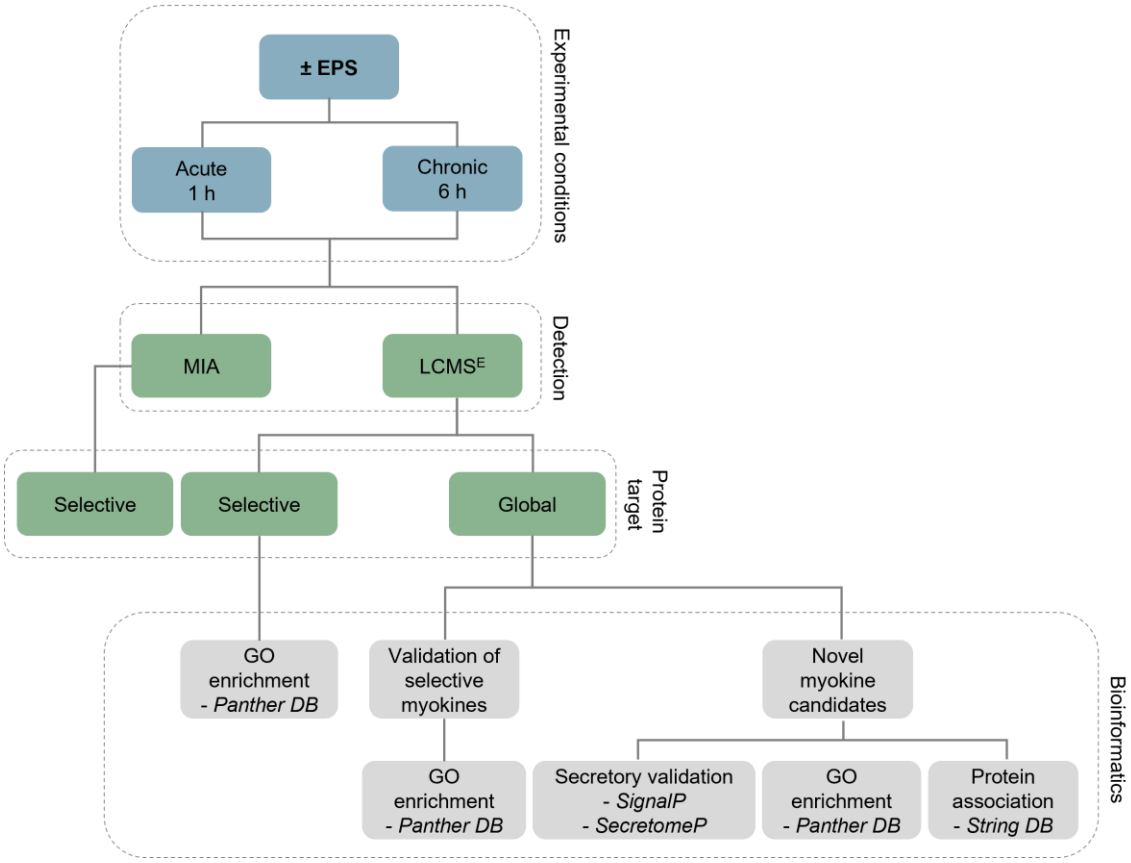

Figure 4.1 Schematic of Chapter 4 experimental design. *This chapter sought to detect and quantify putative myokines in the secretome of unstimulated (- EPS) and stimulated (+ EPS) 2D and 3D SkM models that were developed in Chapter 3. EPS, Electrical pulse stimulation; LCMS^E, Liquid chromatography tandem mass spectrometry; GO, Gene ontology.*

4.4 References for the selective and global analysis of myokines

Experimental peptide sequences were matched against theoretical peptide sequences (generated from *in silico* digests) via Progenesis QIP. A target list of 29 myokines that were established from a pre-existing 12-plex MIA panel, supported by an additional 16 myokines reported in the literature was used as an initial targeted database. The entire mouse proteome was also searched, for a broader exploratory approach (**Figure 4.2**).

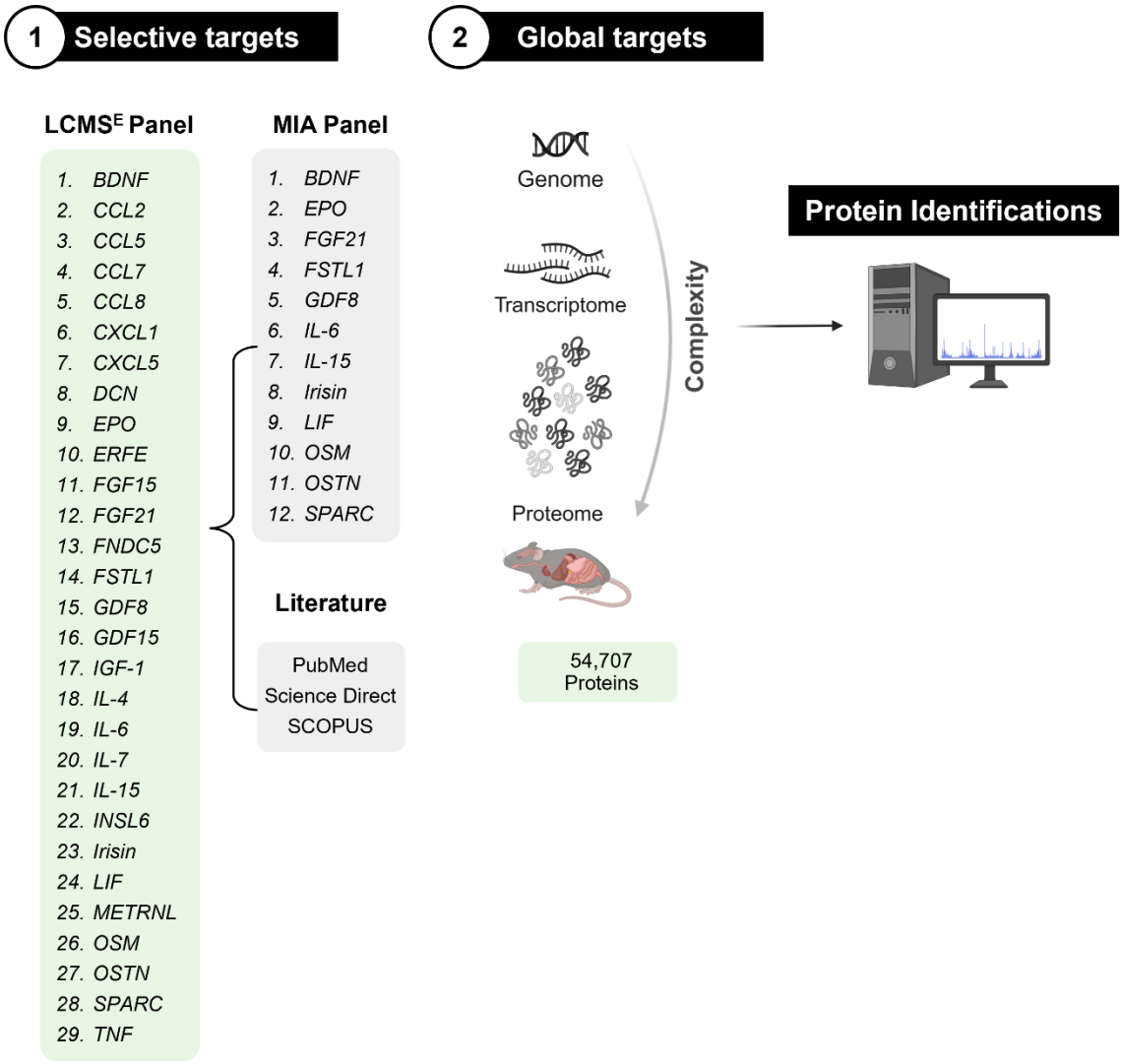

Figure 4.2 Reference lists for protein identifications. *Experimental peptide sequences were matched to target peptide sequences using Progenesis QI for proteomics.* ***(1)*** *Selective targets comprised of 29 myokines that were established from the literature for LCMS^E analysis and a 12-plex panel was used for MIA analysis.* ***(2)*** *The global target consisted of the entire mouse proteome, for a broader exploratory approach. BDNF, Brain-derived neurotrophic factor; CCL2/5/7/8, Chemokine ligand 2/5/7/8; CXCL1/5, C-X-C Motif Chemokine Ligand 1/5; DCN, Decorin; EPO, Erythropoietin; ERFE, Erythroferrone; FGF15/21, Fibroblast growth factor 15/21; FNDC5, Fibronectin type III domain-containing protein 5; FSTL1, Follistatin-like 1; GDF15/8, Growth/differentiation factor 15/8; IGF-1, Insulin-like growth factor 1; IL-15/4/6/7, Interleukin-15/4/6/7; INSL6, Insulin like 6; LIF, Leukaemia inhibitory factor; METRNL, Meteorin-like; OSM, Oncostatin M; OSTN, Osteocrin; SPARC, Secreted protein acidic and rich in cysteine; TNF, Tumour necrosis factor. Canonical and isoform sequences were obtained from UniProt (UniProtKB and Proteome). Image created with biorender.*

4.5 Results

4.5.1 Detection of myokine peptides from acute and chronic ± EPS conditions

4.5.2 Confirmation of acute and chronic ± EPS timepoints

To determine the optimal time course for acute and chronic ± EPS, the secretome from 2D cultures were initially analysed. CM from unstimulated (- EPS) and stimulated (+ EPS) cells were collected immediately after 1 h, 3 h, 6 h, and 24 h ± EPS and prepared for mass spectrometry (Section 2.4.2). A target panel of 29 myokines that included MIA and literature-sourced myokines were used for selective proteomic profiling (**Figure 4.2**). Stimulated and matched unstimulated controls were analysed independently and the mean abundance of each myokine was calculated as described in section 2.4.2.6.

Thirteen myokines were detected in the - EPS condition and 15 in the + EPS condition across all timepoints 1 h, 3 h, 6 h and 24 h. Among the detected myokines, 10 were shared between ± EPS conditions, representing baseline expression (**Figure 4.3**). In the 2D - EPS condition, myokines with a fold changes > 2 between the highest mean condition (HMC) and the lowest mean condition (LMC) in 2D - EPS included CCL7, 6.15 (HMC 3 h, LMC 24 h); DCN, 2.35 (HMC 24 h, LMC 3 h); FNDC5, 2.64 (HMC 6 h, LMC 24 h); FSTL1, 13.87 (HMC 6 h, LMC 24 h); IL-7, 2.37 (HMC, 6 h, LMC 1 h) and SPARC, 7.81 (HMC 6 h, LMC 24 h). Statistically significant change in expression between conditions for a given myokine ($p \leq 0.05$) is reported in **Figure 4.3**. All myokines detected in the - EPS CM had decreased in abundance (>2-fold) from 6 h to 24 h (except for DCN which had increased by 1.5-fold) included CCL7, 3.65; FNDFC5, 2.64; FSTL1, 13.88; INSL6, 2.59; IL-7, 2.25 and SPARC, 7.81 (**Figure 4.3.**)

In the 2D + EPS, the largest fold change was seen in INSL6, 75.97 (HMC 24 h, LMC 1 h) and further notable fold increases in the following myokines: LIF, 33.67 (HMC 24 h, LMC 3 h) and CCL2, 21.6 (HMC 24 h, LMC 1 h). However, there was no statistical significance ($p > 0.05$) between any of the timepoints in this condition. Following stimulation in 2D (+ EPS), the following myokines had fold decreases (>2) from 6 h to 24 h: FSTL1, 2.9; GDF8, 2.3; CXCL1, 2.5; INSL6, 6241.5; FGF15, IL-7 and SPARC. As a result, 6 h was selected as the longest period of exercise mimicry representing chronic exercise timepoint with 1 h selected to mimic acute exercise. The highest mean myokine abundance was observed at 6 h for both -EPS and +EPS conditions (**Figure 4.3**).

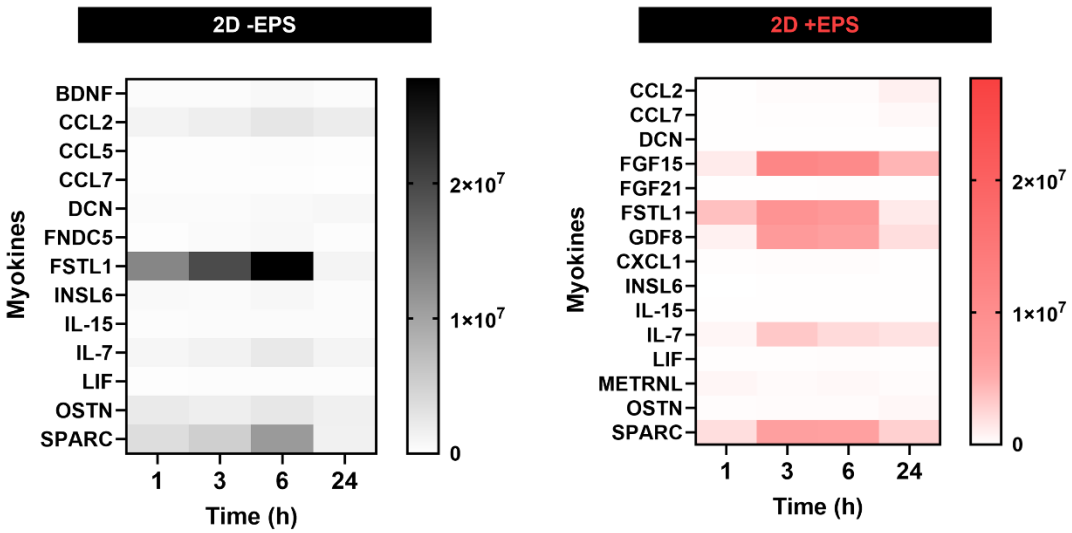

Figure 4.3 LCMS^E – detected myokines from a range of acute and chronic timepoints. *Heat maps show normalisation mean abundance of myokines from 2D - EPS (black) and 2D + EPS (red) conditions. Each box represents a mean normalised abundance (n=3) of a single myokine. Differences between 1 h, 3 h, 6 h and 24 h (- EPS) timepoints were: CCL7 (**p=0.0102; HMC 3 h, LMC, 24 h), DCN (***p=0.0007; HMC 24 h, LMC 3 h), FNDC5, *p=0.0430 (HMC 6 h, LMC 24 h), FSTL1 *p = 0.0326 (HMC 6 h, LMC 24 h), IL-7 **p = 0.0161 (HMC, 6 h LMC 1 h) and SPARC (****p= 0.0001; HMC 6 h, LMC 24 h). However, in the + EPS condition, there were no significant difference between any of the 4 timepoints.*

4.5.3 Unstimulated myokines from acute and chronic conditions

The - EPS condition established a basal myokine secretion profile from 1 h to 6 h. There were 9 myokines identified in 2D CM and 18 in 3D in CM from unstimulated models (**Table 4.1**). In the 2D - EPS condition, 3 myokines revealed a significant difference and > 2-fold increase (in mean relative abundance) between 1 h and 6 h: FNDC5, 2.80 (p=0.0463); INSL6, 2.63 (p=0.0009*)* and FSTL1, 3.68 (p=0.0627) (**Figure 4.4, Ai, Bi**). A minimal change (<2) was recorded for the remaining myokines (**Figure 4.4, Bi**). In the 3D - EPS condition, all but one detected myokine (GDF15, $p > 0.05$), exhibited increased relative expression from 1 h to 6 h (**Figure 4.4, Aii**). Notable fold increases (>2) and significance ($p \leq 0.05$) were reported for the following myokines in 3D - EPS: DCN, 7.37 (p=0.0033); FNDC5, 6.84 (p=0.0399); GDF8, 2.78 (p=0.0492); IGF-1, 7.80 (p=0.0138); INSL6, 10.21 (p=0.0125); IL-4, 7.23 (p=0.0143*)*; IL-6, 10.43 (p=0.0042); IL-7, 26.75 (p=0.0019); LIF, 16.42 (p=0.0025); OSM, 14.27 (p=0.0057); OSTN, 18.11 (p=0.0007) and TNF, 617.28 (p=0.0065) (**Figure 4.4, Aii, Bii**). The following myokines revealed an insignificant ($p > 0.05$) difference between 1 h and 6 h but a > 2-fold change: CCL5 (5.27), EPO (2.24) and SPARC (2.13) (**Figure 4.4, Bii**). Notably, IL-15 was also detected at 1 h (9.35 a.u ± 16.19, n=1) and 6 h (2.11×10^3 a.u ± 1.24×10^3, n=3) but excluded from ANOVA analysis due to low sample number for statistical comparison.

Table 4.1 Putative myokine identifications in 2D and 3D - EPS CM. *Experimental peptide sequences were matched to 29 known myokine protein sequences from the UniProt database. Data is sorted according to the greatest unique peptide matches and confidence scores. Myokines detected in at least 1 CM sample are reported*

Unique peptides	Confidence score	Mass	Accession no.	Myokine
2D - EPS				
28	135.0	35305.5	P07214	SPARC
20	108.4	35694.5	Q62356	FSTL1
19	84.5	18068.9	P10168	IL-7
13	71.7	14437.5	P61364	OSTN
9	50.0	16554.1	P10148	CCL2
9	52.2	22727.9	Q9QY05	INSL6
9	40.8	22629.3	P09056	LIF
7	25.3	28522.5	P21237	BDNF
4	17.0	23606.1	Q8K4Z2	FNDC5
3D - EPS				
15	108.2	18068.9	P10168	IL-7
14	68.0	24612.1	P08505	IL-6
12	51.9	43662.8	O08689	GDF8
10	67.9	23606.1	Q8K4Z2	FNDC5
9	41.2	16232.8	P07750	IL-4
8	46.0	11284.2	Q03366	CCL7
8	43.1	17606.3	P05017	IGF-1
8	41.6	26180.9	P06804	TNF
6	27.0	40151.2	P28654	DCN
6	39.8	21650.3	P07321	EPO
6	31.8	22629.3	P09056	LIF
6	29.3	14437.5	P61364	OSTN
5	29.5	35305.5	P07214	SPARC
4	16.2	33738.6	Q9Z0J7	GDF15
4	9.4	22727.9	Q9QY05	INSL6
4	23.1	18992.7	P48346	IL-15
3	13.0	30341.8	P53347	OSM
1	4.7	10355.9	P30882	CCL5

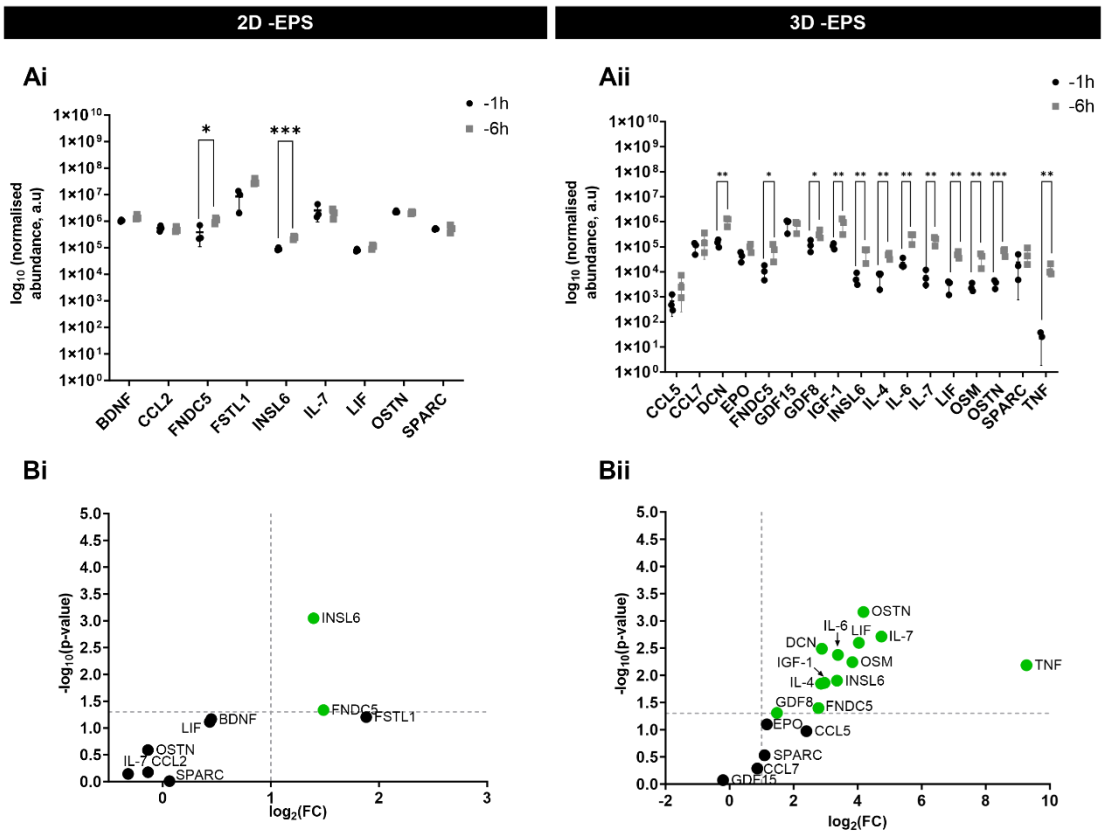

Figure 4.4 LCMS^{E-}detected myokines from 2D and 3D - EPS conditions. *Graphs show quantification of myokine abundance, recalibrated to a normalisation reference and analysed via one-way ANOVA. Data represents triplicate CM samples (n=3) as mean with SD.* ***(Ai)*** *Significances between 1 h and 6 h in 2D: * p=0.0463, FNDC5 and ***p=0.0009, INSL6.* ***(Aii)*** *Significances between 1 h and 6 h in 3D: **p=0.0033, DCN; *p=0.0399, FNDC5, *p=0.0492, GDF8; **p=0.0138, IGF1; **p=0.0125, INSL6; **p=0.0143, IL-4; **p=0.0042, IL-6; **p=0.0019, IL-7; **p=0.0025, LIF; **p=0.0057, OSM and ***p=0.0007, OSTN in In 3D. Significance versus magnitude of change in myokines detected from 1 h and 6 h - EPS conditions. Myokines with p-value ≤0.05 and fold change >2 (highlighted in green) include* ***(Bi)*** *INSL6 and FNDC5 in 2D and* ***(Bii)*** *DCN, FNDC5, IGF-1, INSL6, IL-4, IL-6, IL-7, IL-15, LIF,OSM, OSTN and TNF in 3D.*

4.5.4 Stimulated myokines from acute and chronic conditions

In the 2D + EPS conditions, ten myokines were matched to the targeted reference list whereas five myokines were recorded from the + EPS 3D model CM (**Table 4.2**). In the 2D + EPS condition, there were no significant differences (p>0.05) in the mean abundance of myokines detected between 1 h and 6 h (**Figure 4.5, Ai**). However, minor increases were reported for CCL7, DCN, FGF15, FSTL1 and METRNL, compared to a decrease in abundance of LIF and OSTN (1.78 and 1.53) from 1 h to 6 h was observed, however insignificant (**Figure 4.5, Ai**). Also, in the 2D + EPS condition, fold increases >2 was reported for GDF8 (2.06) and IL-7 (3.48), but this was not significant (**Figure 4.5, Bi**). SPARC was also detected in only 1 CM sample at 1 h with a normalised mean abundance of 3.34 x 10^4 a.u (n=1) and at 6 h, resulting in a normalised mean abundance of 9.39 x 10^3 a.u ± 1.36 x 10^4 (n=3), and was also excluded from acute vs chronic analysis.

A selection of myokines detected in 3D + EPS model increased from 1 h to 6 h (**Figure 4.5, Aii**). LIF showed a significant fold increase of 4.33 (p=0.0241) between 1 h and 6 h + EPS (**Figure 4.5, Bii**). CCL2, IL-15 and OSTN showed no significance and p>0.05 and fold-change < 2. IL-6 was undetected at 1 h but detected at 6 h and had a normalised mean abundance of 5.18 x 10^4 a.u ± 8.01 x 10^3.

Table 4.2 Putative myokine identifications in 2D and 3D + EPS CM. *Experimental peptide sequences were matched to 28 known myokine protein sequences from the UniProt database. Data is sorted according to the greatest unique peptide matches and confidence scores. Myokines detected in at least 1 CM sample are reported.*

Unique peptides	Confidence score	Mass	Accession no.	Myokine
2D + EPS				
24	122.0	35694.5	Q62356	FSTL1
8	34.2	11284.2	Q03366	CCL7
7	42.7	35099.8	Q8VE43	METRNL
5	32.9	14437.5	P61364	OSTN
3	20.3	18068.9	P10168	IL-7
2	15.4	22629.3	P09056	LIF
1	11.7	40151.2	P28654	DCN
1	6.3	25521.0	O35622	FGF15
1	4.9	43662.8	O08689	GDF8
1	5.1	35305.5	P07214	SPARC
3D + EPS				
31	128.0	14437.5	P61364	OSTN
12	81.8	22629.3	P09056	LIF
14	53.7	16554.1	P10148	CCL5
6	36.2	18992.7	P48346	IL-15
1	3.7	24612.1	P08505	IL-6

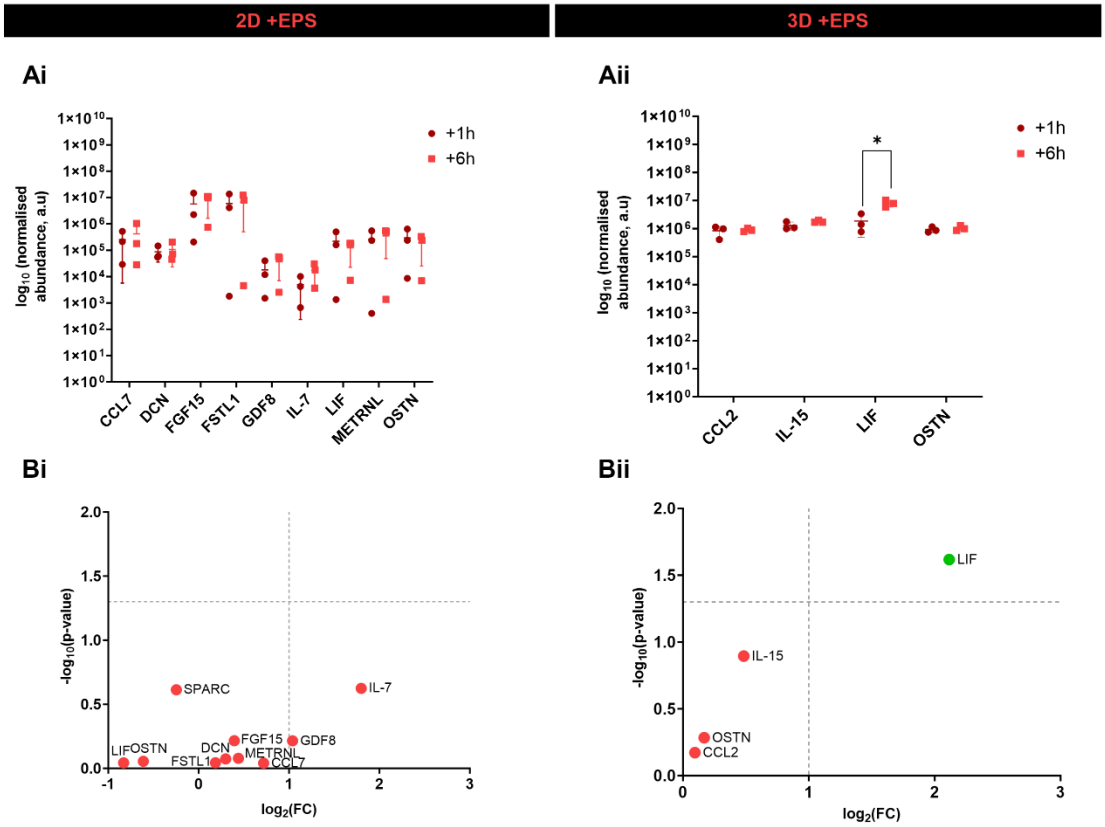

Figure 4.5 LCMS^{E}-detected myokines from 2D and 3D + EPS conditions. *Graphs show quantification of myokine abundance, recalibrated to a normalisation reference and analysed via one-way ANOVA. Data represents triplicate CM samples (n=3) as mean with SD. (**Ai**) There were no significances between 1 h and 6 h in 2D. (**Aii**) In 3D, significances between 1 h and 6 h was *p=0.0241, LIF. (**Bi-Bii**) Significance versus magnitude of change in myokines detected from 1 h and 6 h - EPS conditions. Myokines with p-value ≤0.05 and fold change >2 (highlighted in green) was LIF only in the 3D condition.*

4.5.5 Functional analysis

Despite their significant role in muscle physiology and intercellular communication, many myokines remain uncharacterised. Their intricate pleiotropic signalling pathways and interconnectivity pose characterisation challenges when determining biological relevance. To address these issues, functional GO analysis of the putatively identified myokines showing significant difference in secretion was performed to inform changes in the secretome between + EPS and - EPS conditions in acute (1 h) and chronic (6 h) exercise-mimicking models. Potential gene regulatory pathways controlled by the putative myokines detected using LCMS^{E} were determined (**Tables 4.1 and 4.2**). The effect of myokines on proximal and distal tissues and organs was not investigated in this body of work since a single-cell model was utilised.

Myokine activity was denoted by gene processes, including response to cytokines (GO:0034097), cytokine-mediated signalling pathways (GO:0019221), cytokine activity (GO:0005125), and cytokine receptor binding (GO:0005126) to determine potential

regulatory functions. Skeletal muscle metabolic regulation was also reaffirmed via the assignment to genes that positively regulate metabolic processes (GO:0009893).

Metabolic process regulation was noted as an associated function in both 2D / 3D ± EPS conditions. GO analysis indicated that autonomously contracting 2D and 3D models (- EPS) released myokines could be assigned to hormone activity (appendix data, **Table A2**), suggesting potential roles in endocrine function. In 3D non- EPS conditions, a key associated biological process was muscle structure development (GO:0061061), indicating that the unstimulated secretome from 3D culture is integral to developing, maintaining, and repairing muscle structure. Cell death (GO:0008219) and its positive regulation (GO:0043068), and chronic inflammatory response regulation (GO:0002676) were uniquely associated with the biological process of 3D - EPS secretome. The - EPS 3D culture secretome was also assigned to the regulation of ERK1/2 cascade (GO:0070372) and positive regulation of MAPK cascade (GO:0043410). In 2D + EPS and - EPS secretome was linked to regulation (GO:0051239) whereas the 3D + EPS secretome was linked to both regulation (GO:0051239) and negative regulation, GO:005124). 3D - EPS was linked to multicellular organismal processes (GO:0032501), which suggests that myokines associated with these processes are involved in systemic regulation and have the potential to act distally. Multicellular organismal processes (GO:0032501) were associated with all conditions, and gene products of myokines were annotated in the extracellular region of a cell (GO:0005576). This evidence suggests that proteins are candidates for being secreted or acting extracellularly.

4.5.6 Validation of myokine secretion from 2D and 3D models

MIA was performed to verify the presence of myokines from 2D and 3D model secretome. Furthermore, due to a lack of direct comparison between - EPS and + EPS via LCMS^{E}, these group comparisons via MIA were necessary for complete analysis. The effect of EPS on myokine secretion was analysed from 2D cells that were subjected to a single bout of 1 h acute and 6 h chronic EPS on D7. The 3D cell-hydrogel was subjected to 1 h EPS on D21 and 1 h EPS each day from D16 until D21 (Section 2.1.3.7).

The effects of EPS on myokines release were investigated by comparing the stimulated (+ EPS) model to the unstimulated (- EPS) model**.** The following myokines were analysed from CM samples of each condition: BDNF, EPO, IL-6, IL-15, FGF21, FSTL1, Myostatin, Irisin, LIF, OSM, OSTN and SPARC. Not all myokines from the target panel were detected in sample conditions. The following list of those myokines that were undetected, with the remaining being observed (Figure 3.9). In the 2D acute (1 h) condition, IL-5 was not detected in either - EPS or + EPS. GDF8 was only detected in the + EPS condition. In the 2D chronic (6 h) condition, IL-15, GDF8 and OSM were detected in - EPS but not

+ EPS CM samples. In the 3D acute (1 hr) condition, EPO and GDF8 were undetected in both - EPS and + EPS conditions. Finally, in the chronic (6 hr) 3D condition, BDNF was undetected in - EPS CM and was produced at low levels after EPS, while EPO and OSM were detected in 3D chronic (6 hr) - EPS CM samples but were undetected in the + EPS condition (**Figure 4.6**).

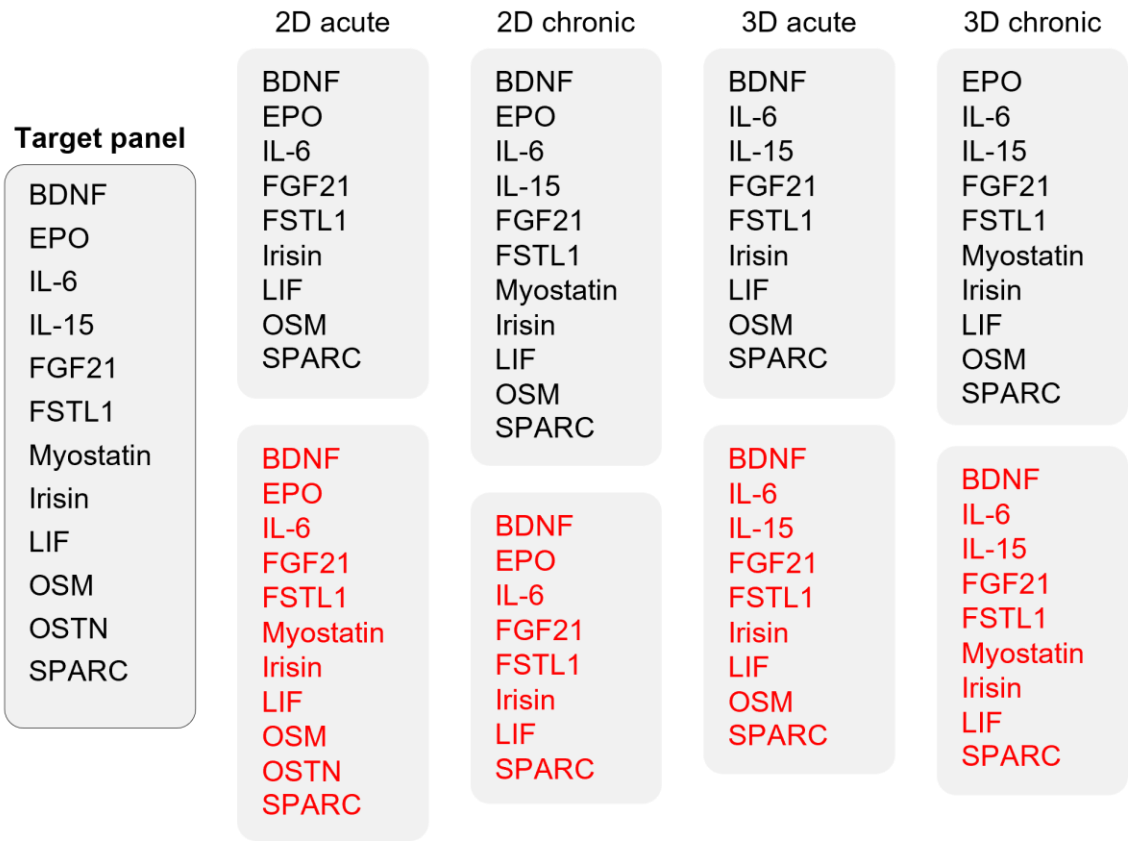

Figure 4.6 Lists of MIA-detected myokines from 2D and 3D ± EPS conditions. *Myokines detected in at least 1 condition were reported in models. - EPS (black) + EPS (red).*

Analysis of differences between - EPS and + EPS CM, the 2D acute (1 h) condition was largely inducible by EPS. There were fold-increases in the median concentration of the following myokines: BDNF (2.76), EPO, (3.39), FSTL1 (2.02) Irisin, (3.17), LIF, (2.20). There was minimal change in IL-6 (1.10) and OSM (1.39). FGF21 was the only myokine that had a 1.65-fold decrease following stimulation (**Figure 4.7, Ai**). The 2D chronic condition (**Figure 4.7, Aii**) presented as an exclusively reducible condition, with a decrease in all myokines after + EPS: with fold decreases in BDNF, (50.08); EPO, (2.66); FGF21, (4.10); FSTL1, (16.53); Irisin, (137.15); LIF, (5.68); SPARC, (11.28). In the 3D acute condition (**Figure 4.7, Bi**), IL-15 and OSM had higher median concentration following EPS, although only minor fold changes were seen of 1.04 and 1.05, respectively (**Figure 4.7, Bi**). The remaining myokines decreased after + EPS, with fold decreases seen for IL-6 (189.88), FGF21 (54.03), FSTL1 (16.58), Irisin (2.76), LIF (1.54),

SPARC (17.16) (**Figure 4.7, Bi**). Finally, the 3D chronic (6 h) condition (**Figure 4.7, Bii**) revealed a fold decrease in IL-6 (3.24) and SPARC (98.10). A fold increase was seen in FSTL1 (2.46), whereas FGF21, Irisin and LIF had ≤ 1.07-fold change in all factors (**Figure 4.7, Bii**). No significant differences (p>0.05) were reported between - EPS and + EPS in either acute and chronic 2D and 3D conditions (**Figure 4.7**).

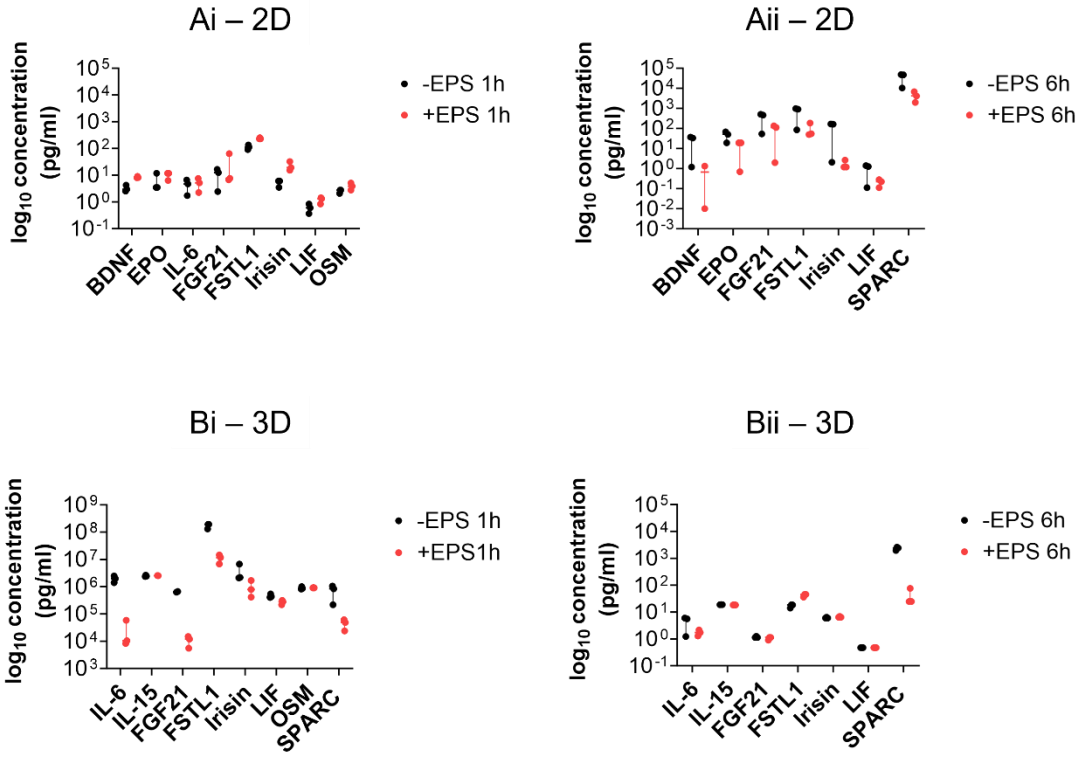

Figure 4.7 MIA-detected myokines from 2D and 3D ± EPS conditions. *Quantification of myokine concentration at 1 h and 6 h in* ***(A)*** *2D and* ***(B)*** *3D, analysed via the Mann-Whitney test, followed by Holm-Šídák's post hoc procedure. Data represents triplicate CM samples (n=3) as median with range. No significant differences (p>0.05) were reported between - EPS and + EPS.*

4.5.7 Summary of myokines detected via LCMS^{E} and MIA

In MIA analysis, the most commonly detected myokines were IL-6, FGF21, FSTL1, Irisin, LIF and SPARC. Secondly, BDNF was present in all conditions except the 3D chronic - EPS. Unique myokines were detected in - EPS or + EPS conditions or the 2D and 3D models. OSM was detected in all conditions besides the chronic + EPS conditions in 2D and 3D. LCMS^{E} comparison of acute and chronic ± EPS revealed the most common myokines shared across all conditions were LIF and OSTN. Secondly, IL-7 and SPARC were detected in all conditions, excluding the 3D + EPS condition. The following unique myokines were detected in a single condition only: BDNF and CCL2 (2D - EPS); FGF15 and METRNL (2D + EPS); EPO, GDF15, IGF-1IL-4,M OSM and TNF (3D - EPS). No unique myokines were identified in the 3D + EPS condition. A summary of shared and

unique number of myokines identified by each detection method is summarised in **Figure 4.8**.

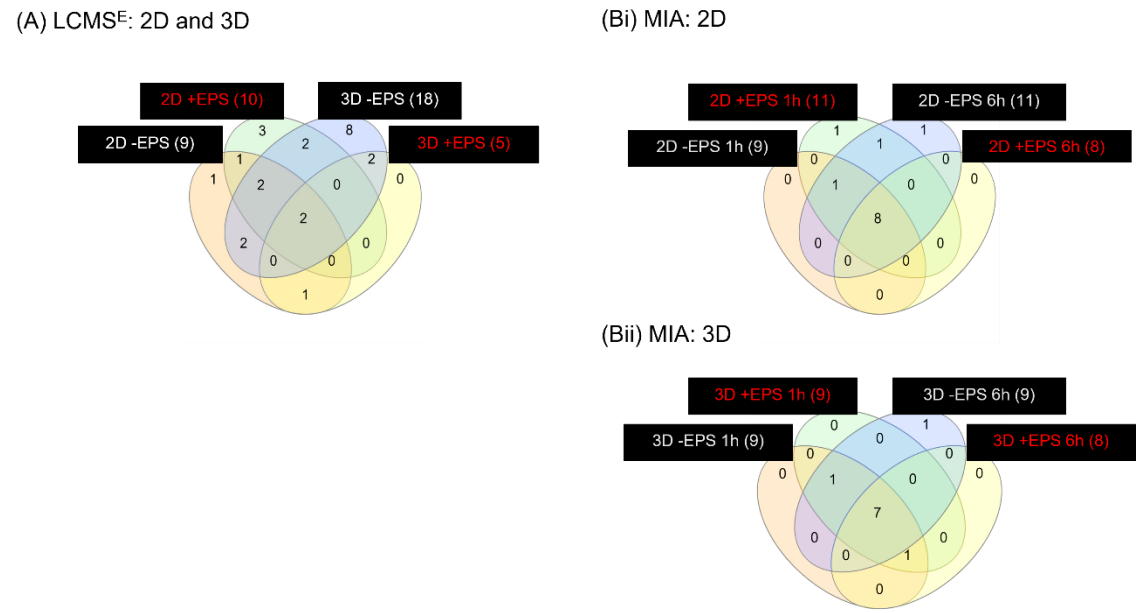

Figure 4.8 Summary of myokines detected from 2D and 3D ± EPS conditions via LCMS^E and MIA. *MIA examined - EPS vs. + EPS while LCMS^E analysis investigated acute vs chronic (±) EPS.*

4.5.8 Global profiling

Global profiling of the conditioned media of 2D and 3D samples revealed the successful identification of proteins >200 per condition. LCMS^E detected peptides were matched to proteins and identified 1210 in the 2D - EPS condition, 397 in 2D + EPS condition, the 215 in the 3D - EPS condition and 349 in the 3D + EPS condition. The complete protein details can be accessed via additional files (https://doi.org/10.6084/m9.figshare.27997763.v1).

4.5.8.1 Secretory Pathway Characterisation

Proteins directed to the secretory pathway may serve as potential myokines. A step toward identifying novel myokines was made via signal peptides (SP) predictions after screening against all five known types of signal peptides (Teufel *et al.*, 2022). Several proteins of interest were identified among the top 10 secreted proteins with the highest confidence score (**Table 4.3**) and the presence of SP, including Serotransferrin (0.980), Ceruloplasmin (0.979), C3/C5 convertase (1.000), Complement C3 (0.977), Fibronectin (0.960), Gelsolin (0.975) and Complement factor B (0.977). Plots of SP type, cleavage location and probabilities are featured in the appendix (Appendix data, **Figure A2**). Further analysis of the highest-ranked secreted proteins by confidence score (**Table 4.3**) for non-signal peptide secretion was conducted using SecretomeP. This identified

Negative elongation factor E/isoform 2 of Negative elongation factor E (P19426/ P19426-2) with a NN-score of 0.741 and RNA-binding protein/ RNA-binding protein 25 (B2RY56, NN-score 0.622). Histone H4 (P62806) also produced an NN-score of 0.791, predicting non-canonical secretion, however, it does not fulfil the role of signalling molecules from muscle cells.

4.5.8.2 Functional classification

Candidate myokine IDs with pathway characterisation were inputted into Panther DB, to assess GO assignments. GO enrichment and pathway analysis to identify biological processes and pathways associated with candidate myokines, supporting their functional characterisation. GO biological process of candidate myokines showed Serotransferrin to be involved in biological process involved in interspecies interaction between organisms (GO:0044419), immune system process (GO:0002376), localisation (GO:0051179) and response to stimulus (GO:0050896). Ceruloplasmin is associated with localisation only. Gelsolin is associated with biological regulation (GO:0065007), cellular process (GO:0009987), developmental process (GO:0032502) and multicellular organismal process (GO:0032501). Complement factor B is shown to be involved in biological process involved in interspecies interaction between organisms (GO:0044419) biological regulation (GO:0065007), immune system process (GO:0002376) and again, response to stimulus (GO:0050896). Complement factor C3 remained unclassified, while C3/C5 convertase and fibronectin had no hits. For non-classically secreted proteins, negative elongation factor E was associated only with biological regulation (GO:0065007), and its isoform was unclassified. RNA-binding protein/ RNA-binding protein 25 and Histone 4 were associated with cellular processes (GO:0009987). Consequently, we propose Serotransferrin, Gelsolin, and Complement factor B are the likely myokine candidates that were able to be characterised thus far due to SP prediction and biological processes attributed to myokines and myokine-related GO.

Table 4.3 Protein IDs from the CM of 2D and 3D - EPS and + EPS 2D models. *Proteins are matched against the whole mouse genome. The top 10 proteins detected are reported from 4 conditions and are sorted by the highest confidence scores/unique peptides. The list comprises previously known and detected myokines (bold) as well as novel myokine candidates.*

Unique peptides	Confidence score	Mass (Da)	Accession no.	Protein
2D - EPS				
53	523.18	243371.64	B7ZNJ1	Fibronectin
46	502.54	204568.08	A0A2I3BPQ5	Zinc finger
30	356.16	188023.95	P01027	Complement C3
30	305.32	70745.57	P07724	Albumin
24	254.54	121949.95	Q61147	Ceruloplasmin
28	248.71	35305.50	P07214	**SPARC**
7	220.92	42668.22	P19426	Negative elongation factor E
17	218.55	78890.94	Q921I1	Serotransferrin
11	202.06	99894.16	B2RY56	RNA-binding protein
12	197.94	245942.68	Q61043	Ninein
2D + EPS				
16	175.5873	70745.57	P07724	Albumin
6	126.0729	42079.02	P60710	Actin_ cytoplasmic 1
22	122.0082	35694.49	Q62356	**FSTL1**
3	105.9791	42408.26	P62737	Actin_ aortic smooth muscle
11	101.5674	78890.94	Q921I1	Serotransferrin
8	79.6956	83623.54	P11499	Heat shock protein
13	73.8184	204497	E9Q784	Zinc finger CCCH domain-containing protein 13
7	69.3331	15208.04	P16045	Galectin-1
9	66.6568	143427.5	A2A4P0	ATP-dependent RNA helicase
8	63.7908	39812.19	P05064	Fructose-bisphosphate aldolase A
3D - EPS				
20	183.93	86340.88	P13020	Gelsolin
10	116.76	86373.26	P04186	Complement factor B
13	108.17	18068.85	P10168	**IL-7**
11	107.42	70745.57	P07724	Albumin
15	92.21	204568.1	A0A2I3BPQ5	Zinc finger CCCH type containing 13

Unique peptides	Confidence score	Mass (Da)	Accession no.	Protein
11	68.04	24612.11	P08505	**IL-6**
9	67.94	23606.05	Q8K4Z2	**FNDC5**
5	65.50	92612.41	Q99J31	Oligophrenin-1
7	60.32	42079.02	P60710	Actin_ cytoplasmic 1
8	60.05	11367.36	P62806	Histone H4
3D + EPS				
21	221.9287	70745.57	P07724	Albumin
23	186.0308	125009.7	E9PZD8	Ceruloplasmin
22	165.5098	204568.1	A0A2I3BPQ5	Zinc finger CCCH type containing 13
29	127.9937	14437.54	P61364	**OSTN**
12	109.0423	188023.9	P01027	Complement C3
16	108.6065	42668.22	P19426	Negative elongation factor E
11	92.0033	99894.16	B2RY56	RNA-binding protein 25
9	81.8349	22629.29	P09056	**LIF**
12	81.1231	86605.56	B8JJM5	C3/C5 convertase
8	74.7766	78890.94	Q921I1	Serotransferrin

4.5.8.3 Protein network analysis

Proteins identified via untargeted analysis (**Table 4.3**) demonstrated protein-protein interactions (PPI) (**Figure 4.9**). SRING analysis of the top 10 detected proteins revealed biological relevance amongst the secretome from all models (PPI enrichment *p*-value: 6.79×10^{-11}, **Figure 4.9, A**). Further analysis of interactions between candidate myokines, also revealed a robust network, with significant biological relevance (PPI enrichment p-value < 1.0×10^{-16}). The candidate myokines detected were clustered into 3 groups for potential functions or biological processes – an acute phase response (**Figure 4.9, B, red**), complement activation and regulation of complement cascade (**Figure 4.9, B, green**), and homeostatic iron regulator (HFE)-transferrin receptor Complex (**Figure 4.9, B, blue**). The STRING maps were extended to show other interactions with the proteins detected. In this way, the networks show potential dependencies and relationships within complex signalling events that implicate the detected proteins (**Figure 4.9**).

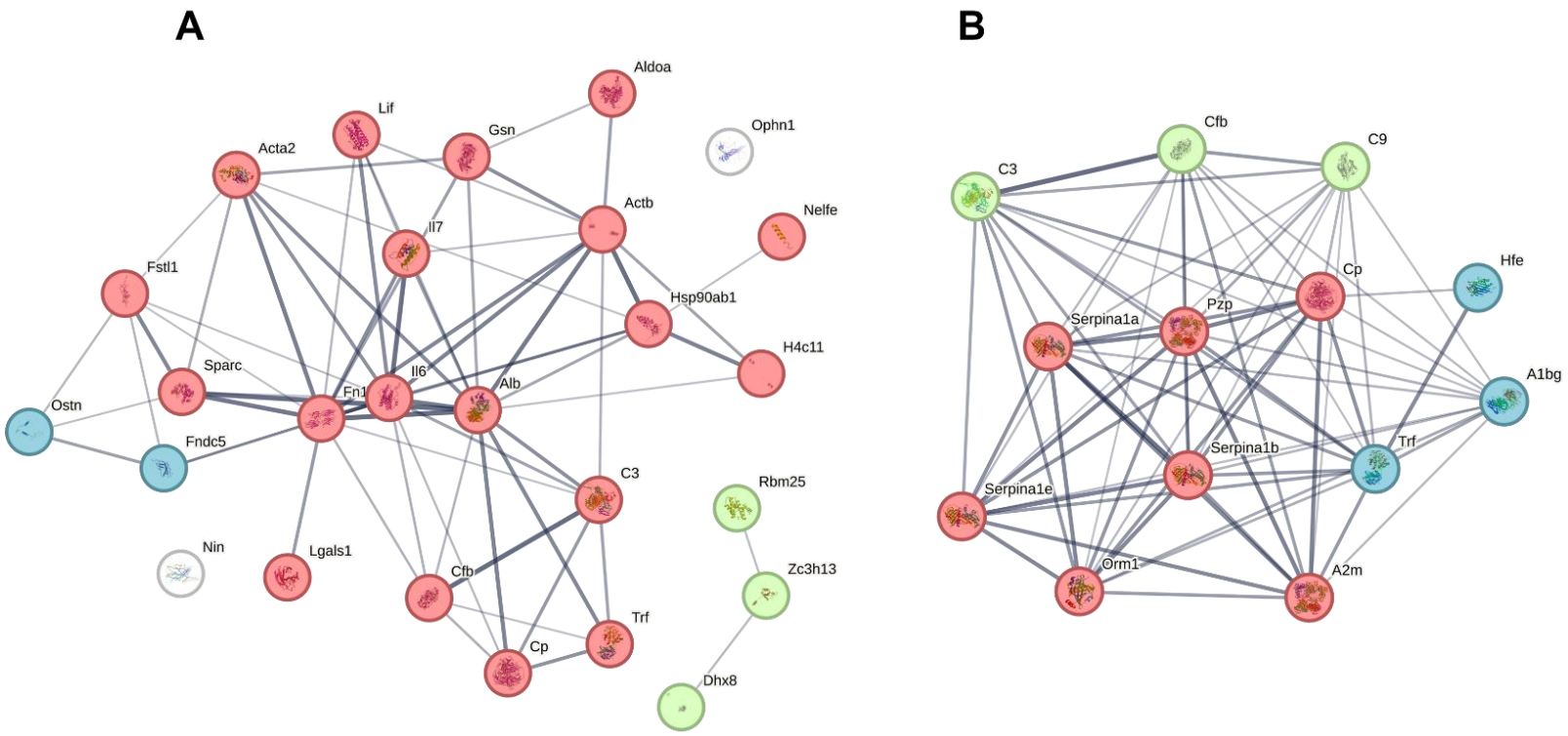

Figure 4.9 String networks displaying PPI interactions and network grouping from 2D and 3D ± EPS condition, identified via global analysis (progenesis QIP). (A) *Protein interactions of the top 10 secreted proteins in all conditions: 26 nodes, 66 edges and a PPI enrichment p-value: 6.79 x 10^{-11}. Proteins are clustered into post-translational protein phosphorylation (red), Dhx8, Rbm25, Zc3 h13 (green) and Dip2-like domain, and Negative regulation of dendrite extension (blue).* ***(B)*** *Interactions between the candidate myokines – Serotransferrin (sTrf), Ceruloplasmin (Cp) and Complement factor B (Cfb), with additional nodes are shown (based on the underlying protein interaction databases). 13 nodes, 67 edges and PPI enrichment p-value<1.0 x 10^{-16}. Proteins are clustered into acute phase response (red), complement activation, regulation of complement cascade (green) and HFE-transferrin receptor complex (blue). Line thickness joining nodes, indicate the degree of confidence prediction. Nodes are individual proteins within a network, that are connected by edges. Edges are the connections or interactions between nodes, indicating relationships or associations between the proteins. Dhx8, DEAD-box helicase 8; Rbm25, RNA binding motif protein 25; Zc3h13, Zinc finger CCCH-type containing 13; Dip2-like domain, DIP2-like domain.*
regulation of complement cascade (green) and HFE-transferrin receptor complex (blue). Line thickness joining nodes, indicate the degree of confidence prediction. Nodes are individual proteins within a network, that are connected by edges. Edges are the connections or interactions between nodes, indicating relationships or associations between the proteins. Dhx8, DEAD-box helicase 8; Rbm25, RNA binding motif protein 25; Zc3h13, Zinc finger CCCH-type containing 13; Dip2-like domain, DIP2-like domain.

4.6 Discussion

This chapter demonstrates that the custom SkM models developed in chapter 2 exhibit functionality, evidenced by the secretion of myokine proteins. Furthermore, this study demonstrated that myokine secretion can be controlled through variable exercise-mimicking protocols, namely acute and chronic electrical pulse stimulation (EPS). Baseline myokines were detected in models that were not subjected to external stimuli, presenting a challenge in truly controlling the SkM contraction phenomenon, to manipulate myokine release. Detection of myokines still remains a challenge however, application of integrative selective proteomic profiling methods identified myokines of interest and successive mining of the secretome against the mouse proteome, indicated novel myokines in the secretome of differentiated C2C12 cells models. Therefore, our study expands the knowledge base of differentiated mouse skeletal muscle secretome.

4.6.1 Integrated analysis is necessary for myokine detection

In both selective and global LCMS^E analysis, CCL8, CXCL1, CXCL5, ERFE and FGF21 were not detected. Furthermore, GDF8 was not detected in the global analysis of the secretome and in several conditions in both 2D and 3D, ± EPS from MIA analysis. Detection of GDF8 is challenging because MIA may not distinguish between different forms. GDF8/myostatin is regulated by proteolytic cleavage and exists in various forms – precursor, pro-peptide, and mature protein, which are often not specified in studies. Besides, the sensitivity of the detection method applied may not be sufficient to identify the low abundant forms. Furthermore, GDF8 is associated with latent-transforming growth factor beta-binding protein 3 (LTBP-3) in the ECM, where LTBP-3 sequesters pro-myostatin and thereby limits its signalling activity (Anderson *et al.*, 2008). However, MS can detect and characterise specific GDF8/myostatin proteoforms via discrete peptide fragments (Peiris *et al.*, 2014). As the differential forms of GDF8 show differential activity this identification of isoforms is crucial (Peiris *et al.*, 2014). Moreover, the absence or disruption of GDF8, a potent negative regulator of hypertrophy, results in skeletal muscle hypertrophy in humans (Rodriguez *et al.*, 2014).

Detection of low molecular weight, lowly abundant proteins can be analytically challenging. One reason is abundant high molecular weight proteins that can mask their identification and quantitation (Sarihan *et al.*, 2023). The 12 most abundant proteins in serum and plasma comprise about 95% of the total protein content, often obscuring the detection of lower-abundance proteins like hormones and cytokines (myokines) (Mittenbühler *et al.*, 2023). Therefore, their depletion in conditioned media or sera is important for improved myokine detection. This study used serum-free media during the collection of CM to avoid such detection issues. Immunoglobulins and albumin are highly

abundant proteins present over a wide range of isoelectric points and molecular weights, but their depletion is common using commercially available kits (Militello *et al.*, 2022). Albumin also constitutes roughly 50% of total protein mass in plasma (Whitham *et al.*, 2018) and was amongst the top 10 proteins (by confidence score) that matched against whole mouse genome search in global analysis, thus is also highly abundant in conditioned media. Immunodepleting can enrich and increase the detection of low abundance proteins (Tu *et al*., 2010). Furthermore, centrifugal ultrafiltration with molecular weight cut-offs could have been used to retain proteins of interest and remove high abundant ones. Other strategies to deplete high-abundant proteins, particularly from serum, include protein precipitation with organic solvent or other inorganic salts (Cai & Yang, 2017). Treatment of samples with a commercial affinity resin removes abundant albumin and immunoglobulins, so that these proteins do not hinder analysis of less abundant proteins (Jedrychowski *et al.*, 2015).

We report the successful detection of FNDC5/irisin in all conditions via MIA, despite its detection being contended (Albrecht *et al.*, 2015, 2020). It was detected in MIA across all conditions, but in $LCMS^{E}$, detection was limited to the unstimulated (- EPS) 2D and 3D CM, both selective and global analysis. This could be due to inefficient deglycosylation. N-glycosylation is required for FNDC5 stabilisation (Nie & Liu, 2017) and deglycosylation with PNGase, has been reported to produce incomplete deglycosylation (Jedrychowski *et al.*, 2015) compared to more efficient glycosylation mixtures (Ruan *et al.*, 2018). In other cases, PNGase has been found to be as effective as enzyme mix reagents (Albrecht *et al.*, 2020).

4.6.2 Myokines in the - EPS condition as evidence for spontaneous contraction

Firstly, a comparison of - EPS and + EPS (via MIA) revealed that both conditions share common myokines. The shared myokines contributed to a baseline secretion profile from C2C12 cells. Since myokines are defined as contraction-induced proteins and spontaneous contraction was observed in 2D models (Appendix data, **Table A1**), we can infer that - EPS models secrete endogenous myokines. Similarly, evidence of passive tissue-engineered 3D C2C12 models have been produced previously (**Table 1.1**) The 3D model, was under static tensile strain, as a stimulus for myokine secretion (discussed in Chapter 2).

4.6.3 Mimicking exercise through EPS

In our study, we applied two protocols to stimulate SkM at 20 V, 10 ms and 1 Hz, with different EPS durations to mimic acute and chronic conditions. Previous studies have modelled acute exercise either using single bouts of exercise for acute and repeated

bouts for chronic conditions (Valero-Breton *et al.*, 2020), or via modulating duration and frequency of stimulations such as acute contractions involving short-term, high- or low-frequency stimulation while chronic contractions involve long-term, continuous low-frequency stimulation (Nikolić *et al.*, 2017). The diversity of *in vitro* EPS protocols, reflecting various exercise types and intensities, likely accounts for differences in detected myokines (Nintou *et al*., 2022), complicating comparisons with *in vivo* exercise. Moreover, direct comparisons between *in vitro* EPS and *in vivo* exercise are challenging and should be approached with caution, as *in vitro* studies control only a few parameters, while *in vivo* exercise activates multiple signalling pathways based on intensity and duration (Egan & Zierath, 2013). To determine acute and chronic exercise timepoints, this study initially investigated a range of time points (1,3,6 and 24 h). There was a higher mean abundance of myokines at 6 h EPS compared to 24 h for ± EPS CM, which reinforced 6 h as chronic ± EPS timepoint. Furthermore, protocols in conventional 2D cell culture of myotubes establish 1-6 h of EPS (Nikolić *et al.*, 2017).

In this study both MS analysis, and MIA analysis identified similar myokines under both acute and chronic conditions, although when investigating quantification of these factors, differential responses were observed between conditions. In particular, $LCMS^{E}$ did not differentiate between acute and chronic conditions in both selective and global analysis. This suggests that, according to $LCMS^{E}$ analysis, *in vitro* EPS-mimicry may not be able to distinguish ± EPS duration. Computational matching and grouping of runs may inadvertently enforce similarity between samples. Furthermore, the +EPS samples had the same biological origin, treatments other than EPS duration. This would lead to the same expression or at least highly overlapping set of proteins.

4.6.4 Controlling myokine profiles through EPS

Selective $LCMS^{E}$ analysis revealed remarkable differences between ± EPS. The greatest number of myokines was identified in the 3D - EPS CM (18) compared to 3D + EPS CM (5). However, a similar number of myokines were identified in the 2D - EPS CM (9) and 2D + EPS CM (10) via $LCMS^{E}$. Furthermore, there were 813 more myokines in the 2D - EPS global analysis compared to the + EPS 2D model. Since the 3D + EPS model consisted of repeated bouts of acute EPS, and at low frequency, accumulative exercise bouts may have been less effective in release of the potentially beneficial myokines. In fact, in rat model the frequency of exercise was shown to impact myokine release. Low-frequency bouts led to insufficient stimulation for optimal myokine secretion, potentially diminishing their beneficial effects (Farrash *et al.*, 2021).

The ± EPS models in the current study altered the myokine levels, which enables targeted research into the roles and functions of secreted proteins. EPS in 3D increased

the average normalised abundance ($LCMS^E$) of secreted factors compared to the unstimulated model. Thereby demonstrating that EPS indeed promotes higher secretion levels of certain myokines. EPS-induced myokines in 3D, detected by $LCMS^E$ all exclusively increased at 6 h from 1 h.

Contrary to $LCMS^E$, EPS-induced myokines from acute and chronic states (detected by MIA) were altered and therefore characterised as inducible or reducible factors. EPS is commonly known to upregulate or increase myokines (Chen *et al*., 2019; Mengeste *et al*., 2022; Nedachi *et al*., 2008; Nikolić *et al*., 2017; Raschke *et al*., 2013; Scheler *et al*., 2013; Tarum *et al*., 2017) and less commonly known to downregulate or decrease after EPS (Ishiuchi, Sato, Komatsu, *et al*., 2018). Interestingly, only two myokines in the literature are characterised as distinct exercise-reducible factors – CCL5 (Ishiuchi, Sato, Komatsu, *et al*., 2018) and CXCL10 (Ishiuchi, Sato, Tsujimura, *et al*., 2018). CXCL10 was not included in our study for myokine selection and therefore not analysed, however CCL5 was detected in the 3D - EPS and + EPS conditions and increased from 1 h to 6 h following stimulation. As these are both chemotactic factors, it is plausible that CXCL10 may be released in a similar manner. Myokines in the 2D acute state were largely inducible as they increased with EPS. Comparatively, the chronic exercise (6 h EPS) state was wholly reducible. This meant the prolonged exercise led to a state of suppression or downregulation which could be due to overstimulation or fatigue or even a higher level of inflammation, which are yet to be determined.

In the 3D model, the acute state secreted myokines that were mainly reducible, and the chronic 3D state presented a combination of both types of regulation in myokines response. This suggests that myokines can be upregulated in one exercise paradigm but downregulated in another, depending on specific characteristics of contraction as representative of different physical activities. This has also been demonstrated *in vivo* (Little *et al*., 2018). This pleiotropic effect of exercise on the nature of myokine secretions are important, as it allows the SkM to contribute to various physiological functions and adapt to different conditions, such as exercise or disease.

4.6.5 Myokine release in response to stress

Exercise induces adaptations related to stress signalling pathways in muscle (Ost *et al.*, 2016) which may contribute to the profile of myokines released or an increase in stress-associated myokines in the unstimulated conditions. - EPS may induce a stress response that promotes the release of stress-associated myokines, while + EPS suppresses these. Cell death (GO:0008219) and its positive regulation (GO:0043068) was only associated with the biological process of 3D - EPS. This suggests that the myokines secreted from the 3D - EPS model might be involved in the modulation of cell survival or maintenance

of muscle tissue homeostasis in response to stress or injury. Furthermore, the metabolic effect of acute exercise largely triggers a rapid response involving stress defence, protein turnover, and a dysregulated redox balance, which also accounts for the increased number of myokines in the - EPS conditions (Petriz *et al.*, 2017). Furthermore, GDF15, a is a known stress-responsive myokine and a biomarker of stress, post-exercise (Johann *et al.*, 2021; Laurens *et al.*, 2020) which exclusively detected in the 3D - EPS model. FGF21 was present across all conditions (via MIA detection) suggesting that some level of stress may be present with ± EPS models. GDF15 was only present in the 3D - EPS condition (detected via $LCMS^{E}$). Indeed, an intense bout of strenuous exercise can cause muscle injury and an acute stress response, releasing 'rescue factors' like FGF21 and GDF15, which are not typically induced by regular exercise (Ost *et al.*, 2016).

The reduced myokines after + EPS may be as a result of altered tissue integrity, perhaps by sarcomeric lesions (Grande *et al.*, 2023). Evidence suggests that low frequency EPS protocols (1 Hz), as in our EPS protocol, leads to no marked cellular damage (Lambernd *et al.*, 2012; Tarum *et al.*, 2017). However, lesions can be prevalent with increased EPS intensity and even lower frequency of EPS such as 0.1 Hz has been suggested to maintain sustained contractions (Nedachi *et al.*, 2008; Orfanos *et al.*, 2016).

4.6.6 Gene ontology analysis of $LCMS^{E}$ – detected myokines

Skeletal muscle as an endocrine organ is affirmed via the assignment of proteins identified to genes that positively regulate 'metabolic processes' (GO:0009893). Extracellular annotation via gene ontology confirms that the targeted proteins detected may function outside the cell, hypothetically, to exert their physiological effects. In our study, the 3D secretome was assigned to regulation of the ERK1/2 cascade, which may be owing to IL-6 as a major influencing factor. Indeed, studies have demonstrated that myokines, such as IL-6 and BDNF, are actively involved in the regulation of the ERK1/2 signalling pathway and the broader MAPK cascade (Smith *et al.*, 2023; Johnson *et al.*, 2022). Additionally, this pathway assignment informs the type of exercise response mimicked as the MAPK pathway, particularly ERK1/2, plays a role in the adaptations that occur in skeletal muscle in response to resistance exercise (Moore *et al.*, 2011).

Chronic inflammatory response regulation (GO:0002676) is also exclusive to the 3D non-EPS condition, which could be owing to the presence of TNF as it is also exclusive to that condition, which has been reported to be involved in systemic inflammation. It has been previously shown that exercise-induced IL-6 inhibits TNF production in the presence of low-grade inflammation. This may explain a lack of TNF detection in the + EPS condition, alongside IL-6 $LCMS^{E}$-detection in 3D (Steensberg *et al.*, 2002).

However, since MIA-detected IL-6 is present in all conditions, rendering the aforementioned inconclusive.

4.6.7 Verification of cell secreted proteins

Identification of non-canonical protein secretion represents a further challenge during secretome analysis. The classical secretion of proteins is based on a short signal peptide located in the N-terminal of proteins, that allows for translocation into the ER, the subsequent transport to the Golgi, and then packaging into transport vesicles. Hence, proteins that are secreted via the classical secretory pathway can be predicted by computational tools such as SignalP. Unconventional secreted proteins lack a signal sequence and bypass the ER-Golgi compartment; the signal peptide hypothesis does not hold true in unconventional protein secretion and complicates a prediction. Therefore, further SecretomeP analysis was performed. Studies have demonstrated unconventional protein secretion. Thus, to fully characterise myokines, their functions need to be determined. Furthermore, verification of active secretion of such proteins remains challenging as their release can also be a result of cell death and cellular contamination. Different attempts have been made to increase the confidence of such potentially secreted proteins and to exclude contaminants. Most often, a dual approach was applied, in which secretome and proteome data were compared, either in a label-free manner or upon SILAC or iTRAQ labelling (Chan *et al*., 2011; Ojima *et al*., 2014). The rationale behind this approach is the assumption that actively secreted proteins should have a higher abundance in the secretome than the cellular proteome. Further confidence can be achieved through the comparison of samples with their time-matched controls. Therefore, secretome analysis should be carefully considered.

4.6.8 Proposed novel myokines

In this chapter, potential novel myokines were identified among the top 10 detected proteins through global analysis, selected based on a high-confidence match between the observed peptides and the mouse proteome, a predicted secretory pathway and myokine-associated functional classification. Of the candidate myokines identified, serotransferrin (sTrf), has been previously detected as a secreted muscle factor (Roca-Rivada *et al*., 2012) and detected via LCMS as a differentially expressed protein, linked to female muscle metabolism (Militello *et al*., 2022). Although sTrf remains unclassified as a myokine, it has been indicated in iron metabolism (Golizeh *et al*., 2017) with Transferrin receptor protein 1 (Tfr1) an essential receptor in mediating iron uptake via endocytosis, critical for regulating brown and beige fat thermogenesis (J. Li *et al*., 2020). Therefore, sTrf may have a similar target as other myokines, such as FNDC5, in adipose tissue browning (J. Li *et al*., 2020). Another correlation exists with OSTN, which binds

directly to Tfr1 on beige adipocytes, inhibiting cAMP/PKA-dependent thermogenic induction in a cell-autonomous way (Jin *et al.*, 2023). Additionally, its secretion may be regulated by excessive iron accumulation, which can negatively impact myokine synthesis and lead to impaired protein production and secretion (Halon-Golabek *et al.*, 2019). We have therefore identified a novel myokine with a potential role in iron metabolism.

4.6.9 Limitations

A limitation in the experimental design involving analysis of EPS and non- EPS data is present in this study. Although the relative abundance of myokine IDs was compared in the results, the LCMS^{E} data from the groups were not analysed together. This was due to discrepancies in sample complexity, retention time, dynamic range, sensitivity and biological variability which created misalignment for peptide matches. As a result, +EPS and -EPS could not be directly compared. Furthermore, the analysis may have influenced the same IDs generated between timepoints analysed together i.e., EPS 1 h and 6 h physiological data.

Mass spectrometry has a broad dynamic range, allowing for the detection of a wide range of analytes. However, several issues can affect its accuracy and sensitivity. Ionisation efficiency can vary between different proteins. Highly abundant species may ionise well, but they can also saturate the detector, overshadowing less abundant molecules. Additionally, species interference can occur when ions from different compounds overlap in the mass spectrum, complicating the identification and quantification of target analytes. Furthermore, compounds that co-elute during chromatographic separation can suppress the signals of each other, a phenomenon known as ion suppression, which can lead to inaccurate or underrepresented data for certain analytes. Therefore, interpretation of myokine quantification via different methods should be considered carefully. Furthermore, inter-study comparisons should be made by alignment of identified putative myokines with the *in silico* secretome reported by other studies, as a means to support proteomic profiling (Hartwig *et al.*, 2014). Myokine characterisation still remains poor, from the nomenclature such as distinction of irisin (as a cleaved myokine, derived from the extracellular domain of transmembrane precursor FNDC5) and FNDC5 itself. Interchangeability of both has led to contention between their detection in the glycosylated and deglycosylated form (Chen *et al*., 2019b; X. Liu *et al*., 2023). MIA and LCMS^{E} identified irisin and FDNC5, respectively. Furthermore, there is no myokine database available to cross-reference novel discoveries by method besides the use of published studies. Secretion of myokines such as irisin are secretion of irisin is modulated by N-glycosylation (Nie & Liu, 2017). Therefore, a balance needs to be

achieved between optimising myokine secretion following contraction and their detection.

In this chapter, the global analysis study also limited the identification of novel myokines to the top 10 proteins from each condition only, and expansion of this could lead to identification of further myokine candidates. Expansion of our reference list to prototypic peptides could also be included into the selective profiling such as BAIBA (W. Lee *et al*., 2018; Molfino *et al*., 2019) and Fractalkine (CX3CL1) (Rutti *et al.*, 2014) and lactate (Brooks *et al.*, 2023).

4.7 Conclusion

EPS significantly modulated both the concentration and abundance of myokines in our 2D and 3D SkM models, highlighting the potential of EPS protocols to effectively regulate myokine secretion. However, it is crucial to account for baseline myokine secretion in unstimulated conditions when evaluating the effects of EPS-induced myokine release. The detection of myokines via mass spectrometry was shown to be the most viable method, with both selective and global analysis strategies, albeit relative quantification. The complete effects of EPS on the integrity of myocytes and their subsequent contractile and secretory functions needs to be further elucidated. Candidate myokines were potentially identified, including sTrf which requires further investigation to fully understand its role in muscle function and response to stimuli. The variation in myokine abundance and concentration has prompted a deeper exploration of their temporal dynamics, extending beyond immediate detection. In the following chapter, we profile myokines after ± EPS, to establish a comprehensive understanding of myokine secretion patterns in response to exercise.

5 Investigating The Temporal Dynamics of Myokines

5.1 Introduction

5.1.1 Exercise duration and intensity affects post-exercise cardiometabolic responses

There is substantial research supporting the physiological benefits of exercise (Nishii *et al*., 2023), including a phenomenon, commonly known as the 'afterburn effect', referred to as excess post-exercise oxygen consumption (Foureaux *et al*., 2006; Kocoloski and Crecelius, 2014). EPOC is associated with an elevation in metabolism (Børsheim & Bahr, 2003). The duration of EPOC can vary with exercise intensity, duration and individual fitness levels (Kocoloski and Crecelius, 2014). Comparison of EPOC duration following different exercise modalities, reveals that resistance exercises led to a longer EPOC than steady-state aerobic exercises (Scott *et al*., 2006). Resistance training with high intensity and volume, performed with short rest intervals (as with circuit training), is thought to have greater impact on EPOC. Meanwhile, short rest intervals (<60 s) increased the EPOC magnitude, but not the overall energy expenditure (Farinatti *et al*., 2013). A further human metabolomics review reported metabolite concentrations before and within 24 h after endurance or resistance exercise in blood, urine, or sweat. Within these studies, 196 metabolites changed their concentration significantly within 24 h after exercise in at least two experiments (Schranner *et al*., 2020). These studies provided insights into how different variables, such as exercise type and intensity affect EPOC and, subsequently demonstrated that energy expenditure is valuable for optimising exercise programs to maximise metabolic health. The secretion of myokines post-exercise aids in recovery, influencing muscle repair and adaptation, which is crucial for sustained EPOC. EPOC not only reflects the physiological recovery phase but also sustains and amplifies the release and effects of myokines, linking SkM activity to systemic health benefits. Myokines like IL-6 are released during and after exercise, contributing to EPOC by enhancing metabolic rate and promoting fat oxidation (Leal *et al*., 2018).

Expectedly, type of exercise, affects the post-exercise response. A short period of exercise (45-min cycling), albeit vigorous, has been shown to increase in the net energy expenditure by 750 kcal, with metabolic rate elevated for up to 14.2 hours (Knab *et al*., 2011). Additionally, 40 minutes of aerobic training elevates resting energy expenditure for 19 hours in women. High intensity, intermittent resistance exercise, unlike continuous exercise**,** results in significant energy expenditure during post-exercise periods (Scott *et al*., 2009, 2011). A further study measured the resting energy expenditure and respiratory exchange ratio at baseline and at 24-, 48-, and 72-hours following resistance training. Results indicated that a single-set resistance training session effectively elevated these metrics for up to 72 hours post-training in overweight college males (Heden *et al*., 2011).

However, both low- and high-intensity exercise yield similar effects on 24-h energy expenditure or nutrient oxidation, however, women were found to have slightly higher 24-h fat oxidation rates (Melanson *et al.*, 2002). Further studies reported no measurable difference in factors such as VO_2 in the hours post high-intensity interval training (HIIT) and exercise and suggested a longer post-exercise collection period may be necessary to capture small changes in energy expenditure induced by HIIT, due to the relatively small differences from baseline (Skelly *et al.*, 2014). Meanwhile, another study found no difference in 3-h excess post-exercise oxygen consumption following HIIT and continuous moderate-intensity training (END), reporting that both had returned to baseline levels by 45 min postexercise (Williams *et al.*, 2013). Thus, even if EPOC is comparable and short-lived across training types, the distinct myokine profiles induced by different exercise modalities may drive longer-term systemic adaptations and recovery processes.

5.1.2 Myokines post-exercise

Understanding the temporal dynamics of myokine release is crucial for not only timing of analytical secretome analysis, but also for potentially refining exercise intervention protocols to enhance specific myokine-associated health benefits in particular disease. While there are a few studies and reviews which highlight the benefits of myokines during both rest and post-exercise phases; a foundational study by Louis *et al* (2007) analysed myokine responses 1, 2, 4, 8 and 24 h post-exercise and found myokines (IL-6, IL-8, and TNF-α and GDF8) exhibited a biphasic response post-exercise, with an initial elevation immediately after exercise, a return to baseline at 1 h, and a subsequent increase peaking between 2–24 hours depending on the cytokine and exercise modality (Louis *et al.*, 2007).

The post EPS period plays a critical role in influencing SkM adaptations, including size and function. An 8-hour rest period following EPS has been shown to induce human muscle cell enlargement (Tarum *et al*., 2017). Additionally, tissue constructs demonstrate a linear increase in force production with extended culture time. Within the initial 2 hours post EPS, ATP content in human SkM cells significantly increases, while AMPK phosphorylation peaks after 8 hours (Lambernd *et al*., 2012).

With a large and growing number of myokines identified in the literature as secreted peptides in response to SkM contraction (**Table 1.3**), it is unsurprising that the temporal dynamics may be unique and changeable for any given myokine under a multitude of different exercise conditions. Comprehensive characterisation of myokine release profiles over time has not been thoroughly investigated and remains a gap in myokine research (Sun *et al.*, 2024). This characterisation must go beyond identifying the specific time point of myokine release post-exercise to include detailed analysis of its dynamics over an extended period. A recent review by Bettariga *et al* (2024) suggested that a single exercise bout induces varied increases in myokine expression, up to 60 minutes post-exercise, generally returning to baseline from 180 min to 24 h post-exercise. However, this analysis was restricted to IL-15, SPARC, OSM, and DCN, underscoring the limited data available on post-exercise myokine dynamics. The confirmation of both IL-6 and LIF function during activation of myotube mTORC1 signalling in a time- and dose-dependent fashion (Severinsen & Pedersen, 2020) provides further evidence that investigation of time course myokine release is important to study.

In **Table 5.1**, we consolidate the limited studies to date using *in vitro* cell culture models, exercised human subjects, and individuals exposed to exercise or exercise-mimetic protocols, with post-exercise timepoint measurements. However, due to potential sources of heterogeneity and variable human and animal studies, drawing precise conclusions about timing of myokine release is challenging. To our knowledge, this is the first dedicated time course analysis of myokines, secreted from *in vitro* models, measured up to 72 hours post-exercise.

Table 5.1 Studies demonstrating the post-exercise duration and sampling, beyond immediate collection (0 h). *While there are other considerations for exercise induction besides electrical, highlighted in Chapter 1, we focus on the EPS as a common exercise inducible method for comparison to in vivo studies.*

Study	Exercise	Subject	Post-exercise duration (h)
(Albrecht *et al.*, 2015)	160 km endurance race	*In vivo* (human)	3
(Barlow & Solomon, 2019)	EPS: 40 V, 1 Hz, 2 ms, ~ 1 h	*In vitro* (C2C12 cells)	2
(Bessa *et al.*, 2016)	High-intensity aerobic and anaerobic training exercises: bench presses + 1 h cycling	*In vivo* (human)	3, 6 , 12, 24, 48, 72
(Broholm *et al.*, 2011)	Resistance exercise, 20 min	*In vivo* (human) *In vitro* (primary human cells)	6, 24 and 48
(Cuevas-Ramos *et al.*, 2012)	Treadmill exercise, two weeks	*In vivo* (human)	1, 4
(Garneau *et al.*, 2020)	Acute bout of moderate intensity cycling	*In vivo* (human)	0, 1, 2, 3 h, 4, 12, and 24
(Gonzalez-Franquesa, Stocks, *et al.*, 2021)	Cycling – acute, 0.5h; endurance, 0.5h + x5 resistance exercise	*In vitro* (C2C12 cells)	Acute: 0.5, 1 Endurance: 0.25 -, 0.5, 1, 1.5, 2, 3
(Han *et al.*, 2020)	Treadmill, 0.25 h,1 h or until exhaustion	*In vivo* (mouse)	1
(Hojman *et al.*, 2019)	Cycling, high-intensity interval-based biking, 2h	*In vitro* (primary human cells)	2
(Ji *et al.*, 2024)	Moderate, vigorous continuous exercise and high intensity interval exercise continuous exercise	*In vivo (human)*	0.5, 1.5
(Kanzleiter *et al.*, 2014)	Acute resistance exercise - every 3 min	*In vivo* (human) and *In vitro* (primary human cells)	0.5, 1, 1.5 and 2
(Nam *et al.*, 2024)	Treadmill endurance exercise targeting 300 kcal expenditure at 70% of age-predicted maximal heart rates	*In vivo* (human)	0.5-, 1-, 2
(Norheim *et al.*, 2014)	Combined strength and endurance training, 12 weeks	*In vivo* (human) and	2

		In vitro (primary human cells)	
(Matthews *et al.*, 2009)	120 min of bicycle exercise	*In vivo* (human)	3, 5, 8, 24, 48 and 72
(Ostrowski *et al.*, 1998)	Marathon, ~3 h	*In vivo* (human)	2
(Raschke *et al.*, 2013)	Cycle at 70% VO2max, 60 min and 2h rest	*In vitro* (primary human cells)	0.5 and 2
(Roca-Rivada *et al.*, 2012)	Voluntary wheel-induced exercise, 6 days	*In vivo* (mouse)	12
(Švec *et al.*, 2022)	Downhill running protocol	*In vivo* (human)	0.5 , 1, and 14 days

5.2 Aims and objectives

The inherent variability in the abundance and concentration of myokines revealed immediately after ± EPS in Chapter 4 led to the hypothesis that SkM cells exhibit temporal dynamic release of myokines for extended periods, post ± EPS. Therefore, the main aim of this chapter was to determine profiles of myokine release, following acute and chronic ± EPS. To test this, the following experimental objectives were employed: (1) Establish staged intervals of myokine release as 0-, 24-, 48-, and 72-hours, post ± EPS from acute and chronic 2D and 3D models. (2) Quantify myokine abundance post ± EPS via LC-MS^{E}. Finally, (3) Validate post ± EPS myokine secretion levels via MIA.

5.3 Experimental design

SkM models were stimulated (+ EPS) in SFM for a duration of 1 h (acute) or 6 h (chronic). An unstimulated control model (- EPS) was subjected to time-matched durations of incubation, in SFM. To investigate the temporal myokine release from models, CM was harvested at 0-, 24-, 48-, and 72-h intervals, post ± EPS. Fresh, pre-warmed SFM was added after each collection time point, following two washes, to remove any residual CM. Myokines were detected in the CM by LCMS^{E} and MIA and using known targets outlined in **Figure 4.2**, detected via peptide and protein analysis (**Figure 5.1**).

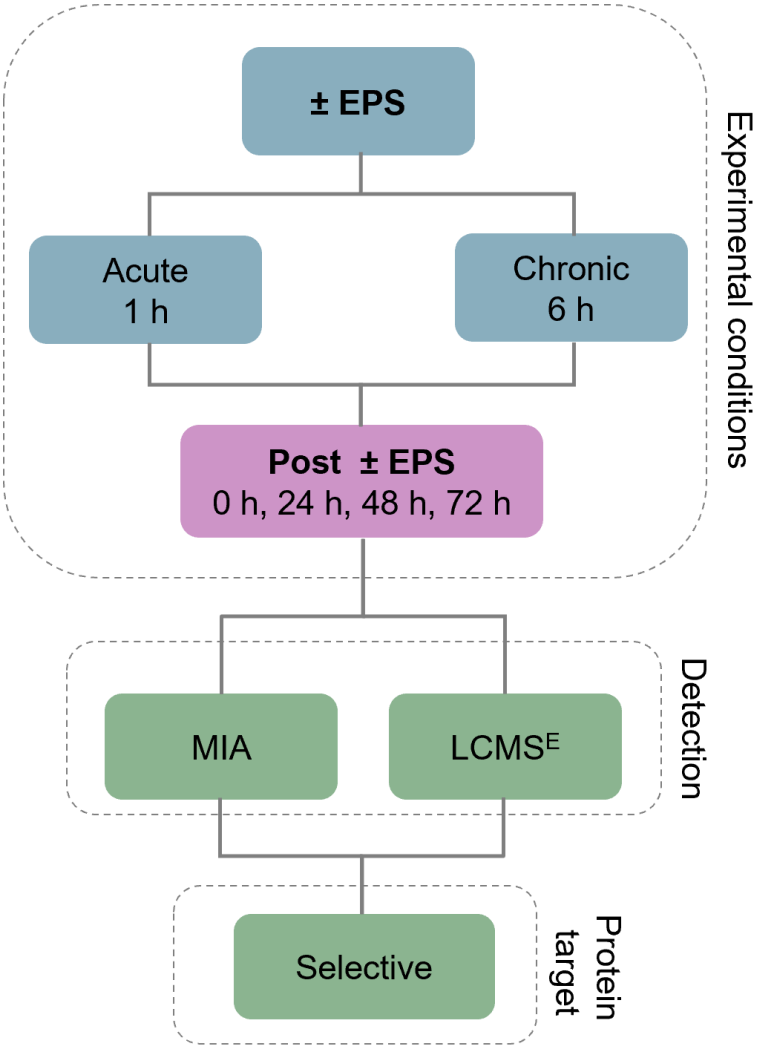

Figure 5.1 Schematic representation of the experimental design for Chapter 5. *SkM models (2D and 3D) underwent either ± EPS via acute (1 h) or chronic (6 h) stimulation periods. Subsequently, SkM models were subjected to 0-, 24-, 48-, and 72-hour post ± EPS durations. The CM was subjected to selective analysis after LCMS^{E} and MIA methodologies.*

5.4 Results

5.4.1 The effect of LCMS^{E}-detected myokines secretion post ± EPS,

Herein, the changes in myokine abundance (> 2-fold change, FC) after ± EPS, at the following timepoints 0, 24, 48 and 72 h were determined by LCMS^{E} are reported. Fold changes with respect to the lowest detected signal for a given myokine are reported in the text. Significant changes are displayed and reported in **Figures 5.3-5.7**.

5.4.1.1 Myokines from 2D and 3D - EPS models

In the - EPS condition, the models are not electrically stimulated but exhibited spontaneous, unstimulated contractions (Chapter 2). Despite the lack of external stimulation, the cells remain responsive, secreting myokines after 1 h and 6 h incubation in SFM. This condition provides a baseline for spontaneous myokine secretion, offering insights into signalling activity in the absence of active stimulation (**Figure 5.2**).

The abundance of CCL2, IL-7 and SPARC alternated from 0 h to 72 h. These myokines showed a biphasic response following 1 h and 6 h incubation in the control model. The shorter 1 h incubation period began with an increase in the first 24 h, followed by a decrease at 48 h then another increase at 72 h. The opposite pattern existed in the longer (6 h) incubation period. FSTL1 presents peak abundance at R0, in both 1 h and 6 h conditions, indicating an early or rapid response to spontaneous contraction, particularly with longer (6 h) incubation at a higher intensity (**Figure 5.2**).

In the 3D 1 h condition, DCN and IGF-1 showed an increased response after - EPS, with a peak abundance at 72 h. This showed a delayed response in these myokines after a short incubation (1 h period) of spontaneous contraction. Meanwhile, GDF15 had a sustained effect following 1 h period, compared to a peak abundance at 48 h in the 6 h period. Furthermore, in the longer 6 h period, CCL7, DCN, GDF8 and IGF-1 increase post - EPS and peaked at 48 h then decreased at 72 h. Therefore, these myokines showed both a delayed and transient response to spontaneous contraction (**Figure 5.2**).

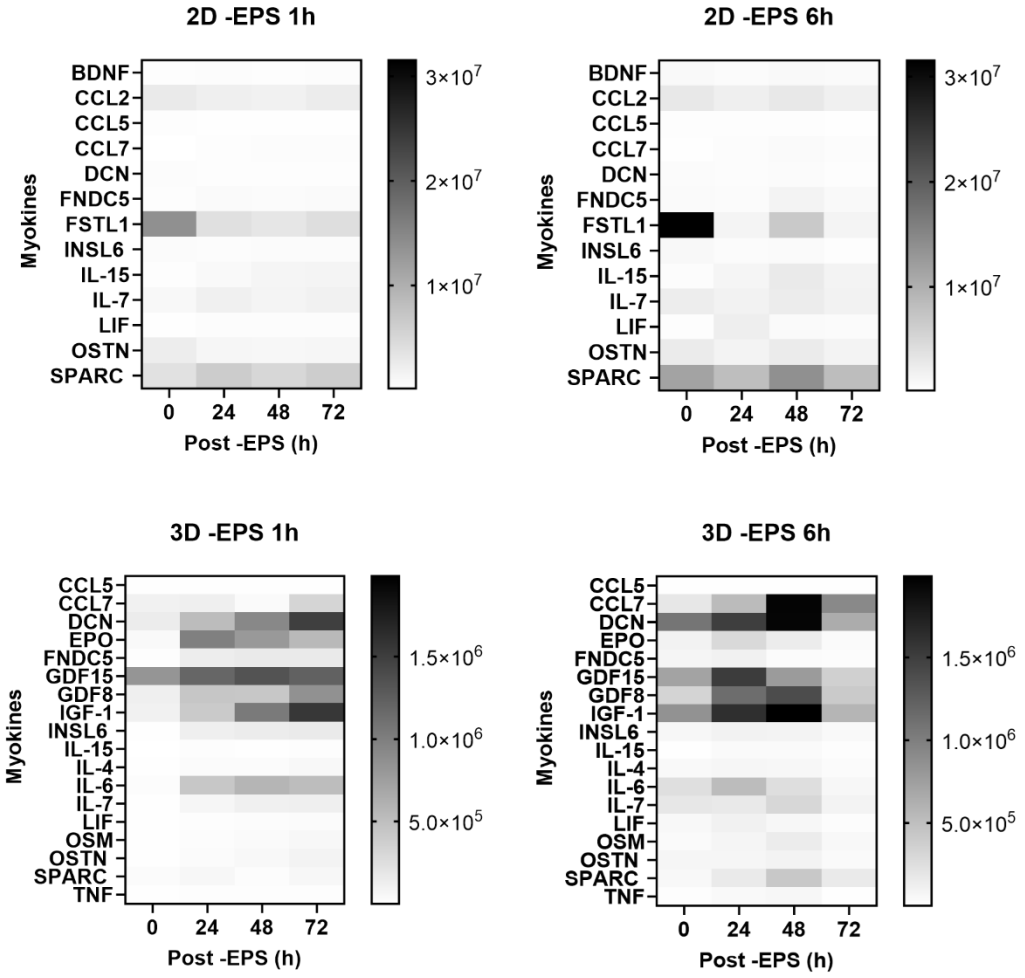

Figure 5.2 Heat maps of mean normalisation abundance of myokines identified from - EPS 2D and 3D conditions. *Each box represents a mean normalised abundance (n=3) of a single myokine.*

After 1 h - EPS of the 2D cells, the subsequent fold-changes are reported for the following myokines: CCL7 showed a 3.41-fold increase from 0 h to 48 h. FNDC5 (2.81), IL-15 (5.64) and LIF (2.36) also showed increases, but from 0 h to 72 h. FSTL1 (4.46) and OSTN (2.15) showed fold-decreases from 48 h to 0 h. Fold increases in the 2D - EPS The 6 h condition included CCL7 (3.56) and IL-15 (7.07) from 0 h to 48 h. Further increases were present with FNDC5 (2.78) from 24 h to 48 h and LIF (8.10) from 0 h to 24 h. FSTL1 and INSL6 showed 22.56- and 2.62-fold decreases, respectively, from 0 h to 72 h (**Figure 5.3**).

Myokines accumulated in the media after - EPS 1 h in 3D, which resulted in the following fold-increases: CCL5 (11.26), DCN, 10.20), GDF8 (7.11), IGF-1 (14.33), INSL6 (27.82), IL-4 (8.28), IL-7 (17.35), LIF (10.03), OSM (22.32), OSTN (26.67) from 0 h to 72 h only. CCL7 (8.82) and SPARC (2.69) had increases from 48 h to 72 h. FNDC5 (14.72) and IL-6 (24.44) increased between 0 h to 48 h. EPO (23.19) increased from 0 h to 24 h and

considerable increases were also present with IL-15 (1625.57) and TNF (703.80) in the first 24 h, post EPS. However, IL-15 should be interpreted with caution due to the low sample size The longer 3D - EPS 6 h condition resulted in the following myokines with fold increases from 0 h to 48 h CCL7 (10.46), GDF8 (4.16), IL-15 (16.04), OSM (3.94), SPARC (8.36). However, the majority of myokines demonstrated fold-decreases: CCL5 (9.23) from 24 h to 72 h; DCN (3.02), IGF-1 (3.26), IL-7 (3.39), OSTN (2.62) and TNF (8.63) from 48 h to 72 h; EPO (8.32), FNDC5 (6.64), GDF15 (4.13), INSL6 (2.44), IL-4 (2.68), IL-6 (8.55) and LIF (6.60) from 24 h to 72 h (**Figure 5.4**).

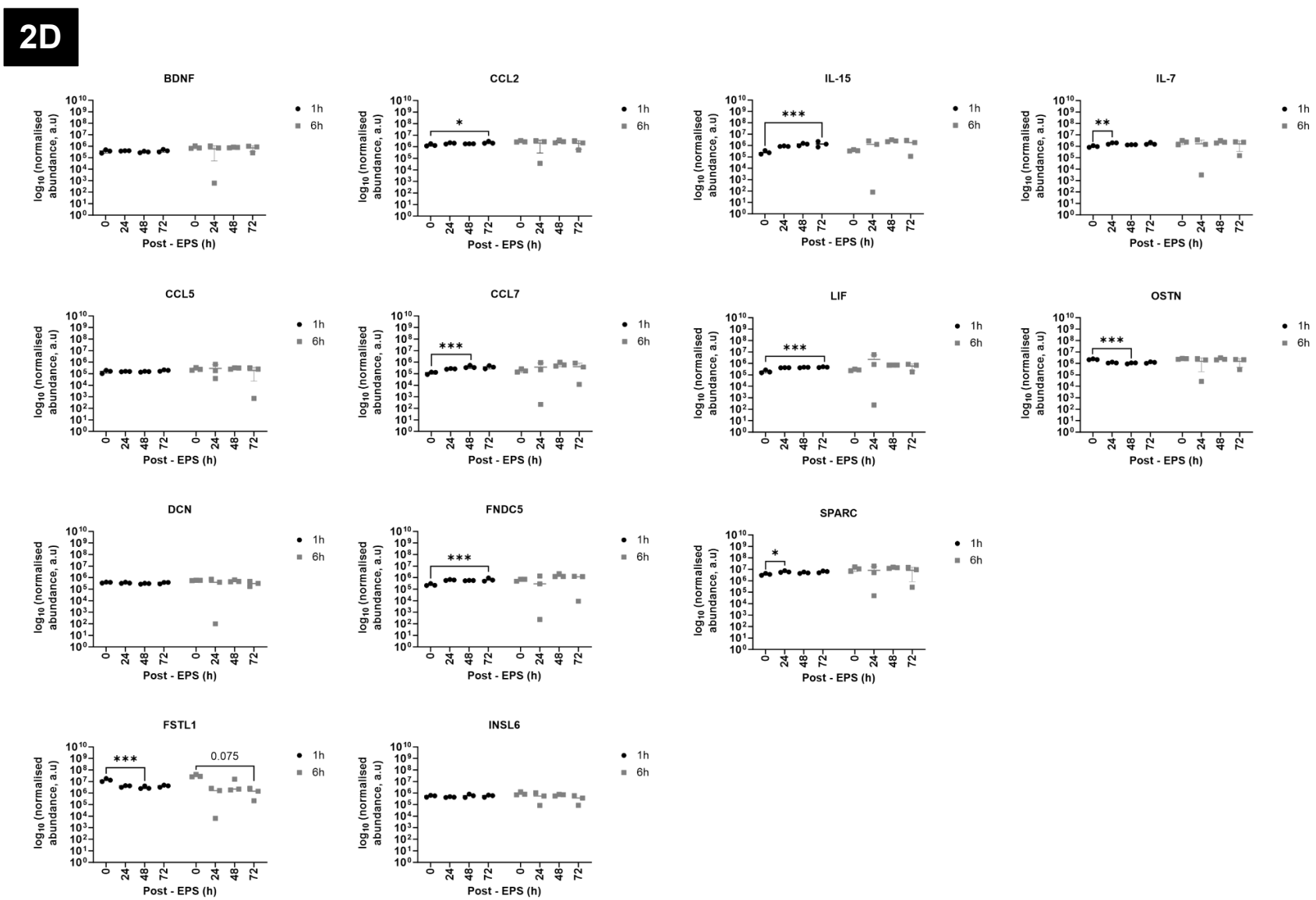

Figure 5.3 Quantification of myokine abundance in 2D CM. Data represents triplicate CM samples (n=3) as mean with SD. *Significance between the (HMC and LMC) post - EPS timepoints are presented in the 2D acute condition only: CCL2 (p=0.0542; 72 h, 0 h), CCL7 (p=0.0010; 48 h, 0 h), FNDC5 (p=0.0007; 72 h, 0 h), FSTL1 (p=0.0004; 0 h, 48 h), IL-15 (p=0.0015; 72 h, 0 h), IL-7 (p=0.0084; 24 h, 0 h), LIF (p=0.0004; 72 h, 0 h), OSTN (p=0.0002; 0 h, 48 h) and SPARC (0.0221; 24, 0 h). There were no significance differences between the post - EPS timepoints for any myokines in the 2D 6 h condition (p>0.05).*

3D

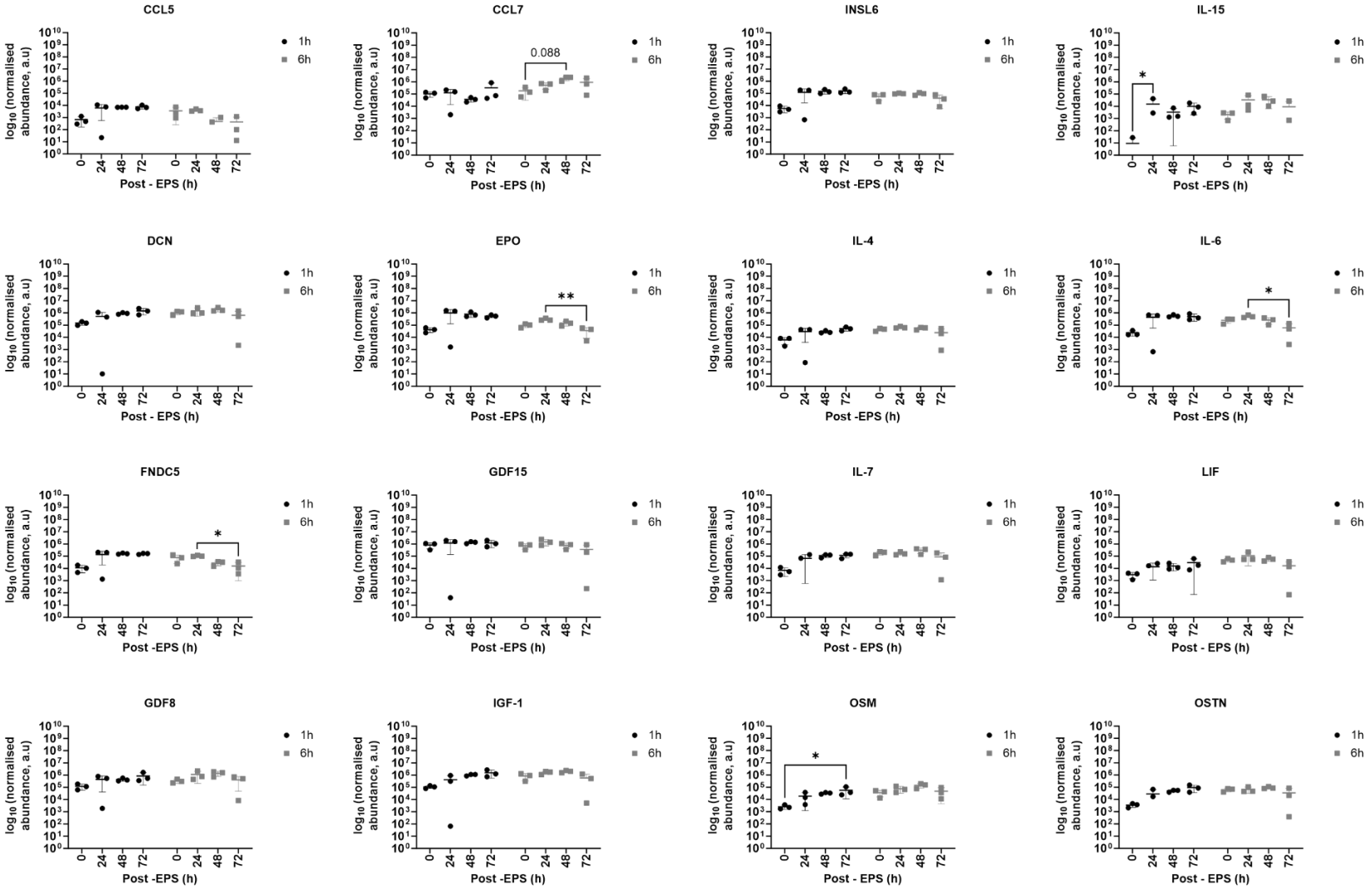
CCL5
CCL7
0.088
INSL6
IL-15
DCN
EPO
IL-4
IL-6
FNDC5
GDF15
IL-7
LIF
GDF8
IGF-1
OSM
OSTN
log10 (normalised abundance, a.u)
Post - EPS (h)
Post -EPS (h)
1h
6h
0
24
48
72
*
**

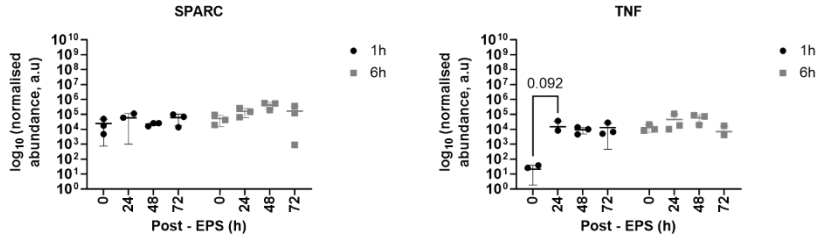

Figure 5.4 Quantification of myokine abundance in 3D CM. *Data represents triplicate CM samples (n=3) as mean with SD. Significance post - EPS periods exist for the following myokines including p values for HMC and LMC in the acute condition: IL-15 (1 h p=0.0587; 24 h, 0 h), OSTN (1 h p=0.0045; 72 h, 0 h) and in the chronic condition: EPO (p=0.0181; 24 h, 72 h), FNDC5 (p=0.0237; 24 h, 72 h), IL-6 (p=0.0510; 24 h, 72 h).*

5.4.1.2 Myokines from stimulated models

The EPS-stimulated conditions provide controlled electrical pulses that actively induce contraction which can elicit more predictable and controlled exercise mimicry.

CCL2 and LIF presented a distinct biphasic response following 1 h and 6 h EPS in 2D, where their abundance increases after 24 h, decreased at 48 h then increased again at 72 h . FGF15, FSTL1, GDF8 and SPARC remain most abundant immediately after EPS, and decrease post + EPS following both 1 h and 6 h EPS, reflecting an immediate physiological response to acute and chronic stimulus. In 2D, acute (1 h) and chronic (6 h) EPS exhibit almost mirrored profiles, suggesting consistent the duration of EPS, is independent of subsequent temporal myokine release (**Figure 5.5**).

Acute EPS of the 3D model secretes LIF as the only myokine to gradually increase and peak in abundance at 72 h. IL-15 and LIF increased, peaked and subsequently decreased following 6 h EPS in 3D. Furthermore, the majority of detected myokines, with the exception of IL-6 showed peak abundance at 48 h, following 6 h chronic EPS (**Figure 5.5**).

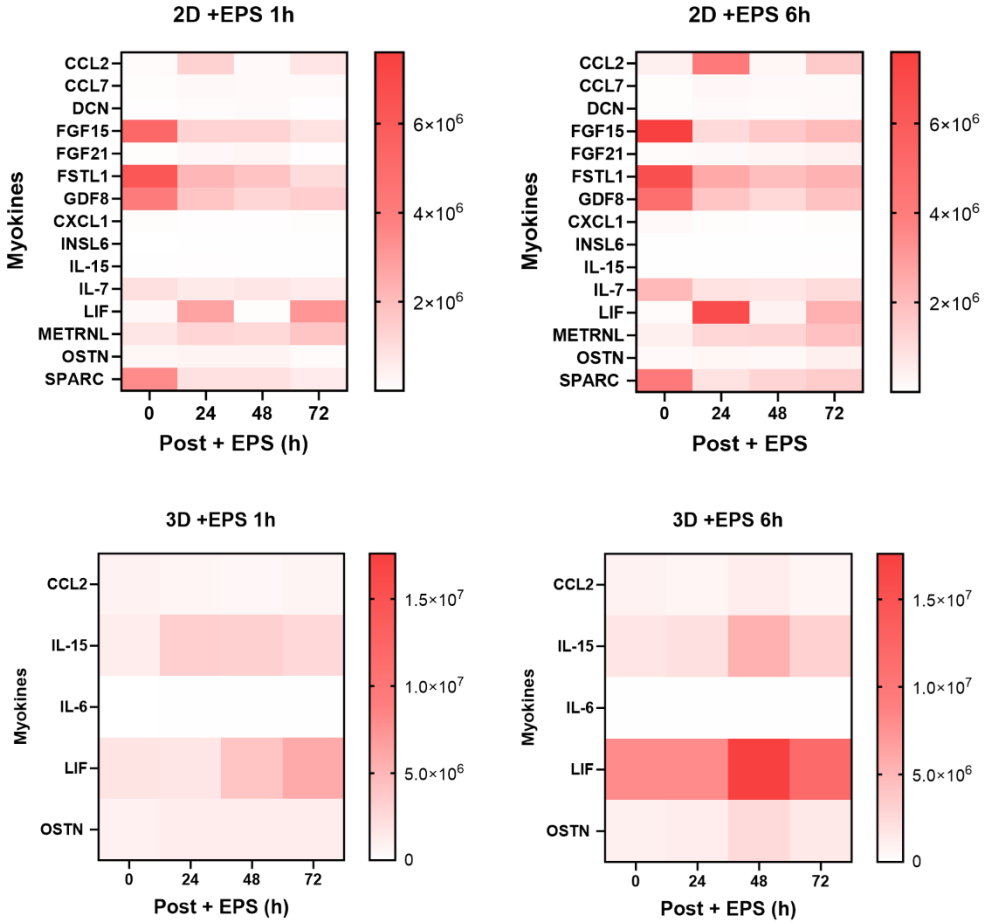

Figure 5.5 Heat maps of myokine normalised abundance in + EPS 2D and 3D conditions. *Each box represents a mean normalised abundance (n=3) of a single myokine.*

Changes between timepoints (0 h, 24 h, 48 h, 72 h) following 1 h and 6 h + EPS are reported (>2 FC). In the stimulated 2D + EPS 1 h condition, the following myokines presented increases: CCL2 (12.69) and CCL7 (3.18) from 0 h to 24 h. INSL6 presented a substantial 169.43-fold increase, and METRNL, a smaller 2.40-fold increase from 0 h to 72 h. LIF also increased by 38.87-fold from 48 h to 72 h. Fold decreases were present from 48 h to 72 h with DCN (3.18), from 0 h to 72 h with FGF15 (6.23), FSTL1 (6.05), GDF8 (3.39) and SPARC (5.81). FGF21 (6.05) decreased from 48 h to 72 h and IL-15 (10.33) and OSTN (3.29) decreased from 24 h to 72 h. Following chronic stimulation in 2D (+ EPS 6 h), a 2.59 and a greater 59.77-fold increases are seen in CCL7 and LIF, respectively, from 0 h to 24 h. Further increases are seen with DCN (2.12), FGF21 (3.91), METRNL (4.10) and OSTN (2.56) from 0 h to 72 h; INSL6 (2.65) from 0 h to 48 h and IL-15 (5.14) from 48 h to 72 h. CCL2 decreased by 17.19-fold from 24 h to 48 h. FGF15 (7.04) and SPARC (5.00) decreased from 0 h to 24 h and FSTL1 (3.47), GDF8 (4.15), CXCL1 (3.12), IL-7 (2.73) also reduced abundance from 0 h to 48 h (**Figure 5.6**).

The 3D + EPS 1 h condition increased the abundance of IL-15 by 2.65-fold from 0 h to 24 h. LIF also increased in abundance by 3.53-fold from 24 h to 72 h post + EPS. Chronic (6 h) stimulation increased the abundance of IL-15 (3.05), LIF (2.20) and OSTN (2.46) from 0 h to 48 h (**Figure 5.7**)

2D

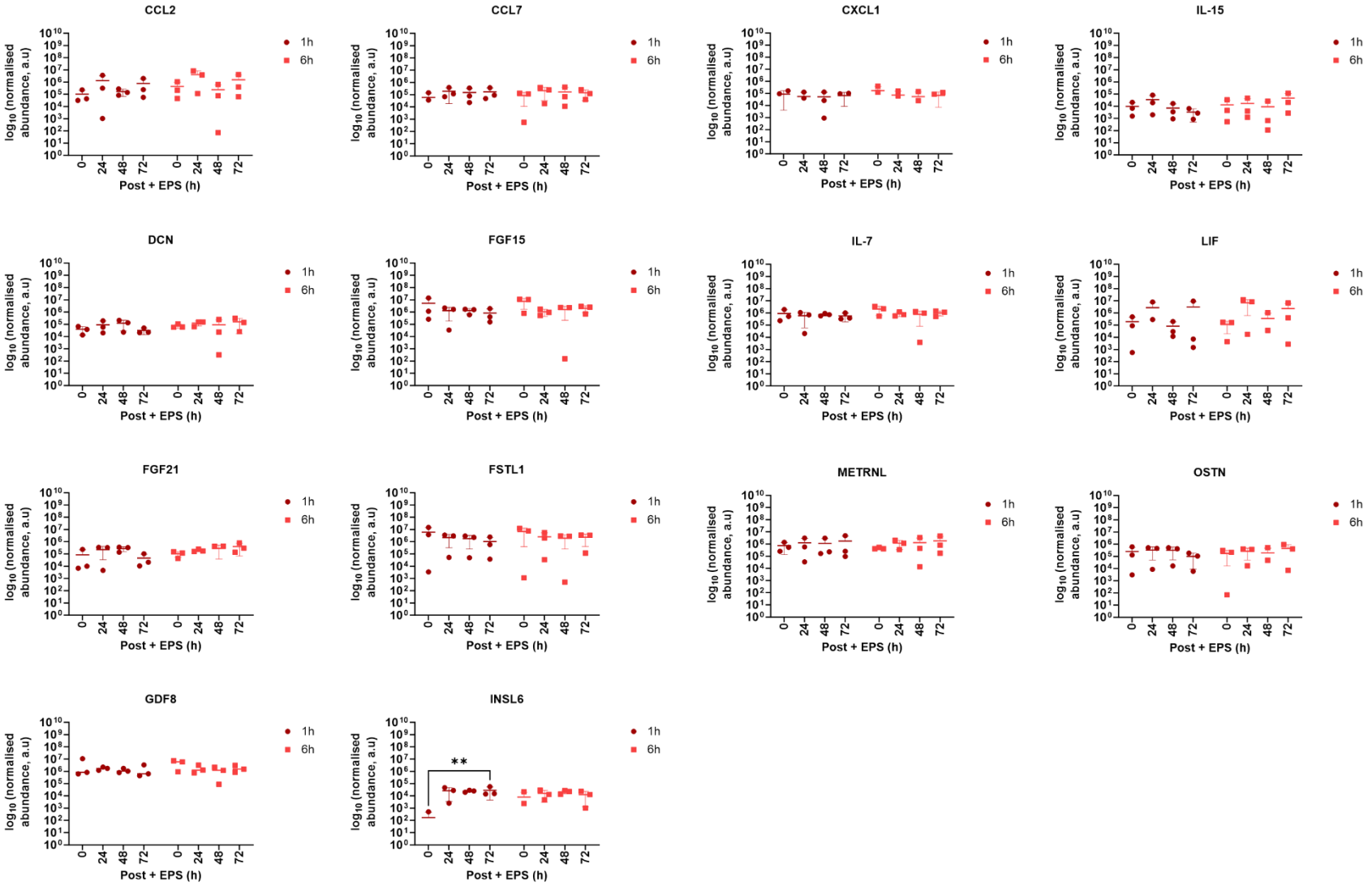

Figure 5.6 Quantification of myokine abundance from 2D + EPS CM. *Data represents triplicate CM samples (n=3) as mean with SD of myokine secretion after + EPS, following 1 h and 6 h EPS in 2D. Significance between the (HMC and LMC) post + EPS timepoints are presented in the 1 h acute only: INSL6 (p=0.003; 72 h, 0 h). There were no significance differences between the post + EPS timepoints for any myokines in the 2D chronic condition (p>0.05).*

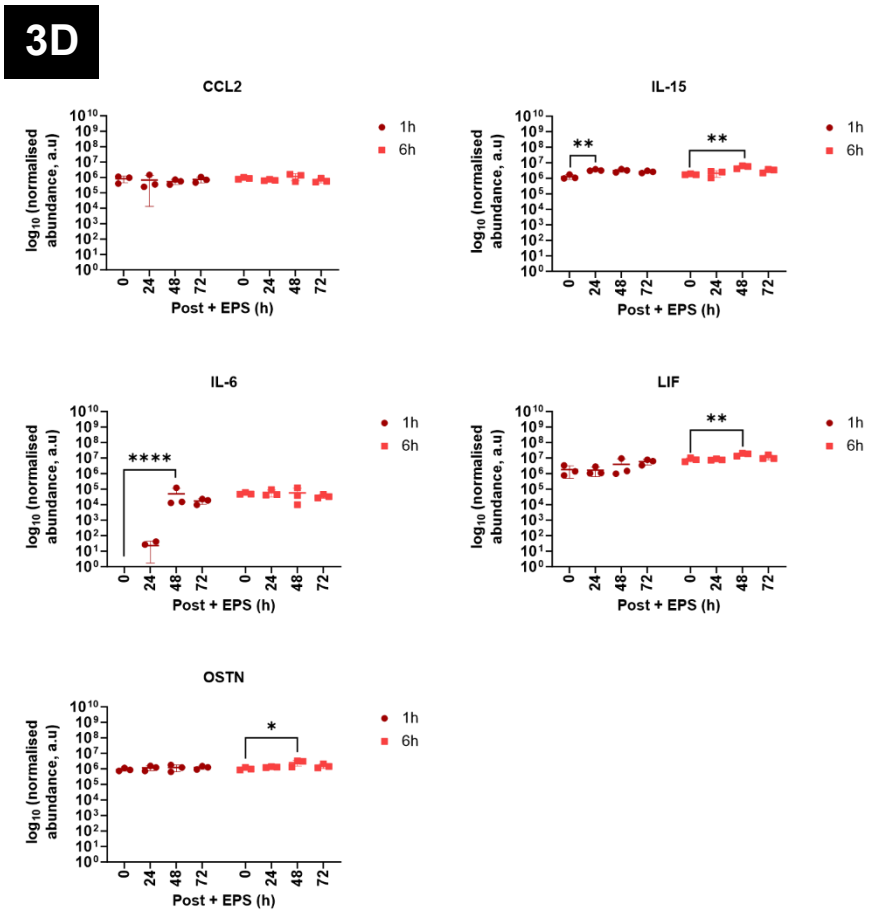

Figure 5.7 Quantification of myokine abundance from 3D + EPS CM. *Data represents triplicate CM samples (n=3) as mean with SD of myokine secretion after + EPS, following 1 h and 6 h EPS in 3D. Significance between the (HMC and LMC) post + EPS timepoints are presented in the 1 h acute condition: IL-15 (p=0.0023; 24 h, 0 h) and IL-6 (p=0.0000; 48 h, 0 h). In the chronic condition, IL-15 (p=0.0119; 48 h, 0 h), LIF (p=0.0118; 48 h, 0 h) and OSTN (p=0.0544; 48 h, 0 h).*

5.4.2 Validation of MIA-detected myokines post ± EPS

Myokine secretion was profiled using MIA as a secondary validation method, assessing concentrations after acute and chronic ± EPS. Here, we report the fold changes between post ± EPS periods, thus depicting a profile of myokine release at 24, 48 and 72 h post ± EPS (compared to 0 h) and then staged 24 h differences between timepoints. Significances are displayed and reported in **Figures 5.8-5.11**.

5.4.2.1 Myokines from the 2D - EPS model

In the 2D - EPS 1 h condition, BDNF levels were significantly elevated post -EPS, showing fold-increases of 23.64 at 24 h, 46.97 and 40.16 at 72 h from 0 h. In the - EPS 6 h condition, there was an early 27.36-fold decrease from 0 h to 24 h and notable fold-increases from 24 h to 48 h (41.77) and 24 h to 72 (21.01). The acute (1 h) EPO response revealed an initial 11.50-fold increase at 24 h, followed by a gradual return to baseline with 10.07- and 8.27-fold-increases from 0 h to 48 and 72 h, respectively. In the chronic

state, there was also a 3.65-fold decrease at 48 h from baseline (0 h) and 2.61-fold-increase from 48 h to 72 h. IL-6 levels exhibited variability post - EPS 1 h, with a peak fold-increase from 0 h to 72 h (57.13). In the 2D - EPS 6 h condition, IL-6 exhibited an initial 21.78-fold-decrease at 24 h and a subsequent 2.14-fold-decrease at 72 h from 0 h. Following acute - EPS, there were decreasing low levels of IL-15 detected at earlier timepoints with median concentrations of 6.10 pg/mL (24 h), 3.42 pg/mL (48 h) and 2.61 pg/mL (72 h) and a notable of 2.34-fold decrease from 24 h to 72 h. IL-15 was only detected immediately after chronic - EPS (2.97 pg/mL). FGF21 immediately after acute - EPS was at a median concentration of 12.55 pg/mL (0 h) and increased by 95.32-fold at 24 h (1196.74 pg/mL), peaking at 2083.92 pg/mL at 48 h with a 165.98-fold increase. There was also a notable fold-increase between 48 h and 72 h (2.68). Following the chronic condition, FGF21 exhibited a 7.98-fold decrease in the first 24 h but increased between 24 h and 48 h (10.29) and 24 h and 72 h (14.72). FSTL1 showed a significant fold-increases of 22.90 at 24 h, 47.59 at 48 h and 27.26 at 72 h, from 0 h. There was also 2.08 increase from 24 h to 48 h. In the chronic condition, there was an initial fold decrease at 24 h (10.03) from 0 h. However, fold-increases persist between 24 h and 48 h (13.32) and 48 h and 72 h (7.49). MSTN surged at 24 h post - EPS (192.95 pg/mL), followed by reduced levels at 48 h (45.88 pg/mL) and elevated at 72 h (95.75 pg/mL). Notable fold reductions between 24 h and 48 h (4.21) and 24 h and 72 h (2.02). In the chronic condition, post 6 h - EPS, MSTN was initially measured at 182.15 pg/mL but was undetected during post - EPS, which indicates low expression or rapid degradation. Irisin demonstrated a 31.48-fold at 24 h from 0 h which suggests a robust myogenic response at the start of the post - EPS period, followed by 10.40-fold and 26.75-fold increases at 28h and 72 h, respectively. A reduction in irisin occurred after the chronic condition, with 92.16-fold decrease from 0 h (6.04 pg/mL) to 24 h (190.08 pg/mL) post - EPS. However, fold-increases were noted between 24 h and 48 h (37.68) and 24 h to 72 h (70.5). LIF after 1 h - EPS showed low, stable levels with minor fluctuations in fold increases at 24 h (4.87), 48 h (4.25) and 72 h (3.63) from baseline (0 h), indicative of a consistent response in the post - EPS period. After 6 h - EPS, a fold-decrease of 5.66 was determined at 24 h from baseline. OSM release fluctuated slightly in the acute condition with fold increases at 24 h (4.18), 48 h (2.56) and 72 h (3.02) from 0 h. After the 6 h condition, OSM was only detected immediately at 0h at (5.16 pg/mL) and absence of data indicates potential downregulation or degradation in the CM. OSTN levels were similar in the post - EPS 1 h condition between 24 and 72 h. OSTN was not detected in the chronic condition. SPARC after acute - EPS showed relatively stable levels during post - EPS timepoints. Fold-increases existed between 0 h and 24 h (47.09), 48 h (54.18) and 72 h (48.65) (**Figure 5.8**).

2D

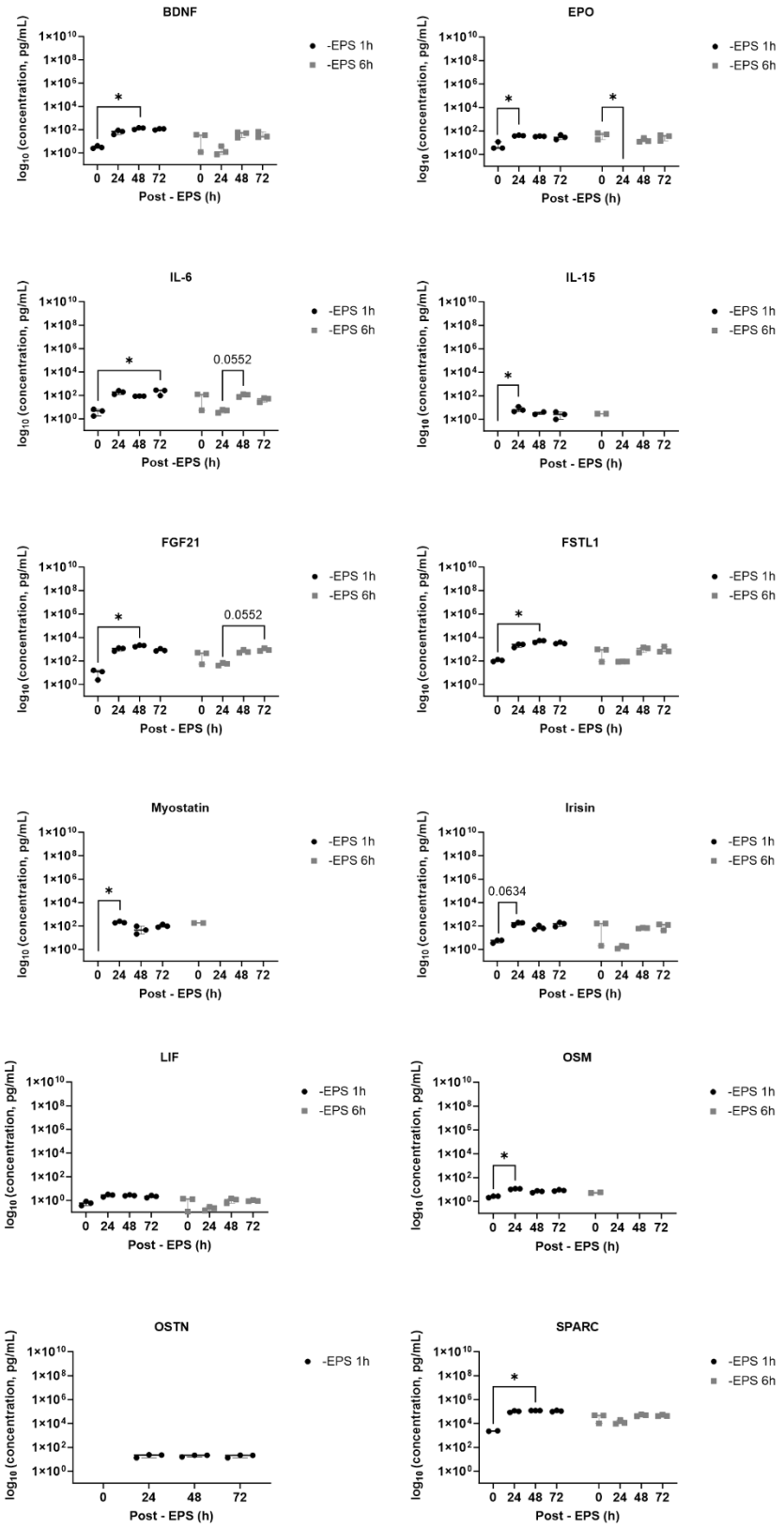

Figure 5.8 Myokine secretion after 1 h and 6 h - EPS from the 2D model. *The following myokines were significant in the post- EPS timepoints BDNF -1 h (p=0.0279) between 0 h vs.48 h; EPO -1 h (p=0.0455) between 0 h vs. 24 h; EPO -6 h (p=0.0372) between 0 h vs. 24 h; IL-6 -1 h (p=0.0395) between 0 h vs. 72 h; IL-15 -1 h (p=0.0164) between 0 h vs. 24 h; FGF21 -1 h (p=0.0134) between 0 h vs. 48 h; FSTL1 -1 h (p=0.0194) between 0 h vs. 48 h; Myostatin -1 h (p=0.0125) between 0 h vs. 24 h; OSM -1 h (p=0.0134) between 0 h vs. 24 h and SPARC -1 h (p=0.0395) between 0 vs. 48 h. Data was analysed by Kruskal-Wallis test, followed by Dunn's correction post-hoc test.*

5.4.2.2 Myokines from the 3D - EPS model

BDNF was only detected at 0 h – in the acute condition, 528687.63 pg/mL and was strikingly lower at 4.00 pg/mL in the chronic condition. EPO remained undetected in the acute condition. However, in the chronic period, EPO showed a marked fold-increase at 24 h from 0 h then decreased and remained unchanged until 72 h with consistent 7.77-fold decreases from 24 h to 48 h to 72 h. IL-6 showed minor fold-decreases after acute - EPS, during the post - EPS timepoints. However, in the chronic condition, there was a notable 3.58-fold increase from 0 h to 24 h, followed by a 6.60-fold-decrease from 24 to 48 h. FGF21 showed notable fold-decreases between 24 h to 48 h (7.41) and 24 h to 48 h (6.11). FSTL1 after acute - EPS showed a fold-increases between 48 h and 72 h (4.64). Furthermore, fold-decreases of 8.78 at 24 h and 4.72 between 24 h and 48 h. A marked 58.78-fold increase following chronic - EPS occurred at 24 h post - EPS from baseline (0 h), followed by subsequent decreases at 48 h (3.50) and 72 h (19.45). Fold-decreases persisted between 24 h to 48 h (205.64) and 72 h (1143.27), declining to 5.56 from 48 h to 72 h. Irisin level peaked after acute - EPS, in the first 48 h with a fold-increase of 2.65 and 2.81 from 0 h to 24 h and 48 h, respectively. Fold decreases persisted between 24 h and 72 h (2.39) and 48 h and 72 h (2.53). The chronic 3D - EPS 6 h state also revealed an initial elevation after 24 h with a fold-increase of 13.70 from 0 h, and low, consistent levels before and after. Similarly, fold-decreases persisted during post - EPS, from 24 h to 48 h (13.70) and 72 h (12.81). LIF after chronic - EPS, presented a fold-increase in the first 24 h of post - EPS, by 2.34-fold from baseline. Between post - EPS timepoints, LIF levels decreased from 24 h by 2.34-fold at 48 h and 2.66-fold at 72 h. OSM after chronic - EPS, presented a maximal concentration of 11.29 pg/mL at 24 h post - EPS and a 12.12-fold increase from 0 h. SPARC after chronic - EPS, showed a notable fold decrease from 0 h to 48 (2.90) and subsequent decrease by 5.49-fold from 0 h to 72 h and between 24 h, 24 h and 48 h (2.24-fold) and 24 h and 72 h (4.25-fold) (**Figure 5.9**).

3D

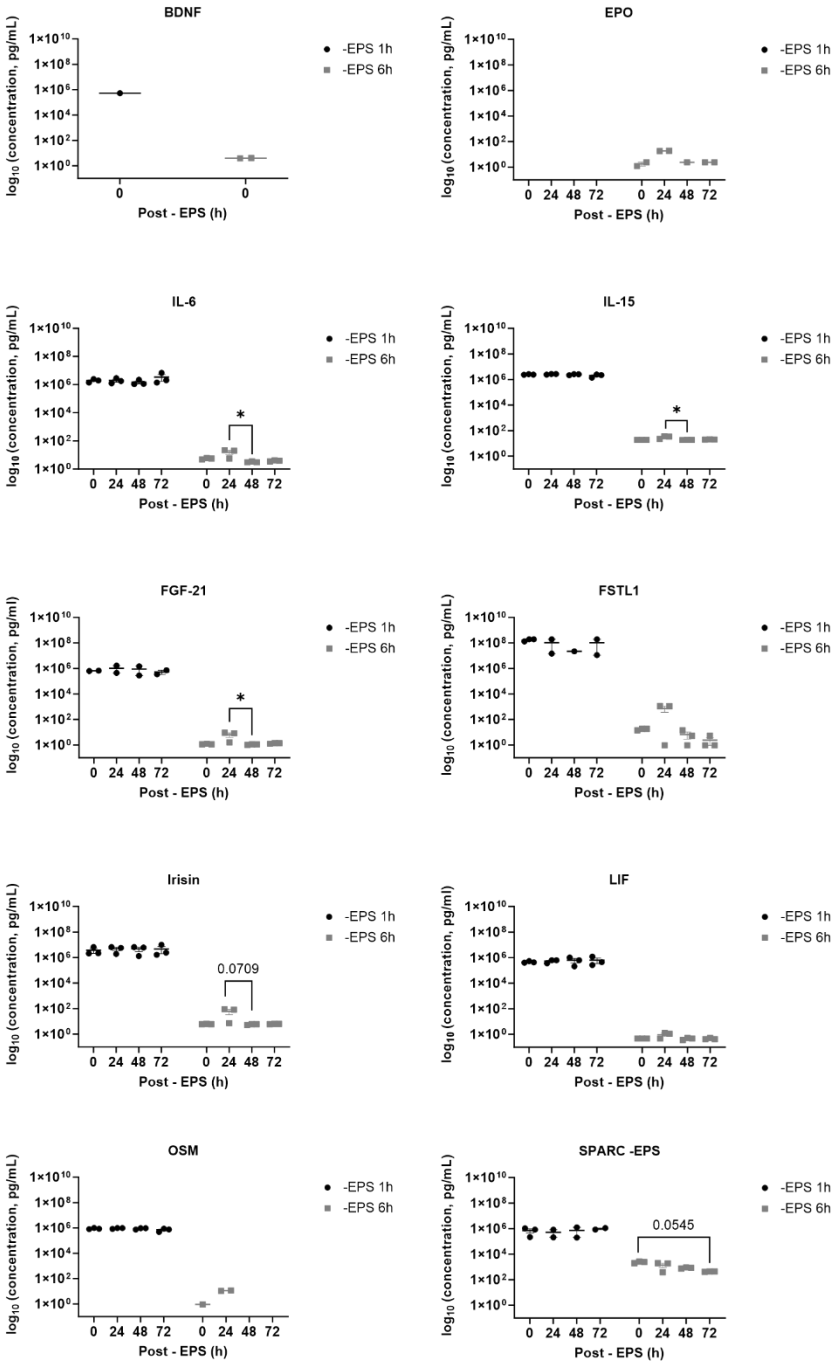

Figure 5.9 Myokine secretion after 1 h and 6 h - EPS from the 3D model. *In the 3D - EPS condition, the following myokines presented significance between 24 h and 48 h post - EPS timepoints: IL-6 (p=0.0266), IL-15 (p=0.0279) and FGF21 (0.0129), after chronic - EPS. Data was analysed by Kruskal-Wallis test, followed by Dunn's correction post-hoc test.*

5.4.2.3 Myokines from the 2D + EPS model

BDNF revealed fold increases of 8.18 at 24 h and 5.61 at 48 h from 0 h during post + EPS, with a diminishing response up to 72 h with a 7.44-fold increase at 72 h from 0 h. After 6 h + EPS, there was a 638.76-fold increase in BDNF concentration at 24 h from very low level at 0 h (0.01 pg/mL to 6.39 pg/mL). A fold-increase of 2.43 at 48 h with a return to negligible concentrations. This indicated a transient effect with rapid degradation or downregulation following initial release. EPO levels after 1 h EPS, showed a fold-increase from 0 h to 24 h (2.65) at 24 h followed by fold-decreases thereafter and between post + EPS timepoints: 4.03 (24 h to 48 h) and 3.43 (24 h to 72 h) indicating diminishing response to acute + EPS over time. EPO after chronic + EPS was initially detected at 19.06pg/mL at 0 h and sustained at 24 h (18.65 pg/mL). After acute + EPS, IL-6 markedly increased from baseline by 135.90-fold at 24 h, by 36.78-fold at 48 h to 91.58-fold. There was a 3.70-fold-decrease between 24 h and 48 h. After chronic + EPS, IL-6 was present at 5.53 pg/mL at 24 h and then was undetected thereafter at 48 h and 72 h which suggests a potential rapid response of IL-6 after chronic + EPS. Acute 1 h + EPS IL-15 is only detected in the 24 h condition following both the acute and chronic EPS. FGF21 levels after acute EPS, showed a noteworthy fold-increase from 0 h to 24 h (343.04), and subsequent stabilised concentrations at 48 h (2611.21 pg/mL) and 72 h (2178.07) which resulted in 286.14- and 243.27-fold increases from 0 h to 48 h and 72 h, respectively. Increasing levels of FGF21 were seen after chronic + EPS with 16.93 (24 h), 90.03 (48 h) and 137.16 (72 h) fold-increases from 0 h. FSTL1 levels revealed fold-increases from 0 h to 24 h (9.25), 48 h (9.73) and 72 h (23.00) and steady fold-increases between + EPS timepoints, particularly 24 h to 72 h (2.49) and 48 h to 72 h (2.36). After chronic + EPS, FSTL1 levels declined significantly after 24 h with peak median concentration of 853.24 pg/mL and 15.65-fold increase from 0 h. MSTN was only detected following acute EPS at 24 h (448.30 pg/mL), albeit markedly and at 48 h (20.98 pg/mL) with a 21.37-fold reduction between these timepoints. Irisin following acute EPS, decreased revealed fold-increases of at 24 h (9.63), 48 h (6.95) and 72 h (4.88) from 0 h. After chronic + EPS, a notably high at 144.86-fold increase was present from 0 h (1.19 pg/mL) to 24 h (172.22 pg/mL), with subsequent decrease in concentration in the post + EPS period. LIF after acute + EPS, presented only a meaningful 5.17-fold increase from 0 h to 24 h. However, during the post + EPS period, fold-decreases persisted between 24 h and 48 h (2.97) and 24 h and 72 h (3.78). LIF levels after chronic EPS remained very low and were almost unchanged immediately after + EPS at 0 h (0.22 pg/mL) and at 24 h (0.34 pg/mL). OSM exhibited an initial 24 h response with a 15.02-fold increase from 0 h to 24 h after acute + EPS but decreased from 48 h to 72 h. OSM remained undetected after chronic, 6 h + EPS. OSTN was only measured following acute EPS, at 24 h (63.65 pg/mL) and persisted at 48 h (60.83

pg/mL) which further increased to a maximum concentration of 96.94 pg/mL at 72 h. SPARC levels remained consistently high during the after 1 h + EPS, with 58.73, 53.10, 53.83-fold increases at 24 h, 48 h and 72 h. Following 6 h + EPS, SPARC revealed a fold-decreases of 3.21 (24 h), 8.98 (48 h) and 11.75 (72 h) from 0 h. Decreases persisted between 24 h and 48 h (2.80) and 24 h and 72 h (3.66) (**Figure 5.10**).

2D

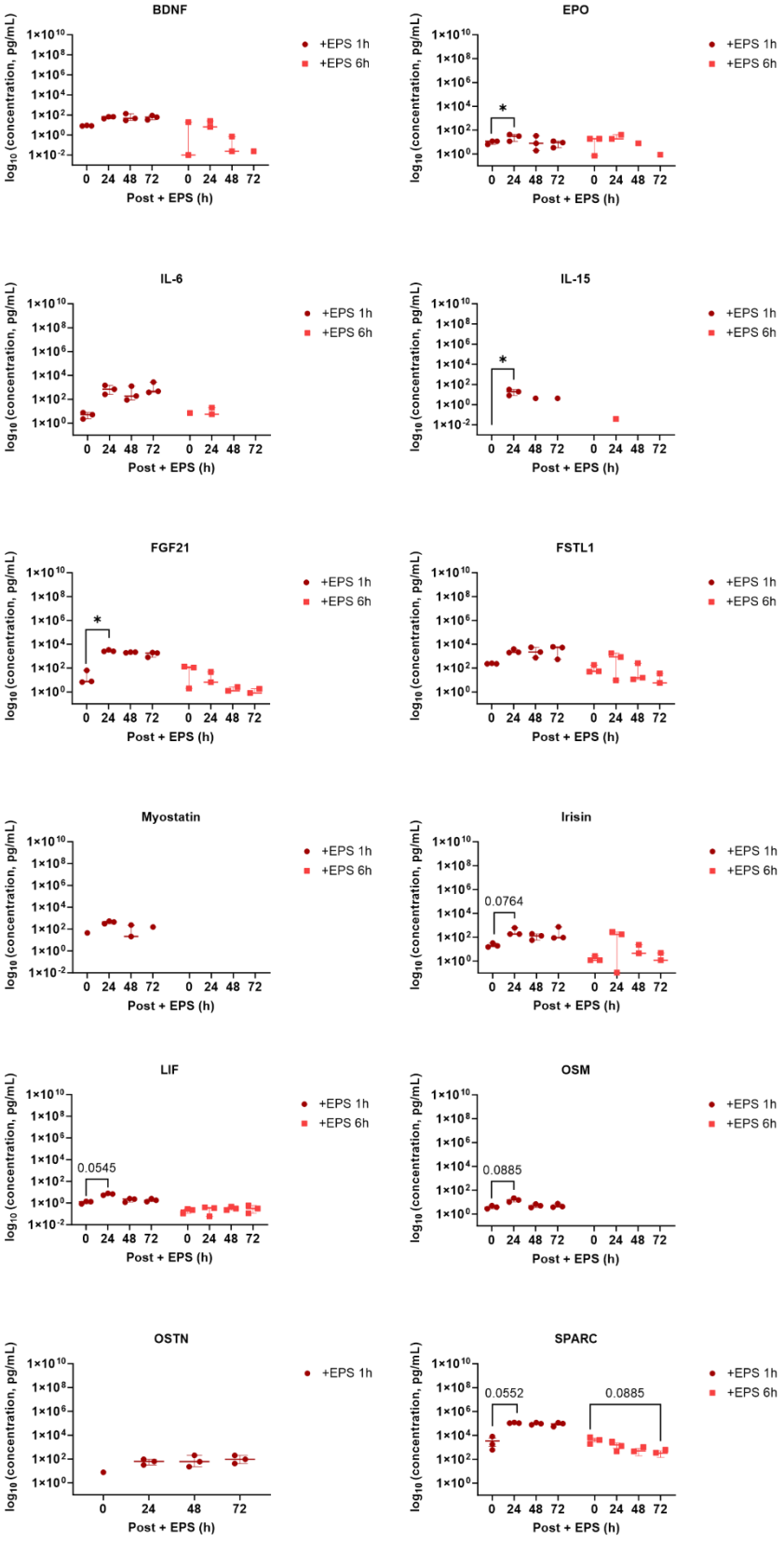

Figure 5.10 Myokine secretion after 1 h and 6 h + EPS of the 2D model. *In the 2D + EPS condition, the following myokines presented significance between 0 h and 24 h post + EPS timepoints: EPO (p=0.0372), IL-15 (p=0.0473), FGF21 (p=0.0134), after acute + EPS. Data was analysed by Kruskal-Wallis test, followed by Dunn's correction post-hoc test.*

5.4.2.4 Myokine secretion from the 3D + EPS model

BDNF at 1 h post + EPS showed a 4.35-fold increase at 24 h but remained almost undetected 6 h post + EPS, at level of 0.23 pg/mL at 24 h (**Figure 5.11**). EPO post + EPS, was detected at low levels at 24 h (3.34 pg/mL), 48 h (2.38 pg/mL) and 72 h (3.34 pg/mL). At 1 h post + EPS, IL-6 shows marked fold-increases at 24 h (172.18) and 48 h (195.58), and 72 h (172.18) compared to baseline. At 6 h post + EPS: moderate increases at 24 h (2.75), 48 h (3.73), and 72 h (3.97) are detected. IL-15 levels remained steady with no fold change in the post + EPS period with a maximal concentration of 2530080.70 pg/mL at 0 h after 1 h + EPS and 23.55 pg/mL at 72 h after 6 h + EPS. Following acute + EPS, FGF21 exhibited fold-increases at 24 h (45.44), 48 h (52.72), and 72 h (40.77) from 0 h, though slightly decreasing by the later timepoints. At 1 h post + EPS, FSTL1 showed a moderate fold-increase at 24 h (3.04), followed by greater fold-increases at 48 h (6.29) and 72 h (16.58) from 0 h. Notable fold-increases persisted between post + EPS timepoints at 24 h and 48 h (2.07), 24 h and 72 h (5.46) and 48 h and 72 h (2.64). At 6 h post + EPS a steady 4.73-fold increase at 24 h, followed a marked 47.91-fold increase at 48 h from 0 h. Between timepoints, a notable 10.12-fold increase was present at 48 h to 72 h. Irisin after acute + EPS showed moderate fold increases at 24 h (2.33), 48 h (3.07), and 72 h (2.65) from 0 h. At 6 h post + EPS irisin levels remained steady at 6-9 pg/mL between 0 h - 72 h. Smaller changes were present between timepoints, for acute and chronic EPS. LIF exhibited high concentrations in the acute condition, peaking at 398547.40 pg/mL and almost undetected after chronic + EPS period at (>1 pg/mL) with no noteworthy fold change (<2). SPARC exhibited notable fold-increases after acute + EPS at 24 h (14.60), 48 h (17.64), and 72 h (16.77) from 0 h and minor increases at later timepoints (72/24 and 72/48). At 6 h post + EPS, SPARC exhibited fold increases at 24 h (19.05), 48 h (17.47), and 72 h (16.63) from 0 h (**Figure 5.11**).

3D

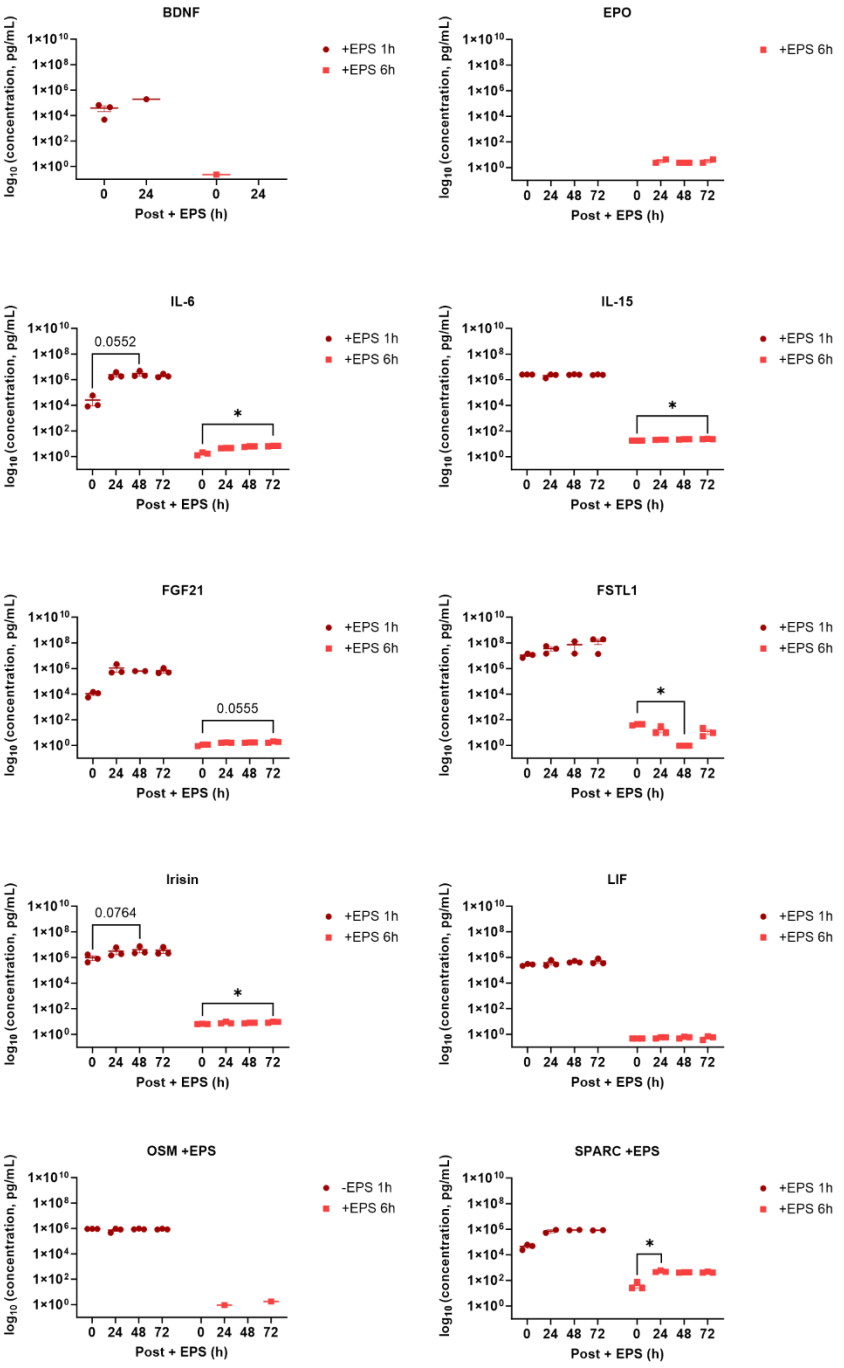

Figure 5.11 Myokine secretion after 1 h and 6 h + EPS of the 3D model. *In the 3D + EPS condition, the following myokines presented significance after chronic + EPS: IL-6 (p=0.0153), IL-15 +6 h (p=0.0211) and Irisin (p=0.0405) between 0 and 72 h; FSTL1 (p=0.0114) between 0 h and 48; and SPARC (p=0.0270) between 0 h and 24 h. Data was analysed by Kruskal-Wallis test, followed by Dunn's correction post-hoc test.*

5.5 Discussion

5.5.1 Dynamics of myokine abundance across 2D and 3D models

This chapter focused on the timing and secretion patterns of myokines from 2D and 3D models, influenced by stimulation modality and duration. The analysis from 0 h to 72 h post ± EPS highlighted the diverse temporal patterns of myokine release, as some myokines responded consistently across conditions, while others were specific to prolonged EPS. This is implicative of *in vivo* exercise duration which accounts over 50% variance of IL-6 levels in plasma (Fischer, 2006). These findings emphasise the complexity of time-dependent myokine dynamics in SkM to different EPS conditions and suggests a potential distinct regulatory role of immediate, sustained, and downregulated myokines. The 2D and 3D - EPS models under acute and chronic conditions, represent models that are incubating in SFM for 1 h or 6 h, respectively. Therefore, the myokines secreted at 0 h, 24 h, 48 h or 72 h post 1 h and 6 h incubation periods, are possibly by spontaneous contraction or a basal level of unstimulated myokine release. In the 2D 1 h - EPS model, some myokines present as early responders, particularly LIF, which peaked at 24 h. This observation is supported by Broholm and Pedersen (2010), who observed that the amount of LIF in differentiation media increased 24 h after media change by differentiated human myotubes. This indicates that the formation of myotubes with sarcomeric contractile apparatus may be sufficient to endogenously induce myokines following contraction. However, the aforementioned study failed to characterise the myotubes. In contrast, the 2D and 3D models were characterised with both structural and developmental maturity features.

5.5.2 Myokine responses from the 3D *in vitro* model

With the exception of EPO, the 3D ± EPS model secretes myokines in response to both acute and chronic conditions. This demonstrates that the 3D model, regardless of the presence or absence of EPS, may be system capable of mimicking both immediate (acute) and sustained (chronic) muscle activity. This analysis underscores the distinct time-specific myokine responses, with 3D + EPS chronic conditions highlighting for their capacity to maintain potential extended signalling, in contrast to the more transient signalling profiles observed in other regimens. Therefore, this model may better represent physiological responses *in vivo*.

In the 3D model, BDNF was only detected once, at 24 h following acute + EPS, and is absent in the post ±EPS period after both acute and chronic ± EPS. This suggests that BDNF may exhibit a distinct acute response from C2C12 cells, independent of ± EPS duration or the application of EPS itself. A similar, early response is seen in a study which found that BDNF levels increased after 10 minutes of moderate hand biking and reduced

when participants continued at high intensity for a marathon distance (Rojas Vega *et al.*, 2008). The absence of BDNF after 0h underscores that secretion profiles can change significantly over time. Furthermore, BNDF has been associated with local action and not released into the circulation when secreted by mouse SkM cells, since its overexpression did not alter plasma BDNF levels (Matthews *et al.*, 2009). This further validates the acute BDNF activity observed in this study from the 3D model.

5.5.3 Myokine degradation in the post ± EPS period

The 2D - EPS condition revealed degradation of myokines - IL-15, Myostatin and OSM were not detected beyond 24 h. This detection method also revealed differences in concentration of myokines, after acute stimulation the myokines were released at a higher concentration, particularly from the 3D models. The variability in myokine levels observed under different protocols highlighted the importance of assessing how various regimens impact specific myokine levels over time. LIF exhibited high concentrations in the acute condition, peaking at 398547.40 pg/mL and almost undetected after chronic + EPS period at (>1 pg/mL) with no noteworthy changes. Time-course analysis revealed the rate at which myokine levels returned to baseline, which is critical for evaluating both recovery phases and the overall efficacy of exercise interventions. Additionally, myokines that were undetectable immediately after ± EPS (Chapter 4) may represent localised rather than systemic responses, warranting further investigation following contraction.

5.5.4 Variable changes in the post ± EPS period

MIA analysis particularly highlighted the distinct temporal patterns of myokine secretion across acute and chronic conditions, with key differences between 2D and 3D models. MIA analysis revealed high-amplitude secretions of myokines in the post + EPS period from the acute 3D model.

FSTL1 has been found to be predominately elevated after acute exercise bouts, namely 0.5 to 2 h, supporting its acute response following 2D EPS (Nam *et al.*, 2024). However, further analysis in this study, which expanded the post ± EPS duration, revealed that FSTL1 secreted from the unstimulated (- EPS) 3D model exhibited consistently high fold-decreases the post-EPS period; between 24 h and 48 h (205.64) and 24 h and 72 h (1143.27). In an unstimulated model, SkM cells secrete FSTL1 over a longer period. IIn this study, changes in concentration were among the highest with BDNF after 6 h stimulation (+ EPS) in 2D, with a 638.76-fold increase at 24 h from immediate collection. FGF21 levels showed a fold-increase from 0 h to 24 h (343.04) and INSL6 presented a substantial 169.43-fold increase from 0 h to 72 h, both in the acute 2D + EPS model. Supporting evidence has shown that serum FGF-21, FSTL-1, and BDNF have all been

shown to increase in serum plasma after an acute bout of high intensity exercise (Ji *et al*., 2024).

Further evidence of variable change is provided from the 3D model at 1 h post + EPS IL-6 shows marked fold-increases at 24 h (172.18) and 48 h (195.58), and 72 h (172.18) compared to baseline. Demonstrating that our + EPS models indeed stimulates myokines at a substantial level, which persist in the post + EPS period. The greatest reported increase in plasma IL-6 (8000-fold) was found after a 246 km foot race (Goussetis *et al.*, 2009). Thereby showing differences between *in vitr*o and *in vivo* post-exercise changes. Notably, the distinction between plasma myokines and CM myokines from SkM requires careful comparison. While plasma myokines are released into circulation and to exert demonstrated systemic effects, CM myokines are only secreted into a localised environment, with the potential to only affect adjacent cells directly or itself. There is high variability between *in vivo* studies. Plasma concentrations of IL-6 is known to peak upon, or shortly after, exercise cessation (Tamura *et al.*, 2011). Particularly showing remarkable increases immediately after exercise including ~100-fold and ~1000-fold increases in IL-6 before exercise which declined rapidly in the period following exercise (Ostrowski *et al.*, 1999; Steensberg *et al.*, 2000). However, some have indicated no change in plasma IL-6 levels and SPARC levels (Bessa *et al.*, 2016) (Garneau *et al.*, 2020).

5.5.5 Myokine dynamics as indicators of inflammatory responses

The fluctuations in myokine abundance and concentration in the post ± EPS period could be linked to the progression and resolution of inflammation, as myokines play critical roles in regulating both pro-inflammatory and anti-inflammatory processes. Thus, the changes in myokine levels over time may reflect the dynamic nature of the inflammatory response and its resolution. The abundance of CCL2, IL-7 and SPARC alternated from 0 h to 72 h. These myokines showed a biphasic response following 1 h and 6 h incubation in the control model. In longer 6 h period, CCL7 abundance increased post - EPS and peaked at 48 h followed by a decrease at 72 h in both 2D and 3D unstimulated models. CCL7 has been shown to mediate inflammatory response in regeneration and disease progression (Boss-Kennedy *et al*., 2024; Chang *et al*., 2022). Thus, this biphasic response may be indicative of a transient response which may mimic inflammatory action. IL-15 and LIF abundance increased, peaked and subsequently decreased following 6 h +EPS in 3D, reflecting a fine-tuning process of these myokines following in chronic stimulation. Furthermore, considerable increases in abundance were also present with IL-15 (1625.57) and TNF (703.80) in the first 24 h, post - EPS 1h in 3D. IL-15 has been found to have both pro-inflammatory (Ye, 2015) and anti-inflammatory

(Bazgir *et al.*, 2015) properties. Like, IL-6, FSTL1 in recent years has been considered in the regulation of inflammation (G. Li *et al*., 2020).

5.5.6 Limitations

The complex nature of myokines, combined with the two approaches used for their detection, made it challenging to determine the dynamics of individual myokines. Factors such as myokine half-life and experimental conditions undoubtedly influenced the measurements obtained. However, it was important to interpret both metrics together to understand myokine dynamics comprehensively and infer their potential roles. Although the post ± EPS period was extensive, this study did not investigate time points before 24 hours. Time intervals closer to the exercise-like protocol, such as 3, 6, 12, 24, 48, and 72 hours, should be explored (Bessa *et al.*, 2016)Ideally, comparison to human sera is required to accurately infer myokine dynamics and roles. Therefore, a range of in vitro protocols (beyond 20 V, 1 Hz, 10 ms) should be executed to maximise potential comparisons.

5.6 Conclusion

Time-course analysis potentially determined optimal time points for detection of myokines, ensuring accurate profiling beyond 0 h (Chapter 4). Variations in myokine levels highlight the complex regulatory mechanisms that sustain SkM homeostasis which may promote some of the systemic benefits of exercise. This study highlighted that the beneficial effects of exercise, i.e. myokines, are prevalent up to 72 h. Furthermore, the 3D ± EPS model appears to be a versatile system, capable of mimicking both immediate (acute) and sustained (chronic) myokine secretion. The distinction of the post ± EPS period concerning exercise-mimicry requires clarity. However, the *in vitro* models in this study have established myokine dynamics, bypassing the confounding factors present in human subjects.

6 General Discussion

6.1 Summary of findings

The initial phase of this program of research focussed on the methodological development and tissue-engineered *in vitro* SkM models, with enhanced maturity and functionality, for effective analysis of the contraction-induced secretome. Review of the literature in Chapter 1, enabled the classification of SkM characterisation into three categories: structural, developmental, and functional maturity features. Chapter 3, detailed the development of a 3D model, guided by the characterisation of key sarcomeric markers, including α-Actinin and MyHC II, in both 2D and 3D models, as well as dystrophin as structural features, in the final 3D model. Evaluation of *in vitro* SkM models highlighted that structural markers could be indicative of contractile capability, but not standalone indicators of maturity. This is because passive (non-contractile) models, still showed expression of sarcomeric proteins as discussed in Chapter 1. However, increased sarcomere formation has been linked to elevated contractile activity in both 2D and 3D *in vitro* models (Ikeda *et al*., 2017b). Furthermore, during myogenesis, MRF4 transcript levels increase, coinciding with myofiber maturation (Weis *et al.*, 2000) and reflecting its role in mature muscle (Zammit, 2017). Therefore, MRF4 was incorporated as a marker of developmental maturity for the 3D model, to address its redundancy in existing SkM models (**Table 1.1**) and enhance the robustness of the characterisation framework. Further characterisation of the *in vitro* models developed in this study was carried out following the application of tensile strain to cell-laden models using two stimuli: MCT6 and MTSIP (Chapter 3). The models developed direction-dependent properties, influenced by the applied stimuli and supported by anchorage of the model. The MCT6 model increased α-Actinin MFI and exhibited cellular alignment in the direction of the tension compared to unstrained models. Furthermore, MT and IF staining of the SkM fibres revealed alignment and lengthened fibres via MTSIP. The effect of the EPS remained undetermined as both the stimulated and unstimulated models expressed the same markers of maturity and ECM-cell distribution. Moreover, contraction was not observed in the final 3D model, and it was thereby classified as a passive model. This model was supported by passive, non-contractile models summarised in **Table 1.1**, as well as secretome studies confirming myokine detection without evidence of SkM contraction (**Table 1.2**).

A range of myokines, including prototype and common myokines such as IL-6, Irisin, and BDNF, among others, were successfully detected and profiled in both models in Chapter 4. The unstimulated model offered valuable insight into the endogenous contraction and basal secretory functions of SkM cells, influenced by mechanical cues, without EPS. Chapter 4 substantiated the hypothesis that myokines are secreted immediately following contraction and are modulated by the duration of stimulation. This study

showed that two time points: 1 hour (acute); and 6 hours (chronic) ± EPS, produced distinct myokine profiles across the different models. For example, LIF (3D) was the only myokine to show a significant increase in abundance and fold-increase from 1 h to 6 h stimulation, highlighting the impact of EPS on models with different dimensional structures. The 3D chronically stimulated model also detected IL-6, which was undetected at 1 h, which further demonstrates that the timing of stimulation (acute vs. chronic) influenced the immediate presence of some myokines. Potential interactions between myokines and the effects of EPS were further observed. EPS selectively influenced myokine dynamics, suggesting a possible interdependence between IL-6 and TNF, as TNF was undetected in the 3D + EPS condition while IL-6 was present. This indicated a potentially beneficial myokine response, where IL-6, as an anti-inflammatory myokine (Keller *et al.*, 2006) was detected in the absence of TNF, which is a pro-inflammatory myokine. Alternatively, further exploration of the pathways involved in IL-6 and TNF could clarify whether they act independently or influence each other. For example, IL-6 might reduce TNF through NF-κB inhibition. Indeed, IL-6 can suppress activation of NF-κB signalling, which regulates TNF expression, thereby reducing inflammation (Rafik *et al*., 2024).. Furthermore, inhibition of both IL-6 and TNF-α has enhanced anti-inflammatory effects (Namakanova *et al.*, 2022), demonstrating that IL-6 can also be pro-inflammatory. In the context of physiological exercise, training reduces TNF levels but not IL-6 (Smart *et al.*, 2011). This reinforces IL-6's protective effects against inflammation. In this way, the 3D EPS model mimics exercise. Finally, in Chapter 4, global secretome analysis via LCMS^{E} identified the most 1210 proteins from the 2D - EPS condition, similar to proteins identified in the secretome from human primary SkM (Mengeste *et al.*, 2022) and greater than other C2C12 mouse studies (Deshmukh *et al*., 2015b; Grube *et al*., 2018; Henningsen *et al*., 2010). In contrast, fewer proteins were identified in the 2D + EPS condition (397), the 3D - EPS controls (215) and the 3D + EPS condition (349). This underscored the 2D model's capacity for producing a diverse secretome profile and demonstrates how the secretome outcomes are influenced by C2C12 monolayer culture compared to 3D culture. Additionally, ± EPS models showed how the 'exercise regime' as well as other stimuli influenced both the number and type of myokines detected. Notably, LCMS^{E} analysis did not distinguish between acute and chronic conditions, as the same myokines were identified. However, differences in the relative abundance of myokines were affected significantly (from in the 2D + EPS condition) such as LIF in the 3D + EPS model between 1 h and 6, which could potentially indicate more representative myokine profile in 3D compared to 2D. h. Studies reveal that shorter EPS durations such as 3 h can effectively increase specific myokines like irisin, while longer durations of 24-48 hours have resulted in wider metabolic adaptations and a more extensive range of myokines secreted (Mengeste *et al.*, 2022; Sugimoto *et*

al., 2022). However, variable EPS parameters such as intensity and model type, limits the direct comparison between studies.

The final research hypothesis proposed that SkM cells secrete myokines in a time-dependent manner, lasting up to 72 h. Chapter 5 revealed trends in myokine secretion beyond the immediate 1 h and 6 h inductions (+ EPS) or incubation in SFM (- EPS) in both 2D and 3D models. Indeed, exercise has been explored beyond stimulation induction, predominant in human studies (**Table 5.1**), however the 'post-exercise' effects *in vitro* had not been extensively investigated up to 72 h. This investigation was crucial to provide a controlled environment to study myokine dynamics, without the complexities and variability of whole-organism systems. Furthermore, the concept of exerkines suggests exercise-induced secreted factors might be broader and not limited to SkM alone (Brooks *et al.*, 2023; Gonzalez-Franquesa, Stocks, *et al.*, 2021; Magliulo *et al.*, 2021).

The key findings from chapter 5 were that myokines secreted from *in vitro* models were indeed detected up to 72 h post ± EPS. Myokines displayed temporal secretion profiles, being secreted in an acute, transient, and biphasic manner following ± EPS. Through sustained release of anti-inflammatory myokines, Chapter 5 supported inference made in Chapter 4 that the unstimulated 3D model triggered inflammatory myokines, with an interdependence between TNF and IL-6 in inflammation and ± EPS. Chapter 5 showed that in the 3D - EPS model, TNF showed a substantial (703.80-fold) increase in the first 24 h of incubation in SFM. This was followed by a 24.44-fold increase in IL-6 between 0 h to 48 h and subsequent 8.63-fold decrease in TNF from 48 h to 72 h. However, this same response in - EPS demonstrates that it is not regulated by + EPS and could be due to spontaneous contraction observed within the 3D model. Overall, the sustained presence of myokines suggests potential endocrine functions, highlighting the relevance of these models for studying the long-term effects of EPS on systemic metabolism.

6.2 2D vs. 3D models

The outcomes of 2D and 3D secretome analysis are inherently influenced by the characteristics and conditions of the respective models. Structurally, with regards to the ECM, the 2D C2C12 model was matrix-free, which does not replicate the native ECM environment found *in vivo* while the C2C12 cells in 3D were encapsulated in a collagen-geltrex matrix, likely promoting more natural cell behaviour and potentially enhancing myokine secretion. Studies indicate that muscle contraction in these 3D environments significantly increases the secretion of myokines like irisin (Sugimoto *et al.*, 2022). Since 3D environments, such as collagen hydrogels, replicate the ECM's biochemical and mechanical properties, to promote myoblast differentiation into myotubes (Camman *et*

al., 2023). Strain alone may also be sufficient to induce myokine secretion from the 3D models. Mechanical strain applied to muscle constructs has been shown to influence myokine secretion, following endurance and high-intensity training (Suresh Kumar *et al.*, 2023). Furthermore, the differentiation period between 2D and 3D culture was found to differ, with differentiation taking three times longer in 3D compared to 2D and could represent more physiological differentiation. Longer culture periods are typical for 3D SkM models with the longest myogenic culture time is reported in a 3D bio-printed fibrous hydrogel structure, lasting up to 21 days (Costantini, Testa, Mozetic, *et al*., 2017). Furthermore, both models underwent separate methods of chronic stimulation. In the 2D model, a single 6 h EPS was delivered at D7, whereas in 3D, 1 h repeated EPS over 6 days was applied. Therefore, EPS in 3D also contributed to model development during differentiation, as it was applied during culture and not purely as an end point stimulation as applied in 2D. Comparing continuous stimulation to the repeated, cumulative chronic stimulation in 3D would clarify the effects of these two stimulation modes (as discussed in section 6.9). However, the cells, SFM conditions, EPS duration were consistent across models in this study. With consideration to the differences mentioned, their secretome, in this instance, could be compared. Mass spectrometry (nano- $LCMS^E$) analysis of the secretome from hiPSCs cultured in 3D showed a significantly greater abundance of unique proteins, including EV-related proteins and growth factors, compared to the 2D culture (Cui *et al.*, 2024). This finding is similar to the differences observed in myokine secretions between 2D and 3D within this thesis.

6.3 EPS as viable approach for *in vitro* exercise-mimicry

EPS generally offers a controlled approach to muscle mimicry by replicating the electrical signals that trigger muscle contraction, thereby simulating exercise-induced responses including myokine secretion. Particularly, EPS can be used to modulate metabolic responses and trigger metabolic pathways of SkM cells using various parameters (Nikolić *et al*., 2012; Valero-Breton *et al*., 2020). The frequency of EPS pulses, typically characterised as low frequency, ranging from 0.2 to 2 Hz are known to mimic endurance exercise (Lambernd *et al*., 2012; Nikolić *et al*., 2012), whereas moderate frequency of 1 to 30 Hz can mimic resistance exercise (Scheler *et al*., 2013). High-frequency EPS up to 100 Hz is can mimic resistance exercise, both acutely and chronically (Valero-Breton *et al.*, 2020).

EPS can be a ‘double-edged’ approach to exercise mimicry since it does not fully replicate the complete range of responses observed with exercise. However, EPS is advantageous in that it controls or limits the redundancy of the complex integrative human physiology. This is because there are multiple overlapping pathways and mechanisms that contribute to the exercise response (Hawley *et al*., 2021), which make

it difficult to isolate or target specific genes or pathways to predict or modulate outcomes consistently. In this way, EPS is less challenging to standardise and simplifies myokine responses. However, how this relates to specific exercise regimes and interactive effects with other tissue responses cannot be addressed *in vitro.*

Furthermore, in human studies or multicellular systems, there is typically a disregard for anthropometric characteristics of study subjects, with the application of the same training protocol to both male and female humans, different ages and ranges of physical capabilities (Militello *et al.*, 2022). In particular, exercise can be sex-dependent due to biological differences, influenced by hormones, muscle composition, metabolism, and cardiovascular function thus further influencing physiological responses (Fulghum *et al.*, 2022). A rare study applied different EPS protocols for myotubes (biopsies) from young male subjects (10 V, 0.1 Hz and 2ms for 24 h) and middle-aged women (30 V, 2 ms and 1 Hz for 48 h), although this study did not describe how these tailored protocols were derived (Mengeste *et al.*, 2022). RNA-Seq and microarray analysis from this study identified both shared and differentially regulated proteins following the gender-tailored protocols. This suggests that EPS may consistently activate certain genes across different donors and cell types when exercises are adjusted for anthropometrics, leading to some elements of a universal protein response yet concurrently maintaining donor specific patterns of protein secretion.

The number of myokines identified in the secretome of both 2D and 3D models appeared relatively consistent across conditions, with similar profiles observed at both 1 h and 6 h, regardless of the presence or absence of EPS. However, there were significant differences in the concentration of the myokines released (Chapter 4). This highlights two key aspects of myokine secretion as presence vs. regulation. EPS affects secretion levels, showing its impact on magnitude but not on the diversity of myokines. These findings are supported by higher intensity and longer duration exercise resulted in increased circulating concentrations of IL-6 in humans (Carson, 2017). Furthermore, EPS has also been shown to significantly increase some myokines from a 3D-engineered muscle model, such as BDNF after 3 h and not others (cathepsin B). This highlights the selective modulation of myokine secretion by EPS and the importance of specific stimulation protocols in determining which myokines are upregulated (Sugimoto *et al.*, 2022). This study showed EPS-evoked muscle contractile stimulation. Furthermore, in Chapters 4 and 5, a baseline of myokine secretion is altered by EPS induction and EPS duration. LCMS^{E} revealed notable differences between - EPS (18) and + EPS (5) myokines in the 3D model. Therefore, the method of detection has a significant impact on the outcome and comparison should be carefully considered. Indeed, the kinetics of myokine release during and after exercise can vary depending on

the detection method, affecting the interpretation of their roles in systemic health (Raimondo *et al*., 2016). Therefore, detection methods complicate the detection of myokines.

EPS may affect the integrity of the tissues with porosity observed after chronic EPS (Chapter 3), that consequently could have to fewer myokines secreted and detected in the 3D + EPS model (Chapter 4). Although EPS using the C-Pace has been reported to not induce cytotoxicity in human SkM cell cultures (Scheler *et al*., 2015), the carbon electrodes in the present work were observed to have residue post EPS which may be due to salt absorption, electrolysis by-products and proteins from media potentially affecting the viability of the cells and quality, particularly electrolysis observed around the electrodes regions within the 2D cell models (Morimoto *et al*., 2020; Nikolić and Aas, 2019). As a result, toxins may have leached into the media to induce unspecific effects and even cell death; the latter of which was observed microscopically as loss of elongated cell structure and twitch contractility by 24 h (data not shown). Metabolically and chemically inert platinum electrodes have been used to circumvent this (Alave Reyes-Furrer *et al*., 2021). However, consideration of the effect of the ionic current flowing through the sample should also be considered, as electrodes with smaller surface areas provide higher current density and targeted electric field distribution (when compared to larger ones), which could affect the stimulation delivered to the cells and ultimately alter contractility across a model system (Rabbani *et al*., 2024).

Matching of the exact EPS conditions could produce a more reliable control model, by assembly of the culture dish with unstimulated cells connected to C-Dish™ has performed previously (Mengeste *et al*., 2022). This would provide the control cells with the same electrode exposure and could account for any electrode-induced differences. Furthermore, since the cell electrodes are submerged in culture media, the media volume and coverage, may affect the sarcomeric development of myotubes and subsequent functional properties such as contraction (Cooper *et al*., 2004), although this was controlled for within this thesis ensuring standard volumes were utilised throughout.

Overall, EPS offers a wide range of parameter variations – including single pulses vs. pulse trains, pulse duration, frequency, voltage, and the various combinations of these factors. Furthermore, there is no consensus on which protocol corresponds to specific exercise regimes, such as resistance or endurance training. This makes SkM exercise mimicry challenging and complicates direct comparison of protocols and results with other studies. Thus, EPS should be regarded as a method for inducing SkM contraction, with protocols broadly classified as acute or chronic, rather than as exact *in vivo* exercise protocols (Carter & Solomon, 2019).

6.4 Evaluating culture conditions

Unstimulated cells were washed and placed in SFM for the same duration as the + EPS condition. A possible limitation of using SFM is the reduction in proteins including growth factors, hormones, minerals and vitamins normally found within serum with prolonged incubation. Although C2C12 cells can proliferate and differentiate in SFM, lack of serum is found to effect metabolic characteristics of SkM cells (Jang *et al*., 2022). Nutrient scarcity has been found to rapidly decrease muscle protein synthesis by approximately 80%, with mTOR and P70S6K activities declining by 50% and 95%, respectively, within 30 minutes, and staying suppressed for up to 4 hours in C2C12 cells (Carson *et al.*, 2018). Thus, the SFM provides a defined environment, minimising variability and contamination from serum-derived factors (Auber *et al.*, 2019) but perhaps limiting the myokine secretion potential of the models and not being reflective of *in vivo* conditions.

Since cells during differentiation were enriched with IGF-1, which was also a target myokine in this work, detection of IGF-1 in SFM was assessed. An important study identified that EPS-CM induced metallothionein 1/2 and Slc30a2 gene expression in the absence of C2C12 myotubes, indicating that EPS can induce both cell-mediated and non-cell-mediated effects. However, the direct effects of EPS on C2C12 myotube function (AMPK phosphorylation, myokine secretion) were mainly caused by EPS-induced contraction and not due to EPS-induced changes in cell culture media (Evers-Van Gogh *et al*., 2015). Positively, for the studies in chapters 4 and 5, IGF-1 was not detected in either SFM media or stimulated SFM for 1, 3, 6 and 24 h. This ensured the effective washing in SFM and during experimentation. However, four myokines were identified, though with low precision and accuracy (>30 ppm). Unstimulated SFM identified DCN and FNDC5 with confidence scores of 4.7 and 4.4. This score reflects the likelihood that the identified myokine corresponds to a specific compound. Therefore, a high confidence score suggests a robust match, whereas a low score may indicate ambiguities or poor matches. In proteomics, according to Progenesis QI, confidence score was assigned based on various physiochemical properties of the ion matches. While stimulated SFM identified METRNL and EPO also with very low confidence scores of 4.59 and 4.18, respectively. For perspective, the average confidence score, taken from the top 10 proteins identified of the 4 conditions investigated in this body of work (**Table 4.3**) revealed an average confidence score of 154.84. Given that their measurements fell outside the detection were low, they were excluded from consideration as valid identifications.

6.5 Evaluating the - EPS model

The myokines detected from the - EPS secretome were described as basal myokines or spontaneous-contractile-induced myokines. Interestingly, a model of occasional spontaneous contractions from cultured human SkM myotubes was deemed a resting model with non-contracting muscle cells (Norheim *et al.*, 2011). At rest, skeletal muscle maintains muscle tone, crucial for postural stability and energy efficiency. This tone results from the intrinsic viscoelastic properties of muscle fibres and the continuous ATP hydrolysis by myosin motors, even without active contraction (Nelson *et al.*, 2020). This also indicates that the contraction was limited or non-existent when unstimulated and native SkM does not contract. To confirm the resting state of SkM, examination of the myosin filaments through conformation and actin attachment (Hill *et al.*, 2021), or resting muscle tone (Masi & Hannon, 2008), which can be examined via electromyography.

6.6 Further potential inducers of myokines

The 2D model, spontaneous myotube contraction was observed (Chapter 3), which was absent in the 3D model. Since, myokines were detected in both unstimulated 2D and 3D models, even in the absence of mechanical strain in 2D, it suggests that myokine release was not solely dependent on mechanical stimulation. This points to the possibility that other factors, could be driving myokine secretion. The fact that myokines were detected in both unstimulated 2D and 3D models indicates that myokine secretion can occur in different culture environments, regardless of the presence of spontaneous contraction. However, the 3D model may better mimic *in vivo* conditions (as discussed previously), where SkM cells are exposed to a complex interplay of biochemical and mechanical cues. This highlights the importance of considering the physical context and cell-matrix interactions, which may influence myokine release beyond mechanical contraction alone (Maleiner *et al.*, 2018). An alternative source of myokines could be the ECM, which envelops myofibers as a meshwork that serves as a reservoir for proteins, including collagens, proteoglycans, glycoproteins (Loreti & Sacco, 2022). Membrane-bound proteins can be cut or ‘shed’ away as ectodomain-shed proteins. Similar to myokines, they are released into the extracellular space and can function as signalling molecules (Mori *et al.*, 2023). An example of this is seen with the release of TNF (a target myokine in our studies), that is regulated by the enzyme TNF converting enzyme (TACE), which cleaves membrane-bound TNF, shedding its ectodomain to produce the soluble (myokine) protein (Barberà-Cremades *et al.*, 2017). However, the mechanisms underlying myokine secretion must be clarified by SPs, as demonstrated in Chapter 4, to discern cell-secreted factors.

Switching the cell culture medium to an SFM buffer has been shown to trigger the release of significant amounts of proteins from C2C12 cells (Furuichi *et al*., 2018). This was significant enough to mask contraction-regulated IL-6 secretion. Nonetheless, media changes are crucial to limit the detection of non-specific proteins and to remove any residual secreted factors to better represent each post ± EPS period. In other cell types such as human SkM myoblasts, serum starvation has greatly triggered their differentiation (Le Bihan *et al.*, 2012).

6.7 Serotransferrin as a novel myokine and its potential endocrine action

Among the top 10 proteins ranked by confidence score, and due its detection as a secretory protein, specifically in metabolism, the presence of a signal peptide (SP) and Gene Ontology (GO) classification (as discussed in Chapter 4), Serotransferrin was identified as novel myokine identified in this study. Notably, Serotransferrin is specific to its presence in serum, while transferrin is the broader term for the protein itself.

A study by Golizeh *et al*. (2017) showed an increased turnover of serotransferrin and ceruloplasmin in diet-controlled patients with type 2 diabetes. As serotransferrin is involved in iron transport, its altered turnover could reflect a role in regulating muscle metabolism and broader systemic processes, supporting the idea of serotransferrin acting as a myokine. OSTN, another myokine, mechanistically interacts with transferrin receptor 1 (Tfr1) and inhibits Tfr1-mediated thermogenic activation in beige adipocytes through a cAMP/PKA-dependent pathway (Jin *et al.*, 2023). OSTN's inhibition of Tfr1-mediated thermogenic activation in beige adipocytes suggests a link between iron regulation and thermogenesis, which may further implicate serotransferrin as a myokine involved in metabolic and thermogenic processes. Further studies implicate Tfr1 (Transferrin receptor protein 1) as an essential receptor in mediating iron uptake via endocytosis, critical for regulating brown and beige fat thermogenesis (J. Li *et al*., 2020). Therefore Tfr1, and by extension the proteins interacting with it (Serotransferrin and OSTN), may be involved in regulating energy expenditure, further supporting the concept of myokines, like the novel myokine serotransferrin, impacting broader metabolic and thermogenic processes. So far, several myokines including irisin (Boström *et al*., 2012; Gamas *et al*., 2015; Nie & Liu, 2017) and METRNL (Rao *et al.*, 2014) with roles in thermogenesis and the browning of white adipose tissue. Knocking down serotransferrin or chelating iron with deferoxamine markedly inhibits adipogenesis and mitochondrial biosynthesis (Hargreaves & Spriet, 2020); however, treating adipocytes with either iron or transferrin stimulates lipolysis (Rumberger *et al.*, 2004). Together, these points suggest that iron metabolism, mediated by Tfr1, serotransferrin, and related proteins, is

integral to thermogenesis and adipocyte function. Furthermore, serotransferrin may influence these processes by regulating iron uptake, which in turn impacts energy expenditure, brown adipose tissue activation, and lipolysis.

By binding free iron, transferrin reduces the generation of reactive oxygen species (ROS) that can lead to oxidative stress and muscle damage. Excess free iron can exacerbate damage in muscle tissues, particularly during conditions like intense exercise or injury. Therefore, serotransferrin may indirectly support muscle repair and regeneration through iron delivery and oxidative protection. By identifying serotransferrin as a myokine in the present study, a role of exercise in key metabolic pathways mediated by iron binding and transport may newly be postulated.

6.8 Summary of key contributions to knowledge

This research sought to establish accessible, contractile-inducible murine SkM models with active secretory function. A key innovation was the application of tensile strain to the cell-laden Collagen-Geltrex hydrogels using a custom platform. The novel model is also compatible with the commercially available C-Pace Ion Optix EP system, enabling the simultaneous stretch and EPS. Additionally, a novel classification framework was developed to systematically characterise SkM models, addressing a gap in the literature and potentially setting new standards for model development. Existing SkM models have shown particular limitations in their ability to represent highly developmental markers of maturity. Therefore, the engineering of a functional, mouse myocyte-derived construct in this body of work, contributed to the limited mature *in vitro* models. Acute and chronic contractile activity was stimulated to promote secretome production. Moreover, untargeted LC-MS^{E} analysis of the CM revealed potential for the discovery of a novel myokine, thus expanding the known myokinome. Finally, insight into the temporal dynamics of myokines after acute and chronic contraction-induction was demonstrated, again highlighting important features and considerations that are often over-looked in myokine research and SkM model development.

6.9 Future Directions

Building on this thesis would involve contribution to the different aspects of the project from SkM model development to its application, specifically for the study of myokines.

SkM is the largest tissue in the human body, constituting around 40% of total body mass and acting as a reservoir for 50–75% of total body protein (Frontera & Ochala, 2015; Sánchez Riera *et al*., 2021). SkM is highly heterogeneous, varying in fibre type composition, cellular and subcellular characteristics, motor unit type, myosin isoform expression, and functional roles (e.g., postural vs. phasic muscles). SkM also exhibits

significant plasticity and adaptability, responding to exercise, ageing, and other environmental stimuli. Moreover, variability exists between different cell sources which have genetic and metabolic characteristics that influence experimental outcomes (Abdelmoez *et al.*, 2020). Considering these factors together, SkM tissue engineering can pose significant challenges. Development of highly sophisticated, physiological and readily applicable *in vitro* SkM model largely depend on the specific research objective, but an ideal model should mimic the physiological, mechanical, and biochemical properties of SkM. Thereby this section will focus on ideas for further development of the 3D SkM model from Chapter 3.

6.9.1 Optimisation of the 3D model

The final model presented in this thesis was expedited to enable secretomics testing and achieve the project's aims. Future iterations could build on the existing model by incorporating biomaterial and tissue engineering strategies, including cells and scaffolding, into the final 3D construct.

Cells: Replacing the C2C12 cell type, which lack many of the specialised characteristics of *in vivo* skeletal muscle (Deshmukh *et al*., 2015a) with primary human cells and co-cultures would be ideal for the reasons discussed in Chapter 1. The cells would then be differentiated using defined media 3 components, as previous, which morphologically showed to enhance the SkM cells (Chapter 3).

Scaffolding: The hydrogel rod provided a 3D fibrillar framework and as the ECM enabled the interaction of the cells within it with its composition. The cell-matrix suspension was cast into the moulds (section 2.1.3.4). Incorporation of a chamber-like system into the MTSIP would minimise manual handling, media volume and material by creating an enclosed channel for cell-hydrogel suspensions to be pipetted into.

Anchorage and strain: The goal here would be to achieve SkM fibre alignment, which reflects directional dependence of structural and functional properties in SkM that necessitates force transmission and contraction (Jana, Levengood and Zhang, 2016). Directionality is generated by mechanical forces for developing SkM (Sunadome *et al.*, 2023) and tensile forces were achieved via the MTSIP system anchors (section 2.1.3.6). The application of manual tensile strain via the MTSIP, was an incredibly positive feature which accelerated the development of the 3D model (Chapter 3). Furthering the application of tensile strain cyclically can produce dense and highly oriented tissue whereby the cells and the collagen fibres could be aligned in the direction of stretching (Bansai *et al*., 2019; Okano & Matsuda, 1997). The use of the slider in the MTSIP model can be optimised to induce incremental and diverse strain magnitudes as well as cyclic stimulation mechanical stimulation in addition to EPS.

EPS: In this research program a single EPS protocol was applied, and chronic stimulation was either continuous 6 h (in the 2D model) or repeated 1 h bouts over 6 days (in the 3D model). Application of electrical pulses using the C-Pace, commonly applied in *in vitro* studies (Orfanos *et al.*, 2016) can replicate the action potentials sent from motor neurons to muscle fibres, which are responsible for initiating muscle contractions. Furthermore, strategic implementation of rest periods is effective in training outcomes. Alternatively, a previous study reported that the force production ability of myotubes decreased rapidly after the cessation of continuous EPS, accompanied by changes in atrophy-related gene expression (Fujita *et al.*, 2010) , indicating the importance of continuous EPS without rest. Thus, comparison is needed to determine the effectiveness of continuous and intermittent stimulation.

3D Imaging: The 2D C2C12 model and an earlier 3D spheroid model exhibited contraction (Chapter 3). However, contraction was not detected in the final 3D rod model which was used in the secretomics study. This was due to the cell-hydrogel thickness and the inability to visualise individual contracting myotubes or whole cell contractions. Thus, as live contractions were unable to be investigated the project utilised FFPE processing to embed the cell-hydrogel models following harvest, which renders 3D systems into endpoint 2D-imaging, potentially leading to the loss of valuable information or interpretation of observations. High resolution confocal microscopy such as the Zeiss Lightsheet z.1 confocal microscope (Germany) could be used for visualising 3D C2C12 cells within the matrix. Tracking cells with markers for visualisation of SkM features in the cell-hydrogel rods before strain, after strain and after + EPS could also be applied. Furthermore, this 3D live imaging would circumvent questions raised regarding cell porosity which may be artefactual, caused by the FFPE process. Additionally, analysis of cell distribution within the hydrogel and confirmation of cellular orientation could be made possible by 3D imaging.

Contraction analysis: In this body of work, contractility as a measure of SkM function was not undertaken due to resource limitations. The 20 second video recordings taken can be analysed using the Myocyter to characterise contractility via two key parameters – the velocity and amplitude of muscle contractions (Grune *et al.*, 2019). Other means of quantifying contraction could be used such as MuscleJ (Mayeuf-Louchart *et al.*, 2018) and Muscle Motion (Mummery *et al.*, 2017), both as open source and accessible softwares for high throughput analysis of *in vitro* SkM contraction. Furthermore, monitoring contraction via live cell recording would clarify the dynamic events of muscle EPS-induced contraction as well as the rate of recurrence of unstimulated contractions. This could be made possible using the Lightsheet described above.

Application: Broadly, the advantages of the *in vitro* models were to exploit and isolate myokine effects, test hypotheses under controlled condition, in response to simulated exercise-like conditions. The model is well-suited for secretomics studies, as it aims to develop a healthy myoid. Chapters 4 and 5 have successfully shown that both 2D and 3D models are capable of secreting detectable and dynamic myokines. Therefore, CM with known myokines, modulated though EPS, can be used to study the paracrine and endocrine effects, an aspect not explored in this work. As a developing model, the MTSIP provides opportunities for adaptation and exploration of interactions between the ECM and SkM under tensile strain and investigation electromechanical coupling of EPS-induced electrical activity (EPS) and mechanical properties in 3D.

Based on a recent bibliometric analysis of research on exercise-regulated myokines from 2003 to 2023 (Sun *et al.*, 2024), there is a still insufficient knowledge about how exercise parameters (intensity, duration, frequency) influence the release and function of specific myokines. This research focuses on the mimicry of *in vivo* effects of exercise, potentially leading to the development of the contentious 'exercise in a pill' exploration (Guerrieri, Moon, and van Praag, 2017). However, further research is needed to identify the myokines responsible for exercise benefits and translate these findings into therapeutic interventions. Additionally, more studies are required to understand the long-term effects of myokine modulation on systemic health and disease prevention.

Development and application of the 3D MTSIP model was mainly discussed here, however an interest was directed toward the intriguing phenomenon of spontaneous SkM contractility observed in 2D, potentially driven by sarcomere dynamics (Gunther & Kruse, 2010; Kono *et al*., 2020). Pertinent to myokine secretion, the flux of intracellular calcium, rather than the contraction itself has been identified as the trigger for IL-6 secretion during contraction (Furuichi *et al*., 2018). Implicitly, mechanisms of myokine release such as intracellular biochemical processes have to be considered. This highlights the complexity of muscle regulation, which is typically dominated by neural inputs and calcium signalling. Thus, further research into the balance between intrinsic and extrinsic factors that dictate muscle contraction is needed.

6.10 Final Conclusion

Myokine research is critical for elucidating the intricate muscle-body crosstalk that contributes to the systemic benefits of exercise. They exert beneficial effects, influencing metabolism (Ahima & Park, 2015; Argilés *et al*., 2016b; Huh, 2018), cardiovascular (Esposito *et al*., 2015), cognitive (Delezie and Handschin, 2018b; Pedersen, 1987) and immune processes (Bay & Pedersen, 2020). The development of robust SkM models is essential to advancing our understanding of myokine study. The consensus was that

functional characterisation represents a definitive marker of SkM maturity for *in vitro* SkM models, because it ensures maturity, structural fidelity, better physiological accuracy of experimental outcomes. Thus, a standard of maturity was indicated which supported a level of comparison and reproducibility of between *in vitro* SkM models. However, SkM models, by virtue of the secretion can indicate functionality. Therefore, secretomics can be a valuable additional dimension to SkM model characterisation. With the well-established benefits of exercise and its growing use as a therapy, interest in mimicking exercise *in vitro* through EPS has also increased, though this remains a complex challenge due to the systemic nature of exercise as a stimulus (Hawley *et al*., 2021). This research demonstrated that myokine secretion can be effectively modulated by optimising EPS protocols with stimulation parameters designed to mirror training regimens. This indicates that the pleiotropic effects of exercise can, to some degree, be replicated via controlled myokine release. However, *in vitro* exercise-mimicry is best considered a generalised model of skeletal muscle contraction, suitable for both acute and chronic applications, rather than a faithful representation of a specific exercise type. Overall, understanding the differences in myokine responses based on stimulation duration and how this affects the post-contraction period of myokine secretion, provides valuable insights into optimising muscle training, recovery, and therapeutic interventions.

References

Abdelmoez, A.M. *et al.* (2020) 'Comparative profiling of skeletal muscle models reveals heterogeneity of transcriptome and metabolism', *American Journal of Physiology - Cell Physiology*, 318(3), pp. C615–C626. Available at: https://doi.org/10.1152/ajpcell.00540.2019.

Aboalola, D. and Han, V.K.M. (2017) 'Different effects of insulin-like growth factor-1 and insulin-like growth factor-2 on myogenic differentiation of human mesenchymal stem cells', *Stem Cells International*, 2017. Available at: https://doi.org/10.1155/2017/8286248.

Adams, V. (2018) 'Electromyostimulation to fight atrophy and to build muscle: facts and numbers', *Journal of Cachexia, Sarcopenia and Muscle*. Wiley Blackwell, pp. 631–634. Available at: https://doi.org/10.1002/jcsm.12332.

Aguilar-Agon, K.W. *et al.* (2019) 'Mechanical loading stimulates hypertrophy in tissue-engineered skeletal muscle: Molecular and phenotypic responses', *Journal of Cellular Physiology*, 234(12), pp. 23547–23558. Available at: https://doi.org/10.1002/jcp.28923.

Ahima, R.S. and Park, H.K. (2015) 'Connecting myokines and metabolism', *Endocrinology and Metabolism*, 30(3), pp. 235–245. Available at: https://doi.org/10.3803/EnM.2015.30.3.235.

Ahmad, S.S. *et al.* (2020) 'Implications of Insulin-Like Growth Factor-1 in Skeletal Muscle and Various Diseases', *Cells*. NLM (Medline). Available at: https://doi.org/10.3390/cells9081773.

Ahmadi, M.N. *et al.* (2023) 'Brief bouts of device-measured intermittent lifestyle physical activity and its association with major adverse cardiovascular events and mortality in people who do not exercise: a prospective cohort study', *The Lancet Public Health*, 8(10), pp. e800–e810. Available at: https://doi.org/10.1016/S2468-2667(23)00183-4.

Alave Reyes-Furrer, A. *et al.* (2021) 'Matrigel 3D bioprinting of contractile human skeletal muscle models recapitulating exercise and pharmacological responses', *Communications Biology*, 4(1). Available at: https://doi.org/10.1038/s42003-021-02691-0.

Albrecht, E. *et al.* (2015) 'Irisin - A myth rather than an exercise-inducible myokine', *Scientific Reports*, 5. Available at: https://doi.org/10.1038/srep08889.

Albrecht, E. *et al.* (2020) 'Irisin: Still chasing shadows', *Molecular Metabolism*, 34, pp. 124–135. Available at: https://doi.org/10.1016/j.molmet.2020.01.016.

Alcazar, J. *et al.* (2019) 'On the Shape of the Force-Velocity Relationship in Skeletal Muscles: The Linear, the Hyperbolic, and the Double-Hyperbolic', *Frontiers in Physiology*. Frontiers Media SA. Available at: https://doi.org/10.3389/fphys.2019.00769.

Aminoff, M.J. (2005) 'Myology, Basic and Clincal, 3rd Edition, edited by Andrew G. Engel and Clara Franzini-Armstrong, 2 vols., 1960 pp., ill., New York, McGraw-Hill, 2004, $395', *Muscle & nerve; Muscle Nerve*. Hoboken: Wiley Subscription Services, Inc., A Wiley Company, p. 531. Available at: https://doi.org/10.1002/mus.20246.

Anderson, S.B., Goldberg, A.L. and Whitman, M. (2008) 'Identification of a novel pool of extracellular pro-myostatin in skeletal muscle', *Journal of Biological Chemistry*, 283(11), pp. 7027–7035. Available at: https://doi.org/10.1074/jbc.M706678200.

Argilés, Josep M. *et al.* (2016) 'Skeletal Muscle Regulates Metabolism via Interorgan Crosstalk: Roles in Health and Disease', *Journal of the American Medical Directors Association*, 17(9), pp. 789–796. Available at: https://doi.org/10.1016/j.jamda.2016.04.019.

Argilés, Josep M *et al.* (2016) 'Skeletal Muscle Regulates Metabolism via Interorgan Crosstalk: Roles in Health and Disease', *Journal of the American Medical Directors Association*, 17(9), pp. 789–796. Available at: https://doi.org/10.1016/j.jamda.2016.04.019.

Asano, T. *et al.* (2015) 'Optogenetic induction of contractile ability in immature C2C12 myotubes', *Scientific reports*, 5(1), p. 8317. Available at: https://doi.org/10.1038/srep08317.

Ascenzi, F. *et al.* (2019) 'Effects of IGF-1 isoforms on muscle growth and sarcopenia', *Aging Cell*, 18(3). Available at: https://doi.org/10.1111/acel.12954.

Asfour, H.A., Allouh, M.Z. and Said, R.S. (2018) 'Myogenic regulatory factors: The orchestrators of myogenesis after 30 years of discovery', *Experimental biology and medicine (Maywood, N.J.)*, 243(2), pp. 118–128. Available at: https://doi.org/10.1177/1535370217749494.

Aswad, H. *et al.* (2014) 'Exosomes participate in the alteration of muscle homeostasis during lipid-induced insulin resistance in mice', *Diabetologia*, 57(10), pp. 2155–2164. Available at: https://doi.org/10.1007/s00125-014-3337-2.

Auber, M. *et al.* (2019) 'Serum-free media supplements carry miRNAs that co-purify with extracellular vesicles', *Journal of Extracellular Vesicles*, 8(1). Available at: https://doi.org/10.1080/20013078.2019.1656042.

Baik, J. *et al.* (2023) ‘Establishment of Skeletal Myogenic Progenitors from Non-Human Primate Induced Pluripotent Stem Cells’, *Cells*, 12(8). Available at: https://doi.org/10.3390/cells12081147.

Bakooshli, M.A. *et al.* (2019) ‘A 3D culture model of innervated human skeletal muscle enables studies of the adult neuromuscular junction’, *eLife*, 8, p. e44530. Available at: https://doi.org/10.7554/eLife.44530.001.

Balshaw, T.G. *et al.* (2023) ‘The effect of specific bioactive collagen peptides on function and muscle remodeling during human resistance training’, *Acta Physiologica*, 237(2). Available at: https://doi.org/10.1111/apha.13903.

Balu, D. *et al.* (2016) ‘Ca2+ effects on glucose transport and fatty acid oxidation in L6 skeletal muscle cell cultures’, *Biochemistry and Biophysics Reports*, 5, pp. 365–373. Available at: https://doi.org/10.1016/j.bbrep.2016.01.007.

Bansai, S. *et al.* (2019) ‘Effect of cyclic stretch on tissue maturation in myoblast-laden hydrogel fibers’, *Micromachines*, 10(6). Available at: https://doi.org/10.3390/mi10060399.

Barberà-Cremades, M. *et al.* (2017) ‘P2X7 receptor induces tumor necrosis factor-α converting enzyme activation and release to boost TNF-α production’, *Frontiers in Immunology*, 8(JUL). Available at: https://doi.org/10.3389/fimmu.2017.00862.

Barlow, J. and Solomon, T.P.J. (2019) ‘Conditioned media from contracting skeletal muscle potentiates insulin secretion and enhances mitochondrial energy metabolism of pancreatic beta-cells’, *Metabolism: Clinical and Experimental*, 91, pp. 1–9. Available at: https://doi.org/10.1016/j.metabol.2018.11.004.

Barohn, J., Dimachkie, M. and Jackson, C. (2014) ‘A PATTERN RECOGNITION APPROACH TO THE PATIENT WITH A SUSPECTED MYOPATHY Richard’, *Neur cli*, 32(3), pp. 569–vii. Available at: https://doi.org/10.1016/j.ncl.2014.04.008.A.

Bay, M.L. and Pedersen, B.K. (2020) ‘Muscle-Organ Crosstalk: Focus on Immunometabolism’, *Frontiers in Physiology*. Frontiers Media S.A. Available at: https://doi.org/10.3389/fphys.2020.567881.

Bazgir, B. *et al.* (2015) ‘Effects of eccentric and concentric emphasized resistance exercise on IL-15 serum levels and its relation to inflammatory markers in athletes and non-athletes’, *Asian Journal of Sports Medicine*, 6(3). Available at: https://doi.org/10.5812/asjsm.27980.

Belizário, J.E. *et al.* (2016) 'Skeletal muscle wasting and renewal: a pivotal role of myokine IL-6', *SpringerPlus*, 5(1), pp. 1–15. Available at: https://doi.org/10.1186/s40064-016-2197-2.

Benoit, B. *et al.* (2017) 'Fibroblast growth factor 19 regulates skeletal muscle mass and ameliorates muscle wasting in mice', *Nature Medicine*, 23(8), pp. 990–996. Available at: https://doi.org/10.1038/nm.4363.

Bentzinger, F.C., Wang, Y.X. and Rudnicki, M.A. (2012) 'Building Muscle: Molecular Regulation of Myogenesis', *Cold Spring Harb Perspect Biol*, 4(2), p. a008342. Available at: https://doi.org/10.1101/cshperspect.a008342.

van den Berg, L.E.M.M. *et al.* (2011) 'A case of adult Pompe disease presenting with severe fatigue and selective involvement of type 1 muscle fibers', *Neuromuscular Disorders*, 21(3), pp. 232–234. Available at: https://doi.org/10.1016/j.nmd.2010.11.016.

Bergeron, R. *et al.* (1999) *Effect of AMPK activation on muscle glucose metabolism in conscious rats*, *Endocrinol. Metab*.

Bersini, S. *et al.* (2018) 'Engineering an Environment for the Study of Fibrosis: A 3D Human Muscle Model with Endothelium Specificity and Endomysium', *Cell Reports*, 25(13), pp. 3858-3868.e4. Available at: https://doi.org/10.1016/j.celrep.2018.11.092.

Bessa, A.L. *et al.* (2016) *EXERCISE INTENSITY AND RECOVERY: BIOMARKERS OF INJURY, INFLAMMATION, AND OXIDATIVE STRESS*. Available at: www.nsca.com.

Bettadapur, A., Suh, Gio C., *et al.* (2016) 'Prolonged Culture of Aligned Skeletal Myotubes on Micromolded Gelatin Hydrogels', *Scientific Reports*, 6(1), pp. 1–14. Available at: https://doi.org/10.1038/srep28855.

Bettariga, F. *et al.* (2024) 'Exercise training mode effects on myokine expression in healthy adults: A systematic review with meta-analysis', *Journal of Sport and Health Science* [Preprint]. Elsevier B.V. Available at: https://doi.org/10.1016/j.jshs.2024.04.005.

Bian, W. *et al.* (2012) 'Local tissue geometry determines contractile force generation of engineered muscle networks', *Tissue Engineering - Part A*, 18(9–10), pp. 957–967. Available at: https://doi.org/10.1089/ten.tea.2011.0313.

Le Bihan, M.C. *et al.* (2012) 'In-depth analysis of the secretome identifies three major independent secretory pathways in differentiating human myoblasts', *Journal of Proteomics*, 77, pp. 344–356. Available at: https://doi.org/10.1016/j.jprot.2012.09.008.

Boesten, L.S.M. *et al.* (2005) 'Tumor necrosis factor-α promotes atherosclerotic lesion progression in APOE*3-leiden transgenic mice', *Cardiovascular Research*, 66(1), pp. 179–185. Available at: https://doi.org/10.1016/j.cardiores.2005.01.001.

Böl, M. *et al.* (2014) 'On the anisotropy of skeletal muscle tissue under compression', *Acta Biomaterialia*, 10(7), pp. 3225–3234. Available at: https://doi.org/10.1016/j.actbio.2014.03.003.

Børsheim, E. and Bahr, R. (2003) *Effect of Exercise Intensity, Duration and Mode on Post-Exercise Oxygen Consumption*, *Sports Med*.

Boss-Kennedy, A. *et al.* (2024) 'Muscle cell-derived Ccl8 is a negative regulator of skeletal muscle regeneration', *The FASEB Journal*, 38(14). Available at: https://doi.org/10.1096/fj.202400184R.

Boström, P. *et al.* (2012) 'A PGC1-α-dependent myokine that drives brown-fat-like development of white fat and thermogenesis', *Nature*, 481(7382), pp. 463–468. Available at: https://doi.org/10.1038/nature10777.

Bouzakri, K. *et al.* (2011) 'Bimodal effect on pancreatic β-cells of secretory products from normal or insulin-resistant human skeletal muscle', *Diabetes*, 60(4), pp. 1111–1121. Available at: https://doi.org/10.2337/db10-1178.

Braun, T. and Gautel, M. (2011) 'Transcriptional mechanisms regulating skeletal muscle differentiation, growth and homeostasis', *Nature Reviews Molecular Cell Biology*, pp. 349–361. Available at: https://doi.org/10.1038/nrm3118.

Broholm, C. *et al.* (2011) 'LIF is a contraction-induced myokine stimulating human myocyte proliferation', *J Appl Physiol*, 111, pp. 251–259. Available at: https://doi.org/10.1152/japplphysiol.01399.2010.-The.

Broholm, C. and Pedersen, B.K. (2010) *Leukaemia inhibitory factor-an exercise-induced myokine*.

Brooks, G.A. *et al.* (2023) 'Lactate as a myokine and exerkine: drivers and signals of physiology and metabolism', *Journal of applied physiology (Bethesda, Md. : 1985)*. NLM (Medline), pp. 529–548. Available at: https://doi.org/10.1152/japplphysiol.00497.2022.

Brunetti, J. *et al.* (2021) 'Nanopattern surface improves cultured human myotube maturation', *Skeletal Muscle*, 11(1). Available at: https://doi.org/10.1186/s13395-021-00268-3.

Burch, N. *et al.* (2010) 'Electric Pulse Stimulation of Cultured Murine Muscle Cells Reproduces Gene Expression Changes of Trained Mouse Muscle', *PLoS ONE*, 5(6). Available at: https://doi.org/10.3929/ethz-b-000018607.

Bydak, B. *et al.* (2022) 'Characterizing Extracellular Vesicles and Particles Derived from Skeletal Muscle Myoblasts and Myotubes and the Effect of Acute Contractile Activity', *Membranes*, 12(5). Available at: https://doi.org/10.3390/membranes12050464.

Cadot, B., Gache, V. and Gomes, E.R. (2015) 'Moving and positioning the nucleus in skeletal muscle-one step at a time', *Nucleus*, 6(5), pp. 373–381. Available at: https://doi.org/10.1080/19491034.2015.1090073.

Cai, T. and Yang, F. (2017) 'Strategies for Characterization of Low-Abundant Intact or Truncated Low-Molecular-Weight Proteins From Human Plasma', in *Enzymes*. Academic Press, pp. 105–123. Available at: https://doi.org/10.1016/bs.enz.2017.08.004.

Camman, M. *et al.* (2023) 'Anisotropic dense collagen hydrogels with two ranges of porosity to mimic the skeletal muscle extracellular matrix', *Biomaterials Advances*, 144. Available at: https://doi.org/10.1016/j.bioadv.2022.213219.

Capel, A.J. *et al.* (2019) 'Scalable 3D printed molds for human tissue engineered skeletal muscle', *Frontiers in Bioengineering and Biotechnology*, 7(FEB). Available at: https://doi.org/10.3389/fbioe.2019.00020.

del Carmen Ortuño-Costela, M. *et al.* (2019) 'iPSCs: A powerful tool for skeletal muscle tissue engineering', *Journal of Cellular and Molecular Medicine*, 23(6), pp. 3784–3794. Available at: https://doi.org/10.1111/jcmm.14292.

Carnes, M.E. and Pins, G.D. (2020) 'Skeletal muscle tissue engineering: Biomaterials-based strategies for the treatment of volumetric muscle loss', *Bioengineering*. MDPI AG, pp. 1–39. Available at: https://doi.org/10.3390/bioengineering7030085.

Carson, B.P. (2017) 'The potential role of contraction-induced myokines in the regulation of metabolic function for the prevention and treatment of type 2 diabetes', *Frontiers in Endocrinology*, 8(MAY), pp. 1–8. Available at: https://doi.org/10.3389/fendo.2017.00097.

Carson, B.P. *et al.* (2018) 'Regulation of muscle protein synthesis in an in vitro cell model using ex vivo human serum', *Experimental Physiology*, 103(6), pp. 783–789. Available at: https://doi.org/10.1113/EP086860.

Carter, S. and Solomon, T.P.J. (2019) 'In vitro experimental models for examining the skeletal muscle cell biology of exercise: the possibilities, challenges and future developments', *Pflugers Archiv European Journal of Physiology*. Springer Verlag, pp. 413–429. Available at: https://doi.org/10.1007/s00424-018-2210-4.

Cha, S.H., Lee, H.J. and Koh, W.G. (2017) 'Study of myoblast differentiation using multi-dimensional scaffolds consisting of nano and micropatterns', *Biomaterials Research*, 21(1). Available at: https://doi.org/10.1186/s40824-016-0087-x.

Chakravarthy, M. V. *et al.* (2000) 'Insulin-like growth factor-I extends in vitro replicative life span of skeletal muscle satellite cells by enhancing G1/S cell cycle progression via the activation of phosphatidylinositol 3'-kinase/Akt signaling pathway', *Journal of Biological Chemistry*, 275(46), pp. 35942–35952. Available at: https://doi.org/10.1074/jbc.M005832200.

Chal, J. and Pourquié, O. (2017) 'Making muscle: Skeletal myogenesis in vivo and in vitro', *Development (Cambridge)*, 144(12), pp. 2104–2122. Available at: https://doi.org/10.1242/dev.151035.

Chan, C.Y.X., McDermott, J.C. and Siu, K.W.M. (2011) 'Secretome Analysis of Skeletal Myogenesis Using SILAC and Shotgun Proteomics', *International Journal of Proteomics*, 2011, pp. 1–13. Available at: https://doi.org/10.1155/2011/329467.

Chan, X.C.Y., McDermott, J.C. and Siu, K.W.M. (2007) 'Identification of secreted proteins during skeletal muscle development', *Journal of Proteome Research*, 6(2), pp. 698–710. Available at: https://doi.org/10.1021/pr060448k.

Chanda, A. and Callaway, C. (2018) 'Tissue Anisotropy Modeling Using Soft Composite Materials', *Applied bionics and biomechanics*, 2018, pp. 4838157–4838159. Available at: https://doi.org/10.1155/2018/4838157.

Chang, T.T., Chen, C. and Chen, J.W. (2022) 'CCL7 as a novel inflammatory mediator in cardiovascular disease, diabetes mellitus, and kidney disease', *Cardiovascular Diabetology*. BioMed Central Ltd. Available at: https://doi.org/10.1186/s12933-022-01626-1.

Chen, H., Zhong, J., Wang, J., Huang, R., *et al.* (2019a) 'Enhanced growth and differentiation of myoblast cells grown on E-jet 3D printed platforms', *International Journal of Nanomedicine*, 14, pp. 937–950. Available at: https://doi.org/10.2147/IJN.S193624.

Chen, S.Q. *et al.* (2019b) 'Icariin induces irisin/FNDC5 expression in C2C12 cells via the AMPK pathway', *Biomedicine and Pharmacotherapy*, 115(April). Available at: https://doi.org/10.1016/j.biopha.2019.108930.

Chen, W., Nyasha, M.R., Koide, M., Tsuchiya, M., *et al.* (2019c) 'In vitro exercise model using contractile human and mouse hybrid myotubes', *Scientific Reports*, 9(1), pp. 1–9. Available at: https://doi.org/10.1038/s41598-019-48316-9.

Chiron, S. *et al.* (2012) 'Complex interactions between human myoblasts and the surrounding 3D fibrin-based matrix', *PLoS ONE*, 7(4), pp. 2–9. Available at: https://doi.org/10.1371/journal.pone.0036173.

Conceição, M.S. *et al.* (2018) 'Muscle Fiber Hypertrophy and Myonuclei Addition: A Systematic Review and Meta-analysis', *Medicine and Science in Sports and Exercise*, 50(7), pp. 1385–1393. Available at: https://doi.org/10.1249/MSS.0000000000001593.

Cooper, S.T. *et al.* (2004) 'C2C12 Co-culture on a fibroblast substratum enables sustained survival of contractile, highly differentiated myotubes with peripheral nuclei and adult fast myosin expression', *Cell motility and the cytoskeleton*, 58(3), pp. 200–211. Available at: https://doi.org/10.1002/cm.20010.

Costa, M.L. *et al.* (2004) 'Desmin: Molecular interactions and putative functions of the muscle intermediate filament protein', *Brazilian Journal of Medical and Biological Research*, 37(12), pp. 1819–1830. Available at: https://doi.org/10.1590/S0100-879X2004001200007.

Costantini, M., Testa, S., Fornetti, E., *et al.* (2017) 'Engineering muscle networks in 3d gelatin methacryloyl hydrogels: Influence of mechanical stiffness and geometrical confinement', *Frontiers in Bioengineering and Biotechnology*, 5(APR), pp. 1–8. Available at: https://doi.org/10.3389/fbioe.2017.00022.

Costantini, M., Testa, S., Mozetic, P., *et al.* (2017) 'Microfluidic-enhanced 3D bioprinting of aligned myoblast-laden hydrogels leads to functionally organized myofibers in vitro and in vivo', *Biomaterials*, 131, pp. 98–110. Available at: https://doi.org/10.1016/j.biomaterials.2017.03.026.

Csapo, R., Gumpenberger, M. and Wessner, B. (2020) 'Skeletal Muscle Extracellular Matrix – What Do We Know About Its Composition, Regulation, and Physiological Roles? A Narrative Review', *Frontiers in Physiology*, 11(March), pp. 1–15. Available at: https://doi.org/10.3389/fphys.2020.00253.

Cuevas-Ramos, D. *et al.* (2012) 'Exercise Increases Serum Fibroblast Growth Factor 21 (FGF21) Levels', *PloS one*, 7(5), p. e38022. Available at: https://doi.org/10.1371/journal.pone.0038022.

Cui, M. *et al.* (2024) 'Unlocking the Potential of Human-Induced Pluripotent Stem Cells: Cellular Responses and Secretome Profiles in Peptide Hydrogel 3D Culture', *Cells*, 13(2). Available at: https://doi.org/10.3390/cells13020143.

Danilov, K. *et al.* (2017) 'Electrical pulse stimulation decreases electrochemical Na+ and K+ gradients in C2C12 myotubes', *Biochemical and Biophysical Research*

Communications, 493(2), pp. 875–878. Available at: https://doi.org/10.1016/j.bbrc.2017.09.133.

Davidenko, N., Schuster, Carlos F., *et al.* (2016) 'Evaluation of cell binding to collagen and gelatin: a study of the effect of 2D and 3D architecture and surface chemistry', *Journal of Materials Science: Materials in Medicine*, 27(10), pp. 1–14. Available at: https://doi.org/10.1007/s10856-016-5763-9.

Delezie, J. and Handschin, C. (2018) 'Endocrine crosstalk between Skeletal muscle and the brain', *Frontiers in Neurology*, 9(AUG). Available at: https://doi.org/10.3389/fneur.2018.00698.

Denes, Lance T. *et al.* (2019) 'Culturing C2C12 myotubes on micromolded gelatin hydrogels accelerates myotube maturation', *Skeletal Muscle*, 9(1), pp. 1–10. Available at: https://doi.org/10.1186/s13395-019-0203-4.

Deng, H.P. *et al.* (2015) 'Insulin down-regulates the expression of ubiquitin E3 ligases partially by inhibiting the activity and expression of AMP-activated protein kinase in L6 myotubes', *Bioscience Reports*, 35(4). Available at: https://doi.org/10.1042/BSR20150017.

DeRosa, C.M. *et al.* (2022) 'Simultaneous N-Deglycosylation and Digestion of Complex Samples on S-Traps Enables Efficient Glycosite Hypothesis Generation', *ACS Omega* [Preprint]. Available at: https://doi.org/10.1021/acsomega.2c08071.

Deshmukh, Atul S. *et al.* (2015a) 'Deep proteomics of mouse skeletal muscle enables quantitation of protein isoforms, metabolic pathways, and transcription factors', *Molecular and Cellular Proteomics*, 14(4), pp. 841–853. Available at: https://doi.org/10.1074/mcp.M114.044222.

Deshmukh, Atul S, Cox, J., *et al.* (2015b) 'Secretome analysis of lipid-induced insulin resistance in skeletal muscle cells by a combined experimental and bioinformatics workflow', *Journal of Proteome Research*, 14(11), pp. 4885–4895. Available at: https://doi.org/10.1021/acs.jproteome.5b00720.

Dhindsa, S. *et al.* (2019) 'Acute effects of insulin on skeletal muscle growth and differentiation genes in men with type 2 diabetes', *European Journal of Endocrinology*, 181(6), pp. K55–K59. Available at: https://doi.org/10.1530/EJE-19-0514.

Dreher, S.I. *et al.* (2024) 'IGF1 promotes human myotube differentiation toward a mature metabolic and contractile phenotype', *American Journal of Physiology - Cell Physiology*, 326(5), pp. C1462–C1481. Available at: https://doi.org/10.1152/ajpcell.00654.2023.

Duffy, R.M., Sun, Y. and Feinberg, A.W. (2016) 'Understanding the Role of ECM Protein Composition and Geometric Micropatterning for Engineering Human Skeletal Muscle', *Annals of Biomedical Engineering*, 44(6), pp. 2076–2089. Available at: https://doi.org/10.1007/s10439-016-1592-8.

Eckel, J. (2019) 'Myokines in metabolic homeostasis and diabetes', *Diabetologia*, 62(9), pp. 1523–1528. Available at: https://doi.org/10.1007/s00125-019-4927-9.

Egan, B. and Zierath, J.R. (2013) 'Exercise metabolism and the molecular regulation of skeletal muscle adaptation', *Cell Metabolism*, pp. 162–184. Available at: https://doi.org/10.1016/j.cmet.2012.12.012.

Engler, A.J. *et al.* (2004) 'Myotubes differentiate optimally on substrates with tissue-like stiffness', *The Journal of cell biology*, 166(6), pp. 877–887. Available at: https://doi.org/10.1083/jcb.200405004.

Engler, A.J. *et al.* (2006) 'Matrix Elasticity Directs Stem Cell Lineage Specification', *Cell*, 126(4), pp. 677–689. Available at: https://doi.org/10.1016/j.cell.2006.06.044.

Esposito, G. *et al.* (2015) 'Dermcidin: A skeletal muscle myokine modulating cardiomyocyte survival and infarct size after coronary artery ligation', *Cardiovascular Research*, 107(4), pp. 431–441. Available at: https://doi.org/10.1093/cvr/cvv173.

Etienne, J. *et al.* (2020) 'Skeletal muscle as an experimental model of choice to study tissue aging and rejuvenation', *Skeletal Muscle*, 10(1), pp. 1–16. Available at: https://doi.org/10.1186/s13395-020-0222-1.

Evers-Van Gogh, Inkie J.A. *et al.* (2015) 'Electric pulse stimulation of myotubes as an in vitro exercise model: Cell-mediated and non-cell-mediated effects', *Scientific Reports*, 5. Available at: https://doi.org/10.1038/srep10944.

Faraldi, M. *et al.* (2022) 'Acute changes in free and extracellular vesicle-associated circulating miRNAs and myokine profile in professional sky-runners during the Gran Sasso d'Italia vertical run', *Frontiers in Molecular Biosciences*, 9. Available at: https://doi.org/10.3389/fmolb.2022.915080.

Farinatti, P., Castinheiras Neto, A.G. and da Silva, N.L. (2013) 'Influence of Resistance Training Variables on Excess Postexercise Oxygen Consumption: A Systematic Review', *ISRN Physiology*, 2013, pp. 1–10. Available at: https://doi.org/10.1155/2013/825026.

Farrash, W.F. *et al.* (2021) 'Myokine Responses to Exercise in a Rat Model of Low/High Adaptive Potential', *Frontiers in Endocrinology*, 12. Available at: https://doi.org/10.3389/fendo.2021.645881.

Febbraio, Mark A *et al.* (2003) 'Hepatosplanchnic clearance of interleukin-6 in humans during exercise', *Am J Physiol Endocrinol Metab*, 285, pp. 397–402. Available at: https://doi.org/10.1152/ajpendo.00134.2003.-The.

Feher, J. (2012) '3.5 - Contractile Mechanisms in Skeletal Muscle', in J. Feher (ed.) *Quantitative Human Physiology*. Elsevier Inc, pp. 249–258. Available at: https://doi.org/10.1016/B978-0-12-382163-8.00028-1.

Fischer, C.P. *et al.* (2004) 'Supplementation with vitamins C and E inhibits the release of interleukin-6 from contracting human skeletal muscle', *Journal of Physiology*, 558(2), pp. 633–645. Available at: https://doi.org/10.1113/jphysiol.2004.066779.

Fischer, C.P. (2006) *Interleukin-6 in acute exercise and training: what is the biological relevance?*, *Exerc. Immunol. Rev*.

Florin, A. *et al.* (2020) 'The secretome of skeletal muscle cells: A systematic review', *Osteoarthritis and Cartilage Open*. Elsevier Ltd. Available at: https://doi.org/10.1016/j.ocarto.2019.100019.

Foureaux, G., Mauro De Castro Pinto, K. and Dâmaso, A. (2006) *Effects of excess post-exercise oxygen consumption and resting metabolic rate in energetic cost*, *Rev Bras Med Esporte*.

Franchi, M. V, Reeves, N.D. and Narici, M. V (2017) 'Skeletal muscle remodeling in response to eccentric vs. concentric loading: Morphological, molecular, and metabolic adaptations', *Frontiers in Physiology*, 8(JUL), pp. 1–16. Available at: https://doi.org/10.3389/fphys.2017.00447.

Frontera, W.R. and Ochala, J. (2015) 'Skeletal Muscle: A Brief Review of Structure and Function', *Behavior Genetics*, 45(2), pp. 183–195. Available at: https://doi.org/10.1007/s00223-014-9915-y.

Frühbeis, C. *et al.* (2015) 'Physical exercise induces rapid release of small extracellular vesicles into the circulation', *Journal of extracellular vesicles*, 4(1), pp. 28239-n/a. Available at: https://doi.org/10.3402/jev.v4.28239.

Fujita, H. *et al.* (2010) 'Rapid decrease in active tension generated by C2C12 myotubes after termination of artificial exercise', *Journal of Muscle Research and Cell Motility*, 31(4), pp. 279–288. Available at: https://doi.org/10.1007/s10974-010-9230-9.

Fujita, H. *et al.* (2011) 'Designing of a Si-MEMS device with an integrated skeletal muscle cell-based bio-actuator', *Biomedical Microdevices*, 13(1), pp. 123–129. Available at: https://doi.org/10.1007/s10544-010-9477-3.

Fujita, H., Nedachi, T. and Kanzaki, M. (2007) 'Accelerated de novo sarcomere assembly by electric pulse stimulation in C2C12 myotubes', *Experimental Cell Research*, 313(9), pp. 1853–1865. Available at: https://doi.org/10.1016/j.yexcr.2007.03.002.

Fulghum, K. *et al.* (2022) 'Influence of biological sex and exercise on murine cardiac metabolism', *Journal of Sport and Health Science*, 11(4), pp. 479–494. Available at: https://doi.org/10.1016/j.jshs.2022.06.001.

Furuichi, Y., Manabe, Y., Takagi, M., Aoki, M. and Fujii, Nobuharu L. (2018) 'Evidence for acute contraction-induced myokine secretion by C2C12 myotubes', *PLoS ONE*, 13(10), pp. 1–15. Available at: https://doi.org/10.1371/journal.pone.0206146.

Gamas, L. *et al.* (2015) 'Irisin and Myonectin Regulation in the Insulin Resistant Muscle: Implications to Adipose Tissue: Muscle Crosstalk', *Journal of diabetes research*, 2015, pp. 359158–359159. Available at: https://doi.org/10.1155/2015/359159.

García-Lizarribar, A. *et al.* (2023) '3D bioprinted functional skeletal muscle models have potential applications for studies of muscle wasting in cancer cachexia', *Biomaterials Advances*, 150. Available at: https://doi.org/10.1016/j.bioadv.2023.213426.

Garneau, L. *et al.* (2020) 'Plasma Myokine Concentrations After Acute Exercise in Non-obese and Obese Sedentary Women', *Frontiers in Physiology*, 11. Available at: https://doi.org/10.3389/fphys.2020.00018.

Geach, T.J., Hirst, E.M.A. and Zimmerman, L.B. (2015) 'Contractile activity is required for Z-disc sarcomere maturation in vivo', *Genesis*, 53(5), pp. 299–307. Available at: https://doi.org/10.1002/dvg.22851.

Gholobova, D. *et al.* (2018) 'Human tissue-engineered skeletal muscle: a novel 3D in vitro model for drug disposition and toxicity after intramuscular injection', *Scientific Reports*, 8(1), pp. 1–14. Available at: https://doi.org/10.1038/s41598-018-30123-3.

Gholobova, D. *et al.* (2020) 'Vascularization of tissue-engineered skeletal muscle constructs', *Biomaterials*, 235(December). Available at: https://doi.org/10.1016/j.biomaterials.2019.119708.

Gilbert, P.M. *et al.* (2010) 'Substrate elasticity regulates skeletal muscle stem cell self-renewal in culture', *Science*, 329(5995), pp. 1078–1081. Available at: https://doi.org/10.1126/science.1191035.

Gillies, A. and Lieber, R. (2011) 'Structure and function of the skeletal muscle extracellular matrix', *Muscle and Nerve*, pp. 318–331. Available at: https://doi.org/10.1002/mus.22094.

Golizeh, M. *et al.* (2017) 'Increased serotransferrin and ceruloplasmin turnover in diet-controlled patients with type 2 diabetes HHS Public Access', *Radic Biol Med*, 113, pp. 461–469. Available at: https://doi.org/10.1016/j.freeradbiomed.

Gomarasca, M., Banfi, G. and Lombardi, G. (2020) *Myokines: The endocrine coupling of skeletal muscle and bone*. United States: Elsevier. Available at: https://doi.org/10.1016/bs.acc.2019.07.010.

Gonzalez, L. and Trigatti, B.L. (2017) 'Macrophage Apoptosis and Necrotic Core Development in Atherosclerosis: A Rapidly Advancing Field with Clinical Relevance to Imaging and Therapy', *Canadian journal of cardiology*, 33(3), pp. 303–312. Available at: https://doi.org/10.1016/j.cjca.2016.12.010.

Gonzalez-Franquesa, A., Stocks, B., *et al.* (2021) 'Discovery of thymosin β4 as a human exerkine and growth factor', *American Journal of Physiology: Cell Physiology*, 321(5), pp. C770–C778. Available at: https://doi.org/10.1152/ajpcell.00263.2021.

Gonzalez-Franquesa, A., Peijs, L., *et al.* (2021) 'Insulin and 5-aminoimidazole-4-carboxamide ribonucleotide (Aicar) differentially regulate the skeletal muscle cell secretome', *Proteomes*, 9(3). Available at: https://doi.org/10.3390/proteomes9030037.

Gonzalez-Gil, A.M. and Elizondo-Montemayor, L. (2020) 'The Role of Exercise in the Interplay between Myokines, Hepatokines, Osteokines, Adipokines, and Modulation of Inflammation for Energy Substrate Redistribution and Fat Mass Loss: A Review', *Nutrients*, 12(6), p. 1899. Available at: https://doi.org/10.3390/nu12061899.

Goussetis, E. *et al.* (2009) 'Spartathlon, a 246 kilometer foot race: Effects of acute inflammation induced by prolonged exercise on circulating progenitor reparative cells', *Blood Cells, Molecules, and Diseases*, 42(3), pp. 294–299. Available at: https://doi.org/10.1016/j.bcmd.2009.01.003.

Gronek, P. *et al.* (2020) 'A Review of Exercise as Medicine in Cardiovascular Disease: Pathology and Mechanism', *Aging and disease*, 11(2), pp. 327–340. Available at: https://doi.org/10.14336/AD.2019.0516.

Grube, L. *et al.* (2018) 'Mining the Secretome of C2C12 Muscle Cells: Data Dependent Experimental Approach to Analyze Protein Secretion Using Label-Free Quantification and Peptide Based Analysis', *Journal of Proteome Research*, 17(2), pp. 879–890. Available at: https://doi.org/10.1021/acs.jproteome.7b00684.

Grune, T. *et al.* (2019) 'The "MYOCYTER" – Convert cellular and cardiac contractions into numbers with ImageJ', *Scientific Reports*, 9(1). Available at: https://doi.org/10.1038/s41598-019-51676-x.

Guerrieri, D., Moon, H.Y. and van Praag, H. (2017) 'Exercise in a Pill: The Latest on Exercise-Mimetics', *Brain Plasticity*, 2(2), pp. 153–169. Available at: https://doi.org/10.3233/bpl-160043.

Gueugneau, M. *et al.* (2018) 'Increased Serpina3n release into circulation during glucocorticoid-mediated muscle atrophy', *Journal of Cachexia, Sarcopenia and Muscle*, 9(5), pp. 929–946. Available at: https://doi.org/10.1002/jcsm.12315.

Gumerson, J.D. and Michele, D.E. (2011) 'The dystrophin-glycoprotein complex in the prevention of muscle damage', *Journal of Biomedicine and Biotechnology*. Available at: https://doi.org/10.1155/2011/210797.

Gundersen, K. and Bruusgaard, J.C. (2008) 'Nuclear domains during muscle atrophy: Nuclei lost or paradigm lost?', *Journal of Physiology*, pp. 2675–2681. Available at: https://doi.org/10.1113/jphysiol.2008.154369.

Gunther, S. and Kruse, K. (2010) *Spontaneous sarcomere dynamics*. Available at: http://www.uni-saarland.de;-stefan;

Guo, X. *et al.* (2014) 'In vitro differentiation of functional human skeletal myotubes in a defined system', *Biomaterials Science*, 2(1), pp. 131–138. Available at: https://doi.org/10.1039/c3bm60166h.

Hajduchova, D. *et al.* (2023) 'Modelling Duchenne muscular dystrophy in vitro with newly generated, blood cell-derived induced pluripotent stem cell line ORIONi003-A', *Stem Cell Research*, 71. Available at: https://doi.org/10.1016/j.scr.2023.103187.

Halon-Golabek, M. *et al.* (2019) 'Iron Metabolism of the Skeletal Muscle and Neurodegeneration', *Frontiers in Neuroscience*. Frontiers Media S.A. Available at: https://doi.org/10.3389/fnins.2019.00165.

Hamill, K.J. *et al.* (2015) 'Alpha Actinin-1 Regulates Cell-Matrix Adhesion Organization in Keratinocytes: Consequences for Skin Cell Motility', *Journal of Investigative Dermatology*, 135(4), pp. 1043–1052. Available at: https://doi.org/10.1038/jid.2014.505.

Hamrick, M.W. (2012) 'The skeletal muscle secretome: an emerging player in muscle–bone crosstalk', *BoneKEy Reports*, 1(4). Available at: https://doi.org/10.1038/bonekey.2012.60.

Han, M.S. *et al.* (2020) 'Regulation of adipose tissue inflammation by interleukin 6', *Proceedings of the National Academy of Sciences of the United States of America*, 117(6), pp. 2751–2760. Available at: https://doi.org/10.1073/pnas.1920004117.

Hargreaves, M. and Spriet, L.L. (2020) 'Skeletal muscle energy metabolism during exercise', *Nature Metabolism*. Nature Research, pp. 817–828. Available at: https://doi.org/10.1038/s42255-020-0251-4.

Hartwig, S. *et al.* (2014) 'Secretome profiling of primary human skeletal muscle cells', *Biochimica et Biophysica Acta - Proteins and Proteomics*, 1844(5), pp. 1011–1017. Available at: https://doi.org/10.1016/j.bbapap.2013.08.004.

Hawley, J.A., Joyner, M.J. and Green, D.J. (2021) 'Mimicking exercise: what matters most and where to next?', in *Journal of Physiology*. Blackwell Publishing Ltd, pp. 791–802. Available at: https://doi.org/10.1113/JP278761.

Heden, T. *et al.* (2011) 'One-set resistance training elevates energy expenditure for 72 h similar to three sets', *European Journal of Applied Physiology*, 111(3), pp. 477–484. Available at: https://doi.org/10.1007/s00421-010-1666-5.

Heher, P. *et al.* (2015) 'A novel bioreactor for the generation of highly aligned 3D skeletal muscle-like constructs through orientation of fibrin via application of static strain', *Acta Biomaterialia*, 24, pp. 251–265. Available at: https://doi.org/10.1016/j.actbio.2015.06.033.

Henningsen, J. *et al.* (2010) 'Dynamics of the skeletal muscle secretome during myoblast differentiation', *Molecular and Cellular Proteomics*, 9(11), pp. 2482–2496. Available at: https://doi.org/10.1074/mcp.M110.002113.

Hernández-Hernández, J.M. *et al.* (2017) 'The myogenic regulatory factors, determinants of muscle development, cell identity and regeneration', *Seminars in Cell and Developmental Biology*. Elsevier Ltd, pp. 10–18. Available at: https://doi.org/10.1016/j.semcdb.2017.11.010.

Hesketh, S.J. (2024) 'Advancing cancer cachexia diagnosis with -omics technology and exercise as molecular medicine', *Sports Medicine and Health Science*. KeAi Communications Co., pp. 1–15. Available at: https://doi.org/10.1016/j.smhs.2024.01.006.

Hill, C. *et al.* (2021) 'Myosin-based regulation of twitch and tetanic contractions in mammalian skeletal muscle', *eLife*, 10. Available at: https://doi.org/10.7554/eLife.68211.

Hingst, J.R. *et al.* (2018) 'Exercise-induced molecular mechanisms promoting glycogen supercompensation in human skeletal muscle', *Molecular Metabolism*, 16. Available at: https://doi.org/10.1016/j.molmet.2018.07.001.

Hiscock, N. *et al.* (2004) 'Skeletal myocytes are a source of interleukin-6 mRNA expression and protein release during contraction: evidence of fiber type specificity', *The FASEB Journal*, 18(9), pp. 992–994. Available at: https://doi.org/10.1096/fj.03-1259fje.

Hojman, P. *et al.* (2019) 'IL-6 release from muscles during exercise is stimulated by lactate-dependent protease activity', *American journal of physiology. Endocrinology and metabolism*, 316(5). Available at: https://doi.org/10.1152/ajpendo.00414.2018.

Honda, M. *et al.* (2022) 'Pathophysiological levels of GDF11 activate Smad2/Smad3 signaling and induce muscle atrophy in human iPSC-derived myocytes', *American Journal of Physiology - Cell Physiology*, 323(5), pp. C1402–C1409. Available at: https://doi.org/10.1152/AJPCELL.00341.2022.

Hong, J. *et al.* (2019) 'Cell-electrospinning and its application for tissue engineering', *International Journal of Molecular Sciences*, 20(24), p. 6208. Available at: https://doi.org/10.3390/ijms20246208.

Hoshiba, T. and Yamaoka, T. (2019) 'CHAPTER 1. Extracellular Matrix Scaffolds for Tissue Engineering and Biological Research', *Decellularized Extracellular Matrix*. Royal Society of Chemistry, p. 1. Available at: https://doi.org/10.1039/9781788015998-00001.

Hsu, C.P. *et al.* (2018) 'Sarcomeric and non-muscle α-actinin isoforms exhibit differential dynamics at skeletal muscle Z-lines', *Physiology & behavior*, 75(5), pp. 213–228. Available at: https://doi.org/10.1002/cm.21442.

Huang, G., Xu, F. and Zhang, W. (2020) 'Engineering Biomaterials and Approaches for Mechanical Stretching of Cells in Three Dimensions', *Frontiers in bioengineering and biotechnology*, 8, p. 589590. Available at: https://doi.org/10.3389/fbioe.2020.589590.

Huang, Ngan F. *et al.* (2006) 'Myotube assembly on nanofibrous and micropatterned polymers', *Nano Letters*, 6(3), pp. 537–542. Available at: https://doi.org/10.1021/nl060060o.

Huang, Y.-C.C. *et al.* (2005) 'Rapid formation of functional muscle in vitro using fibrin gels', *Journal of Applied Physiology*, 98(2), pp. 706–713. Available at: https://doi.org/10.1152/japplphysiol.00273.2004.

Huh, J.Y. (2018) 'The role of exercise-induced myokines in regulating metabolism', *Archives of Pharmacal Research*. Available at: https://doi.org/10.1007/s12272-017-0994-y.

Hurd, S.A. *et al.* (2015) 'Development of a biological scaffold engineered using the extracellular matrix secreted by skeletal muscle cells', *Biomaterials*, 49, pp. 9–17. Available at: https://doi.org/10.1016/j.biomaterials.2015.01.027.

Husmann, I. *et al.* (1996) *MINI REVIEW Growth Factors in Skeletal Muscle Regeneration*, *ytokine & Growth Factor Review~*.

Ikeda, K., Ito, A., Sato, M., *et al.* (2017) 'Effects of heat stimulation and l-ascorbic acid 2-phosphate supplementation on myogenic differentiation of artificial skeletal muscle tissue constructs', *Journal of Tissue Engineering and Regenerative Medicine*, 11(5), pp. 1322–1331. Available at: https://doi.org/10.1002/term.2030.

Ikeda, K., Ito, A., Imada, R., *et al.* (2017b) 'In vitro drug testing based on contractile activity of C2C12 cells in an epigenetic drug model', *Scientific Reports*, 7. Available at: https://doi.org/10.1038/srep44570.

Işin, S. *et al.* (2023) 'Effect of ascorbic acid on collagen and some inflammatory mediators in rats', *Ankara Universitesi Veteriner Fakultesi Dergisi*, 70(3), pp. 303–308. Available at: https://doi.org/10.33988/auvfd.1019201.

Ito, A. *et al.* (2014) 'Induction of functional tissue-engineered skeletal muscle constructs by defined electrical stimulation', *Scientific Reports*, 4. Available at: https://doi.org/10.1038/srep04781.

Jana, S., Levengood, S.K.L. and Zhang, M. (2016) 'Anisotropic Materials for Skeletal-Muscle-Tissue Engineering', *Advanced materials (Weinheim)*, 28(48), pp. 10588–10612. Available at: https://doi.org/10.1002/adma.201600240.

Jang, M. *et al.* (2022) 'Serum-free cultures of C2C12 cells show different muscle phenotypes which can be estimated by metabolic profiling', *Scientific Reports*, 12(1). Available at: https://doi.org/10.1038/s41598-022-04804-z.

Jedrychowski, M.P. *et al.* (2015) 'Detection and Quantitation of Circulating Human Irisin by Tandem Mass Spectrometry', *Cell metabolism*, 22(4), pp. 734–740. Available at: https://doi.org/10.1016/j.cmet.2015.08.001.

Jensen, J.H. *et al.* (2020) 'Large-scale spontaneous self-organization and maturation of skeletal muscle tissues on ultra-compliant gelatin hydrogel substrates', *Scientific Reports*, 10(1), pp. 1–10. Available at: https://doi.org/10.1038/s41598-020-69936-6.

Ji, M., Cho, C. and Lee, S. (2024) 'Acute effect of exercise intensity on circulating FGF-21, FSTL-1, cathepsin B, and BDNF in young men', *Journal of Exercise Science and Fitness*, 22(1), pp. 51–58. Available at: https://doi.org/10.1016/j.jesf.2023.11.002.

Jia, T. *et al.* (2021) 'FGF-2 promotes angiogenesis through a SRSF1/SRSF3/SRPK1-dependent axis that controls VEGFR1 splicing in endothelial cells', *BMC Biology*, 19(1). Available at: https://doi.org/10.1186/s12915-021-01103-3.

Jiao, A. *et al.* (2018) 'Regulation of skeletal myotube formation and alignment by nanotopographically controlled cell-secreted extracellular matrix', *Journal of Biomedical Materials Research - Part A*, 106(6), pp. 1543–1551. Available at: https://doi.org/10.1002/jbm.a.36351.

Jin, L. *et al.* (2023) 'The muscle-enriched myokine Musclin impairs beige fat thermogenesis and systemic energy homeostasis via Tfr1/PKA signaling in male mice', *Nature Communications*, 14(1). Available at: https://doi.org/10.1038/s41467-023-39710-z.

Jin, L., Lin, Z. and Xu, A. (2016) 'Fibroblast Growth Factor 21 Protects against Atherosclerosis via Fine-Tuning the Multiorgan Crosstalk', *Diabetes & metabolism journal*, 40(1), pp. 22–31. Available at: https://doi.org/10.4093/dmj.2016.40.1.22.

Johann, K., Kleinert, M. and Klaus, S. (2021) 'The role of gdf15 as a myomitokine', *Cells*. MDPI. Available at: https://doi.org/10.3390/cells10112990.

Jones, J.M. *et al.* (2018) 'An Assessment of Myotube Morphology, Matrix Deformation, and Myogenic mRNA Expression in Custom-Built and Commercially Available Engineered Muscle Chamber Configurations', *Frontiers in Physiology*. Frontiers Media SA. Available at: https://doi.org/10.3389/fphys.2018.00483.

Kanzleiter, T. *et al.* (2014) 'The myokine decorin is regulated by contraction and involved in muscle hypertrophy', *Biochemical and Biophysical Research Communications*, 450(2), pp. 1089–1094. Available at: https://doi.org/10.1016/j.bbrc.2014.06.123.

Kawakami, Y. *et al.* (2006) 'Human skeletal muscle size and architecture: Variability and interdependence', *American journal of human biology*, 18(6), pp. 845–848. Available at: https://doi.org/10.1002/ajhb.20561.

Keipert, S. *et al.* (2014) 'First published Decem-ber 17', *Am J Physiol Endocrinol Metab*, 306, pp. 469–482. Available at: https://doi.org/10.1152/ajpendo.00330.2013.-UCP1-Tg.

Keller, C. *et al.* (2006) 'Differential regulation of IL-6 and TNF-α via calcineurin in human skeletal muscle cells', *Cytokine*, 36(3–4), pp. 141–147. Available at: https://doi.org/10.1016/j.cyto.2006.10.014.

Khodabukus, A. *et al.* (2018) 'In Vitro Tissue-Engineered Skeletal Muscle Models for Studying Muscle Physiology and Disease', *Advanced Healthcare Materials*. Available at: https://doi.org/10.1002/adhm.201701498.

Khodabukus, A., Madden, L., Prabhu, Neel K, *et al.* (2019) 'Electrical stimulation increases hypertrophy and metabolic flux in tissue-engineered human skeletal muscle',

Biomaterials, 198(July), pp. 259–269. Available at: https://doi.org/10.1016/j.biomaterials.2018.08.058.

Kim, C.S. *et al.* (2019) 'Deficiency of fibroblast growth factor 21 aggravates obesity-induced atrophic responses in skeletal muscle', *Journal of Inflammation (United Kingdom)*, 16(1). Available at: https://doi.org/10.1186/s12950-019-0221-3.

Kim, H., Kim, M.C. and Asada, H.H. (2019) 'Extracellular matrix remodelling induced by alternating electrical and mechanical stimulations increases the contraction of engineered skeletal muscle tissues', *Scientific Reports*, 9(1). Available at: https://doi.org/10.1038/s41598-019-39522-6.

Kim, J.H. *et al.* (2018) '3D Bioprinted Human Skeletal Muscle Constructs for Muscle Function Restoration', *Scientific Reports*. Springer Science and Business Media LLC. Available at: https://doi.org/10.1038/s41598-018-29968-5.

Kim, J.H. *et al.* (2020) 'Neural cell integration into 3D bioprinted skeletal muscle constructs accelerates restoration of muscle function', *Nature communications*, 11(1), p. 1025. Available at: https://doi.org/10.1038/s41467-020-14930-9.

Kim, K.H. *et al.* (2013) 'Autophagy deficiency leads to protection from obesity and insulin resistance by inducing Fgf21 as a mitokine', *Nature Medicine*, 19(1), pp. 83–92. Available at: https://doi.org/10.1038/nm.3014.

King, W. and Kissel, J. (2013) 'Multidisciplinary approach to the management of myopathies', *CONTINUUM Lifelong Learning in Neurology*, 19(6), pp. 1650–1673. Available at: https://doi.org/10.1212/01.CON.0000440664.34051.4d.

Kinney, M.C. *et al.* (2017) 'Reduced skeletal muscle satellite cell number alters muscle morphology after chronic stretch but allows limited serial sarcomere addition', *Muscle and Nerve*, 55(3), pp. 384–392. Available at: https://doi.org/10.1002/mus.25227.

Kitakaze, T. *et al.* (2016) 'The collagen derived dipeptide hydroxyprolyl-glycine promotes C2C12 myoblast differentiation and myotube hypertrophy', *Biochemical and Biophysical Research Communications*, 478(3), pp. 1292–1297. Available at: https://doi.org/10.1016/j.bbrc.2016.08.114.

Knab, A.M. *et al.* (2011) 'A 45-minute vigorous exercise bout increases metabolic rate for 14 hours.', *Medicine and science in sports and exercise*, 43(9), pp. 1643–1648. Available at: https://doi.org/10.1249/mss.0b013e3182118891.

Kocoloski, G. and Crecelius, A.R. (2014) *Alterations and Specifications of Excess Post-Exercise Oxygen Consumption: A Review*. Available at:

http://ecommons.udayton.edu/hss_fac_pubhttp://ecommons.udayton.edu/hss_fac_pub/57.

Kokubu, Y. *et al.* (2019) 'Phenotypic Drug Screening for Dysferlinopathy Using Patient-Derived Induced Pluripotent Stem Cells', *Stem Cells Translational Medicine*, 8(10), pp. 1017–1029. Available at: https://doi.org/10.1002/sctm.18-0280.

Komori, T. and Morikawa, Y. (2022) 'Essential roles of the cytokine oncostatin M in crosstalk between muscle fibers and immune cells in skeletal muscle after aerobic exercise', *Journal of Biological Chemistry*, 298(12). Available at: https://doi.org/10.1016/j.jbc.2022.102686.

Kondash, M.E. *et al.* (2020) 'Glucose Uptake and Insulin Response in Tissue-engineered Human Skeletal Muscle', *Tissue Engineering and Regenerative Medicine*, 17(6), pp. 801–813. Available at: https://doi.org/10.1007/s13770-020-00242-y.

Kono, F. *et al.* (2020) 'Nanoscopic changes in the lattice structure of striated muscle sarcomeres involved in the mechanism of spontaneous oscillatory contraction (SPOC)', *Scientific Reports*, 10(1). Available at: https://doi.org/10.1038/s41598-020-73247-1.

Krieger, J. *et al.* (2018) '3D skeletal muscle fascicle engineering is improved with TGF-β1 treatment of myogenic cells and their co-culture with myofibroblasts', *PeerJ*, 2018(7), pp. 1–24. Available at: https://doi.org/10.7717/peerj.4939.

Lacombe, J., Armstrong, M.E.G., *et al.* (2019) 'The impact of physical activity and an additional behavioural risk factor on cardiovascular disease, cancer and all-cause mortality: A systematic review', *BMC Public Health*, 19(1). Available at: https://doi.org/10.1186/s12889-019-7030-8.

Lambernd, S. *et al.* (2012) 'Contractile activity of human skeletal muscle cells prevents insulin resistance by inhibiting pro-inflammatory signalling pathways', *Diabetologia*, 55(4), pp. 1128–1139. Available at: https://doi.org/10.1007/s00125-012-2454-z.

Langelaan, M.L.P. *et al.* (2011) 'Advanced maturation by electrical stimulation: Differences in response between C2C12 and primary muscle progenitor cells', *Journal of Tissue Engineering and Regenerative Medicine*, 5(7), pp. 529–539. Available at: https://doi.org/10.1002/term.345.

Laurens, C. *et al.* (2020) 'Growth and differentiation factor 15 is secreted by skeletal muscle during exercise and promotes lipolysis in humans', *JCI insight*, 5(6), pp. 1–14. Available at: https://doi.org/10.1172/jci.insight.131870.

Lauritzen, H.P.M.M. *et al.* (2013) 'Contraction and AICAR stimulate IL-6 vesicle depletion from skeletal muscle fibers in vivo', *Diabetes*, 62(9), pp. 3081–3092. Available at: https://doi.org/10.2337/db12-1261.

Leal, Luana G, Lopes, M.A. and Batista, M.L. (2018) 'Physical exercise-induced myokines and muscle-adipose tissue crosstalk: A review of current knowledge and the implications for health and metabolic diseases', *Frontiers in Physiology*, 9(SEP), pp. 1–17. Available at: https://doi.org/10.3389/fphys.2018.01307.

Lee, I.H. *et al.* (2018) 'Study of muscle contraction induced by electrical pulse stimulation and nitric oxide in C2C12 myotube cells', *Journal of exercise nutrition & biochemistry*, 22(1), pp. 22–28. Available at: https://doi.org/10.20463/jenb.2018.0004.

Lee, J.H. and Jun, H.S. (2019) 'Role of myokines in regulating skeletal muscle mass and function', *Frontiers in Physiology*, 10(JAN), pp. 1–9. Available at: https://doi.org/10.3389/fphys.2019.00042.

Lee, L.A. *et al.* (2019) 'The ancient sarcomeric myosins found in specialized muscles', *Skeletal Muscle*, 9(1), pp. 1–15. Available at: https://doi.org/10.1186/s13395-019-0192-3.

Lee, W. *et al.* (2018) 'BAIBA Attenuates the Expression of Inflammatory Cytokines and Attachment Molecules and ER Stress in HUVECs and THP-1 Cells', *Pathobiology*, 85(5–6), pp. 280–288. Available at: https://doi.org/10.1159/000490497.

Legård, G.E. and Pedersen, B.K. (2019) 'Muscle as an Endocrine Organ', in *Muscle and Exercise Physiology*. Available at: https://doi.org/10.1016/b978-0-12-814593-7.00013-x.

Lehman, W. *et al.* (2009) 'Structural Basis for the Activation of Muscle Contraction by Troponin and Tropomyosin', *Journal of Molecular Biology*, 388(4), pp. 673–681. Available at: https://doi.org/10.1016/j.jmb.2009.03.060.

Li, G. *et al.* (2020) 'Follistatin like protein-1 modulates macrophage polarization and aggravates dextran sodium sulfate-induced colitis', *International Immunopharmacology*, 83. Available at: https://doi.org/10.1016/j.intimp.2020.106456.

Li, J. *et al.* (2020) 'Transferrin Receptor 1 Regulates Thermogenic Capacity and Cell Fate in Brown/Beige Adipocytes', *Advanced Science*, 7(12). Available at: https://doi.org/10.1002/advs.201903366.

Li, L. *et al.* (2023) 'Advances in research on cell models for skeletal muscle atrophy', *Biomedicine and Pharmacotherapy*. Elsevier Masson s.r.l. Available at: https://doi.org/10.1016/j.biopha.2023.115517.

Li, Y. *et al.* (2016) 'Magnetically actuated cell-laden microscale hydrogels for probing strain-induced cell responses in three dimensions', *NPG Asia Materials*, 8(1). Available at: https://doi.org/10.1038/am.2015.148.

Lieber, R.L. and Ward, S.R. (2011) 'Skeletal muscle design to meet functional demands', *Philosophical Transactions of the Royal Society B: Biological Sciences*, 366(1570), pp. 1466–1476. Available at: https://doi.org/10.1098/rstb.2010.0316.

Lin, Z. *et al.* (2015) 'Fibroblast growth factor 21 prevents atherosclerosis by suppression of hepatic sterol regulatory element-binding protein-2 and induction of adiponectin in mice', *Circulation*, 131(21), pp. 1861–1871. Available at: https://doi.org/10.1161/CIRCULATIONAHA.115.015308.

Lindegaard, B. *et al.* (2013) 'Expression of Fibroblast Growth Factor-21 in Muscle Is Associated with Lipodystrophy, Insulin Resistance and Lipid Disturbances in Patients with HIV', *PLoS ONE*, 8(3). Available at: https://doi.org/10.1371/journal.pone.0055632.

Little, H.C. *et al.* (2018) 'Multiplex quantification identifies novel exercise-regulated myokines/cytokines in plasma and in glycolytic and oxidative skeletal muscle', *Molecular and Cellular Proteomics*, 17(8), pp. 1546–1563. Available at: https://doi.org/10.1074/mcp.RA118.000794.

Liu, J. *et al.* (2018) 'Current Methods for Skeletal Muscle Tissue Repair and Regeneration', *BioMed Research International*, 2018(10), pp. 146–155. Available at: https://doi.org/10.1155/2018/1984879.

Liu, X. *et al.* (2020) 'Type i collagen promotes the migration and myogenic differentiation of C2C12 myoblasts: Via the release of interleukin-6 mediated by FAK/NF-κB p65 activation', in *Food and Function*. Royal Society of Chemistry, pp. 328–338. Available at: https://doi.org/10.1039/c9fo01346f.

Liu, X. *et al.* (2023) 'Fndc5/irisin deficiency leads to dysbiosis of gut microbiota contributing to the depressive-like behaviors in mice', *Brain Research*, 1819. Available at: https://doi.org/10.1016/j.brainres.2023.148537.

López, S.M. *et al.* (2020) 'Creation and characterization of an immortalized canine myoblast cell line: Myok9', *Mammalian Genome*, 31(3–4), pp. 95–109. Available at: https://doi.org/10.1007/s00335-020-09833-5.

Loreti, M. and Sacco, A. (2022) 'The jam session between muscle stem cells and the extracellular matrix in the tissue microenvironment', *npj Regenerative Medicine*. Nature Research. Available at: https://doi.org/10.1038/s41536-022-00204-z.

Louis, E. *et al.* (2007) 'Time course of proteolytic, cytokine, and myostatin gene expression after acute exercise in human skeletal muscle', *Journal of Applied Physiology*, 103(5), pp. 1744–1751. Available at: https://doi.org/10.1152/japplphysiol.00679.2007.

Lovering, R.M. *et al.* (2011) 'Physiology, structure, and susceptibility to injury of skeletal muscle in mice lacking keratin 19-based and desmin-based intermediate filaments', *American Journal of Physiology - Cell Physiology*, 300(4), pp. 803–813. Available at: https://doi.org/10.1152/ajpcell.00394.2010.

Luan, X. *et al.* (2019) 'Exercise as a prescription for patients with various diseases', *Journal of sport and health science*, 8(5), pp. 422–441. Available at: https://doi.org/10.1016/j.jshs.2019.04.002.

Lundsgaard, A.-M. and Kiens, B. (2014) 'Gender Differences in Skeletal Muscle Substrate Metabolism - Molecular Mechanisms and Insulin Sensitivity', *Frontiers in endocrinology (Lausanne)*, 5, p. 195. Available at: https://doi.org/10.3389/fendo.2014.00195.

Madden, L., Juhas, M., Kraus, William E., *et al.* (2015) 'Bioengineered human myobundles mimic clinical responses of skeletal muscle to drugs', *eLife*, 2015(4), pp. 1–14. Available at: https://doi.org/10.7554/eLife.04885.

Maffioletti, S. *et al.* (2018) 'Three-Dimensional Human iPSC-Derived Artificial Skeletal Muscles Model Muscular Dystrophies and Enable Multilineage Tissue Engineering', *Cell Reports*, 23(3), pp. 899–908. Available at: https://doi.org/10.1016/j.celrep.2018.03.091.

Magliulo, L. *et al.* (2021) 'The wonder exerkines-novel insights: a critical state-of-the-art review', *Molecular and Cellular Biochemistry* [Preprint]. Available at: https://doi.org/10.1007/s11010-021-04264-5.

Maleiner, B. *et al.* (2018) 'The importance of biophysical and biochemical stimuli in dynamic skeletal muscle models', *Frontiers in Physiology*. Frontiers Media S.A. Available at: https://doi.org/10.3389/fphys.2018.01130.

Manabe, Y. *et al.* (2012) 'Characterization of an Acute Muscle Contraction Model Using Cultured C2C12 Myotubes', *PLoS ONE*, 7(12), p. e52592. Available at: https://doi.org/10.1371/journal.pone.0052592.

Manabe, Y. *et al.* (2014) 'Redox proteins are constitutively secreted by skeletal muscle', *Journal of Physiological Sciences*, 64(6), pp. 401–409. Available at: https://doi.org/10.1007/s12576-014-0334-7.

Manabe, Y. *et al.* (2016) 'Evaluation of an in vitro muscle contraction model in mouse primary cultured myotubes', *Analytical Biochemistry*, 497, pp. 36–38. Available at: https://doi.org/10.1016/j.ab.2015.10.010.

Manabe, Y., Miyatake, S. and Takagi, M. (2012) *Myokines: Do they really exist?*, *J Phys Fitness Sports Med*.

Mao, W. *et al.* (2019) 'Electrospun nanohybrid hydrogels for enhanced differentiation of myoblasts', *Journal of Industrial and Engineering Chemistry*, 80, pp. 838–845. Available at: https://doi.org/10.1016/j.jiec.2019.07.012.

Marotta, M., Bragós, R. and Gómez-Foix, A.M. (2004) 'Design and performance of an electrical stimulator for long-term contraction of cultured muscle cells', *BioTechniques*, 36(1), pp. 68–73. Available at: https://doi.org/10.2144/04361ST01.

Marshall, C.J. (1995) *Specificity of Receptor Tyrosine Kinase Signaling: Transient versus Sustained Extracellular Signal-Regulated Kinase Activation Review*, *Cell*.

Martin, N.R.W. *et al.* (2015) 'Neuromuscular Junction Formation in Tissue-Engineered Skeletal Muscle Augments Contractile Function and Improves Cytoskeletal Organization', *Tissue Engineering Part A*. Mary Ann Liebert Inc, p. 2595. Available at: https://doi.org/10.1089/ten.tea.2015.0146.

Masi, A.T. and Hannon, J.C. (2008) 'Human resting muscle tone (HRMT): Narrative introduction and modern concepts', *Journal of Bodywork and Movement Therapies*, 12(4), pp. 320–332. Available at: https://doi.org/10.1016/j.jbmt.2008.05.007.

Masuda, S. *et al.* (2018) 'Chemokine (C-X-C motif) ligand 1 is a myokine induced by palmitate and is required for myogenesis in mouse satellite cells', *Acta Physiologica*, 222(3). Available at: https://doi.org/10.1111/apha.12975.

Matthews, V.B. *et al.* (2009) 'Brain-derived neurotrophic factor is produced by skeletal muscle cells in response to contraction and enhances fat oxidation via activation of AMP-activated protein kinase', *Diabetologia*, 52(7), pp. 1409–1418. Available at: https://doi.org/10.1007/s00125-009-1364-1.

Mayeuf-Louchart, A. *et al.* (2018) 'MuscleJ: A high-content analysis method to study skeletal muscle with a new Fiji tool', *Skeletal Muscle*, 8(1). Available at: https://doi.org/10.1186/s13395-018-0171-0.

Medler, S. (2019) 'Mixing it up: The biological significance of hybrid skeletal muscle fibers', *Journal of Experimental Biology*. Company of Biologists Ltd, p. 1OBITUARY. Available at: https://doi.org/10.1242/jeb.200832.

Melanson, E.L. *et al.* (2002) 'Effect of exercise intensity on 24-h energy expenditure and nutrient oxidation', *J Appl Physiol*, 92, pp. 1045–1052. Available at: https://doi.org/10.1152/japplphysiol.00706.2001.-The.

Mendias, C.L. *et al.* (2012) 'Transforming growth factor-beta induces skeletal muscle atrophy and fibrosis through the induction of atrogin-1 and scleraxis', *Muscle and Nerve*, 45(1), pp. 55–59. Available at: https://doi.org/10.1002/mus.22232.

Mengeste, A.M. *et al.* (2022) 'Insight Into the Metabolic Adaptations of Electrically Pulse-Stimulated Human Myotubes Using Global Analysis of the Transcriptome and Proteome', *Frontiers in Physiology*, 13. Available at: https://doi.org/10.3389/fphys.2022.928195.

Merceron, T.K. *et al.* (2015) 'A 3D bioprinted complex structure for engineering the muscle–tendon unit', *Biofabrication*. IOP Publishing. Available at: https://doi.org/10.1088/1758-5090/7/3/035003.

Mertens, J. *et al.* (2014) 'Engineering muscle constructs for the creation of functional engineered musculoskeletal tissue', *Regen Med*, 9(1), pp. 89–100. Available at: https://doi.org/10.2217/rme.13.81.

Meyer, G.A. and Lieber, R.L. (2011) 'Elucidation of extracellular matrix mechanics from muscle fibers and fiber bundles', *Journal of Biomechanics*, 44(4), pp. 771–773. Available at: https://doi.org/10.1016/j.jbiomech.2010.10.044.

Mijailovich, S.M. *et al.* (2019) 'Nebulin and titin modulate cross-bridge cycling and length-dependent calcium sensitivity', *Journal of General Physiology*, 151(5), pp. 680–704. Available at: https://doi.org/10.1085/jgp.201812165.

Militello, R. *et al.* (2022) 'Modulation of Plasma Proteomic Profile by Regular Training in Male and Female Basketball Players: A Preliminary Study', *Frontiers in Physiology*, 13. Available at: https://doi.org/10.3389/fphys.2022.813447.

Mills, Richard J. *et al.* (2019) 'Development of a human skeletal micro muscle platform with pacing capabilities', *Biomaterials*, 198(September), pp. 217–227. Available at: https://doi.org/10.1016/j.biomaterials.2018.11.030.

Mittenbühler, M.J. *et al.* (2023) 'Isolation of extracellular fluids reveals novel secreted bioactive proteins from muscle and fat tissues', *Cell Metabolism*, 35(3), pp. 535-549.e7. Available at: https://doi.org/10.1016/j.cmet.2022.12.014.

Molfino, A. *et al.* (2019) 'Longitudinal physical activity change during hemodialysis and its association with body composition and plasma BAIBA levels', *Frontiers in Physiology*, 10(JUN). Available at: https://doi.org/10.3389/fphys.2019.00805.

Mondrinos, M.J. *et al.* (2021) 'Surface-directed engineering of tissue anisotropy in microphysiological models of musculoskeletal tissue', *Science Advances*. American Association for the Advancement of Science (AAAS). Available at: https://doi.org/10.1126/sciadv.abe9446.

Moo, E.K. and Herzog, W. (2018) 'Single sarcomere contraction dynamics in a whole muscle', *Scientific Reports*, 8(1). Available at: https://doi.org/10.1038/s41598-018-33658-7.

Moon, H.Y. *et al.* (2016) 'Running-Induced Systemic Cathepsin B Secretion Is Associated with Memory Function', *Cell Metabolism*, 24(2), pp. 332–340. Available at: https://doi.org/10.1016/j.cmet.2016.05.025.

Moon, H.Y. *et al.* (2019) 'Conditioned media from AICAR-treated skeletal muscle cells increases neuronal differentiation of adult neural progenitor cells', *Neuropharmacology*, 145, pp. 123–130. Available at: https://doi.org/10.1016/j.neuropharm.2018.10.041.

Moore, D.R. *et al.* (2011) 'Resistance exercise enhances mTOR and MAPK signalling in human muscle over that seen at rest after bolus protein ingestion', *Acta Physiologica*, 201(3), pp. 365–372. Available at: https://doi.org/10.1111/j.1748-1716.2010.02187.x.

Mori, Shuuichi *et al.* (2023) 'Proteolytic ectodomain shedding of muscle-specific tyrosine kinase in myasthenia gravis', *Experimental Neurology*, 361. Available at: https://doi.org/10.1016/j.expneurol.2022.114300.

Morifuji, M. *et al.* (2010) 'Post-exercise carbohydrate plus whey protein hydrolysates supplementation increases skeletal muscle glycogen level in rats', *Amino Acids*, 38(4), pp. 1109–1115. Available at: https://doi.org/10.1007/s00726-009-0321-0.

Morimoto, Y., Onoe, H. and Takeuchi, S. (2020) 'Biohybrid robot with skeletal muscle tissue covered with a collagen structure for moving in air', *APL Bioengineering*. AIP Publishing. Available at: https://doi.org/10.1063/1.5127204.

Mudera, V. *et al.* (2010) 'The effect of cell density on the maturation and contractile ability of muscle derived cells in a 3D tissue-engineered skeletal muscle model and determination of the cellular and mechanical stimuli required for the synthesis of a postural phenotype', *Journal of Cellular Physiology*, 225(3), pp. 646–653. Available at: https://doi.org/10.1002/jcp.22271.

Mueller, C. *et al.* (2021) 'Effects of External Stimulators on Engineered Skeletal Muscle Tissue Maturation', *Advanced Materials Interfaces*. Wiley-VCH Verlag. Available at: https://doi.org/10.1002/admi.202001167.

Mukund, K and Subramaniam, S. (2020) ‘Skeletal muscle: A review of molecular structure and function, in health and disease’, *Wiley interdisciplinary reviews.Systems biology and medicine*, 12(1), p. e1462. Available at: https://doi.org/10.1002/wsbm.1462 [doi].

Mummery, C.L. *et al.* (2017) ‘New Methods in Cardiovascular Biology MUSCLEMOTION A Versatile Open Software Tool to Quantify Cardiomyocyte and Cardiac Muscle Contraction In Vitro and In Vivo’. Available at: https://doi.org/10.1161/CIRCRESAHA.

Muñoz-Cánoves, P. *et al.* (2013) ‘Interleukin-6 myokine signaling in skeletal muscle: A double-edged sword?’, *FEBS Journal*, pp. 4131–4148. Available at: https://doi.org/10.1111/febs.12338.

Murphy, A.C.H. and Young, P.W. (2015) ‘The actinin family of actin cross-linking proteins – a genetic perspective’, *Cell & bioscience*, 5(1), p. 49. Available at: https://doi.org/10.1186/s13578-015-0029-7.

Murphy, M.M. *et al.* (2011) ‘Satellite cells, connective tissue fibroblasts and their interactions are crucial for muscle regeneration’, *Development*, 138(17), pp. 3625–3637. Available at: https://doi.org/10.1242/dev.064162.

Nagamine, K. *et al.* (2018) ‘Contractile Skeletal Muscle Cells Cultured with a Conducting Soft Wire for Effective, Selective Stimulation’, *Scientific Reports*, 8(1). Available at: https://doi.org/10.1038/s41598-018-20729-y.

Nakamura, T. *et al.* (2017) ‘Development and evaluation of a removable tissue-engineered muscle with artificial tendons’, *Journal of Bioscience and Bioengineering*, 123(2), pp. 265–271. Available at: https://doi.org/10.1016/j.jbiosc.2016.08.003.

Nam, J.S. *et al.* (2024) ‘Follistatin-like 1 is a myokine regulating lipid mobilization during endurance exercise and recovery’, *Obesity*, 32(2), pp. 352–362. Available at: https://doi.org/10.1002/oby.23949.

Namakanova, O.A. *et al.* (2022) ‘Therapeutic Potential of Combining IL-6 and TNF Blockade in a Mouse Model of Allergic Asthma’, *International Journal of Molecular Sciences*, 23(7). Available at: https://doi.org/10.3390/ijms23073521.

Nedachi, T., Fujita, H. and Kanzaki, M. (2008) ‘Contractile C2C12 myotube model for studying exercise-inducible responses in skeletal muscle’, *American Journal of Physiology - Endocrinology and Metabolism*, 295(5). Available at: https://doi.org/10.1152/ajpendo.90280.2008.

Negrini, K.A. *et al.* (2024) ‘Role of Oncostatin M in Exercise-Induced Breast Cancer Prevention’, *Cancers*, 16(15). Available at: https://doi.org/10.3390/cancers16152716.

Nelson, S.R. *et al.* (2020) 'Imaging ATP Consumption in Resting Skeletal Muscle: One Molecule at a Time', *Biophysical Journal*, 119(6), pp. 1050–1055. Available at: https://doi.org/10.1016/j.bpj.2020.07.036.

Neunhäuserer, D. *et al.* (2011) 'Human skeletal muscle: transition between fast and slow fibre types', *Pflügers Archiv*, 461(5), pp. 537–543. Available at: https://doi.org/10.1007/s00424-011-0943-4.

Nguyen, J. *et al.* (2024) 'Culture substrate stiffness impacts human myoblast contractilitydependent proliferation and nuclear envelope wrinkling', *Journal of Cell Science*, 137(6). Available at: https://doi.org/10.1242/jcs.261666.

Nichol, J.W. *et al.* (2010) 'Cell-laden microengineered gelatin methacrylate hydrogels', *Biomaterials*, 31(21), pp. 5536–5544. Available at: https://doi.org/10.1016/j.biomaterials.2010.03.064.

Nie, Y. and Liu, D. (2017) 'N-Glycosylation is required for FDNC5 stabilization and irisin secretion', *Biochemical Journal*, 474(18), pp. 3167–3177. Available at: https://doi.org/10.1042/BCJ20170241.

Nielsen, S. and Pedersen, B.K. (2008) 'Skeletal muscle as an immunogenic organ', *Current Opinion in Pharmacology*, pp. 346–351. Available at: https://doi.org/10.1016/j.coph.2008.02.005.

Nieuwoudt, S., Mulya, A., Fealy, Ciarán E., *et al.* (2017) 'In vitro contraction protects against palmitate-induced insulin resistance in C2C12 myotubes', *American Journal of Physiology - Cell Physiology*, 313(5), pp. C575–C583. Available at: https://doi.org/10.1152/ajpcell.00123.2017.

Nikolić, N., Skaret Bakke, S., Tranheim Kase, E., Rudberg, I., Flo Halle, I., Rustan, Arild C, *et al.* (2012) 'Electrical pulse stimulation of cultured human skeletal muscle cells as an in vitro model of exercise', *PLoS ONE*, 7(3), p. e33203. Available at: https://doi.org/10.1371/journal.pone.0033203.

Nikolić, N. *et al.* (2017) 'Electrical pulse stimulation of cultured skeletal muscle cells as a model for in vitro exercise – possibilities and limitations', *Acta Physiologica*. Blackwell Publishing Ltd, pp. 310–331. Available at: https://doi.org/10.1111/apha.12830.

Nikolić, N. and Aas, V. (2019) 'Electrical pulse stimulation of primary human skeletal muscle cells', in *Methods in Molecular Biology*. Humana Press Inc., pp. 17–24. Available at: https://doi.org/10.1007/978-1-4939-8897-6_2.

Nishii, K., Aizu, N. and Yamada, K. (2023) 'Review of the health-promoting effects of exercise and the involvement of myokines', *Fujita Medical Journal*. Fujita Medical Society, pp. 171–178. Available at: https://doi.org/10.20407/fmj.2022-020.

Niu, W. *et al.* (2010) 'Contraction-related stimuli regulate GLUT4 traffic in C 2 C 12-GLUT4myc skeletal muscle cells', *Am J Physiol Endocrinol Metab*, 298, pp. 1058–1071. Available at: https://doi.org/10.1152/ajpendo.00773.2009.-Muscle.

Norheim, F. *et al.* (2011) 'Proteomic identification of secreted proteins from human skeletal muscle cells and expression in response to strength training'. Available at: https://doi.org/10.1152/ajpendo.00326.2011.-Regu.

Norheim, F. *et al.* (2014) 'The effects of acute and chronic exercise on PGC-1α, irisin and browning of subcutaneous adipose tissue in humans', *The FEBS journal*, 281(3), pp. 739–749. Available at: https://doi.org/10.1111/febs.12619.

Ojima, K. *et al.* (2014) 'Proteomic analysis of secreted proteins from skeletal muscle cells during differentiation', *EuPA Open Proteomics*, 5, pp. 1–9. Available at: https://doi.org/10.1016/j.euprot.2014.08.001.

Ojuka, E.O. *et al.* (2003) ' Raising Ca 2+ in L6 myotubes mimics effects of exercise on mitochondrial biogenesis in muscle ', *The FASEB Journal*, 17(6), pp. 675–681. Available at: https://doi.org/10.1096/fj.02-0951com.

Okano, T. and Matsuda, T.T. (1997) 'Tissue Engineered Skeletal Muscle: Preparation Of Highly Dense, Highly Oriented Hybrid Muscular Tissues', *Cell Transplantation*, 7(1), pp. 71–82. Available at: https://doi.org/10.1016/S0963-6897(97)00067-5.

Olfert, I.M. *et al.* (2016) 'Advances and challenges in skeletal muscle angiogenesis', *American journal of physiology. Heart and circulatory physiology*, 310(3), pp. H326–H336. Available at: https://doi.org/10.1152/ajpheart.00635.2015.

Oost, L.J. *et al.* (2019) 'Fibroblast growth factor 21 controls mitophagy and muscle mass', *Journal of Cachexia, Sarcopenia and Muscle*, 10(3), pp. 630–642. Available at: https://doi.org/10.1002/jcsm.12409.

Oosterheert, W. *et al.* (2022) 'Structural basis of actin filament assembly and aging', *Nature*, 611(7935), pp. 374–379. Available at: https://doi.org/10.1038/s41586-022-05241-8.

Orfanos, Z. *et al.* (2016) 'Breaking sarcomeres by in vitro exercise', *Scientific Reports*, 6. Available at: https://doi.org/10.1038/srep19614.

Osaki, T., Sivathanu, V. and Kamm, R.D. (1980) 'Biomaterials', *Biomaterials*, 156, pp. 65–76. Available at: https://doi.org/10.1016/j.biomaterials.2017.11.041.

Osaki, T., Sivathanu, V. and Kamm, R.D. (2018) 'Crosstalk between developing vasculature and optogenetically engineered skeletal muscle improves muscle contraction and angiogenesis', *Biomaterials*, 156, pp. 65–76. Available at: https://doi.org/10.1016/j.biomaterials.2017.11.041.

Ost, M. *et al.* (2016) 'Regulation of myokine expression: Role of exercise and cellular stress', *Free Radical Biology and Medicine*, 98, pp. 78–89. Available at: https://doi.org/10.1016/j.freeradbiomed.2016.02.018.

Ostrovidov, S., Ahadian, S., Ramon-Azcon, J., Hosseini, V., Fujie, T., Parthiban, S. Prakash, *et al.* (2017) 'Three-dimensional co-culture of C2C12/PC12 cells improves skeletal muscle tissue formation and function', *Journal of Tissue Engineering and Regenerative Medicine*, 11(2), pp. 582–595. Available at: https://doi.org/10.1002/term.1956.

Ostrowski, K. *et al.* (1998) 'Evidence that interleukin-6 is produced in human skeletal muscle during prolonged running', *Journal of Physiology*, 508(3), pp. 949–953. Available at: https://doi.org/10.1111/j.1469-7793.1998.949bp.x.

Ostrowski, K. *et al.* (1999) 'Pro- and anti-inflammatory cytokine balance in strenuous exercise in humans'.

Pal, M., Febbraio, M.A. and Whitham, M. (2014) 'From cytokine to myokine: the emerging role of interleukin-6 in metabolic regulation', *Immunology and cell biology*, 92(4), pp. 331–339. Available at: https://doi.org/10.1038/icb.2014.16.

Pang, K.T. *et al.* (2023) 'Insight into muscle stem cell regeneration and mechanobiology', *Stem Cell Research and Therapy*. BioMed Central Ltd. Available at: https://doi.org/10.1186/s13287-023-03363-y.

Passey, S. *et al.* (2011) 'Stretching skeletal muscle in vitro: Does it replicate in vivo physiology?', *Biotechnology Letters*, pp. 1513–1521. Available at: https://doi.org/10.1007/s10529-011-0610-z.

Pedersen, B.K. (1987) 'Brain, behavior and immunity', *Brain, behavior and immunity*, 25(5), pp. 811–816.

Pedersen, B. K. *et al.* (2003) 'Searching for the exercise factor: Is IL-6 a candidate?', *Journal of Muscle Research and Cell Motility*, 24(2–3), pp. 113–119. Available at: https://doi.org/10.1023/A:1026070911202.

Pedersen, B.K. (2010) ‘Muscles and their myokines’, *Journal of experimental biology*, 214(2), pp. 337–346. Available at: https://doi.org/10.1242/jeb.048074.

Pedersen, B.K. (2019a) ‘Physical activity and muscle–brain crosstalk’, *Nature Reviews Endocrinology*. Available at: https://doi.org/10.1038/s41574-019-0174-x.

Pedersen, B.K. (2019b) ‘The Physiology of Optimizing Health with a Focus on Exercise as Medicine’, *Annual Review of Physiology*, 81(1). Available at: https://doi.org/10.1146/annurev-physiol-020518-114339.

Pedersen, B.K. and Saltin, B. (2015) ‘Exercise as medicine - evidence for prescribing exercise as therapy in 26 different chronic diseases’, *Scandinavian journal of medicine & science in sports*, 25(S3), pp. 1–72. Available at: https://doi.org/10.1111/sms.12581.

Peiris, H.N. *et al.* (2014) ‘Method development for the detection of human myostatin by high-resolution and targeted mass spectrometry’, *Journal of Proteome Research*, 13(8), pp. 3802–3809. Available at: https://doi.org/10.1021/pr5004642.

Perry, L., Flugelman, M.Y. and Levenberg, S. (2017) ‘Elderly Patient-Derived Endothelial Cells for Vascularization of Engineered Muscle’, *Molecular Therapy*, 25(4), pp. 935–948. Available at: https://doi.org/10.1016/j.ymthe.2017.02.011.

Peter, A.K. *et al.* (2011) ‘The costamere bridges sarcomeres to the sarcolemma in striated muscle’, *Progress in Pediatric Cardiology*, 31(2), pp. 83–88. Available at: https://doi.org/10.1016/j.ppedcard.2011.02.003.

Petriz, B.A. *et al.* (2017) ‘The Effects of Acute and Chronic Exercise on Skeletal Muscle Proteome’, *Journal of Cellular Physiology*, 232(2), pp. 257–269. Available at: https://doi.org/10.1002/jcp.25477.

Piccirillo, R. (2019) ‘Exercise-induced myokines with therapeutic potential for muscle wasting’, *Frontiers in Physiology*, 10(MAR), pp. 1–9. Available at: https://doi.org/10.3389/fphys.2019.00287.

Pierdoná, T.M. *et al.* (2022) ‘Extracellular Vesicles as Predictors of Individual Response to Exercise Training in Youth Living with Obesity’, *Frontiers in Bioscience - Landmark*, 27(5). Available at: https://doi.org/10.31083/j.fbl2705143.

Piersma, S.R. *et al.* (2013) ‘Whole gel processing procedure for GeLC-MS/MS based proteomics’, *Proteome Science*, 11(1). Available at: https://doi.org/10.1186/1477-5956-11-17.

Pinckard, K., Baskin, K.K. and Stanford, K.I. (2019) 'Effects of Exercise to Improve Cardiovascular Health', *Frontiers in Cardiovascular Medicine*, 6(June), pp. 1–12. Available at: https://doi.org/10.3389/fcvm.2019.00069.

Pinnell, S.R. (1985) *Regulation of Collagen Biosynthesis by Ascorbic Acid: A Review*, *The Yale Journal Of Biology And Medicine*.

Planavila, A. *et al.* (2013) 'Fibroblast growth factor 21 protects against cardiac hypertrophy in mice', *Nature Communications*, 4. Available at: https://doi.org/10.1038/ncomms3019.

Powell, C.A. *et al.* (2002) 'Mechanical stimulation improves tissue-engineered human skeletal muscle'. Available at: https://doi.org/10.1152/ajpcell.00595.2001.-Human.

Powers, S. *et al.* (2016) 'Disease-Induced Skeletal Muscle Atrophy and Fatigue', *Physiology & behavior*, 48(11), pp. 2307–231. Available at: https://doi.org/doi:10.1249.

Purslow, P.P. (2020) 'The Structure and Role of Intramuscular Connective Tissue in Muscle Function', *Frontiers in Physiology*, 11(May), pp. 1–15. Available at: https://doi.org/10.3389/fphys.2020.00495.

Rabbani, M. *et al.* (2024) 'A Low-Cost, Scalable, and Configurable Multi-Electrode System for Electrical Bio-Interfacing with In-Vitro Cell Cultures', *Applied Sciences (Switzerland)*, 14(1). Available at: https://doi.org/10.3390/app14010162.

Rafik, R., Andrew, R. and Mark, R. (2024) 'NF-κB inhibitors in clinical management for Cancer and diabetes treatment: The IL-6 Potential', *American Heart Journal*, 267, pp. 143–144. Available at: https://doi.org/10.1016/j.ahj.2023.08.062.

Rall, J.A. (2018) 'What makes skeletal muscle striated? Discoveries in the endosarcomeric and exosarcomeric cytoskeleton', *Advances in physiology education*, 42(4), pp. 672–684. Available at: https://doi.org/10.1152/advan.00152.2018.

Rao, L. *et al.* (2018) 'Engineering human pluripotent stem cells into a functional skeletal muscle tissue', *Nature Communications*, 9(1), pp. 1–12. Available at: https://doi.org/10.1038/s41467-017-02636-4.

Rao, R.R. *et al.* (2014) 'Meteorin-like is a hormone that regulates immune-adipose interactions to increase beige fat thermogenesis', *Cell*, 157(6), pp. 1279–1291. Available at: https://doi.org/10.1016/j.cell.2014.03.065.

Raschke, S. *et al.* (2013) 'Identification and Validation of Novel Contraction-Regulated Myokines Released from Primary Human Skeletal Muscle Cells', *PloS one*, 8(4), p. e62008. Available at: https://doi.org/10.1371/journal.pone.0062008.

Raschke, S. and Eckel, J. (2013) 'Adipo-Myokines: Two Sides of the Same Coin-Mediators of Inflammation and Mediators of Exercise', *Mediators of inflammation*, 2013, pp. 1–16. Available at: https://doi.org/10.1155/2013/320724.

Reid, G. *et al.* (2020) 'Next stage approach to tissue engineering skeletal muscle', *Bioengineering*. MDPI AG, pp. 1–30. Available at: https://doi.org/10.3390/bioengineering7040118.

Reimann, L. *et al.* (2017) 'Myofibrillar Z-discs are a protein phosphorylation hot spot with protein kinase C (PKCα) modulating protein dynamics', *Molecular and Cellular Proteomics*, 16(3), pp. 346–367. Available at: https://doi.org/10.1074/mcp.M116.065425.

Riehl, B.D. *et al.* (2012) 'Mechanical Stretching for Tissue Engineering: Two-Dimensional and Three-Dimensional Constructs', *Tissue Engineering Part B: Reviews*. Mary Ann Liebert Inc, p. 288. Available at: https://doi.org/10.1089/ten.teb.2011.0465.

Rigamonti, A.E. *et al.* (2020) 'Effects of an acute bout of exercise on circulating extracellular vesicles: tissue-, sex-, and BMI-related differences', *International Journal of Obesity*, 44(5), pp. 1108–1118. Available at: https://doi.org/10.1038/s41366-019-0460-7.

Roca-Rivada, A. *et al.* (2012) 'Muscle tissue as an endocrine organ: Comparative secretome profiling of slow-oxidative and fast-glycolytic rat muscle explants and its variation with exercise', *Journal of Proteomics*, 75(17), pp. 5414–5425. Available at: https://doi.org/10.1016/j.jprot.2012.06.037.

Rodriguez, J. *et al.* (2014) 'Myostatin and the skeletal muscle atrophy and hypertrophy signaling pathways', *Cellular and Molecular Life Sciences*. Birkhauser Verlag AG, pp. 4361–4371. Available at: https://doi.org/10.1007/s00018-014-1689-x.

Rojas Vega, S. *et al.* (2008) 'Impact of exercise on neuroplasticity-related proteins in spinal cord injured humans', *Neuroscience*, 153(4), pp. 1064–1070. Available at: https://doi.org/10.1016/j.neuroscience.2008.03.037.

Roman, W. and Gomes, E.R. (2018) 'Nuclear positioning in skeletal muscle', *Seminars in cell & developmental biology*, 82, pp. 51–56. Available at: https://doi.org/10.1016/j.semcdb.2017.11.005.

Romancino, D.P. *et al.* (2013) 'Identification and characterization of the nano-sized vesicles released by muscle cells', *FEBS Letters*, 587(9), pp. 1379–1384. Available at: https://doi.org/10.1016/j.febslet.2013.03.012.

Rossi, D. *et al.* (2022) 'The Sarcoplasmic Reticulum of Skeletal Muscle Cells: A Labyrinth of Membrane Contact Sites', *Biomolecules*. MDPI. Available at: https://doi.org/10.3390/biom12040488.

Rowland, L., Bal, N. and Periasamy, M. (2015) 'The role of skeletal-muscle-based thermogenic mechanisms in vertebrate endothermy', *Biological Reviews*, 90(4), pp. 1279–1297. Available at: https://doi.org/10.1111/brv.12157.

Ruan, Q. *et al.* (2018) 'Detection and quantitation of irisin in human cerebrospinal fluid by tandem mass spectrometry', *Peptides*, 103, pp. 60–64. Available at: https://doi.org/10.1016/j.peptides.2018.03.013.

Ruan, Q. *et al.* (2019) 'The effects of both age and sex on irisin levels in paired plasma and cerebrospinal fluid in healthy humans', *Peptides*, 113, pp. 41–51. Available at: https://doi.org/10.1016/j.peptides.2019.01.004.

Rumberger, J.M. *et al.* (2004) 'Transferrin and Iron Contribute to the Lipolytic Effect of Serum in Isolated Adipocytes', *DIABETES*, 53. Available at: http://diabetesjournals.org/diabetes/article-pdf/53/10/2535/375065/zdb01004002535.pdf.

Rutti, S. *et al.* (2014) 'Fractalkine (CX3CL1), a new factor protecting β-cells against TNFα', *Molecular Metabolism*, 3(7), pp. 731–741. Available at: https://doi.org/10.1016/j.molmet.2014.07.007.

Sampath, Srihari C., Sampath, Srinath C. and Millay, D.P. (2018) 'Myoblast fusion confusion: The resolution begins', *Skeletal Muscle*. BioMed Central Ltd. Available at: https://doi.org/10.1186/s13395-017-0149-3.

Sánchez Riera, C. *et al.* (2021) 'Muscle diversity, heterogeneity, and gradients: Learning from sarcoglycanopathies', *International Journal of Molecular Sciences*. MDPI AG, pp. 1–15. Available at: https://doi.org/10.3390/ijms22052502.

Sarihan, M. *et al.* (2023) 'An experimental workflow for enrichment of low abundant proteins from human serum for the discovery of serum biomarkers', *Journal of Biological Methods*, 10, p. e99010001. Available at: https://doi.org/10.14440/jbm.2023.394.

Sasaki-Honda, M. *et al.* (2018) 'A patient-derived iPSC model revealed oxidative stress increases facioscapulohumeral muscular dystrophy-causative DUX4', *Human Molecular Genetics*, 27(23), pp. 4024–4035. Available at: https://doi.org/10.1093/hmg/ddy293.

Sato, S., Nomura, M., Yamana, I., Uchiyama, A., Furuichi, Y., Manabe, Y. and Fujii, Nobuharu L (2019) 'A new in vitro muscle contraction model and its application for analysis of mTORC1 signaling in combination with contraction and beta-hydroxy-beta-methylbutyrate administration', *Bioscience, Biotechnology and Biochemistry*, 83(10), pp. 1851–1857. Available at: https://doi.org/10.1080/09168451.2019.1625261.

Scheler, M. *et al.* (2013) 'Cytokine response of primary human myotubes in an in vitro exercise model', *American Journal of Physiology - Cell Physiology*, 305(8), pp. 877–886. Available at: https://doi.org/10.1152/ajpcell.00043.2013.

Scheler, M. *et al.* (2015) 'Methods for Proteomics-Based Analysis of the Human Muscle Secretome Using an In Vitro Exercise Model', 1295, pp. 1–519. Available at: https://doi.org/10.1007/978-1-4939-2550-6.

Schiaffino, S. *et al.* (2015) 'Developmental myosins: Expression patterns and functional significance', *Skeletal Muscle*, 5(1), pp. 1–14. Available at: https://doi.org/10.1186/s13395-015-0046-6.

Schnyder, S. and Handschin, C. (2015) 'Europe PMC Funders Group Skeletal muscle as an endocrine organ : PGC-1 α , myokines and exercise', *Bone*, 80(1), pp. 115–125. Available at: https://doi.org/10.1016/j.bone.2015.02.008.Skeletal.

Schranner, D. *et al.* (2020) 'Metabolite Concentration Changes in Humans After a Bout of Exercise: a Systematic Review of Exercise Metabolomics Studies', *Sports Medicine - Open*. Springer. Available at: https://doi.org/10.1186/s40798-020-0238-4.

Schwartz, L.M. (2019) 'Skeletal muscles do not undergo apoptosis during either atrophy or programmed cell death-revisiting the myonuclear domain hypothesis', *Frontiers in Physiology*, 10(JAN). Available at: https://doi.org/10.3389/fphys.2018.01887.

Scott, C.B. *et al.* (2006) 'Differences in oxygen uptake but equivalent energy expenditure between a brief bout of cycling and running', *Nutrition and Metabolism*, 3. Available at: https://doi.org/10.1186/1743-7075-3-1.

Scott, C.B. *et al.* (2011) Aerobic, Anaerobic, And Excess Postexercise Oxygen Consumption Energy Expenditure Of Muscular Endurance And Strength: 1-Set Of Bench Press To Muscular Fatigue. Available at: www.nsca-jscr.org.

Scott, C.B., Croteau, A. and Ravlo, T. (2009) Energy Expenditure Before, During, And After The Bench Press. Available at: www.nsca-jscr.org.

Sebille, S. *et al.* (2017) 'Optogenetic approach for targeted activation of global calcium transients in differentiated C2C12 myotubes', *Scientific reports*, 7(1), pp. 11108–11110. Available at: https://doi.org/10.1038/s41598-017-11551-z.

Sekulic-Jablanovic, M. *et al.* (2016) 'Functional characterization of orbicularis oculi and extraocular muscles', *Journal of General Physiology*, 147(5), pp. 395–406. Available at: https://doi.org/10.1085/jgp.201511542.

Seldin, M.M. *et al.* (2012) 'Myonectin (CTRP15), a Novel Myokine That Links Skeletal Muscle to Systemic Lipid Homeostasis', *The Journal of biological chemistry*, 287(15), pp. 11968–11980. Available at: https://doi.org/10.1074/jbc.M111.336834.

Seto, J.T. *et al.* (2011) 'Deficiency of α-actinin-3 is associated with increased susceptibility to contraction-induced damage and skeletal muscle remodeling', *Human Molecular Genetics*, 20(15), pp. 2914–2927. Available at: https://doi.org/10.1093/hmg/ddr196.

Severinsen, M.C.K. and Pedersen, B.K. (2020) 'Muscle-Organ Crosstalk: The Emerging Roles of Myokines', *Endocrine reviews*, 41(4), pp. 594–609. Available at: https://doi.org/10.1210/endrev/bnaa016.

Seyedmahmoud *et al.* (2019) 'Three-Dimensional Bioprinting of Functional Skeletal Muscle Tissue Using GelatinMethacryloyl-Alginate Bioinks', *Micromachines*. MDPI AG. Available at: https://doi.org/10.3390/mi10100679.

Shao, H. *et al.* (2010) 'α-Actinin-4 Is Essential for Maintaining the Spreading, Motility and Contractility of Fibroblasts', *PloS one*, 5(11), p. e13921. Available at: https://doi.org/10.1371/journal.pone.0013921.

Sharma, A. *et al.* (2018) 'Myosin Heavy Chain-embryonic is a crucial regulator of skeletal muscle development and differentiation.', pp. 1–50.

Shima, A., Morimoto, Y., Sweeney, H. Lee, *et al.* (2018) 'Three-dimensional contractile muscle tissue consisting of human skeletal myocyte cell line', *Experimental Cell Research*, 370(1), pp. 168–173. Available at: https://doi.org/10.1016/j.yexcr.2018.06.015.

Shimizu, K. *et al.* (2010) 'Assembly of skeletal muscle cells on a Si-MEMS device and their generative force measurement', *Biomedical Microdevices*, 12(2), pp. 247–252. Available at: https://doi.org/10.1007/s10544-009-9379-4.

Shimizu, K. *et al.* (2017) 'Three-dimensional culture model of skeletal muscle tissue with atrophy induced by dexamethasone', *Bioengineering*, 4(2), p. 56. Available at: https://doi.org/10.3390/bioengineering4020056.

Shimizu, K., Fujita, H. and Nagamori, E. (2013) 'Evaluation systems of generated forces of skeletal muscle cell-based bio-actuators', *Journal of Bioscience and Bioengineering*, pp. 115–121. Available at: https://doi.org/10.1016/j.jbiosc.2012.08.024.

Shimoyama, Y. *et al.* (2010) 'Highly Aligned Skeletal Muscle Fibers', *14th International Conference on Miniaturized Systems for Chemistry and Life Sciences 2010, MicroTAS 2010*, 3(October 2010), pp. 2020–2022.

Sicari, B.M., Londono, R. and Badylak, S.F. (2015) 'Strategies for skeletal muscle tissue engineering: Seed vs. soil', *Journal of Materials Chemistry B*, 3(40), pp. 7881–7895. Available at: https://doi.org/10.1039/c5tb01714a.

Sidorenko, S., Klimanova, E., Milovanova, K., Lopina, Olga D, *et al.* (2018) 'Transcriptomic changes in C2C12 myotubes triggered by electrical stimulation: Role of Ca 2+i -mediated and Ca 2+i -independent signaling and elevated [Na +] i /[K +] i ratio', *Cell Calcium*, 76(May), pp. 72–86. Available at: https://doi.org/10.1016/j.ceca.2018.09.007.

Silva, J.C. *et al.* (2006) 'Absolute Quantification of Proteins by LCMSE', *Molecular & cellular proteomics*, 5(1), pp. 144–156. Available at: https://doi.org/10.1074/mcp.M500230-MCP200.

Skelly, L.E. *et al.* (2014) 'High-intensity interval exercise induces 24-h energy expenditure similar to traditional endurance exercise despite reduced time commitment', *Applied Physiology, Nutrition and Metabolism*, 39(7), pp. 845–848. Available at: https://doi.org/10.1139/apnm-2013-0562.

Smart, N.A. *et al.* (2011) 'Effect of exercise training on interleukin-6, tumour necrosis factor alpha and functional capacity in heart failure', *Cardiology Research and Practice*, 1(1). Available at: https://doi.org/10.4061/2011/532620.

Smith, A.C., Bruce, C.R. and Dyck, D.J. (2005) 'AMP kinase activation with AICAR further increases fatty acid oxidation and blunts triacylglycerol hydrolysis in contracting rat soleus muscle', *Journal of Physiology*, 565(2), pp. 547–553. Available at: https://doi.org/10.1113/jphysiol.2004.081687.

Smith, A.S.T. *et al.* (2012) 'Characterization and optimization of a simple, repeatable system for the long term in vitro culture of aligned myotubes in 3D', *Journal of cellular biochemistry*, 113(3), pp. 1044–1053. Available at: https://doi.org/10.1002/jcb.23437.

Smith, I.C., Adam, H. and Herzog, W. (2020) 'A brief contraction has complex effects on summation of twitch pairs in human adductor pollicis', *Experimental physiology*, 105(4), pp. 676–689. Available at: https://doi.org/10.1113/EP088401.

Snijders, T. *et al.* (2021) 'Myonuclear content and domain size in small versus larger muscle fibres in response to 12 weeks of resistance exercise training in older adults', *Acta Physiologica*, 231(4). Available at: https://doi.org/10.1111/apha.13599.

Snyman, C. *et al.* (2013) 'Simple silicone chamber system for in vitro three-dimensional skeletal muscle tissue formation', *Frontiers in Physiology*, 4. Available at: https://doi.org/10.3389/fphys.2013.00349.

Sonou, T. *et al.* (2007) *Effect of different types of carbohydrate supplementation on glycogen supercompensation in rat skeletal muscle*, スポーツ科学研究.

Staiger, H. *et al.* (2017) 'Fibroblast growth factor 21-metabolic role in mice and men', *Endocrine Reviews*. Oxford University Press, pp. 468–488. Available at: https://doi.org/10.1210/er.2017-00016.

Starkie, R.L. *et al.* (2001) 'Carbohydrate ingestion attenuates the increase in plasma interleukin-6, but not skeletal muscle interleukin-6 mRNA, during exercise in humans', *Journal of Physiology*, 533(2), pp. 585–591. Available at: https://doi.org/10.1111/j.1469-7793.2001.0585a.x.

Steensberg, A. *et al.* (2000) 'Production of interleukin-6 in contracting human skeletal muscles can account for the exercise-induced increase in plasma interleukin-6', *Journal of Physiology*, 529(1), pp. 237–242. Available at: https://doi.org/10.1111/j.1469-7793.2000.00237.x.

Steensberg, A. *et al.* (2002) 'IL-6 and TNF-α expression in, and release from, contracting human skeletal muscle', *American Journal of Physiology - Endocrinology and Metabolism*, 283(6 46-6), pp. 1272–1278. Available at: https://doi.org/10.1152/ajpendo.00255.2002.

Su, R. *et al.* (2021) 'Effects of energy supplements on the differentiation of skeletal muscle satellite cells', *Food Science and Nutrition*, 9(1), pp. 357–366. Available at: https://doi.org/10.1002/fsn3.2001.

Sugimoto, T. *et al.* (2022) 'Investigation of Brain Function-Related Myokine Secretion by Using Contractile 3D-Engineered Muscle', *International Journal of Molecular Sciences*, 23(10). Available at: https://doi.org/10.3390/ijms23105723.

Sun, Z. *et al.* (2024) 'Research trends and hotspot evolution of exercise-regulated myokines: a bibliometric analysis from 2003 to 2023', *Frontiers in Physiology*. Frontiers Media SA. Available at: https://doi.org/10.3389/fphys.2024.1410068.

Sunadome, K. *et al.* (2023) 'Directionality of developing skeletal muscles is set by mechanical forces', *Nature Communications*, 14(1). Available at: https://doi.org/10.1038/s41467-023-38647-7.

Suresh Kumar, H. *et al.* (2023) 'Biomechanical Stimulation of Muscle Constructs Influences Phenotype of Bone Constructs by Modulating Myokine Secretion', *JBMR Plus*, 7(11). Available at: https://doi.org/10.1002/jbm4.10804.

Švec, X. *et al.* (2022) 'Hsp90 as a Myokine: Its Association with Systemic Inflammation after Exercise Interventions in Patients with Myositis and Healthy Subjects', *International*

Journal of Molecular Sciences, 23(19). Available at: https://doi.org/10.3390/ijms231911451.

Sylow, L. *et al.* (2021) 'The many actions of insulin in skeletal muscle, the paramount tissue determining glycemia', *Cell Metabolism*. Cell Press, pp. 758–780. Available at: https://doi.org/10.1016/j.cmet.2021.03.020.

Syverud, B., VanDusen, K. and Larkin, L. (2016) 'Growth Factors for Skeletal Muscle Tissue Engineering', *Cells Tissues Organ*, 202((3-4)), pp. 169–179.

Takagi, S., Nakamura, T. and Fujisato, T. (2018) 'Effect of heat stress on contractility of tissue-engineered artificial skeletal muscle', *Journal of Artificial Organs*, 21(2), pp. 207–214. Available at: https://doi.org/10.1007/s10047-018-1020-y.

Takahashi, H. *et al.* (2013) 'The use of anisotropic cell sheets to control orientation during the self-organization of 3D muscle tissue', *Biomaterials*, 34(30), pp. 7372–7380. Available at: https://doi.org/10.1016/j.biomaterials.2013.06.033.

Takahashi, H., Shimizu, T. and Okano, T. (2018) 'Engineered Human Contractile Myofiber Sheets as a Platform for Studies of Skeletal Muscle Physiology', *Scientific Reports*, 8(1), pp. 13911–13932. Available at: https://doi.org/10.1038/s41598-018-32163-1.

Takisawa, S. *et al.* (2022) 'Vitamin C Is Essential for the Maintenance of Skeletal Muscle Functions', *Biology*, 11(7). Available at: https://doi.org/10.3390/biology11070955.

Talbot, J., Mavez, L. and Maves, L. (2016) 'Skeletal muscle fiber type: using insights from muscle developmental biology to dissect targets for susceptibility and resistance to muscle disease', *Wiley interdisciplinary reviews. Developmental biology*, 5(4), pp. 518–534. Available at: https://doi.org/10.1002/wdev.230.

Tamura, Y. *et al.* (2011) *Upregulation of circulating IL-15 by treadmill running in healthy individuals: Is IL-15 an endocrine mediator of the beneficial effects of endurance exercise?*, *Endocrine Journal*.

Tan, S.J. *et al.* (2015) 'Muscle tissue engineering and regeneration through epigenetic reprogramming and scaffold manipulation', *Scientific Reports*. Springer Science and Business Media LLC. Available at: https://doi.org/10.1038/srep16333.

Tarum, J. *et al.* (2017) 'Electrical pulse stimulation: an in vitro exercise model for the induction of human skeletal muscle cell hypertrophy. A proof-of-concept study', *Experimental Physiology*, 102(11), pp. 1405–1413. Available at: https://doi.org/10.1113/EP086581.

Tezze, C., Romanello, V. and Sandri, M. (2019) 'FGF21 as Modulator of Metabolism in Health and Disease', *Frontiers in physiology*, 10(MAR), p. 419. Available at: https://doi.org/10.3389/fphys.2019.00419.

Thomson, D.M., Fick, C.A. and Gordon, S.E. (2008) 'AMPK activation attenuates S6K1, 4E-BP1, and eEF2 signaling responses to high-frequency electrically stimulated skeletal muscle contractions', *J Appl Physiol*, 104, pp. 625–632. Available at: https://doi.org/10.1152/japplphysiol.00915.2007.-Regulation.

Tomalka, A. *et al.* (2017) 'The active force-length relationship is invisible during extensive eccentric contractions in skinned skeletal muscle fibres', *Proceedings of the Royal Society B: Biological Sciences*, 284(1854), p. 20162497. Available at: https://doi.org/10.1098/rspb.2016.2497.

Trensz, F. *et al.* (2015) 'Increased microenvironment stiffness in damaged myofibers promotes myogenic progenitor cell proliferation', *Skeletal Muscle*, 5(1). Available at: https://doi.org/10.1186/s13395-015-0030-1.

Trinick, J. and Tskhovrebova, L. (2010) 'Roles of titin in the structure and elasticity of the sarcomere', *Journal of Biomedicine and Biotechnology*. Available at: https://doi.org/10.1155/2010/612482.

Tu, C. *et al.* (2010) 'Depletion of abundant plasma proteins and limitations of plasma proteomics', *Journal of Proteome Research*, 9(10), pp. 4982–4991. Available at: https://doi.org/10.1021/pr100646w.

Uchimura, T. *et al.* (2017) 'A human iPS cell myogenic differentiation system permitting high-throughput drug screening', *Stem Cell Research*, 25, pp. 98–106. Available at: https://doi.org/10.1016/j.scr.2017.10.023.

Urciuolo, A. *et al.* (2020) 'Engineering a 3D in vitro model of human skeletal muscle at the single fiber scale', *PloS one*, 15(5), pp. 1–17. Available at: https://doi.org/10.1371/journal.pone.0232081.

Urzì, O. *et al.* (2023) 'Three-Dimensional Cell Cultures: The Bridge between In Vitro and In Vivo Models', *International Journal of Molecular Sciences*. Multidisciplinary Digital Publishing Institute (MDPI). Available at: https://doi.org/10.3390/ijms241512046.

Valero-Breton, M. *et al.* (2020) 'Acute and Chronic Effects of High Frequency Electric Pulse Stimulation on the Akt/mTOR Pathway in Human Primary Myotubes', *Frontiers in Bioengineering and Biotechnology*, 8. Available at: https://doi.org/10.3389/fbioe.2020.565679.

Vandenburgh, H.H., Karlisch, P. and Farr, L. (1988) 'Maintenance of highly contractile tissue-cultured avian skeletal myotubes in collagen gel', *In Vitro Cellular & Developmental Biology*, 24(3), pp. 166–174. Available at: https://doi.org/10.1007/BF02623542.

Vaughan, M. and Lamia, K.A. (2020) *Isolation and Differentiation of Primary Myoblasts from Mouse Skeletal Muscle Explants*.

Velasco-Mallorquí, F. *et al.* (2020) 'New volumetric CNT-doped gelatin–cellulose scaffolds for skeletal muscle tissue engineering', *Nanoscale advances*, 2(7), pp. 2885–2896. Available at: https://doi.org/10.1039/D0NA00268B.

van der Ven, P.F.M.M. *et al.* (1992) 'Differentiation of human skeletal muscle cells in culture : maturation as indicated by titin and des min striation', *Cell And Tissue Research*, 270(1), pp. 189–198. Available at: https://doi.org/10.1007/BF00381893.

Vepkhvadze, T.F., Vorotnikov, A. V. and Popov, D. V. (2021) 'Electrical Stimulation of Cultured Myotubes in vitro as a Model of Skeletal Muscle Activity: Current State and Future Prospects', *Biochemistry (Moscow)*. Pleiades journals, pp. 597–610. Available at: https://doi.org/10.1134/S0006297921050084.

Vesga-Castro, C. *et al.* (2022) 'Contractile force assessment methods for in vitro skeletal muscle tissues', *eLife*. eLife Sciences Publications Ltd. Available at: https://doi.org/10.7554/eLife.77204.

Wang, H. *et al.* (2022) 'Prior AICAR induces elevated glucose uptake concomitant with greater γ3-AMPK activation and reduced membrane cholesterol in skeletal muscle from 26-month-old rats', *FACETS*, 7, pp. 774–791. Available at: https://doi.org/10.1139/facets-2021-0166.

Wang, J. *et al.* (2019) 'Engineered skeletal muscles for disease modeling and drug discovery', *Biomaterials*, 221(August). Available at: https://doi.org/10.1016/j.biomaterials.2019.119416.

Wang, J. *et al.* (2021) 'Three-dimensional tissue-engineered human skeletal muscle model of Pompe disease', *Communications biology*, 4(1), p. 524. Available at: https://doi.org/10.1038/s42003-021-02059-4.

Wang, Y. and Jaenisch, R. (1997) 'Myogenin can substitute for Myf5 in promoting myogenesis but less efficiently', *Development*, 124(13). Available at: https://doi.org/10.1242/dev.124.13.2507 (Accessed: 27 November 2024).

Washio, T. *et al.* (2019) ‘Effect of myofibril passive elastic properties on the mechanical communication between motor proteins on adjacent sarcomeres’, *Scientific Reports*, 9(1). Available at: https://doi.org/10.1038/s41598-019-45772-1.

Webster, C. *et al.* (1988) ‘Fast muscle fibers are preferentially affected in Duchenne muscular dystrophy’, *Cell (Cambridge)*, 52(4), pp. 503–513. Available at: https://doi.org/10.1016/0092-8674(88)90463-1.

Weis, J. *et al.* (2000) ‘Denervation induces a rapid nuclear accumulation of MRF4 in mature myofibers’, *Developmental Dynamics*, 218(3), pp. 438–451. Available at: https://doi.org/10.1002/1097-0177(200007)218:3<438::AID-DVDY1001>3.0.CO;2-6.

Weist, M.R. *et al.* (2013) ‘TGF-β1 enhances contractility in engineered skeletal muscle’, *Journal of tissue engineering and regenerative medicine*, 7(7), pp. 562–571. Available at: https://doi.org/10.1002/term.551.

White, J. *et al.* (2014) ‘Localization of sarcomeric proteins during myofibril assembly in cultured mouse primary skeletal myotubes’, *Anatomical Record*, 297(9), pp. 1571–1584. Available at: https://doi.org/10.1002/ar.22981.

Whitham, M. *et al.* (2018) ‘Extracellular Vesicles Provide a Means for Tissue Crosstalk during Exercise’, *Cell Metabolism*, 27(1), pp. 237-251.e4. Available at: https://doi.org/10.1016/j.cmet.2017.12.001.

Williams, C.B. *et al.* (2013) ‘Changes in mechanisms proposed to mediate fat loss following an acute bout of high-intensity interval and endurance exercise’, *Applied Physiology, Nutrition and Metabolism*, 38(12), pp. 1236–1244. Available at: https://doi.org/10.1139/apnm-2013-0101.

Wohlgemuth, R.P. *et al.* (2024) ‘Strain-dependent dynamic re-alignment of collagen fibers in skeletal muscle extracellular matrix’, *Acta Biomaterialia* [Preprint]. Available at: https://doi.org/10.1016/j.actbio.2024.08.035.

Xie, D. *et al.* (2023) ‘Fluid-Driven High-Performance Bionic Artificial Muscle with Adjustable Muscle Architecture’, *Advanced Intelligent Systems*, 5(6). Available at: https://doi.org/10.1002/aisy.202200370.

Yaffe, D. (1968) Retention Of Differentiation Potentialities During Prolonged Cultivation Of M1yogenic Cells. Available at: https://www.pnas.org.

Yamasaki, K.I. *et al.* (2009) ‘Control of myotube contraction using electrical pulse stimulation for bio-actuator’, *Journal of Artificial Organs*, 12(2), pp. 131–137. Available at: https://doi.org/10.1007/s10047-009-0457-4.

Ye, J. (2015) ‘Beneficial metabolic activities of inflammatory cytokine interleukin 15 in obesity and type 2 diabetes’, *Frontiers of Medicine*. Higher Education Press, pp. 139–145. Available at: https://doi.org/10.1007/s11684-015-0377-z.

Yin, H., Price, F. and Rudnicki, M.A. (2013) ‘Satellite Cells and the Muscle Stem Cell Niche’, *Physiological reviews*, 93(1), pp. 23–67. Available at: https://doi.org/10.1152/physrev.00043.2011.

Yin, W. *et al.* (2024) ‘Erythropoietin regulates energy metabolism through EPO-EpoR-RUNX1 axis’, *Nature Communications* , 15(1). Available at: https://doi.org/10.1038/s41467-024-52352-z.

Yoon, J.H. *et al.* (2011) ‘Proteomic analysis of tumor necrosis factor-alpha (TNF-α)-induced L6 myotube secretome reveals novel TNF-α-dependent myokines in diabetic skeletal muscle’, *Journal of Proteome Research*, 10(12), pp. 5315–5325. Available at: https://doi.org/10.1021/pr200573b.

Yoon, J.H. *et al.* (2015) ‘Proteomic analysis of the palmitate-induced myotube secretome reveals involvement of the annexin A1-formyl peptide receptor 2 (FPR2) pathway in insulin resistance’, *Molecular and Cellular Proteomics*, 14(4), pp. 882–892. Available at: https://doi.org/10.1074/mcp.M114.039651.

Yoshida, T. and Delafontaine, P. (2020) ‘Mechanisms of IGF-1-Mediated Regulation of Skeletal Muscle Hypertrophy and Atrophy’, *Cells*. NLM (Medline). Available at: https://doi.org/10.3390/cells9091970.

Yoshimoto, Y. *et al.* (2020) ‘Methods for Accurate Assessment of Myofiber Maturity During Skeletal Muscle Regeneration’, *Frontiers in Cell and Developmental Biology*, 8(April), pp. 1–12. Available at: https://doi.org/10.3389/fcell.2020.00267.

Young, J. *et al.* (2018) ‘MyoScreen, a High-Throughput Phenotypic Screening Platform Enabling Muscle Drug Discovery’, *SLAS Discovery*, 23(8), pp. 790–806. Available at: https://doi.org/10.1177/2472555218761102.

Yu, S.J. *et al.* (2004) ‘Distinct transcriptional control and action of fibroblast growth factor receptor 4 in differentiating skeletal muscle cells’, *Laboratory Investigation*, 84(12), pp. 1571–1580. Available at: https://doi.org/10.1038/labinvest.3700187.

Yu, W. *et al.* (2024) ‘The myokine CCL5 recruits subcutaneous preadipocytes and promotes intramuscular fat deposition in obese mice’, *American Journal of Physiology - Cell Physiology*, 326(5), pp. C1320–C1333. Available at: https://doi.org/10.1152/ajpcell.00591.2023.

Zammit, P.S. (2017) ‘Function of the myogenic regulatory factors Myf5, MyoD, Myogenin and MRF4 in skeletal muscle, satellite cells and regenerative myogenesis’, *Seminars in Cell and Developmental Biology*. Elsevier Ltd, pp. 19–32. Available at: https://doi.org/10.1016/j.semcdb.2017.11.011.

Zhang, P., Chen, X. and Fan, M. (2007) ‘Signaling mechanisms involved in disuse muscle atrophy’, *Medical Hypotheses*, 69(2), pp. 310–321. Available at: https://doi.org/10.1016/j.mehy.2006.11.043.

Zhao, Y. *et al.* (2018) ‘Conditioned medium from contracting skeletal muscle cells reverses insulin resistance and dysfunction of endothelial cells’, *Metabolism: Clinical and Experimental*, 82, pp. 36–46. Available at: https://doi.org/10.1016/j.metabol.2017.12.008.

Zhu, Z. and Miller, J.B. (1997) ‘MRF4 can substitute for myogenin during early stages of myogenesis’, *Developmental Dynamics*, 209(2), pp. 233–241. Available at: https://doi.org/10.1002/(SICI)1097-0177(199706)209:2<233::AID-AJA9>3.0.CO;2-J.

Zöllner, A.M. *et al.* (2012) ‘Stretching Skeletal Muscle: Chronic Muscle Lengthening through Sarcomerogenesis’, *PLoS ONE*, 7(10). Available at: https://doi.org/10.1371/journal.pone.0045661.

Appendix I

A

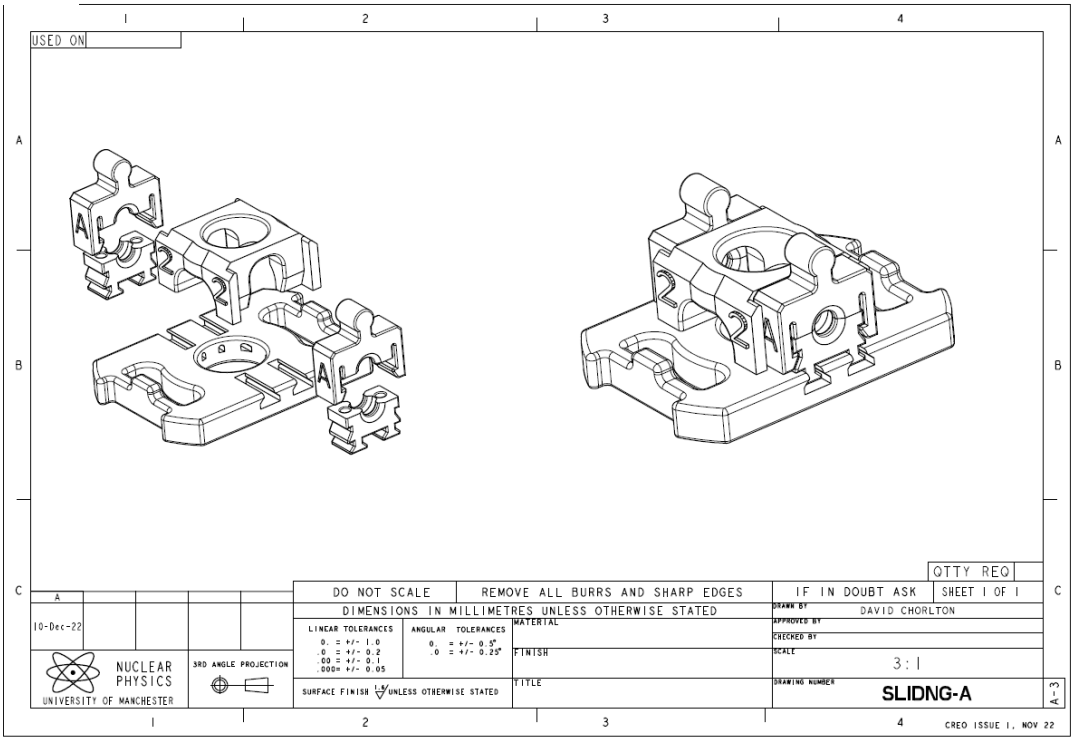

B

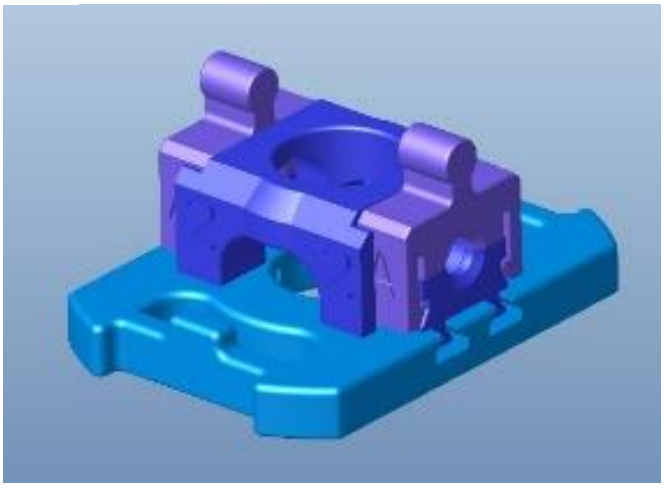

Figure A1 3D MTSIP system designs. *(A) CAD drawing of the 3D MTSIP. (B) A 3D render of the MTSIP prototype.*

Table A1 Videos of skeletal muscle model contractions. Videos can be viewed at: *Nuh Ali M (2024) Contraction of 2D and 3D C2C12 Skeletal Muscle Models. This work is part of a Ph.D. project. figshare. DOI: 10.6084/m9.figshare.28001114.v1. https://doi.org/10.6084/m9.figshare.28001114.v1*

Video no.	Culture Condition	Model	Observation
1	C2C21 cells in defined media 1	2D + EPS	Round myoblasts fuse to form longer, elongated myotubes by day 7 of differentiation.
2	C2C12 contraction in defined media 1	2D + EPS	Myotubes contract as single fibres.
3	C2C12 in defined media 2	2D + EPS	Myotubes contract as single fibres.
4	C2C12 in defined media 2	2D + EPS	Myotubes exhibit cross-linking and contract.
5	C2C12 in defined media 2	2D + EPS	Myotubes appear fused and contract together as 'sheets'.
6	C2C12 in defined media 2	2D - EPS	Spontaneous myotubes contraction
7	C2C12 in defined media 2	3D spheroid + EPS	Minimal contraction at the tissue periphery, visible fibres

Table A2 Gene ontology (GO) characterisation: *Summary of parent GO annotations with respect to biological process, molecular function, and cellular component of secreted proteins from physiological 2D and 3D EPS models. Results are grouped highest to lowest for fold enrichment. FDR > 0.05.*

Function		Number of genes	Fold enrichment	p-value
2D + EPS				
GO biological process				
Regulation of locomotion	GO:0040012	7	9.26	3.79×10^{-6}
Cell motility	GO:0048870	7	9.21	3.93×10^{-6}
Response to cytokine	GO:0034097	5	8.83	1.70×10^{-4}
Response to endogenous stimulus	GO:0009719	6	6.68	1.46×10^{-4}
Regulation of multicellular organismal development	GO:2000026	7	6.5	3.84×10^{-5}
Regulation of phosphorus metabolic process	GO:0051174	6	6.29	2.03×10^{-4}
Regulation of developmental process	GO:0050793	11	6.1	6.58×10^{-8}
Regulation of transport	GO:0051049	7	5.23	1.53×10^{-4}
Regulation of response to stimulus	GO:0048583	12	4.35	3.97×10^{-7}
Regulation of multicellular organismal process	GO:0051239	9	4.04	7.48×10^{-5}
Regulation of signalling	GO:002305	9	3.79	1.27×10^{-4}
Regulation of cell communication	GO:0010646	9	3.78	1.28×10^{-4}
Negative regulation of biological process	GO:0048519	13	3.44	1.04×10^{-6}
Positive regulation of metabolic process	GO:0009893	9	3.42	2.84×10^{-4}

Function		Number of genes	Fold enrichment	p-value
Positive regulation of cellular process	GO:0048522	12	3.09	$1.85x10^{-5}$
Developmental process	GO:0032502	12	3.03	$2.29x10^{-5}$
Regulation of biological process	GO:0050789	15	1.8	$2.52x10^{-4}$
GO Molecular function				
Glycosaminoglycan binding	GO:0005539	5	30.53	$4.51x10^{-7}$
Growth factor receptor binding	GO:0070851	3	29.12	$1.44x10^{-4}$
Sulphur compound binding	GO:1901681	4	19.74	$4.16x10^{-5}$
Molecular function regulator activity	GO:0098772	12	8.2	$2.63x10^{-10}$
Protein binding	GO:0005515	14	2.17	$6.68x10^{-5}$
GO Cellular component				
Extracellular region	GO:0005576	15	8.46	$1.28x10^{-14}$
3D + EPS				
GO biological process				
Animal organ regeneration	GO:0031100	2	> 100	$1.92x10^{-5}$
Regulation of collagen metabolic process	GO:0010712	2	> 100	$8.56x10^{-5}$
Regulation of peptidyl-tyrosine phosphorylation	GO:0050730	3	49.22	$1.82x10^{-5}$
Regulation of ERK1 and ERK2 cascade	GO:0070372	3	39.37	$3.52x10^{-5}$
Cytokine-mediated signalling pathway	GO:0019221	3	38.91	$3.64x10^{-5}$
Negative regulation of transport	GO:0051051	3	25.46	$1.28x10^{-4}$
Positive regulation of protein localization	GO:1903829	3	25.22	$1.31x10^{-4}$
Positive regulation of MAPK cascade	GO:0043410	3	24.56	$1.42x10^{-4}$
Regulation of cell adhesion	GO:0030155	4	20.84	$1.06x10^{-5}$
Regulation of anatomical structure morphogenesis	GO:0022603	4	18.59	$1.67x10^{-5}$
Negative regulation of developmental process	GO:0051093	4	17.43	$2.16x10^{-5}$
Negative regulation of multicellular organismal process	GO:005124	4	14.17	$4.88x10^{-5}$
Cell surface receptor signalling pathway	GO:0007166	5	11.52	$4.96x10^{-6}$
Regulation of immune system process	GO:0002682	4	10.98	$1.33x10^{-4}$
Immune response	GO:0006955	4	10.47	$1.61x10^{-4}$
Cellular response to organic substance	GO:0071310	4	10.09	$1.86x10^{-4}$
Regulation of cell population proliferation	GO:0042127	4	9.85	$2.05x10^{-4}$
Regulation of localization	GO:0032879	5	9.43	$1.35x10^{-5}$
Regulation of developmental process	GO:0050793	5	8.32	$2.52x10^{-5}$
Regulation of multicellular organismal process	GO:0051239	5	6.74	$7.22x10^{-5}$
System development	GO:0048731	5	6.31	$1.00x10^{-4}$
Cellular developmental process	GO:0048869	5	5.78	$1.56x10^{-4}$
GO Molecular function				
Cytokine receptor binding	GO:0005126	4	55.65	$2.18x10^{-7}$
Molecular function regulator activity	GO:0098772	5	10.25	$8.61x10^{-9}$
GO Cellular component				
Extracellular region	GO:0005576	5	8.46	$2.32x10^{-5}$

Function		Number of genes	Fold enrichment	p-value
2D - EPS				
GO biological process				
Granulocyte activation	GO:0036230	2	99.47	2.01E-04
Regulation of monocyte chemotaxis	GO:0090025	2	93.94	2.24E-04
Regulation of macrophage migration	GO:1905521	2	69.02	4.04E-04
Response to interleukin-1	GO:0070555	3	55.75	2.10E-05
neutrophil migration	GO:1990266	3	55.14	2.16E-05
Response to tumour necrosis factor	GO:0034612	3	33.16	9.50E-05
Positive regulation of GTPase activity	GO:0043547	3	20.05	4.09E-04
Regulation of cell-cell adhesion	GO:0022407	4	12.81	2.03E-04
Locomotion	GO:0040011	4	12.76	2.06E-04
Positive regulation of locomotion	GO:0040017	4	10.62	4.14E-04
Regulation of cell adhesion	GO:0030155	5	10.02	8.41E-05
Regulation of multicellular organismal development	GO:2000026	9	9.64	2.86E-08
Positive regulation of developmental process	GO:0051094	7	7.9	8.23E-06
Regulation of locomotion	GO:0040012	5	7.63	3.01E-04
Cell motility	GO:0048870	5	7.59	3.08E-04
Regulation of protein phosphorylation	GO:0001932	5	7.4	3.47E-04
Cell surface receptor signalling pathway	GO:0007166	8	7.09	2.82E-06
Regulation of cell differentiation	GO:0045595	7	7.02	1.78E-05
Regulation of cell population proliferation	GO:0042127	7	6.63	2.61E-05
Positive regulation of cell communication	GO:0010647	7	6.39	3.32E-05
Positive regulation of signalling	GO:0023056	7	6.39	3.32E-05
Immune response	GO:0006955	6	6.04	2.15E-04
Regulation of multicellular organismal process	GO:0051239	9	4.67	1.42E-05
Response to organic substance	GO:0010033	7	4.54	2.98E-04
Regulation of cell communication	GO:0010646	8	3.88	2.44E-04
Cell differentiation	GO:0030154	8	3.58	4.30E-04
Negative regulation of cellular process	GO:0048523	10	3.48	4.08E-05
Negative regulation of biological process	GO:0048519	11	3.36	1.22E-05
Positive regulation of cellular process	GO:0048522	10	2.97	1.76E-04
Regulation of cellular process	GO:0050794	13	1.93	2.71E-04
Granulocyte activation	GO:0036230	2	99.47	2.01E-04
GO Molecular function				
Chemokine receptor binding	GO:0042379	3	64.22	1.39E-05
Hormone activity	GO:0005179	3	37.03	6.89E-05
Glycosaminoglycan binding	GO:0005539	5	35.23	1.97E-07
Growth factor activity	GO:0008083	3	34.28	8.62E-05
Sulphur compound binding	GO:1901681	4	22.77	2.23E-05
Signalling receptor binding	GO:0005102	10	10.27	1.33E-09
Molecular function regulator activity	GO:0098772	10	7.88	1.73E-08

Function		Number of genes	Fold enrichment	p-value
GO Cellular component				
Extracellular region	GO:0005576	13	8.46	9.05E-13
3D - EPS				
GO biological process				
Regulation of interleukin-33 production	GO:0150127	1	> 100	1.64E-03
Lung vasculature development	GO:0060426	2	> 100	3.46E-05
Regulation of chronic inflammatory response	GO:0002676	2	> 100	4.90E-05
Regulation of chemokine (C-X-C motif) ligand 2 production	GO:2000341	2	87.23	2.71E-04
Response to activity	GO:0014823	2	81.42	3.09E-04
Regulation of interleukin-17 production	GO:0032660	3	79.65	8.27E-06
Monocyte chemotaxis	GO:0002548	2	71.84	3.92E-04
T cell selection	GO:0045058	3	70.46	1.17E-05
Regulation of syncytium formation by plasma membrane fusion	GO:0060142	2	69.79	4.14E-04
Regulation of leukocyte adhesion to vascular endothelial cell	GO:1904994	2	69.79	4.14E-04
Regulation of nitric oxide metabolic process	GO:0080164	4	63.44	5.02E-07
Chondroitin sulphate proteoglycan metabolic process	GO:0050654	2	62.63	5.09E-04
Positive regulation of steroid metabolic process	GO:0045940	2	62.63	5.09E-04
Protein kinase B signalling	GO:0043491	3	60.06	1.86E-05
Lymphocyte chemotaxis	GO:0048247	2	56.8	6.13E-04
Regulation of phosphatidylinositol 3-kinase signalling	GO:0014066	5	55.01	3.03E-08
Regulation of amyloid precursor protein catabolic process	GO:1902991	2	54.28	6.69E-04
Response to protozoan	GO:0001562	2	53.1	6.97E-04
Negative regulation of cellular response to insulin stimulus	GO:1900077	2	50.89	7.57E-04
Regulation of cell adhesion mediated by integrin	GO:0033628	2	49.85	7.87E-04
Regulation of macrophage migration	GO:1905521	2	49.85	7.87E-04
Embryo implantation	GO:0007566	2	48.85	8.18E-04
Neuroinflammatory response	GO:0150076	2	44.41	9.82E-04
Regeneration	GO:0031099	4	43.23	2.19E-06
Regulation of myelination	GO:0031641	2	41.4	1.12E-03
Regulation of protein kinase B signalling	GO:0051896	6	40.94	5.56E-09
Positive regulation of hemopoiesis	GO:1903708	7	40.52	2.47E-10
Regulation of interleukin-10 production	GO:0032653	2	38.77	1.28E-03
Regulation of cytokine production involved in inflammatory response	GO:1900015	2	38.77	1.28E-03
Regulation of pathway-restricted SMAD protein phosphorylation	GO:0060393	2	38.16	1.31E-03

Function		Number of genes	Fold enrichment	p-value
Lung alveolus development	GO:0048286	2	37.58	1.35E-03
Response to ethanol	GO:0045471	2	37.01	1.39E-03
Positive regulation of nuclear division	GO:0051785	2	37.01	1.39E-03
Detection of mechanical stimulus	GO:0050982	2	36.46	1.44E-03
Positive regulation of smooth muscle cell migration	GO:0014911	2	36.46	1.44E-03
Positive regulation of lymphocyte differentiation	GO:0045621	4	35.14	4.88E-06
Positive regulation of Ras protein signal transduction	GO:0046579	2	34.89	1.56E-03
Regulation of osteoblast differentiation	GO:0045667	4	33.69	5.74E-06
Regulation of immunoglobulin production	GO:0002637	3	33.31	1.02E-04
Regulation of interleukin-1 production	GO:0032652	3	32.71	1.07E-04
Positive regulation of osteoblast differentiation	GO:0045669	2	32.57	1.78E-03
Regulation of interleukin-8 production	GO:0032677	2	32.57	1.78E-03
Cytokine-mediated signalling pathway	GO:0019221	9	32.42	2.40E-12
Regulation of receptor signalling pathway via STAT	GO:1904892	3	32.14	1.13E-04
Negative regulation of epithelial cell apoptotic process	GO:1904036	2	32.14	1.83E-03
Regulation of smooth muscle cell proliferation	GO:0048660	5	31.97	4.16E-07
Response to tumour necrosis factor	GO:0034612	4	31.93	7.06E-06
Regulation of peptidyl-serine phosphorylation	GO:0033135	4	30.34	8.60E-06
Regulation of generation of precursor metabolites and energy	GO:0043467	3	29.55	1.44E-04
Tissue remodelling	GO:0048771	3	29.08	1.51E-04
Regulation of epithelial cell apoptotic process	GO:1904035	3	29.08	1.51E-04
Myeloid leukocyte activation	GO:0002274	4	28.24	1.13E-05
Organ growth	GO:0035265	3	27.76	1.72E-04
Response to type II interferon	GO:0034341	3	26.74	1.92E-04
Regulation of B cell activation	GO:0050864	3	25.27	2.26E-04
Regulation of fat cell differentiation	GO:0045598	3	24.92	2.35E-04
Regulation of epithelial cell migration	GO:0010632	5	24.72	1.44E-06
Regulation of myeloid cell differentiation	GO:0045637	4	21.15	3.45E-05
Regulation of vasculature development	GO:1901342	5	20.15	3.84E-06
MAPK cascade	GO:0000165	3	19.91	4.49E-04
Regulation of hemopoiesis	GO:1903706	7	19.43	3.58E-08
Leukocyte proliferation	GO:0070661	3	18.79	5.30E-04
Regulation of cell morphogenesis	GO:0022604	4	17.64	6.92E-05
Regulation of tumour necrosis factor superfamily cytokine production	GO:1903555	3	17.12	6.92E-04

Function		Number of genes	Fold enrichment	p-value
Bone development	GO:0060348	3	16.96	7.11E-04
Regulation of neuron death	GO:1901214	5	16.64	9.62E-06
Respiratory tube development	GO:0030323	3	16.36	7.89E-04
B cell activation	GO:0042113	3	16.36	7.89E-04
Negative regulation of cytokine production	GO:0001818	4	15.91	1.02E-04
Myeloid cell differentiation	GO:0030099	4	15.71	1.08E-04
Regulation of neuron differentiation	GO:0045664	3	15.59	9.05E-04
Regulation of adaptive immune response	GO:0002819	3	15.02	1.01E-03
Regulation of MAPK cascade	GO:0043408	9	14.77	2.27E-09
Apoptotic signalling pathway	GO:0097190	4	14.76	1.36E-04
Respiratory system development	GO:0060541	3	14.54	1.10E-03
Regulation of epithelial cell proliferation	GO:0050678	5	14.44	1.89E-05
Negative regulation of growth	GO:0045926	3	13.98	1.23E-03
Regulation of cell activation	GO:0050865	8	13.65	4.32E-08
Anatomical structure maturation	GO:0071695	3	13.62	1.33E-03
Response to cytokine	GO:0034097	9	13.24	5.83E-09
Cell fate commitment	GO:0045165	3	13.13	1.47E-03
Regulation of cell adhesion	GO:0030155	9	13.02	6.74E-09
Regulation of small molecule metabolic process	GO:0062012	4	12.89	2.28E-04
Regulation of secretion by cell	GO:1903530	7	12.34	7.51E-07
Cellular response to organic cyclic compound	GO:0071407	4	11.63	3.36E-04
Positive regulation of locomotion	GO:0040017	6	11.5	8.37E-06
Inflammatory response	GO:0006954	5	11.41	5.75E-05
Negative regulation of phosphorus metabolic process	GO:0010563	4	11.15	3.93E-04
Positive regulation of cell projection organization	GO:0031346	4	10.76	4.50E-04
Regulation of anatomical structure morphogenesis	GO:0022603	8	10.33	3.60E-07
Negative regulation of signalling	GO:0023057	12	10.19	1.54E-05
Positive regulation of developmental process	GO:0051094	12	9.78	8.23E-11
Regulation of transmembrane transport	GO:0034762	5	9.63	1.32E-10
Regulation of system process	GO:0044057	5	9.6	1.27E-04
Positive regulation of cellular component organization	GO:0051130	10	9.58	1.29E-04
Growth	GO:0040007	4	9.39	1.27E-08
Positive regulation of protein localization	GO:1903829	4	9.34	7.46E-04
Regulation of response to biotic stimulus	GO:0002831	4	9.27	7.62E-04
Muscle structure development	GO:0061061	4	9.18	7.84E-04
Regulation of growth	GO:0040008	5	9.13	8.12E-04
Regulation of transferase activity	GO:0051338	6	8.83	1.63E-04

Function		Number of genes		Fold enrichment	p-value
Regulation of locomotion	GO:0040012	8	8.82	3.71E-05	
Negative regulation of intracellular signal transduction	GO:1902532	4	8.72	1.19E-06	
Regulation of multicellular organismal development	GO:2000026	11	8.51	9.82E-04	
Cell death	GO:0008219	7	8.05	5.38E-09	
Enzyme-linked receptor protein signalling pathway	GO:0007167	4	7.94	1.24E-05	
Positive regulation of transport	GO:0051050	7	7.81	1.39E-03	
Negative regulation of response to stimulus	GO:0048585	11	7.71	1.52E-05	
Regulation of monoatomic ion transport	GO:0043269	4	7.71	1.51E-08	
Regulation of cell population proliferation	GO:0042127	11	7.52	1.55E-03	
Positive regulation of programmed cell death	GO:0043068	4	7.45	1.94E-08	
Negative regulation of molecular function	GO:0044092	6	7.13	1.76E-03	
Positive regulation of catalytic activity	GO:0043085	6	6.76	1.21E-04	
Regulation of cellular localization	GO:0060341	6	6.75	1.62E-04	
Cellular response to endogenous stimulus	GO:0071495	6	6.73	1.63E-04	
Regulation of programmed cell death	GO:0043067	9	6.71	1.65E-04	
Regulation of response to stress	GO:0080134	8	6.51	1.90E-06	
Regulation of catabolic process	GO:0009894	5	6.26	1.13E-05	
Regulation of cellular component organization	GO:0051128	13	6.12	9.15E-04	
Regulation of catalytic activity	GO:0050790	9	6.07	4.24E-09	
Defence response to other organism	GO:0098542	5	5.77	4.34E-06	
Positive regulation of nucleobase-containing compound metabolic process	GO:0045935	9	5.63	1.32E-03	
Response to organic substance	GO:0010033	12	5.62	8.08E-06	
Response to endogenous stimulus	GO:0009719	6	5.56	7.41E-08	
Cell motility	GO:0048870	5	5.48	4.63E-04	
Regulation of localization	GO:0032879	10	5.24	1.66E-03	
Immune system process	GO:0002376	10	5.03	3.55E-06	
Homeostatic process	GO:0042592	6	4.91	5.15E-06	
Regulation of molecular function	GO:0065009	10	4.72	9.01E-04	
Regulation of signalling	GO:0023051	13	4.56	9.19E-06	
Regulation of cell communication	GO:0010646	13	4.55	1.57E-07	
Cell development	GO:0048468	9	4.47	1.59E-07	
Regulation of biological quality	GO:0065008	10	3.96	5.22E-05	
Response to chemical	GO:0042221	12	3.65	4.45E-05	
Cellular developmental process	GO:0048869	11	3.53	8.52E-06	
Negative regulation of biological process	GO:0048519	16	3.53	4.04E-05	
Regulation of biosynthetic process	GO:0009889	11	3.38	2.42E-08	

Function		Number of genes	Fold enrichment	p-value
Signalling	GO:0023052	14	3.21	6.10E-05
Regulation of cellular biosynthetic process	GO:0031326	10	3.19	2.65E-06
Cell communication	GO:0007154	14	3.11	2.91E-04
Regulation of cellular metabolic process	GO:0031323	13	3.01	3.93E-06
Regulation of nucleobase-containing compound metabolic process	GO:0019219	9	2.88	2.15E-05
Developmental process	GO:0032502	13	2.73	1.54E-03
Cellular response to stimulus	GO:0051716	14	2.52	6.48E-05
Regulation of metabolic process	GO:0019222	13	2.4	5.61E-05
Regulation of metabolic process	GO:0019222	13	2.4	2.83E-04
Multicellular organismal process	GO:0032501	14	2.24	2.37E-04
Response to stimulus	GO:0050896	16	2.2	2.94E-05
Biological regulation	GO:0065007	18	1.74	5.21E-05
GO Molecular function				
Cytokine activity	Go:0005125	12	63.44	4.39E-20
Hormone activity	Go:0005179	5	44.57	8.36E-08
Glycosaminoglycan binding	Go:0005539	4	20.35	4.00E-05
Molecular function regulator activity	Go:0098772	16	9.11	9.01E-15
Protein binding	Go:0005515	17	2.2	6.34E-06
GO Cellular component				
Extracellular region	Go:0005576	18	8.46	2.14E-17

- A: Serotransferrin (Q921I1), cleave sites position 19 and 20

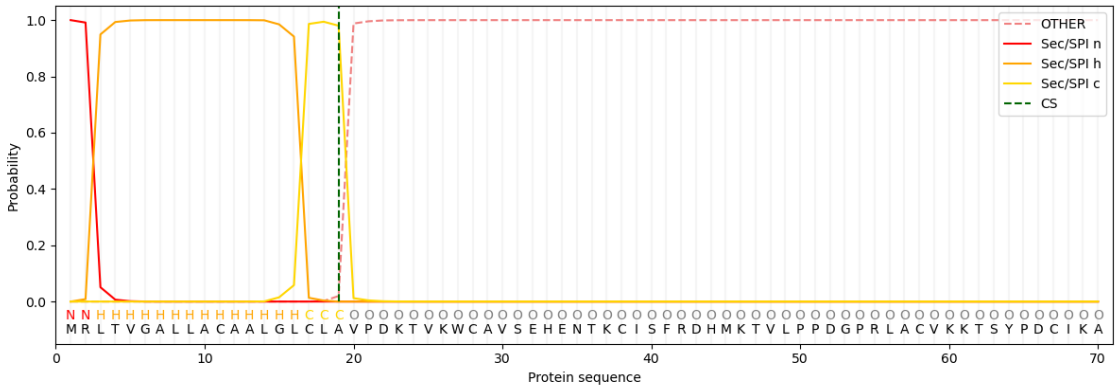

- B: Ceruloplasmin (Q61147), cleave sites position 19 and 20

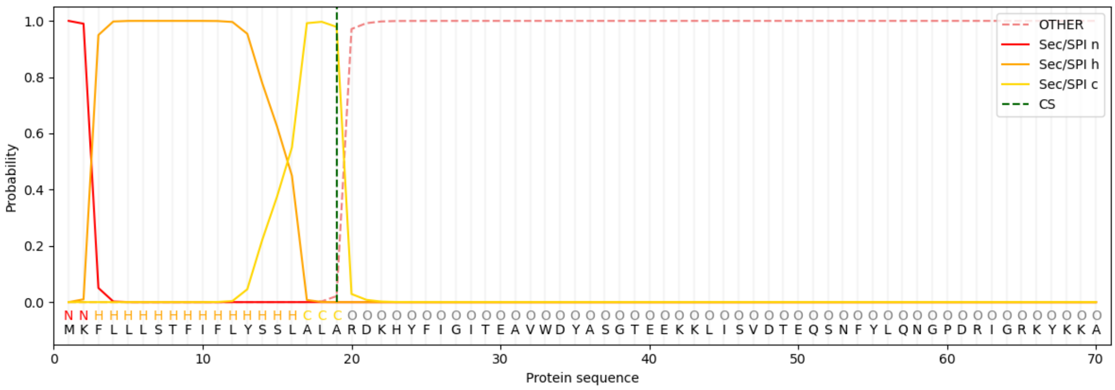

- C: C3/C5 convertase (B8JJM5), cleave sites position 24 and 25

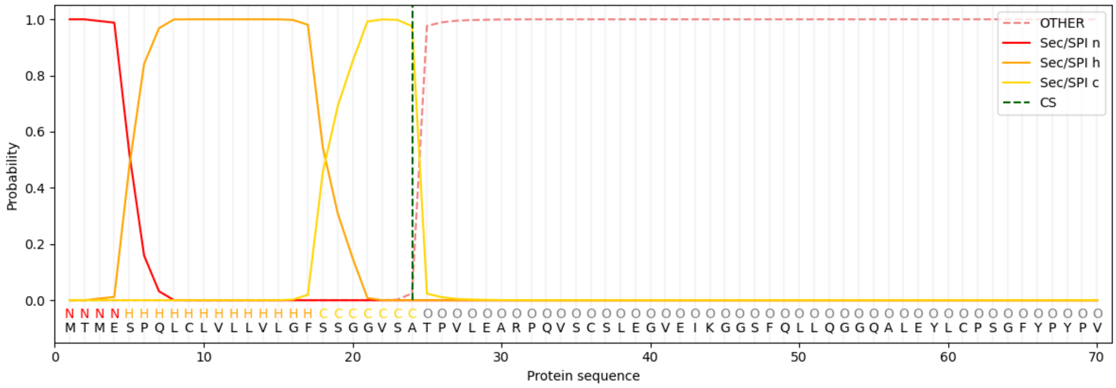

- D: Complement C3 (P01027), cleave sites position 24 and 25

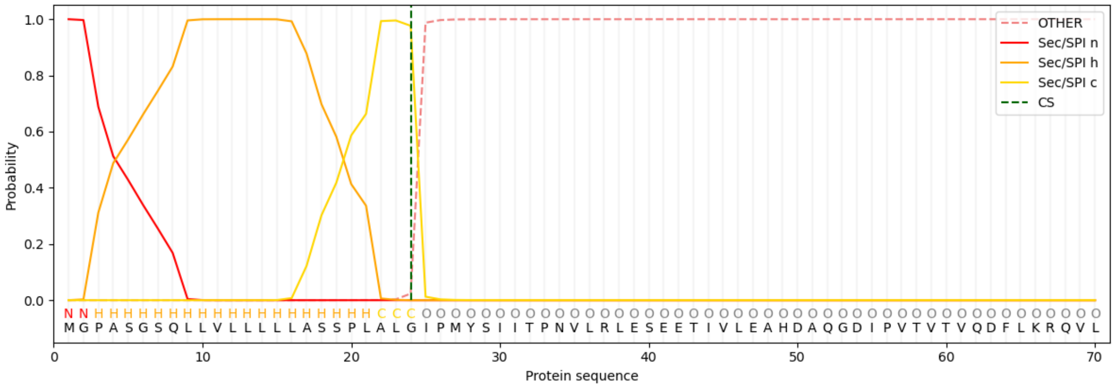

- E: Fibronectin (B7ZNJ1), cleave sites position 24 and 25

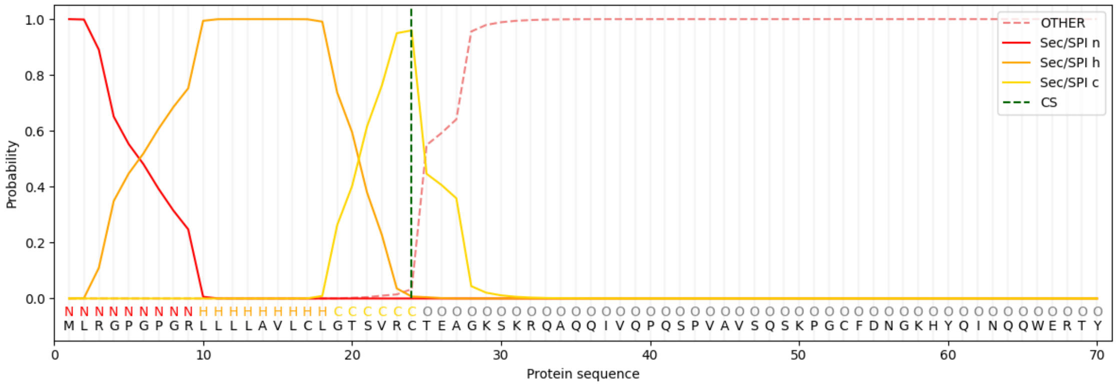

- F: Gelsolin (P13020), cleave sites position 25 and 26

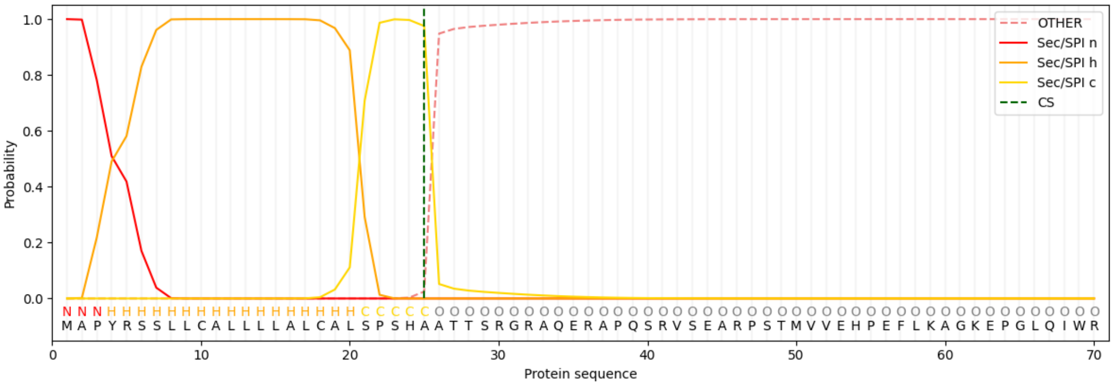

- G: Complement factor B (P04186), cleave sites position 22 and 23:

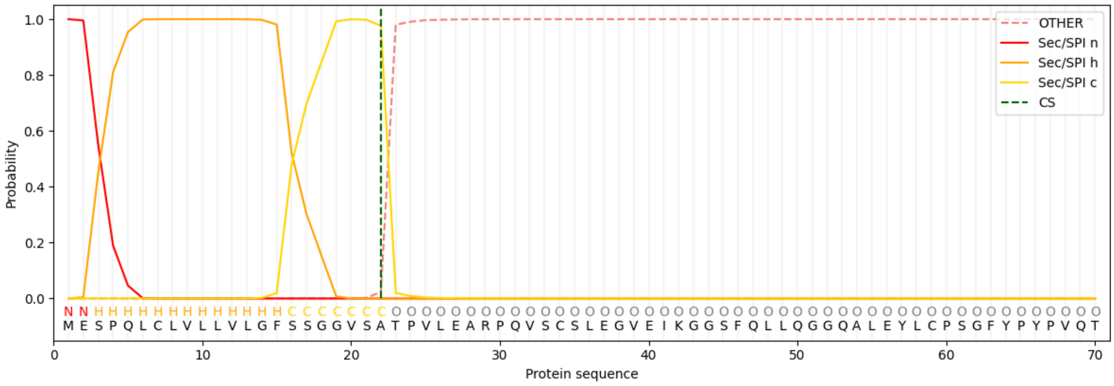

Figure A2 Verification of top 10 secreted proteins in 2D and 3D CM. *Prediction of SPs and cleavage site positions for serotransferrin, fibronectin, complement C3, ceruloplasmin, C3/C5 convertase and gelsolin. The Sec signal peptide (Sec/SPI) signal is annotated. n-region: The n-terminal region of the signal peptide, h-region: The centre hydrophobic region of the signal peptide and the c-region: the c-terminal region of the signal peptide, CS: cleavage site.*

Appendix II

Poster presentations (external)

Muscle and Myokines: Investigating exercise profiles from *in vitro* mouse models. *Advances in Skeletal Muscle Biology in Health and Disease. University of Florida, Myology Institute, USA (2023).*

Skeletal Muscle As An Endocrine Organ: Development Of In Vitro Models. *12th Annual Mellanby Centre Research Day. University of Sheffield, UK (2023).* ***First Prize Award.***

Skeletal Muscle As An Endocrine Organ: Development Of Custom in vitro Models. *Biomaterials & Tissue Engineering Group 21st Annual White Rose Work in Progress Meeting, UK (2022).*

Detecting Myokines from 2D and 3D skeletal muscle models. *British Mass Spectrometry Society, UK (2022).*

Developing A Functional 3D Skeletal Muscle Model For Myokine Investigation. *EMBO: Muscle formation, maintenance, regeneration and pathology. 2022 in Gouvieux, France.*

Detecting Myokines From Skeletal Muscle Models For Cardiometabolic Disease Effects *(2021). British Mass Spectrometry Society, UK (2022).*

Grants

Biochemistry Society Travel Grant - £500